

Dissertation
submitted to the
Combined Faculties for the Natural Sciences and for Mathematics
of the Ruperto–Carola University of Heidelberg, Germany
for the degree of
Doctor of Natural Sciences

presented by
M.Sc. Yu-Ao Chen
born in Qidong Jiangsu (P. R. China)

Oral examination: January 23rd 2008

Quantum Manipulation of Photons and Atoms

* * *

The Application in Quantum Information Processing

Referees:

Prof. Dr. Jian-Wei Pan

Prof. Dr. Jörg Schmiedmayer

Zusammenfassung

Quantenmanipulation von Photonen und Atomen

Quanteninformation wird seit den achtziger Jahren des vergangenen Jahrhunderts ein grosser wissenschaftlicher Wert und grosse Anwendbarkeit bezeugt. Die hier vorgestellte wissenschaftliche Arbeit gliedert sich in zwei Hauptteile: die Manipulation von Multiphotonen-Verschränkung und Quantenspeicher basierend auf atomaren Ensembles. Im ersten Teil werden die experimentellen Methoden von Multiphotonen-Verschränkung weiterentwickelt um fundamentale Fragen der Quantenmechanik zu studieren und bemerkenswerte Anwendungen zur Quantenkommunikation und Quantenrechnungen zu untersuchen. Genauer gesagt handelt es sich dabei um die Demonstration eines Bit-Flip fehlerfreien Transfers von Quanteninformation, die Verletzung der Bell'schen Ungleichung über die Tsirelson Grenze, die Teleportation eines zwei Qubit-Kompositsystems, sowie um eine Einwegquantenrechnung mittels eines Zwei-Photonen-Vier-Qubit-Clusterzustandes. Um die Unskalierbarkeit durch die probabilistischen Eigenschaften in der linearen Quanteninformationsverarbeitung zu überwinden, haben wir im zweiten Teil der vorliegenden Arbeit die Physik von Quantenspeichern basierend auf atomaren Ensembles untersucht. Wir zeigen theoretisch, dass Verschränkung zwischen entfernten Orten deterministisch erzeugt werden kann. Mit den experimentell sorgfältig entwickelten Techniken haben wir eine deterministische Einzelphotonenquelle umgesetzt, die Interferenz von Photonen von unabhängigen atomaren Ensembles erreicht, die Teleportation zwischen einem photonischen und atomaren Qubit verwirklicht, einen neuen Weg zur Erzeugung von robuster Verschränkung zwischen einem atomaren und einem photonischen Qubit entwickelt und speicherbasierten Verschränkungstausch nachgewiesen. Wir glauben, dass die hier dargestellten Techniken den Fortschritt in vielen Feldern wie der globalen Quantenkommunikation, der linearen optischen Quantenrechnung, den Fundamenten der Quantenmechanik usw. eine dramatische Erleichterung bringen werden.

Abstract

Quantum manipulation of photons and atoms

Quantum information has been witnessing great science value and latent application since 1980's. The research work presented here consist of mainly two important parts: manipulations of multi-photon entanglement and atomic ensembles based quantum memory. In first part, the experimental technique multi-photon entanglement is further developed to study fundamental issues in quantum mechanics, remarkable applications to quantum communication and quantum computation. Specifically, we have demonstrated a bit-flip error-free transfer of quantum information, violation of Bell's inequality beyond Tsirelson's bound, teleportation of a two-qubit composite system, as well as the one-way computing by two-photon-four-qubit cluster state. To overcome un-scalability problem due to probabilistic feature in linear optical quantum information processing, we investigated in the second part the physics of atomic ensembles based quantum memory. We show that theoretically, entanglement between distant locations can be deterministically generated. The experimental work has thoroughly developed the necessary techniques and we have achieved deterministic single photon source, and interference of the photons from independent atomic ensembles, teleportation between photonic and atomic qubits, a novel way to create a robust entanglement between an atomic and a photonic qubit, and memory based entanglement swapping. We believe, the developed techniques here would dramatically facilitate progresses in many fields including global quantum communication, linear optical quantum computation and the foundations of quantum mechanics etc.

摘要

光子和原子的量子操纵

量子信息学是基于上世纪物理学最重大的发展之一量子力学的基础之上的，由于其潜在的应用价值和重大的科学意义，上世纪八十年代以来，量子信息学成为一门迅速发展新兴学科，同时引起了各国政府和广大科学界的高度关注。

本文主要研究多光子纠缠以及基于原子系综的量子存储在量子信息处理中的应用。本文主要包括两个部分：多光子纠缠的实验操纵和基于原子系综的量子存储的操纵。

在第一部分中，我们在实验上进一步发展了基于参量下转换的多光子纠缠的实验技术，除了研究多光子纠缠在量子力学基础问题上的性质之外，我们也实现了其在量子通讯以及量子计算学等方向的重要应用：实验实现无比特翻转误差的量子态传输；验证了高于 Tsirelson 极限的贝尔不等式的违背；双光子复杂系统的隐形传态；通过双光子四比特簇态实现了基于测量的高速单向量子计算。

然而，由于源的概率性，限制了基于参量下转换的量子信息处理往更复杂化升级，人们提出了量子存储来解决这一问题。在本文的第二部分，我们从理论上以及实验上研究了基于原子系综的存储可行性。理论研究表明，通过原子系综的帮助，我们可以确定性的在两个距离遥远的地方之间产生最大纠缠态。进一步的，我们发展了必须的实验技术以在实验上研究量子存储：通过读写原子系综产生的非经典光子对，我们实验实现了确定性的单光子源；进一步的我们研究了基于两个独立系综的两个光子之间的相干及其不可区分性；利用两个系综作为一个量子比特，我们实现了从光子比特到原子比特的量子隐形传态；进一步的我们发展了一个更新奇稳定的光子原子纠缠源，基于这样一个纠缠源我们实现了基于量子存储的量子纠缠交换。

最后，我们的实验方法将大大促进未来的全球量子通讯，线性光学量子计算，量子力学基础检验等重要科学问题的研究。

路漫漫其修远兮，

吾将上下而求索。

Contents

| | |
|--|-------------|
| Abstract | i |
| Contents | v |
| List of figures | ix |
| List of Tables | xvii |
| 1 Introduction | 1 |
| 1.1 Basic concepts of quantum information | 1 |
| 1.2 Quantum communication and quantum cryptography | 2 |
| 1.3 Quantum computation | 2 |
| 1.4 Linear optical quantum information processing | 3 |
| 1.5 Objective of this work | 5 |
| | |
| I Manipulation of Photons: Multi-photon Entanglement | 7 |
| | |
| 2 Multi-photon entanglement | 9 |
| 2.1 Polarization-entangled photon pairs | 10 |
| 2.2 Multi-photon entanglement | 12 |
| | |
| 3 Quantum error rejection | 15 |
| 3.1 Introduction | 15 |
| 3.2 Two-bit bit-flip error-rejection code | 16 |
| 3.2.1 Encoding | 16 |
| 3.2.2 A bit flip noisy quantum noisy channel | 17 |
| 3.2.3 Parity check and decoding | 17 |
| 3.2.4 Fault tolerance property | 18 |
| 3.3 Experimental setup | 19 |
| 3.3.1 Noisy quantum channels | 20 |
| 3.4 Experimental results | 20 |
| 3.5 Discussion | 23 |
| | |
| 4 Violation of Bell's Inequality beyond Tsirelson's bound | 25 |
| 4.1 Introduction | 25 |
| 4.2 CHSH-Bell inequality | 25 |
| 4.2.1 Tsirelson's bound | 26 |
| 4.2.2 Violation beyond Tsirelson's bound | 26 |
| 4.3 Experiment proposal | 27 |
| 4.4 Experimental setup | 28 |
| 4.5 Experimental results | 30 |

| | | |
|-----------|--|-----------|
| 4.5.1 | Violation of Mermin's inequality | 31 |
| 4.6 | Discussion | 32 |
| 5 | Teleportation of two-qubit composite system | 33 |
| 5.1 | Introduction | 33 |
| 5.2 | Two-qubit teleportation scheme | 34 |
| 5.3 | A stable high-intensity entangled photon source | 35 |
| 5.4 | Experimental setup | 38 |
| 5.5 | Experimental results | 38 |
| 5.6 | Discussion | 40 |
| 6 | One-way quantum computing | 43 |
| 6.1 | Introduction | 43 |
| 6.2 | State preparation | 44 |
| 6.2.1 | State analysis | 47 |
| 6.3 | Cluster state based one-way computing | 47 |
| 6.3.1 | Grover's algorithm | 48 |
| 6.3.2 | Quantum gates | 49 |
| 6.4 | Discussion | 50 |
| II | Manipulation of Atoms: Quantum Memory | 51 |
| 7 | Atomic ensemble based quantum repeater | 53 |
| 7.1 | Introduction | 53 |
| 7.2 | The DLCZ protocol | 54 |
| 7.2.1 | Light-atoms coupling | 54 |
| 7.2.2 | Entanglement generation | 55 |
| 7.2.3 | Entanglement connection | 55 |
| 7.2.4 | Phase instability analysis | 56 |
| 7.3 | Robust quantum repeater | 56 |
| 7.3.1 | Motivation | 56 |
| 7.3.2 | Basic protocol | 56 |
| 7.3.3 | Entanglement connection and scalability | 59 |
| 7.3.4 | Alternative approach | 61 |
| 7.3.5 | Entanglement purification | 62 |
| 7.4 | Conclusion | 64 |
| 8 | Deterministic single photon source | 65 |
| 8.1 | Introduction | 65 |
| 8.2 | Basic conception | 66 |
| 8.2.1 | Non-classical photon pair generation | 66 |
| 8.2.2 | Single photon source | 69 |
| 8.3 | Discussion | 70 |
| 9 | Interference of photons from independent atomic ensembles | 73 |
| 9.1 | Introduction | 73 |
| 9.2 | Experiment | 74 |
| 9.3 | Experimental results | 77 |
| 9.3.1 | The measurement of HOM dip | 77 |
| 9.3.2 | Time resolved two-photon interference | 79 |
| 9.3.3 | Efficient entanglement generation | 79 |

| | |
|---|------------|
| 9.4 Discussion | 79 |
| 10 Teleportation between photonic and atomic qubits | 81 |
| 10.1 Introduction | 81 |
| 10.2 Experiment scheme | 82 |
| 10.3 Experimental realization | 84 |
| 10.3.1 Phase locking | 84 |
| 10.3.2 Photonic qubit to be teleported | 86 |
| 10.4 Experimental result | 86 |
| 10.5 Discussion – noise estimation | 87 |
| 10.5.1 Bell-state measurement | 87 |
| 10.5.2 Teleportation fidelity | 88 |
| 10.6 Conclusion | 89 |
| 11 A novel entanglement source | 91 |
| 11.1 Introduction | 91 |
| 11.2 Experimental conception | 92 |
| 11.3 Characterization of atom-photon entanglement | 94 |
| 11.3.1 Entanglement visibility | 94 |
| 11.3.2 Storage of entanglement | 95 |
| 11.4 Discussion | 97 |
| 12 Entanglement swapping | 99 |
| 12.1 Introduction | 99 |
| 12.2 Experimental setup | 100 |
| 12.2.1 Atom-photon entanglement | 100 |
| 12.2.2 Entanglement swapping | 102 |
| 12.3 Experimental result | 102 |
| 12.3.1 Violation of CHSH-Bell inequality | 102 |
| 12.3.2 Entanglement witness | 103 |
| 12.3.3 Fidelity | 104 |
| 12.4 Discussion | 105 |
| III Conclusion | 107 |
| 13 Conclusion and outlook | 109 |
| Appendix: Associated Publications | 111 |
| Acknowledgement | 113 |
| Bibliography | 115 |

List of Figures

| | | |
|-----|--|----|
| 2.1 | Principle of type-II spontaneous parametric down-conversion. Inside a nonlinear BBO crystal, an incoming pump photon can decay spontaneously into two photons. Two down-converted photons arise polarized orthogonally to each other. Each photon is emitted into a cone, and the photon on the top cone is vertically polarized while its exactly opposite partner in the bottom cone is horizontally polarized. Along the directions where the two cones intersect, their polarization are undefined; all that is known is that they have to be different, which results in polarization entanglement between the two photons in beams A and B. | 11 |
| 2.2 | Diagram showing the principle of generating three photon (a) and four photon (b) entanglement. The single photon source (S) emits a photon in a polarization state $H + V$, and the entangled photon sources (EPR), each one emits a photon pair in the entangled state $HH + VV$ | 13 |
| 3.1 | Scheme for one bit-flip quantum error-rejection. | 16 |
| 3.2 | Experimental set-up for quantum error-rejection. | 19 |
| 3.3 | Simulated bit-flip noisy quantum channel. The curve represents the desired error rate. | 21 |
| 3.4 | Experimental results for three different initial states $ V\rangle$ (a), $ -\rangle$ (b) and $ L\rangle$ (c), and (d) shows the average QBER (calculated over all the six states). The quadrangle and the triangle dots are corresponding to the cases that error-rejection and no error-rejection was made, and the solid curves and the dot curves show the theoretically prediction of QBER for the cases without and with error rejection respectively. | 22 |
| 4.1 | Experimental setup for generating three-photon GHZ states. An ultraviolet pulse passes twice through the + crystal to generate two pairs of polarization-entangled photons by Type-II spontaneous parametric down-conversion used to perform the preparation of three-photon GHZ state. The ultraviolet laser with a central wavelength of 394 nm has pulse duration of 200fs, a repetition rate of 76 MHz, and an average pump power of 400 mW. We observe about 2×10^4 entangled pairs per second behind 3.6 nm filters (F) of central wavelength 788 nm. Polarizers (Pol.) and quarter wave plates ($\lambda/4$) in front of the detectors are used for performing X or Y measurement. | 29 |
| 4.2 | Typical experimental results for polarization measurements on all three photons in a X basis triggered by the photon 4 at the + polarization. The coincidence rates of $+++$ and $++-$ components are shown as a function of the pump delay mirror position. The high visibility obtained at zero delay implies that three photons are indeed in a coherent superposition. | 30 |
| 4.3 | Experimental results observed for the 5 required configurations: XXX , XYX , YXY , YYX , and YYY | 31 |

| | | |
|-----|---|----|
| 5.1 | Schematic diagram showing the principle of two-qubit teleportation. Alice wants to teleport an unknown state of a system composed of photon 1 and 2 to Bob. To do so, Alice and Bob first share two entangled photon pairs (EPR source), photon pairs 3-5 and 4-6. Alice then carries out a joint Bell-state measurement (BSM) both on photons 1 and 3 and on photons 2 and 4, respectively. On receiving Alice's BSM results via classical communication, Bob can then carry out a corresponding unitary transformation (U) on both photons 5 and to convert them into the original state of photons 1 and 2. | 34 |
| 5.2 | The method to increase the power of the ultraviolet light. A modified mode-locked Ti:sapphire laser (MIRA), pumped with an all-solid-state CW laser Verdi-V18 (operating at 14W), is used to produce high-intensity ultra-fast infrared light pulses. The infrared light pulse passes through the LBO crystal to generate via up-conversion the ultraviolet pulse necessary for parametric down-conversion. Behind the LBO, two cylindrical lenses with orthogonal axes, (one horizontal and one vertical) are used to shape and focus the ultraviolet beam and five dichroic mirrors (DM) are used to separate the ultraviolet from the infrared light. | 36 |
| 5.3 | A schematic diagram of the experimental setup. The ultraviolet pulse passes through a BBO crystal to generate a polarization-entangled photon pair in mode 3 and 5 (that is, the first ancillary entangled photon pair). After the first BBO, a 10-cm-focus lens is introduced to refocus the ultraviolet pulse pumps once more into the second BBO and generates the third entangled photon pair in modes 4 and 6 (that is, the second ancillary photon pair). Prisms 1 and 2, both mounted on step motors, are used to compensate the time delay for the interference on polarizing beam splitters PBS13 and PBS24, respectively. PBS5 and PBS6 are used to verify the teleported state with the help of wave plates in front of them. The photons are all detected by silicon avalanched single-photon detectors. Coincidences are recorded with a coincidence unit clocked by the infrared laser pulses. Pol. are linear polarizers and Filter labels the narrow band filter with $\Delta\lambda_{FWHM} = 2.8\text{nm}$ | 37 |
| 5.4 | Experimental results for the teleportation of the $ \chi\rangle_A$ state and the $ \chi\rangle_B$ state. Each measurement takes 60 h. A , The $ \chi\rangle_A$ state. We measured photon 5 and 6 in $ H\rangle/ V\rangle$ basis. B , The $ \chi\rangle_B$ state. We measured photon 5 in $ +\rangle/ -\rangle$ basis and photon 6 in $ R\rangle/ L\rangle$ basis. The fraction of $ H\rangle V\rangle$ ($ +\rangle R\rangle$) to the sum of all counts shows the fidelity for the teleportation of the $ \chi\rangle_A(\chi\rangle_B)$ state in A(B) | 39 |
| 5.5 | Experimental results for $ \chi\rangle_C$ teleportation. Three complementary bases were used: (A) $ H\rangle/ V\rangle$, (B) $ +\rangle/ -\rangle$ and (C) $ R\rangle/ L\rangle$ corresponding to the three different local measurements $\hat{\sigma}_x\hat{\sigma}_x$, $\hat{\sigma}_y\hat{\sigma}_y$ and $\hat{\sigma}_z\hat{\sigma}_z$. Each measurements takes 60 h. In (A) whenever there is a $ H\rangle H\rangle$ or $ V\rangle V\rangle$ coincidence, the result of the $\hat{\sigma}_x\hat{\sigma}_x$ is +1, whereas $ H\rangle V\rangle$ or $ V\rangle H\rangle$ represents -1. In (B) , $ +\rangle +\rangle$ or $ -\rangle -\rangle$ represents +1, whereas $ +\rangle -\rangle$ or $ -\rangle +\rangle$ represents -1. In (C) , $ R\rangle R\rangle$ or $ L\rangle L\rangle$ displaces +1, whereas $ R\rangle L\rangle$ or $ L\rangle R\rangle$ displaces -1. | 40 |

6.1 Schematic of experimental setup. **(a)**. By pumping a two-crystal structured in a double pass configuration, one polarization entangled photon pair is generated either in the forward direction or in the backward direction. Two QWPs are tilted along their optic axis to vary relative phases between polarization components to attain two desired possibilities for entangled pair creation. Concave mirror and prism are mounted on translation stages to optimize interference on two beam splitters($BS_{1,2}$) or polarizing beam splitters ($PBS_{1,2}$) for achieving the target cluster state. HWPs together with PBS and 8 single-photon detectors (D1-D8) are used for polarization analysis of the output state. IF are 3 nm filters with central wavelength 710 nm. **(b)**. In the place where $BS_{1,2}$ or $PBS_{1,2}$ are located, three apparatuses are for measuring all necessary observables. Setup **(i)** is for Z measurement while setup **(ii)** is used for X measurement for spacial modes. If an α phase shifter is inserted at one of the input modes in (ii), an arbitrary measurement along basis $B(\alpha)$ can be achieved. Setup **(iii)** can be for Z measurement of spacial mode and, simultaneously, for Z measurement of polarization. 45

6.2 Interference fringe observed when the concave mirror and the prism being moved to achieve perfect temporal overlap and to adjust the phase $\theta = 0$. **a** We measure the two fold coincidence between the output modes toward detectors D_1 and D_2 behind 22.5° HWP and PBS, by scanning the position of the prism. The envelope of the observed twofold coincidence varies indicating the visibility of the two photon coherence. Inside the coherent region, the best visibility is obtained at the position where perfect temporal overlap is achieved. **b** We use a piezo translation stage to move the concave mirror to perform a fine scan around the centre of the envelope. By setting the piezo system to a position where we observe maximum twofold coincidence of D_1 - D_2 , we then achieve $\theta = 0$ 46

6.3 Demonstration of Grover’s algorithm. **a**. Equivalent quantum circuit of Grover’s algorithm using box cluster state. The ‘oracle’ encodes the element ‘00’ by measuring along basis $B_{2,3}(\pi)$, while the inverse and readout sections will find this entry with certainty by a single query. **b**. A successful identification probability of $(96.1 \pm 0.2)\%$ is achieved deterministically with feed-forward, while it is $(24.9 \pm 0.4)\%$ without feed-forward. This is in an excellent agreement with theoretical expectations. The trick is that the black box provides only outcomes but not basis information for feed-forward. Thus the oracle encoding is hidden before feed-forward on readout. 48

6.4 Two-qubit quantum gates realizations. **a**. CPhase gate realization with the horse-shoe cluster. **b**. Experimental measured fidelities of output states to the ideal Bell states (unnormalized) in the lab basis. They are $0.954 \pm 0.003, 0.940 \pm 0.004, 0.936 \pm 0.005, 0.910 \pm 0.005$ for outcomes 00,01,10,11 on qubits 2,3 respectively. **c**. Quantum gate implementation that does not generate entanglement with the box cluster. **d**. Measured fidelities of output states to the ideal product states in the lab basis. They are $0.935 \pm 0.005, 0.962 \pm 0.004, 0.969 \pm 0.003, 0.975 \pm 0.003$ for outcomes 00,01,10,11 on qubits 2,3 respectively. 49

| | | |
|-----|--|----|
| 7.1 | <p>Setups for entanglement generation and entanglement swapping in the DLCZ protocol. a). Forward-scattered anti-Stokes photons, generated by an off resonant Write laser pulse via spontaneous Raman transition, are directed to beam splitter (BS) at the center. Entanglement is generated between atomic ensembles at sites a and b, once there is a click on either of the detectors. The inset shows the atomic level structure, with a pair of metastable state $g\rangle$ and $s\rangle$, and excited state $e\rangle$. b). Entanglement has been generated between atomic ensembles (a, b^L) and (b^R, c). The atomic ensembles at site b are illuminated by near resonant Read laser pulses, and the retrieved Stokes photons are subject to BS at the center. A click on either of the detectors will prepare the atomic ensembles at a and c into an entangled state.</p> | 54 |
| 7.2 | <p>Setup for entanglement generation between sites A and B. Forward-scattered anti-Stokes photons, generated by an off-resonant write laser pulse via spontaneous Raman transition, are subject to Bell-state measurement (BSM-I) at the center. The Stokes photons generated at the same site are assumed to have different polarization i.e., $H\rangle$ and $V\rangle$. PBS (PBS_{\pm}) reflects photons with polarization $V\rangle$ ($-\rangle$) and transmits photons with polarization $H\rangle$ ($+\rangle$), where $\pm\rangle = \frac{1}{\sqrt{2}}(H\rangle \pm V\rangle)$. After passing through the PBS_{\pm} and PBS successively, the Stokes photons are detected by single photon detectors. A coincidence count between single photon detectors D_1 and D_4 (D_1 and D_3) or D_2 and D_3 (D_2 and D_4) will project the four atomic ensembles into the complex entangled state $\psi\rangle_{AB}$ up to a local unitary transformation.</p> | 57 |
| 7.3 | <p>Setup for entanglement connection between sites A and C via entanglement swapping. Complex entangled states have been prepared in the memory qubits between sites (A, B_L) and (B_R, C). The memory qubits at site B are illuminated by near resonant read laser pulses, and the retrieved anti-Stokes photons are subject to BSM-II at the center. The Stokes photons at the same site have different polarizations $H\rangle$ and $V\rangle$. After passing through PBS and PBS_{\pm} successively, the Stokes photons are detected by single photon detectors. Coincidence counts between D_1 and D_4 (D_1 and D_3) or D_2 and D_3 (D_2 and D_4) are registered. The memory qubits will be projected into an effectively maximally entangled state ρ_{AC} up to a local unitary transformation. Note that the sequence of PBSs in BSM-II is different from BSM-I. This helps to eliminate the spurious contributions from second-order excitations.</p> | 58 |
| 7.4 | <p>Elementary entangled pairs are first locally generated via the standard DLCZ protocol. The anti-Stokes photons are subject to BSM-I to connect neighboring communication nodes. We also assume the anti-Stokes photons retrieved from atomic ensembles at the same site have different polarization. Note that BSM-I also helps to eliminate the spurious contributions from higher order excitations.</p> | 60 |
| 7.5 | <p>Quantum memory for photonic polarization qubits. Two ensembles are a classical control field. Classical and quantized light fields are fed into the first PBS and will leave at two different outputs of the second PBS. As each atomic cell works as quantum memory for single photons with polarization $H\rangle$ or $V\rangle$ via the adiabatic transfer method, the whole setup is then quantum memory of any single-photon polarization states. The inset shows the relevant level structure of the atoms. The $e\rangle - s\rangle$ transition is coherently driven by the classical control field of Rabi frequency Ω_c, and the $g\rangle - e\rangle$ transition is coupled to a quantized light field.</p> | 62 |

- 7.6 a). Entanglement swapping between adjacent communications nodes A and B . Two pairs of entangled memory qubits are first generated by storing the event-ready entanglement of two photons at each node. Then the two photons stored in the U memory at the two nodes are simultaneously retrieved and subject to a two-photon Bell-state measurement at the center. This entanglement swapping process will in an “event-ready” way entangle the two distant D memory qubits. b). Entanglement connection to extend the communication length. Two well entangled pairs of memory qubits, one across nodes (A, B_L) and (B_R, C) are prepared in parallel. The Bell-state measurement on the two photons released simultaneously from the two memories at node B results in, with a probability of $1/2$, well entangled quantum memories across nodes A and C in a definite Bell state. 63
- 7.7 Setup for quantum entanglement purification. Entangled states have been prepared in the memory qubits between two distant nodes I and J . The memory qubits at the two sites are illuminated by near resonant read laser pulse, and the retrieved entangled photon pairs are directed to two PBS respectively. The photons in mode b_1 and b_2 are detected in $|\pm\rangle = \frac{1}{\sqrt{2}}(|H\rangle \pm |V\rangle)$ basis and the remaining photons in mode a_1 and a_2 are restored in the memory qubits at the two sites respectively. . . 64
- 8.1 Illustration of the experimental setup (a) and the time sequence with the feedback circuit for the *write* and *read* process (b). The atomic ensemble is firstly prepared in the initial state $|a\rangle$ by applying a pump beam resonant with the transition $|b\rangle$ to $|e'\rangle$. A write pulse with the Rabi frequency Ω_w is applied to generate the spin excitation and an accompanying photon of the mode \hat{a}_{AS} . Waiting for a duration Δt , a read pulse is applied with orthogonal polarization and spatially overlap with the write beam in PBS1. The photons, whose polarization is orthogonal to that of the write beam, in the mode \hat{a}_{AS} are spatially extracted from the write beam by PBS2 and detected by detector D1. Similarly, the field \hat{a}_S is spatially extracted from the Read beam and detected by detector D2 (or D3). Here, FC1 and FC2 are two filter cells, BS is a 50/50 beamsplitter, and AOM1 and AOM2 are two acousto-optic modulators. 67
- 8.2 Intensity correlation function $g_{AS,S}^{(2)}$ along the excitation probability p_{AS} with $\delta t = 500$ ns (a) and along the time delay δt between read and write pulses with $p_{AS} = 3 \times 10^{-3}$ (b). The black dots are obtained from current experiment and the curves correspond to a least-square fit procedure according to Eq. (8.2) and (8.3). The observed lifetime is $\tau_c = 12.5 \pm 2.6 \mu\text{s}$ 68
- 8.3 The anti-correlation parameter as a function of p_{AS} (a) and Δt (b). In Fig (a), the data in black correspond to the experiment without feedback circuit, in which each write sequence is followed by one read pulse. The data in red correspond to the experiment with feedback circuit, in which 12 successive write sequences are followed by one read pulse. The red curve is the theoretical evaluation taking into account the fitted background of the black dots. In Fig (b), 12 write sequences were applied in each trial while measuring. 70

| | | |
|------|--|----|
| 9.1 | <p>Illustration of the relevant energy levels of the atoms and arrangement of laser beams (a) and the experimental setup (b). Alice and Bob each keeps a single-photon source at two remote locations. As elucidated in Chapter 8, Alice applies write pulses continuously until an anti-Stokes photon is registered by detector D1. Then she stops the write pulse, holds the spin excitations and meanwhile sends a synchronization signal to Bob and waits for his response (This is realized by the feedback circuit and the acousto-optic modulators, AOM). In parallel Bob prepares a single excitation in the same way as Alice. After they both agree that each has a spin excitation, each of them will apply a read pulse simultaneously to retrieve the spin excitation into a light field \hat{a}_s. The two Stokes photons propagate to the place for entanglement generation and Bell measurement. They overlap at a 50:50 beam splitter (BS) and then will be analyzed by latter half-wave plates ($\lambda/2$), polarized beam splitters (PBS) and single photon detectors Da, Db, Dc, and Dd.</p> | 75 |
| 9.2 | <p>Hong-Ou-Mandel dips in time domain (left panel) and frequency domain (right panel). The circle in the right panel was obtained by setting the polarization of the two photons perpendicular to each other and zero detuning between two read lasers. The Gaussian curves that roughly connect the data points are only shown to guide the eye. The dashed line shows the plateau of the dip. Error bars represent statistical errors, which are \pm one standard deviation.</p> | 76 |
| 9.3 | <p>Hong-Ou-Mandel dips in time domain with coincidence window (2 ns) much shorter than the wave-package length. The red spots are measured under perpendicular polarization and the black ones are measured under parallel cases.</p> | 78 |
| 10.1 | <p>Experimental setup for teleportation between photonic and atomic qubits. The inset shows the structure and the initial populations of atomic levels for the two ensembles. At Bob's site the anti-Stokes fields emitted from U and D are collected and combined at PBS_1, selecting perpendicular polarizations. Then the photon travels 7 m through fibers to Alice's to overlap with the initial unknown photon on a beam-splitter (BS) to perform the Bell-state measurement. The results of the Bell-state measurement are sent to Bob via a classical channel. The results of the Bell-state measurement are sent back to Bob via a classical channel. Bob then perform the verification of the teleported state in the U and D ensembles by converting the atomic excitation to a photonic state. A unitary operation on the converted photon is performed according to the classical information from the results of Bell-state measurement is performed.</p> | 82 |
| 10.2 | <p>Schematic drawing of the phase locking setup. Two Mach-Zehnder interferometers are used to actively stabilize the phases between the arms of write and read paths (a) and between the arms of anti-Stokes and Stokes paths (b), respectively. H/V denotes the horizontal/vertical polarization, and AOM is for an acousto-optic modulator. A polarizer (Pol.) is set at 45° to erase the polarization information. The HWPs ($\lambda/2$) are set at 45° as well to rotate the horizontal polarization to vertical. AS (S) denotes the anti-Stokes (Stokes) photon.</p> | 85 |
| 10.3 | <p>Fidelity of the teleported state in atomic ensembles along storage time. The initial state to be teleported is $H + iV$. Until $8 \mu s$ the fidelity is still well beyond the classical limit of $2/3$. Each experimental point is measured for about four hours (averagely). The curve is a Gaussian fit, due to the Gaussian decay of the retrieve efficiency. The error bars represent the statistical error, i.e. ± 1 standard deviation.</p> | 87 |

| | | |
|------|--|-----|
| 11.1 | Illustration of the scheme of the experiment setup and the relevant energy levels of the ^{87}Rb atoms. Cold ^{87}Rb atoms captured by MOT are initially prepared in state $ a\rangle$. A weak write pulse Ω_w with a beam waist of $240\ \mu\text{m}$ illuminates the atom cloud to generate the spin excitation. The spontaneous Raman scattered anti-Stokes field AS_L and AS_R are detected at $\pm 3^\circ$ to the propagating direction of the write beam, with the beam waist of $70\ \mu\text{m}$, defining the spatial mode of the atomic ensembles L and R , respectively. The two anti-Stokes field are combined on a polarizing beam splitter PBS_1 and sent to the polarization analyzer. This creates the entanglement between the polarization of the anti-Stokes field and the spatial modes of spin excitation of atoms in atomic ensemble. After a controlled storage time τ , the entanglement is verified by retrieving the spin excitation back to the Stokes fields S_L and S_R by a strong read pulse, which is overlapped and counter-propagates to the write beam. After overlap the Stokes fields on PBS_2 , the entanglement can be proved. | 93 |
| 11.2 | Visibility of the interference fringes V between anti-Stokes fields and Stokes fields various with the changing of the detected rate of anti-Stokes field p_{AS} . The solid line is the fit corresponding to Eq.(11.6). The dashed line shows the bound of $1/\sqrt{2}$ which mark the limit to violate the CHSH-type Bell's inequality. | 95 |
| 11.3 | Decay of the S parameter in the Bell's inequality measurement with the storage time τ . The dashed line shows the classical bound of $S = 2$ | 96 |
| 11.4 | The decay of retrieve efficiency and cross correlation $g_{12}^{(2)}$ with the storage time τ . The anti-Stokes detection rate is fixed at $p_{AS} = 2 \times 10^{-3}$. The square dots show the decay process of the retrieve efficiency of the Stokes fields, round dots show the decay of the cross correlation $g_{AS,S}^{(2)}$ between anti-Stokes field and Stokes field. | 97 |
| 12.1 | Illustration of the relevant energy levels of the atoms and the experimental setup. At Alice's site, ^{87}Rb atoms are prepared in the initial state $ a\rangle = 5S_{1/2}, F = 2\rangle$. A write pulse Ω_w with the detuning of $\Delta = -10\ \text{MHz}$ and a beam waist of $240\ \mu\text{m}$ is applied to generate the spin excitation (with one atom excited to $ b\rangle = 5S_{1/2}, F = 1\rangle$ through Raman scattering $ a\rangle \rightarrow e\rangle \rightarrow b\rangle$, where $ e\rangle = 5P_{1/2}, F = 2\rangle$) and an accompanying photon of the anti-Stokes field \hat{a}_{AS} with a beam waist of $70\ \mu\text{m}$. The light modes in channels AS_L and AS_R , tilted $\pm 3^\circ$ relative to the direction of the write beam, are overlapped at PBS_2 selecting perpendicular polarizations and coupled in a single-mode fiber (SMF2) for a future Bell-state measurement. Bob has the same apparatus and simultaneously does the same as Alice. Photon 2 and 3 overlap at BSM through which the entanglement between the two atomic ensembles I and II is generated. After a time interval δt_s , the spin excitations in the two atomic ensembles are retrieved back to single photons and the entanglement can be verified through polarization analysis of photons 1 and 4. | 100 |
| 12.2 | Correlation functions of a CHSH-type Bell's inequality with the storage time $\delta t_s = 500\ \text{ns}$. Error bars represent statistical errors, which are ± 1 standard deviation. | 102 |
| 12.3 | Visibility as a function of the storage time. Black dots are for the visibility and the dashed line shows the threshold for the violation of the CHSH-type Bell's inequality. Error bars represent statistical errors, which are ± 1 standard deviation. | 103 |
| 12.4 | Experimental outcomes of the fractions at different polarization settings. The polarization bases are chosen as (a) $ +\rangle$ and $ -\rangle$, (b) $ H\rangle$ and $ V\rangle$, and (c) $ \odot\rangle$ and $ \oslash\rangle$ respectively. | 104 |

List of Tables

| | | |
|------|---|----|
| 5.1 | Fidelities of quantum teleportation of a two-qubit composite system. | 41 |
| 6.1 | Experimental values of all the observable on the state $ C_4\rangle$ for the entanglement witness \mathcal{W} measurement. Each experimental value corresponds to measure in an average time of 1 sec and considers the Poissonian counting statistics of the raw detection events for the experimental errors. | 47 |
| 9.1 | Correlation functions E and the resulting S | 79 |
| 10.1 | Fidelities of teleporting a photonic qubit at a storage time of $0.5 \mu s$. Data for teleporting each state are collected two hours. The error bars represent the statistical error, i.e. ± 1 standard deviation. | 86 |

Chapter 1

Introduction

Quantum information, a combination of quantum mechanics, information theory and computer science, has provided and will continue to provide profound new insights into fundamental problems relating to both computation and physical science. Because quantum information has latent application value and great science value, it is both the new rapidly developing subject and noticed by lots of governments and scientists from 1980's. It is expected that the flourishing of this new field in the new century may guide the way to revolutionary advances in technology and in our understanding of the physical universe.

1.1 Basic concepts of quantum information

Quantum information processing (QIP) can mainly be divided into two major subfield: quantum communication and quantum computation [1, 2]. Unlike the unproven complexity computational assumptions in classical communication, the security of quantum communication is based on fundamental principles of quantum mechanics [3]. Meanwhile, by taking advantage of microcosmic quantum phenomena such as superposition, entanglement [4, 5, 6] and teleportation [7], a quantum computer and quantum information could, in principle, outperform a classical computer in many difficult computational tasks [8].

While today's digital classical information is encoded in bits, a quantum information is encoded in quantum bits, or qubits [9]. A qubit is a quantum system that can exist in a coherent superposition of two distinguishable states, and can be entangled with other such systems. The two distinguishable states might be, for example, internal electronic states of an individual atom, polarization states of a single photon, spin states of an atomic nucleus, or charges in superconductors. Entanglement [4, 5, 6] is a subtle quantum kind of correlation having no classical analog, and can be roughly described by saying that two systems are entangled when their joint state is more definite and less random than the state of either system by itself. Two obvious properties of classical information are that it can be read and copied without being disturbed, and that the state of a composite system can be fully specified by specifying the state of each of its parts. But information carried by a quantum system flouts such common-sense principles by quantum non-cloning theorem [10]. This allows the absolutely secure transfer of classical messages by means of quantum cryptography or faithful quantum teleportation of unknown quantum states [11, 3]. Unlike the former applications of quantum mechanics, what is used in quantum information is quantum state itself. The basic tasks include generation, manipulation, transfer, and storage of quantum states.

1.2 Quantum communication and quantum cryptography

With ongoing technological improvements, QIP of moderate complexity should soon be feasible in a variety of physical implementations. It is reasonable to hope that one such implementation will eventually enable a full-scale quantum computer [8], but not any time soon. The technology of quantum cryptography such as quantum key distribution (QKD) [12, 11] or dense coding [13] is now pretty mature and much close to commercial realization.

Cryptography is the art of rendering a message unintelligible to any unauthorized party. For a crypto-system to be secure, it should be impossible to unlock the cryptogram without the key. However, classically in practice, this requirement is often weakened so that the system is just extremely difficult to crack, based on unproven assumptions. For instance, the most widely used system in internet and financial business is the asymmetrical crypto-system, which was developed by Ronald Rivest, Adi Shamir, and Leonard Adleman [14], known as RSA. The security of the RSA system is based on computational complexity of the factorization of large integers. In spite of its elegance, this technique suffers from a major flaw. It has not been possible yet to prove whether factoring is “difficult” or not. This implies that the existence of a fast algorithm for factorization cannot be ruled out. In particular, in 1994 Peter Shor discovered a polynomial algorithm allowing fast factorization of integers with a quantum computer [15].

In a society where information and secure communication are of the utmost importance, one cannot tolerate such a threat. Fortunately, quantum communication offers an absolutely secure way for transfer of classical messages by means of quantum cryptography [12, 11, 3]. Quantum cryptography is based on the “one-time pad” crypto-system proposed by Vernam [16]. Once the quantum channel is generated, the secure key can be generated real-time between distant locations. This is so-called QKD. Because of the basic properties of quantum mechanics, the no-cloning theorem [10], no eavesdropper can track any information without being detected; thus, particularly the absolute security is ensured.

Besides the absolutely secure cryptosystems (systems that combine communications and cryptography), quantum physics also allows a sort of “teleportation”. Teleportation is such a condition, one object for example a person, he disappears in one place and appears in another place without moving it. In classical physics, the teleportation machines of science fiction present no problem of principle. One simply measures the state of every atom of the object to be teleported, transmits that information, and any number of copies of the object can be reconstructed by any receiver. But quantum physics fundamentally limits the accuracy of any such process because one cannot experimentally determine an unknown state. In a seminal paper, Bennett, Brassard, Crépeau, Jozsa, Peres and Wootters showed how an unknown quantum state can be “teleported” from one place to another [7]. Namely, by using entanglement, one can transfer the quantum state without getting any information about the state in the course of this transformation. Later, it is found that quantum teleportation is central to quantum communication [17] and plays an important role in a number of quantum computation protocols [18, 19, 20].

1.3 Quantum computation

The art of computing is as old as human history itself. Elegant tools were developed to do complicated computations. The earliest known tool for computation was the abacus, which was invented around 2400 BC. Modern computer science, born in the middle of last century as the combination of mechanical inventions and mathematical theories, has been involved in nearly every field of both natural science and social science, and has now contributed a lot to human civilization.

Indeed, quantum computer can be exploited to perform tasks that would be impossible or very difficult in a classical world.

For example:

- Today’s digital super computers would take billions of years to find the prime factors of a number that is a few hundred digits long, whereas large-scale quantum computers, if they can eventually be built, can perform that task in just seconds [15, 21].
- A classical computer requires a time proportional to N to search for a particular item in a list of N items, whereas a quantum computer can perform the search in a time proportional to the square root of N [22].
- If quantum information rather than classical information is exchanged between processors, then the amount of communication required to perform certain distributed computing tasks can be drastically reduced.
- A quantum computer can efficiently and accurately simulate the evolution of quantum many-body systems and quantum field theories that cannot be simulated on classical computers without making unjustified approximations.
- If quantum information is exchanged, cryptographic protocols can be devised in which privacy is ensured by principles of fundamental physics. In contrast, the security of public-key cryptosystems that are currently in widespread use rests on the assumption that decrypting a message requires a time-consuming computation (such as prime factorization), an assumption that could prove unwarranted if large-scale quantum computers become available.

A new and probably more practical approach is the concept of a “one-way quantum computer” [23]; for its linear optical implementation. Unlike the standard quantum computation based on sequences of unitary quantum logic gates which process qubits, the one-way quantum computer proposed by Raussendorf and Briegel [23] is entirely different. This new model requires qubits to be initialized in a so-called “cluster state” [24]. The computation algorithm is then performed by applying a sequence of one-qubit measurements (whose order and choices determine the algorithm computed) with classical feedforward of their outcomes. The outcomes will directly show the computation result. Remarkably in 2004, by combining cluster-state quantum computation (the one way computer) and KLM, Nielsen proposed that, without using the elaborate teleportation and Z-measurement error correction required in the original KLM scheme, any nontrivial linear optical gate that succeeds with finite probability is sufficient to obtain efficient quantum computation [25].

Of the theoretical discoveries concerning quantum information, one of the most important and unexpected is that noisy quantum devices (if not too noisy) can reliably store and process suitably encoded quantum states. Ordinarily, complex quantum states like those that arise during intermediate stages of a quantum computation are extraordinarily fragile. But if a logical qubit is encoded, not as a single physical qubit, but instead in the form of entanglement among several physical qubits, it becomes far more robust. The new quantum error-correcting codes [26, 27, 28, 29] and fault-tolerant methods [18] will be an essential part of any future effort to create, maintain, and manipulate intricate many-qubit quantum states.

1.4 Linear optical quantum information processing

Recent years, there were scientific breakthroughs of QIP in both experimental and theoretical sides: by exploiting entanglement one can efficiently encode classical messages (quantum dense coding) [13, 30], transfer quantum information to a remote location (quantum teleportation) [7, 31, 32], entangle two remote particles that have no common past (entanglement swapping) [33, 34], purify less entangled states of a larger ensemble into more entangled states of a smaller ensemble [35, 36, 37, 38], demonstration of multi-particle entanglement [39, 40, 41, 42, 43, 44, 45, 46] particle entanglement, experimental violation between quantum mechanics and local realism [47, 48, 49, 50], based on the preparation of highly entangled multi-qubit states simple adaptive one-qubit

measurements one can exploit the so-called “one-way quantum computer” [23, 24, 25, 51] and etc. All these theoretical and experimental results demonstrate that quantum information has become the brand-new application of quantum mechanics.

After spontaneous parametric down conversion (SPDC) [52, 53] became most standard method to generate entangled photon pairs, significant progress in linear optical QIP has been essentially achieved [54], which allows new studies of the fundamentals of quantum theory. For instance, three- [39], four- [42], five- [43] and yet six- [45] photon entanglement were successively demonstrated, and further used to test quantum nonlocality in an “all-versus-nothing” way [49, 50, 55, 56]. Based on the manipulation of photon entanglement, quantum dense coding was first demonstrated in 1996 [30]; quantum teleportation was first demonstrated in 1997 [31] and later freely propagating teleported qubits [57], open destination teleportation [43] and teleportation of two-qubit composite state were realized; entanglement based QKD was simultaneously realized in three different groups [58, 59, 60], and third-man quantum cryptography and quantum secret sharing was also demonstrated [61]; implementations of nondestructive Controlled-NOT gates were reported [62, 63, 64] and etc.

While one of the ultimate dreams is long-distance or even global quantum communication, many efforts have been made in the past years to extend the maximum distances for the observation of entanglement or for the realization of quantum cryptography between distance locations. Using optical fibers as the quantum channel, entanglement has already been achieved between photons separated by 50 km of fiber [65], and QKD has been demonstrated over distances up to around 100 km [3, 66]. Progress has also been made toward entanglement distribution in free space, with the achieved distances of about 10 km [67]. However, in spite of all the developments, the linear optical QIP suffers from some fundamental limitations. To solve photon losses and the decrease in the quality of entanglement requires exponentially large physical resources. As a combination of the ideas of entanglement purification [35, 37], entanglement swapping [33, 34], and most importantly, quantum memory, the quantum repeater protocol [17, 68] enables to establish high-quality long-distance entanglement with resources increasing only polynomially with transmission distance. Thus, it enables long-distance quantum communication.

Early physical implementations of a quantum repeater were based on atoms trapped in high-finesse cavities [69], where strong coupling between atoms and photons is required. However, these techniques require a extremely complicated experimental setup. In a seminal paper [70], Duan *et al.* (DLCZ) proposed an implementation of the quantum repeater by using atomic ensembles and linear optics. In this protocol atomic ensembles are used as memory qubits to avoid the challenging request for strong coupling between atoms and photons. Besides, the DLCZ protocol has built-in entanglement purification and thus is photon-loss tolerant. In the efforts of realizing the atomic ensemble based quantum repeater protocol, significant experimental advances have been achieved recently. Non-classical correlated photon pairs were generated from a MOT and a hot vapor [71, 72]. Controllable single photons were generated from atomic ensembles with the help of event-ready detection and feedforward circuit [73, 74, 75]. Interference of photons emitted from different atomic ensembles are studied [76, 77, 78]. Entanglement between two atomic ensembles either in the same MOT or in two MOTs were generated by detecting single photons [79, 80] and used for memory-bulit-in quantum teleportation between photonic and atomic qubits [81]. Recently, segment of the DLCZ protocol was demonstrated [82].

Photons are ideal quantum information carriers for quantum communication, because they have very weak coupling to the environment and are the fastest. Although for quantum computation, since it requires nonlinear coupling, implementations with stationery system like atoms, ions or solid-state devices seem to be more feasible. Surprisingly, the discovery that some gates could be realized through teleportation [18] shows that photons also offer interesting possibilities for quantum communication, despite the difficulty in storing them. Later, Knill, Laflamme, and Milburn (KLM) [19] showed that, with the help of quantum memory, even with linear optical elements, in principle, universal quantum computation could be realized. This is quite a breakthrough in the field of quantum computing theory. Following these suggestions, various linear optical quantum

computation protocols have been proposed to reduce the complexity of the KLM scheme while improving its theoretical efficiency [83, 25, 84]. Thus, linear optics with photon counting shows the prominent potential as a candidate for practical quantum computing [85].

1.5 Objective of this work

In this thesis we cover both the manipulation of multi-photon entanglement and atomic ensemble based quantum memory. After a brief introduction to the QIP and to the recent progress in linear optical QIP, the work consists of two parts each of which presents a dedicated topic in complete and self-contained form:

- Part I focuses on manipulation of photons: the photon-photon entanglement and its applications in linear optical QIP.
 - In Chapter 2, we theoretically describe how to generate polarization entanglement photons by spontaneous parametric down conversion and briefly introduce how to further generate multi-photon entanglement.
 - In Chapter 3, a bit-flip error rejection code for error-free transfer of quantum information through a noisy quantum channel is experimentally demonstrated. We report a full realization of encoding and decoding process.
 - In Chapter 4, we report an observation of a violation of the Clauser-Horne-Shimony-Holt-Bell inequality beyond Tsirelson's bound by 7 standard deviations. In addition, using part of our results, we obtain a violation of the Mermin inequality by 39 standard deviation.
 - In Chapter 5, we develop and exploit a six-photon interferometer to teleport an arbitrary polarization state of a two-photon composite system.
 - In Chapter 6, a two-photon four-qubit cluster state source is developed and used to implement a highly efficient Grover's search algorithm and high-fidelity two-qubit quantum gates.
- In part II we present theoretical and experimental investigations on atomic ensemble based quantum memory.
 - In Chapter 7, we analyze in detail the seminal quantum memory scheme based on atomic ensembles proposed by Duan-Lukin-Cirac-Zoller (DLCZ) and show that the severe requirement of the phase stability problem in the original protocol makes a long-distance quantum communication impossible. Then we propose a robust quantum repeater architecture building on the DLCZ protocol, which is insensitive to phase stability.
 - In Chapter 8, we first show the atomic ensemble can be used as a storage of single photons and further report a deterministic single photon source.
 - In Chapter 9, we create two independent, synchronized single-photon sources and experimentally investigate the interference between the photons emitted from respective source. Based on quantum memory, polarization entangled photon pair are efficiently generated.
 - In Chapter 10, quantum teleportation between photonic (flying) and atomic (stationary) qubits is reported. An unknown single-photon state is teleported to an atomic qubit, stored for up to 8 microseconds and successfully read out.
 - In Chapter 11, we develop a novel way to efficiently create a stable atom-photon entanglement with inherent built-in quantum memory. The entanglement exists for more than 20 microseconds by violation of CHSH-Bell inequality.

- In Chapter 12, we generate two independent atom-photon entanglement sources, and further entangle the two atomic ensembles in distant location via entanglement swapping.

We conclude this thesis by summarizing its main results and providing an outlook to future work in Chapter 13.

Part I

Manipulation of Photons: Multi-photon Entanglement

Chapter 2

Multi-photon entanglement

Quantum Entanglement, a simple name for superposition in a multiparticle system, is essence of the quantum world. It was first noticed by Schrödinger [5] and since then it has baffled generations of physicists. It is at the heart of the discussions of the Einstein-Podolsky-Rosen (EPR) paradox [4], of Bell's inequality [86], and of the non-locality of quantum mechanics. In recent years, entanglement has become a new focus of activities in quantum physics because of immense theoretical and experimental progress both in the foundation of quantum mechanics and in the new field of quantum information processing.

To generate entangled states of a composite system, there exist various possibilities. First, the subsystems of the composite system could be entangled by controllable interaction, which may implement, e.g., controlled-NOT (CNOT) gate. Second, in some nonlinear decay processes, a parent particle might be splitted into two daughter particles. Then certain conservation laws (e.g., momentum, energy and angular momentum conservations) may enforce that the daughter particles are entangled. Third, the utility of quantum eraser technique [87] will be encountered in the case of polarization entanglement creation. A further possibility is the entanglement creation via projective measurements, as illustrated by entanglement swapping [33] and multi-photon entanglement creation.

Entangled photon sources play a central role in the experimental study of quantum mechanical foundations and are resources for quantum information processing. The early entangled photon source was pairs emitted from an atomic cascade [47, 88, 48]. However, such a source has some drawbacks such as very low collection efficiency for the entangled photons. Fortunately, the process of SPDC [52, 53] provides mechanisms by which pairs of entangled photons can be produced with reasonable intensity and in good purity. Today, the well developed SPDC entangled photon sources, with increasing quality, brightness and numbers of entangled photons, can be routinely realized, which enabled a significant fraction of key progresses in the emerging field of quantum information processing.

In the SPDC process, one uses a non-centrosymmetric crystal with nonlinear electric susceptibility. In such a medium, an incoming higher-energy pump photon can decay with relatively small probability into two lower-energy daughter photons in a way that energy and momentum inside the crystal are conserved. The photon pair is explicitly correlated in energy and momentum or equivalently in space and time. In this chapter, we will give a brief review of SPDC entangled photon source and give a most common method of post-selected generation of multi-photon entanglement, by which we can conveniently observe multi-particle GHZ correlations.

2.1 Polarization-entangled photon pairs

So far, the most widely used photon entanglement source is polarization-entangled photon pairs using the process of non-collinear type-II SPDC process [53]. In the experiment, the desired polarization-entangled state is produced directly out of a single nonlinear beta-barium-borate (BBO) crystal. In that process, the two photons are emitted with different polarization (Fig. 2.1). Photons of each polarization are emitted into one cone in such a way that momenta of two photons always add up to the momentum of the pump photon. Thus, the emission direction of each individual photon is completely uncertain within the cone, but once one photon is registered, and thus its emission direction is defined, the other photon is found just exactly opposite from the pump beam on the other cone. The total quantum mechanical state is therefore extremely rich and is a superposition of all such pairs of emission modes.

The interesting point is now that the crystal can be cut and arranged such that the two cones intersect, as shown in Fig. 2.1. Then, along the lines of intersection, the polarization of neither photon is defined, but what is defined is the fact that the two photons have to have different polarization. This contains all the necessary features of entanglement in a nutshell. Measurement on each of the photons separately is totally random and gives with equal probability vertical or horizontal polarization. But once one photon, for example photon A, is measured, the polarization of another photon B is orthogonal. Choosing an appropriate basis e.g., $|H\rangle$ and $|V\rangle$, where H (V) denotes horizontal (vertical) linear polarization, the state emerging through the two beams A and B is thus a superposition of $|H\rangle|V\rangle$ and $|V\rangle|H\rangle$, i.e.

$$\frac{1}{\sqrt{2}} (|H\rangle_A|V\rangle_B + e^{i\alpha}|V\rangle_A|H\rangle_B), \quad (2.1)$$

where the relative phase α arises from the crystal birefringence, and an overall phase shift is omitted.

Using an additional birefringent phase shifter (or even slightly rotating the down-conversion crystal itself), the value of α can be set as desired, e.g., to the values 0 or π . Somewhat surprisingly, a net phase shift of π may be obtained by a 90° rotation of a quarter wave plate (QWP) in one of the paths. Similarly, a half wave plate (HWP) in one path can be used to change horizontal polarization to vertical and vice versa. One can thus very easily produce any of the four maximally polarization-entangled states (so-called Bell states)

$$\begin{aligned} |\Phi^\pm\rangle &= (|H\rangle|H\rangle \pm |V\rangle|V\rangle)/\sqrt{2} \\ |\Psi^\pm\rangle &= (|H\rangle|V\rangle \pm |V\rangle|H\rangle)/\sqrt{2}. \end{aligned} \quad (2.2)$$

The birefringent nature of the down-conversion crystal complicates the actual entangled state produced, since the ordinary and extraordinary photons have different velocities inside the crystal, and propagate along different directions even though they become collinear outside the crystal (an effect well known from calcite prisms, for example). The resulting longitudinal and transverse walk-offs between the two terms in the state (2.1) are maximal for pairs created near the entrance face, which consequently acquire a relative time delay $\delta T = L(1/u_o - 1/u_e)$ (L is the crystal length, and u_o and u_e are the ordinary and extraordinary group velocities, respectively) and a relative lateral displacement $d = L \tan \rho$ (ρ is the angle between the ordinary and extraordinary beams inside the crystal). If $\delta T \geq \tau_c$, the coherence time of the down-conversion light, then the terms in Eq. (2.1) become, in principle, distinguishable by the order in which the detectors would fire, and no interference will be observed. Similarly, if d is larger than the coherence width, the terms can become partially labeled by their spatial location.

Because the photons are produced coherently along the entire length of the crystal, one can *completely* compensate for the longitudinal walk-off [89]—after compensation, interference occurs pairwise between processes where the photon pair is created at distances $\pm x$ from the middle of the crystal. The ideal compensation is therefore to use two crystals, one in each path, which are

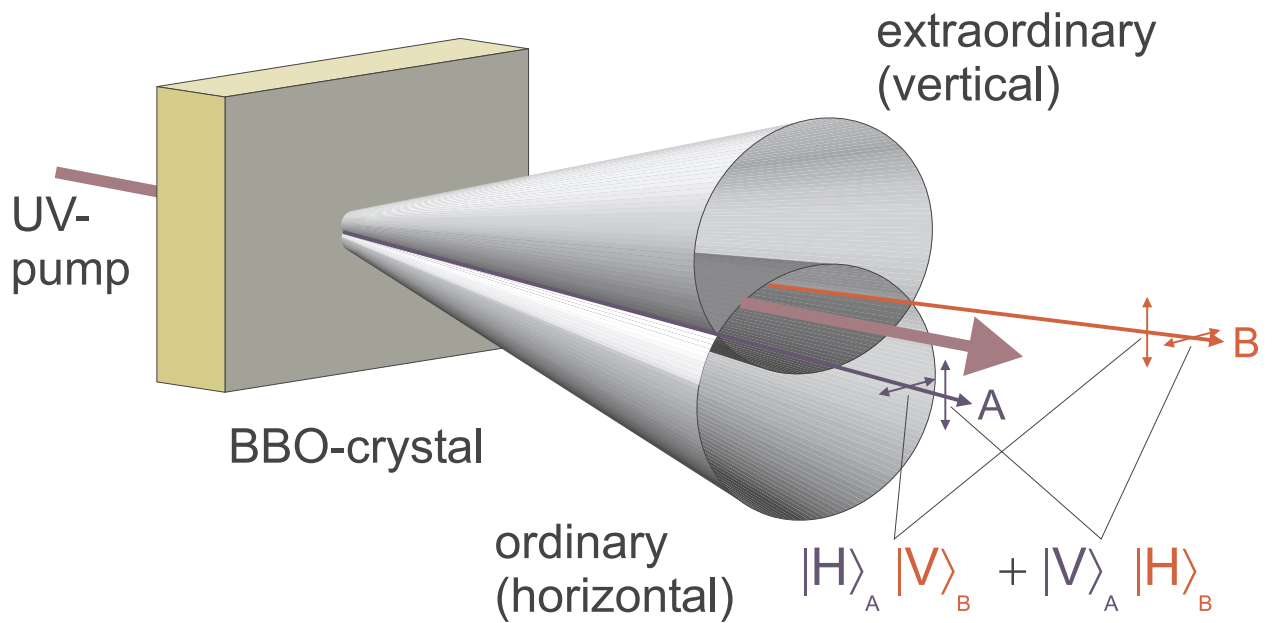


Figure 2.1: Principle of type-II spontaneous parametric down-conversion. Inside a nonlinear BBO crystal, an incoming pump photon can decay spontaneously into two photons. Two down-converted photons arise polarized orthogonally to each other. Each photon is emitted into a cone, and the photon on the top cone is vertically polarized while its exactly opposite partner in the bottom cone is horizontally polarized. Along the directions where the two cones intersect, their polarization are undefined; all that is known is that they have to be different, which results in polarization entanglement between the two photons in beams A and B.

identical to the down-conversion crystal, but only half as long. If the polarization of the light is first rotated by 90° (e.g., with a half wave plate), the retardations of the o and e components are exchanged and complete temporal indistinguishability is restored ($\delta T = 0$). The same method provides optimal compensation for the transverse walk-off effect as well. Here, the compensation crystals were oriented along the same direction as that of the down-conversion crystal.

In this part, except the experiment described in Chapter 6, where the entangled photon source is produced by type-I SPDC, all the other experiments are based on type-II SPDC process.

Moreover, we would like to define that, in this thesis, the polarization of the photon will be analyzed in one of three different basis:

- The X basis, which is defined as the linear polarization basis H/V rotated by 45° , which is denoted as $+/-$;
- The Y basis, which is defined as the circular polarization basis R/L (right-hand/left-hand);
- The Z basis, which is the linear polarization basis H/V .

These polarization bases of X and Y can be expressed in terms of the H/V basis as

$$\begin{aligned} |+\rangle &= \frac{1}{\sqrt{2}} (|H\rangle + |V\rangle), & |-\rangle &= \frac{1}{\sqrt{2}} (|H\rangle - |V\rangle), \\ |R\rangle &= \frac{1}{\sqrt{2}} (|H\rangle + i|V\rangle), & |L\rangle &= \frac{1}{\sqrt{2}} (|H\rangle - i|V\rangle). \end{aligned} \quad (2.3)$$

2.2 Multi-photon entanglement

While Bell's proof of the impossibility of EPR's "elements of reality" [4] was based on statistical predictions and inequalities [86], Greenberger-Horne-Zeilinger (GHZ) showed that a simpler proof can be achieved with perfect correlations and without inequalities [90]. This is in contrast to the case of the Bell experiments with two entangled particles testing Bell's inequalities, where the conflict only arises for the statistical predictions of quantum theory [86, 91]. Further, quantum mechanics can violate the multi-particle Bell-type inequalities imposed by local realism by an amount that grows exponentially with the number of entangled particles [92, 93], that is, for entangled systems of more particles, the conflict between quantum mechanics and local realism becomes even stronger. Besides fundamental interest, entanglement between several particles is also the most important feature of many quantum communication and computation protocols [1], e.g. quantum secret sharing [94] and third-man quantum cryptography [95], as realized using four-photon entanglement [61]. Although the extension from two to a few entangled particles might seem to be only a modest step forward, the implications are rather profound.

As an example of generating multi-photon entanglement, we consider the experiment setup (shown in Fig. 2.2b) for the four-photon entanglement. There exist two entangled photon pair sources (EPR), A and B. Each of them produces a photon pair, denoted as photon 1 and 2, and photon 3 and 4 respectively. For simplicity, let the photon pairs from both sources be in the same entangled state $\frac{1}{\sqrt{2}}(|H\rangle|H\rangle + |V\rangle|V\rangle)$. Then, after passing through the polarizing beam splitter (PBS) the state of the four photon will be in the superposition

$$\frac{1}{2} (|H_1\rangle|H_2\rangle|H_3\rangle|H_4\rangle + |V_1\rangle|V_2\rangle|V_3\rangle|V_4\rangle + |H_1\rangle|H_3\rangle|V_3\rangle|V_4\rangle + |V_1\rangle|V_2\rangle|H_2\rangle|H_4\rangle). \quad (2.4)$$

It is clear that, only for the first two parts $|H_1\rangle|H_2\rangle|H_3\rangle|H_4\rangle$ and $|V_1\rangle|V_2\rangle|V_3\rangle|V_4\rangle$, one observe four-fold coincidence. Therefore as long as we observe four-fold coincidence, we know these four particles are in the superposition

$$|H_1\rangle|H_2\rangle|H_3\rangle|H_4\rangle + |V_1\rangle|V_2\rangle|V_3\rangle|V_4\rangle.$$

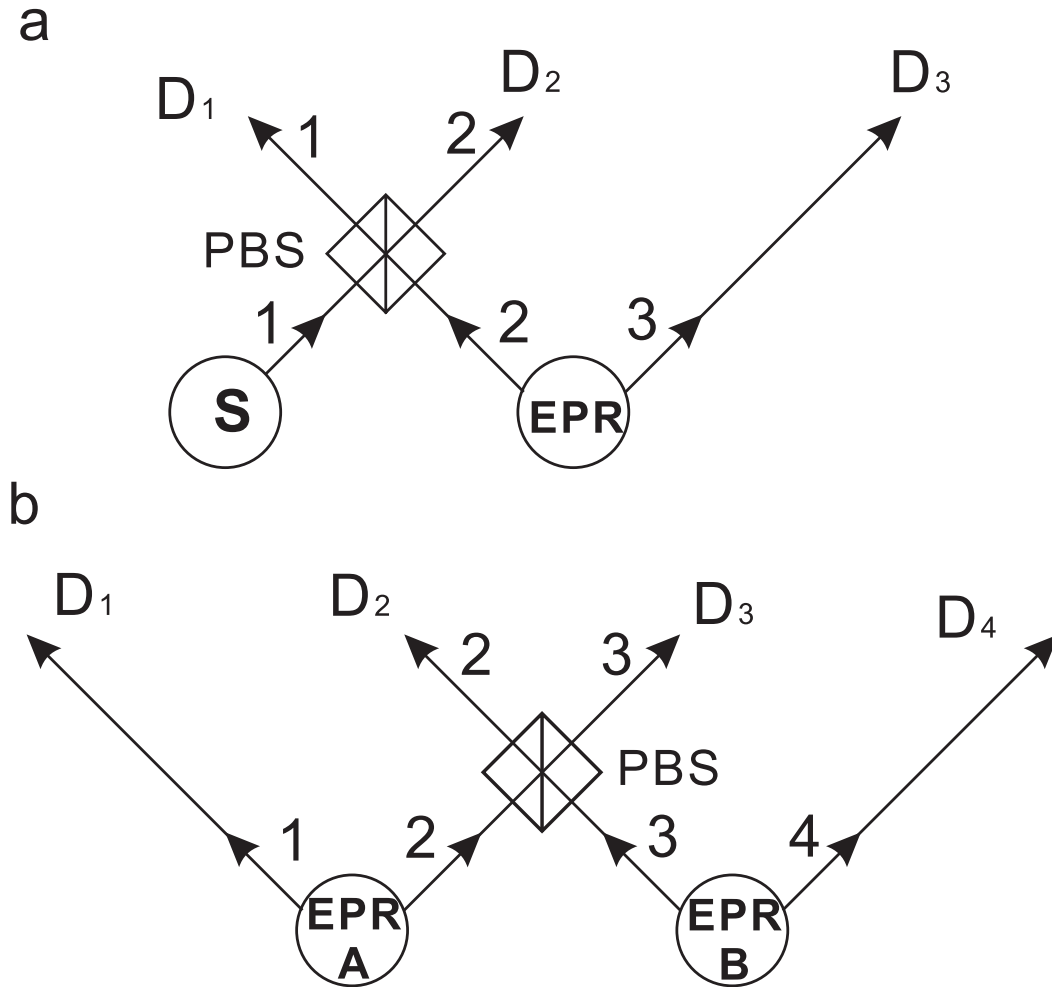


Figure 2.2: Diagram showing the principle of generating three photon (a) and four photon (b) entanglement. The single photon source (S) emits a photon in a polarization state $H + V$, and the entangled photon sources (EPR), each one emits a photon pair in the entangled state $HH + VV$.

Note that the GHZ state is not directly prepared, but we know that the four particles are in a GHZ state under the condition that one particle each is detected in each of the outgoing beams 1, 2, 3 and 4. This is a much weaker condition than any post-selection procedure which might be based on properties of the particles. In an experiment our case will not be distinguishable from the real situation occurring anyway because of finite detector efficiency. That is, from a practical point of view, even if one definitely prepares a full GHZ state one only will observe four-fold coincidence in a fraction of time anyway. Thus, we conclude that using our conditional GHZ-state one will be able to experimentally demonstrate all features of a four-particle GHZ state

$$\frac{1}{\sqrt{2}} (|H_1\rangle|H_2\rangle|H_3\rangle|H_4\rangle + |V_1\rangle|V_2\rangle|V_3\rangle|V_4\rangle). \quad (2.5)$$

In the same way, our scheme can also generate unconditional three-photon GHZ states as shown in Fig. 2.2. Consider one single photon and one entangled photon pair source, the single photon in the state $\frac{1}{\sqrt{2}}(|H\rangle + |V\rangle)$ is guided to a PBS where it is overlapped with one of the photon from the emitted EPR pair in the state $\frac{1}{\sqrt{2}}(|H\rangle|H\rangle + |V\rangle|V\rangle)$. Then, the state of the three photons

immediately after passage through the PBS will be at the superposition

$$\frac{1}{2}(|H_1\rangle|H_2\rangle|H_3\rangle + |V_1\rangle|V_2\rangle|V_3\rangle + |H_2\rangle|V_2\rangle|V_3\rangle + |V_1\rangle|H_1\rangle|H_3\rangle). \quad (2.6)$$

Again by observing three-fold coincidence, we know these three photon are in the three photon GHZ state $|H_1\rangle|H_2\rangle|H_3\rangle + |V_1\rangle|V_2\rangle|V_3\rangle$.

However, since the absence of single photon source, normally we use a weak coherent pulse as the single photon source required in Fig. 2.2. The problem is the double emission from weak coherent pulse will greatly reduce the visibility of generated three photon GHZ state (for more details, see the analyzation in § ??). Thereby, normally we use another way to generate unconditional three-particle GHZ states via so-called entangled entanglement [96]. For example, one could analyze the polarization state of photon 2 in X basis, that is $+/-$ basis as shown in Eq. (2.3). Then the polarization state of the remaining three photons 1, 3 and 4 will be projected into

$$\frac{1}{\sqrt{2}}(|H_1\rangle|H_3\rangle|H_4\rangle + |V_1\rangle|V_3\rangle|V_4\rangle)$$

if and only if detector D_2 detects a single photon in state $|+\rangle$. Correspondingly, the state of photons 1, 3 and 4 will be projected into

$$\frac{1}{\sqrt{2}}(|H_1\rangle|H_3\rangle|H_4\rangle - |V_1\rangle|V_3\rangle|V_4\rangle)$$

if and only if detector D_2 detects a single photon in state $|-\rangle$. In the scheme, the detection of photon 2 actually plays the double role of both getting rid of the last two terms in Eq. (2.4) and projecting the remaining three photons into a spatially separated and freely propagating GHZ state. Such a GHZ-state could be extremely useful both in further test of local realism versus quantum mechanics and in future applications of secret sharing and third-man cryptography.

In the same way, with more photon pairs or single photons and PBSs, one can post-selectly generate more particle entanglement, not only GHZ state but also other kind of multi-particle entanglement e.g. cluster state [45] as well.

Chapter 3

Quantum error rejection

3.1 Introduction

A crucial step in the full realization of long-distance quantum communication is to overcome the problems caused by decoherence and exponential photon loss in the noisy quantum channel [3]. As a general solution, two distant parties could first share highly entangled photon pairs, the transmission of quantum states for various applications in quantum communication can then be achieved by using ancilla entanglement. As the quantum repeater [17], combining entanglement purification [35, 36] and entanglement swapping [33], provides an efficient way to generate highly entangled states between distant locations, many experimental efforts have been made to achieve entanglement swapping, entanglement purification and quantum memory [34, 38, 80, 97], and even the demonstration of a prototype of quantum relay [98, 99]. However, one still has a long way to go before the above techniques can be realistically applied to long-distance quantum communication.

Meanwhile, in the context of quantum error correction (QEC) the way to protect a fragile unknown quantum state is to encode the state into a multi-particle entangled state [26, 27, 28, 29]. Then, the subsequent measurements, i.e. the so-called decoding processes, can find out and correct the error during the quantum operations. This is very different from the classical error correction since the unknown qubit in principle can not be copied [10] or observed exactly. Therefore the simple repetition code used in classical coding is not applicable here. Although the QEC codes are primarily designed for large scale quantum computing, the similar idea is also inspired to implement error-free transfer of quantum information through a noisy quantum channel, i.e. an unknown qubit can be sent to a remote party robustly through a noisy channel if we use the QEC code by encoding and decoding process.

Several QEC protocols have been experimentally demonstrated in the NMR [100, 101] and ion-trap [102] systems. However, the NMR [100, 101] demonstration is not a strict demonstration since no quantum entanglement is involved. And the demonstration in ion-trap [102] is difficult to extend to large distance in the application of quantum communication. So far there's no such implementation using photons. The reason is that all theoretical schemes are based on controlled-NOT operations between single particles. For photons, this operation would require either a strong nonlinear interaction between individual photons, which is extremely difficult to achieve, or ancilla photons [63, 64], which needs too many resources. In 2001, a scheme of the optical realization of quantum error-rejection code over the bit-flip-error channel is considered [103]. It was shown that the controlled-NOT operation in quantum error correction can be done probabilistically by a polarizing beam splitter and one can transfer a qubit robustly over a bit flip channel by the teleportation.

In this chapter, we will report an experimental demonstration of an improved bit-flip error rejection protocol for error-free transfer of quantum information through a noisy quantum channel.

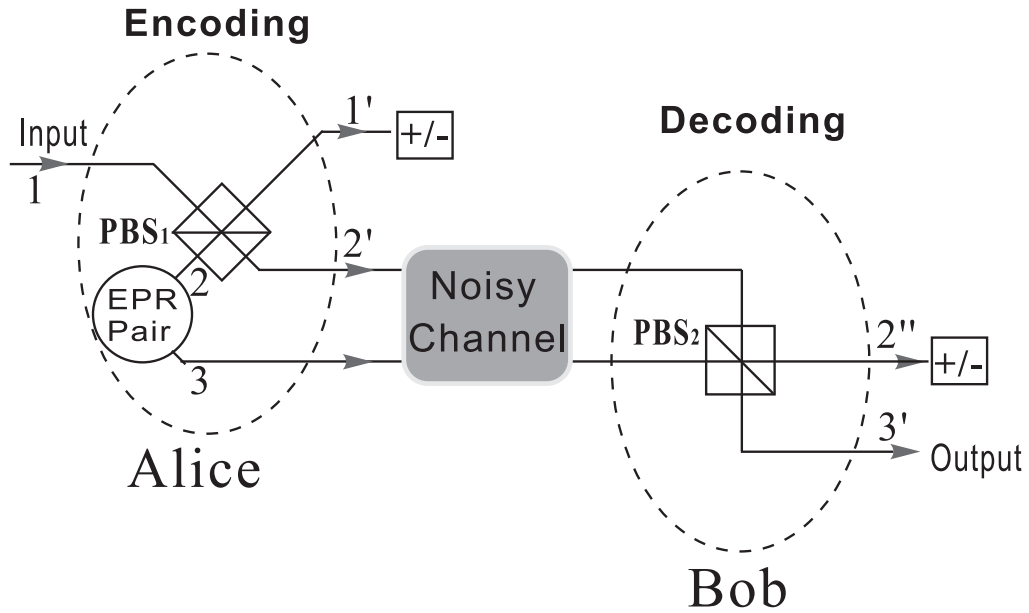


Figure 3.1: Scheme for one bit-flip quantum error-rejection.

In the experiment, an unknown state to be transmitted is encoded into a two-photon entangled state, which is then sent through an engineered noisy quantum channel. At the final stage, the unknown state is decoded by a parity measurement, successfully rejecting the erroneous transmission over the noisy quantum channel.

3.2 Two-bit bit-flip error-rejection code

The main idea in the original scheme is to encode an unknown quantum state of single particle into a two-particle entangled state [103]. After the encoded state is transmitted over the noisy quantum channel, a parity check measurement [104] is sufficient to reject the transmission with bit-flip error instead of correcting the errors to simplify the experimental realization. Such a scheme has the advantage of avoiding the difficult photon-photon controlled-NOT gates necessary for the usual QEC. Moreover, the proposed error rejection scheme promises additional benefit of high efficiency, compared with the QEC based on linear optics quantum logic operations [19], since the crucial feed-forward operations in linear optics QEC will lead to very low efficiency. Although the original scheme is within the reach of the current technology as developed in the recent five-photon experiments [43, 63], it is not optimal in its use of ancilla entangled state because the encoding process is implemented via a Bell-state measurement.

Remarkably, it is found recently [105] that one pair of ancilla entangled states is sufficient to implement the two-photon coding through two quantum parity measurements. Thus, an elegant modification of the previous experiment on four-photon entanglement [42] would allow a full experimental realization of the error rejection code.

3.2.1 Encoding

Suppose that Alice wants to send Bob a single photon in an unknown polarization state

$$|\psi\rangle = \text{Cos}(\theta/2) |H\rangle_1 + e^{i\phi} \text{Sin}(\theta/2) |V\rangle_1, \quad (3.1)$$

to Bob through a noisy quantum channel. As shown in Fig. 3.1, instead of directly sending it to Bob, Alice can encode her unknown state onto a two-photon entangled state with an ancilla pair of entangled photons:

$$|\phi^+\rangle_{23} = \frac{1}{\sqrt{2}}(|HH\rangle_{23} + |VV\rangle_{23}). \quad (3.2)$$

The photon in the unknown polarization state and one photon out of the ancilla entangled photon are superposed at a polarization beam splitting (PBS₁). Behind the PBS₁, with a probability of 50% we obtain the renormalized state corresponding to the three-fold coincidence among modes 1', 2' and 3

$$\begin{aligned} |\psi\rangle_{1'2'3} &= \text{Cos}(\theta/2)|HHH\rangle_{1'2'3} + e^{i\phi}\text{Sin}(\theta/2)|V V V\rangle_{1'2'3} \\ &= |+\rangle_{1'}(\text{Cos}(\theta/2)|HH\rangle_{2'3} + e^{i\phi}\text{Sin}(\theta/2)|VV\rangle_{2'3}) \\ &\quad + |-\rangle_{1'}(\text{Cos}(\theta/2)|HH\rangle_{2'3} - e^{i\phi}\text{Sin}(\theta/2)|VV\rangle_{2'3}). \end{aligned} \quad (3.3)$$

Eq. (3.3), implies that conditional on detecting photon 1' in the |+⟩ polarization state (with probability 50%), the remaining two photons are projected onto the following entangled state:

$$|\psi\rangle_{2'3} = \text{Cos}(\theta/2)|HH\rangle_{2'3} + e^{i\phi}\text{Sin}(\theta/2)|VV\rangle_{2'3}. \quad (3.4)$$

Thus, through a quantum parity measurement between modes 1' and 2', a two-photon encoding operation can be realized.

3.2.2 A bit flip noisy quantum noisy channel

If the qubit with the initial state (3.1) is directly sent through the channel with flipping probability p , the qubit state after passing through the bit flip noisy channel will be

$$\rho = (1-p)|\psi\rangle\langle\psi| + p|\psi_f\rangle\langle\psi_f| \quad (3.5)$$

here

$$\begin{aligned} |\psi_f\rangle &= \text{Cos}(\theta/2)|V\rangle + e^{i\phi}\text{Sin}(\theta/2)|H\rangle \\ &= \text{Sin}(\theta)\text{Cos}(\phi)|\psi\rangle + e^{i\phi}(-\text{Cos}(\theta)\text{Cos}(\phi) + i\text{Sin}(\phi))|\psi_\perp\rangle, \end{aligned} \quad (3.6)$$

Here, $|\psi_\perp\rangle = (e^{i\phi}\text{Sin}(\theta/2))|H\rangle - \text{Cos}(\theta/2)|V\rangle$ is orthogonal to $|\psi\rangle$ (state 3.1). Therefore, for all possible initial states on the Bloch sphere, the average quantum bit error rate (QBER) caused by the noisy channel is

$$E_0 = 1 - \frac{1}{4\pi} \int_0^\pi \int_0^{2\pi} \langle\psi|\rho|\psi\rangle \text{Sin}(\theta) d\theta d\phi = \frac{2}{3}p. \quad (3.7)$$

3.2.3 Parity check and decoding

After finishing the encoding process, Alice sends photons 2' and 3, which are the encoded state (3.4) to Bob through the bit flip noisy quantum channel and Bob will recombine the two photons at the PBS₂ in order to do the parity check to identify and reject the erroneous transmission. If there is no error in the quantum channel, Bob will obtain the same quantum state as in (3.4) after PBS₂. The state between photon 2'' and photon 3' can be rewritten as

$$\begin{aligned} |\psi\rangle_{2''3'} &= |+\rangle_{2''}(\text{Cos}(\theta/2)|H\rangle_{3'} + e^{i\phi}\text{Sin}(\theta/2)|V\rangle_{3'}) \\ &\quad + |-\rangle_{2''}(\text{Cos}(\theta/2)|H\rangle_{3'} - e^{i\phi}\text{Sin}(\theta/2)|V\rangle_{3'}). \end{aligned} \quad (3.8)$$

Thus, projecting photon 2'' into the |+⟩ state with a success probability of 50%, photon 3' will be left in the unknown state $\text{Cos}(\theta/2)|H\rangle + e^{i\phi}\text{Sin}(\theta/2)|V\rangle$. Through the decoding process, i.e. conditional on detecting in mode 2'' one and only one |+⟩-polarized photon, Bob can recover the state originally sent by Alice.

If a bit-flip error occurred for one of the two transmitted photons, the two photons will have different polarizations and exit the PBS_2 in the same output arm. Therefore, no coincidence will be observed between modes $2''$ and $3'$. That is to say, the bit-flip error during the transmission of quantum states over the noisy channel has been simply rejected by the final quantum parity measurement. However, if both bit-flip errors occurred simultaneously for the two transmitted photons, Bob would finally obtain the polarization state of (3.6) via the same quantum parity measurement for decoding operation and the error can not be effectively rejected.

Moreover, from Eq. (3.3) the detection of photon $1'$ in the $|-\rangle$ state also leads to encoding of the initial quantum state in a two photon state, provided the associated phase flip is taken into account. Obviously, as shown in Eq. (3.8) the same holds for the decoding at Bob's: projection onto the $|-\rangle$ state is associated with a phase flip that can be compensated for. The coding and decoding efficiency can thus be increased by a factor of two each.

3.2.4 Fault tolerance property

Specifically, suppose that Alice would send photons to Bob in state (3.4) through the noisy quantum channel with the bit flipping probability p , as analyzed in §3.2.3, with a probability $(1-p)^2$, that is no error occurring in both photons, the final state will be exactly the same as the initial state (3.1), $|\psi\rangle_{3'} = \text{Cos}(\theta/2)|H\rangle_{3'} + e^{i\phi}\text{Sin}(\theta/2)|V\rangle_{3'}$. And if the bit-flipping error occurring in both photons with a probability p^2 , Bob will obtain a wrong state (3.6). Given that in the case with one bit error occurring in one photon, the state will be rejected. The final state in Bob's hand can be described as:

$$\rho' = \frac{(1-p)^2|\psi\rangle\langle\psi| + p^2|\psi_f\rangle\langle\psi_f|}{(1-p)^2 + p^2}. \quad (3.9)$$

Therefore, the final average QBER is

$$\begin{aligned} E_1 &= 1 - \frac{1}{4\pi} \int_0^\pi \int_0^{2\pi} \langle\psi|\rho'|\psi\rangle \text{Sin}(\theta) d\theta d\phi \\ &= \frac{2p^2}{3((1-p)^2 + p^2)} \end{aligned} \quad (3.10)$$

Therefore, the QBER of E_1 will be lower, compared to the QBER of E_0 for any $p < 1/2$. For small p , E_1 is on the order of p^2 . The transmission fidelity can thus be greatly improved by using the quantum error rejection code.

Note that, conditional detection of photons in mode $1'$ implies that there is either zero or one photon in the mode $2'$. But, as any further practical application of such a coding involves a final verification step, detecting a threefold coincidence makes sure that there will be exactly one photon in each of the modes $2'$ and 3 . This feature allows us to perform various operations like, for example, the recombination of two photons at PBS_2 before the final detection. This makes our encoding scheme significantly different from a previous two-photon encoding experiment [106], where there are certain probabilities of containing two photons in one of two encoding modes. Thus, the previous two-photon encoding experiment cannot be applied to the error-rejection code.

Moreover, we would like to emphasize that, compared to the two recent experiments on fault-tolerant quantum information transmission [107, 108] our protocol has two essential advantages. On the one hand, the work in [107] can only encode and send a known state instead of encoding and sending arbitrary unknown states required by many quantum communication protocols. On the other hand, the experiment in [108] can only filtrate half of the single phase-shift error. Thus, if the error rate of the channel is p , after applying the error filtration method the remaining QBER is still larger than $p/2$ even in the ideal case. Note that, the error filtration probability in [108] can be increased by coding a qubit in a larger number of time-bins, however, this would need much more resources. In contrast, our method can in principle reject any one bit-flip error with certainty as analyzed before. In fact, the ability to suppress the first order error (p) to the second order (p^2) is essential to overcome the channel noise in scalable quantum communication.

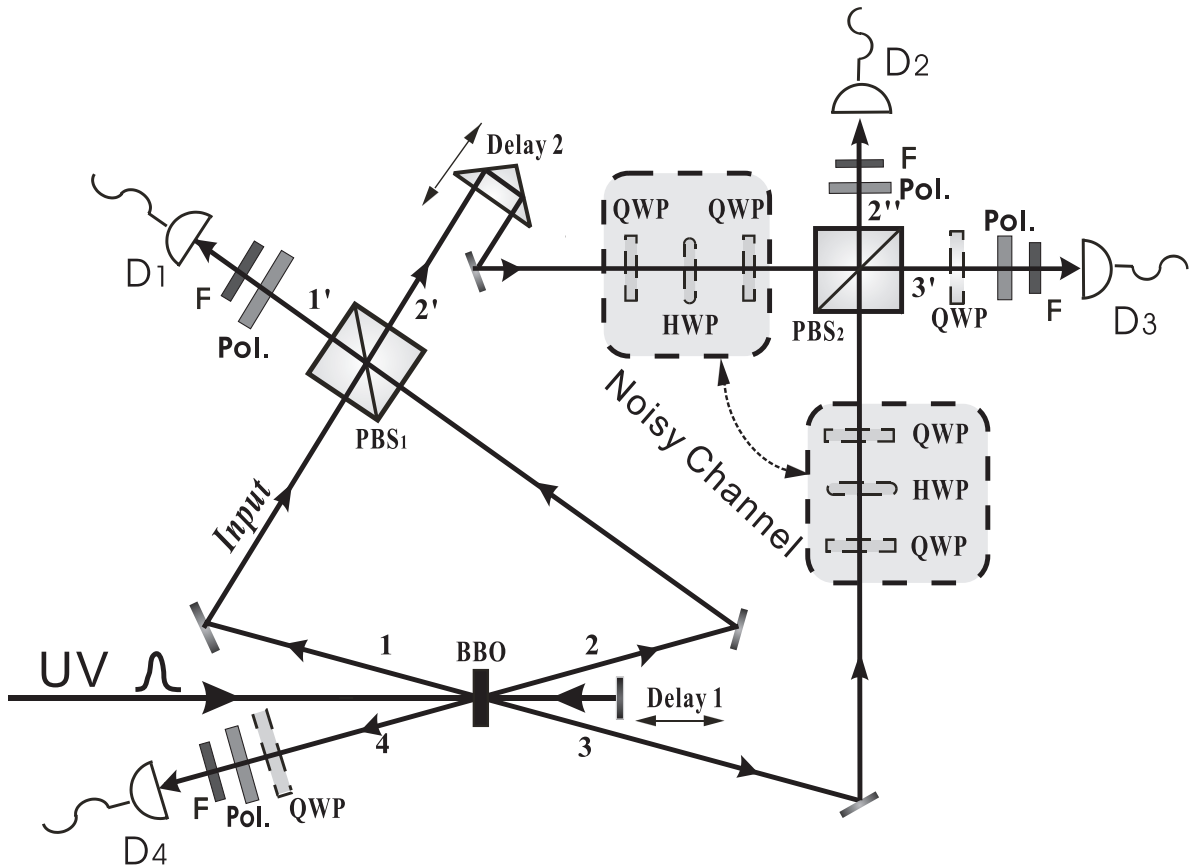


Figure 3.2: Experimental set-up for quantum error-rejection.

3.3 Experimental setup

A schematic drawing of the experimental realization of the error rejection is shown in Fig. 3.2. An ultraviolet pulse (with a duration of 200fs, a repetition rate of 76MHz and a central wavelength of 394nm) passes through a + crystal twice to generate two entangled photon pairs 1, 4 and 2, 3 in the state $|\phi^+\rangle$ [53]. The high quality of two-photon entanglement is confirmed by observing a visibility of $(94 \pm 1)\%$ in the $|+\rangle/|-\rangle$ basis. One QWP and one polarizer (Pol.) in front of detector D_4 are used to perform the polarization projection measurement such that the input photon in mode 1 is prepared in the unknown state.

The two photons in modes 1 and 2 are steered to the PBS_1 where the path length of photon 1 have been adjusted by moving the delay mirror Delay 1 such that they arrive simultaneously. Conditional on detecting photon $1'$ in the $|+\rangle$ polarization, the unknown polarization state was encoded into the modes in $2'$ and 3. The encoded two-photon state is transmitted through the engineered noisy quantum channel and then recombined at the PBS_2 . Furthermore, the path length of photon $2'$ has been adjusted by moving the Delay 2 such that photons in modes $2'$ and 3 arrive at the PBS_2 simultaneously. Through the whole experiment, spectral filtering (with a FWHM 3nm, F in Fig. 3.2) and fiber-coupled single-photon detectors have been used to ensure good spatial and temporal overlap between photons in modes 1 and 2, and photons in modes $2'$ and 3 [109].

To characterize the quality of the encoding and decoding process, we first measure the interference visibility at the PBS_1 . Since photon pairs 1-4 and 2-3 are in the state $|\phi^+\rangle$, it is easy to see that the four-fold coincidence in $1'$, $2'$, 3 and 4 corresponds to a four-photon GHZ state

$\frac{1}{\sqrt{2}}(|HHHH\rangle_{1'2'34} + |VVVV\rangle_{1'2'34})$ [42]. The four-photon entanglement visibility in the $|+\rangle / |-\rangle$ basis was observed to be $(83 \pm 3)\%$. Similarly, the four-photon entanglement visibility in modes $1', 2'', 3'$ and 4 is observed to be $(80 \pm 3)\%$, before introducing artificial channel noise. Note that, the visibility is obtained after compensating the birefringence effect of the PBSes [57].

3.3.1 Noisy quantum channels

In order to show the quantum error rejection code, it is necessary to have a bit-flip noisy quantum channel. In the experiment, the noisy quantum channels are simulated by one HWP sandwiched with two QWPs. Denote the operations of the QWP and HWP as $QWP(\alpha)$ and $HWP(\beta)$ respectively, α and β represent the set angle of the wave plates. i.e.,

$$\begin{aligned} QWP(\alpha) &= \begin{pmatrix} \sin(\alpha) & \cos(\alpha) \\ -\cos(\alpha) & \sin(\alpha) \end{pmatrix}^+ \bullet \begin{pmatrix} e^{-i\frac{\pi}{4}} & 0 \\ 0 & e^{i\frac{\pi}{4}} \end{pmatrix} \bullet \begin{pmatrix} \sin(\alpha) & \cos(\alpha) \\ -\cos(\alpha) & \sin(\alpha) \end{pmatrix} \\ &= \frac{1}{\sqrt{2}} \begin{pmatrix} 1 + i\cos(2\alpha) & -i\sin(2\alpha) \\ -i\sin(2\alpha) & 1 - i\cos(2\alpha) \end{pmatrix}, \end{aligned} \quad (3.11)$$

and

$$HWP(\beta) = -i \begin{pmatrix} \cos(2\beta) & \sin(2\beta) \\ \sin(2\beta) & -\cos(2\beta) \end{pmatrix}. \quad (3.12)$$

Each of two QWP is set at 90° such that the horizontal and vertical polarization will experience 90° phase shift after passing through the QWPs. The total operation matrix will be

$$QWP\left(\frac{\pi}{2}\right) \bullet HWP(\beta) \bullet QWP\left(\frac{\pi}{2}\right) = \begin{pmatrix} -\cos(2\beta) & -i\sin(2\beta) \\ -i\sin(2\beta) & -\cos(2\beta) \end{pmatrix}. \quad (3.13)$$

Rewrite the input photon in the initial state (3.1) as $|\psi\rangle = \begin{pmatrix} \cos(\theta/2) \\ e^{i\phi}\sin(\theta/2) \end{pmatrix}$. The state of the photon after passing through the simulation channel can be written as

$$|\psi(\beta)\rangle = QWP\left(\frac{\pi}{2}\right) \bullet HWP(\beta) \bullet QWP\left(\frac{\pi}{2}\right) \bullet \begin{pmatrix} \cos(\theta/2) \\ e^{i\phi}\sin(\theta/2) \end{pmatrix}. \quad (3.14)$$

By randomly setting the HWP axis to be oriented at $\pm\beta$ with respect to the horizontal direction, the final density matrix can be described as

$$\begin{aligned} \rho(\beta) &= \frac{1}{2}|\psi(\beta)\rangle\langle\psi(\beta)| + \frac{1}{2}|\psi(-\beta)\rangle\langle\psi(-\beta)| \\ &= \frac{1}{2} \begin{pmatrix} 1 + \cos(4\beta)\cos(\theta) & \sin(\theta)(\sin(\phi) - i\cos(4\beta))\sin(\theta) \\ \sin(\theta)(\sin(\phi) - i\cos(4\beta))\sin(\theta) & 1 - \cos(4\beta)\cos(\theta) \end{pmatrix}. \end{aligned} \quad (3.15)$$

On the other hand, consider $p = \sin^2(2\gamma)$ the density matrix (3.5) can be written as

$$\rho = \frac{1}{2} \begin{pmatrix} 1 + \cos(4\gamma)\cos(\theta) & \sin(\theta)(\sin(\phi) - i\cos(4\gamma))\sin(\theta) \\ \sin(\theta)(\sin(\phi) - i\cos(4\gamma))\sin(\theta) & 1 - \cos(4\gamma)\cos(\theta) \end{pmatrix}. \quad (3.16)$$

In comparison with Eq. (3.15) it is clear that with randomly setting the HWP axis to be oriented at $\pm\beta$, the noisy quantum channel can be engineered with a bit-flip error probability of $p = \sin^2(2\beta)$.

3.4 Experimental results

Before starting the experiment, the bit flip error rate of the engineered noisy quantum channel is directly measured by sending in a photon with horizontal polarization. The result is shown in Fig. 3.3, the curve shows the desired error rate for corresponding setting of HWP, and the quadrangle

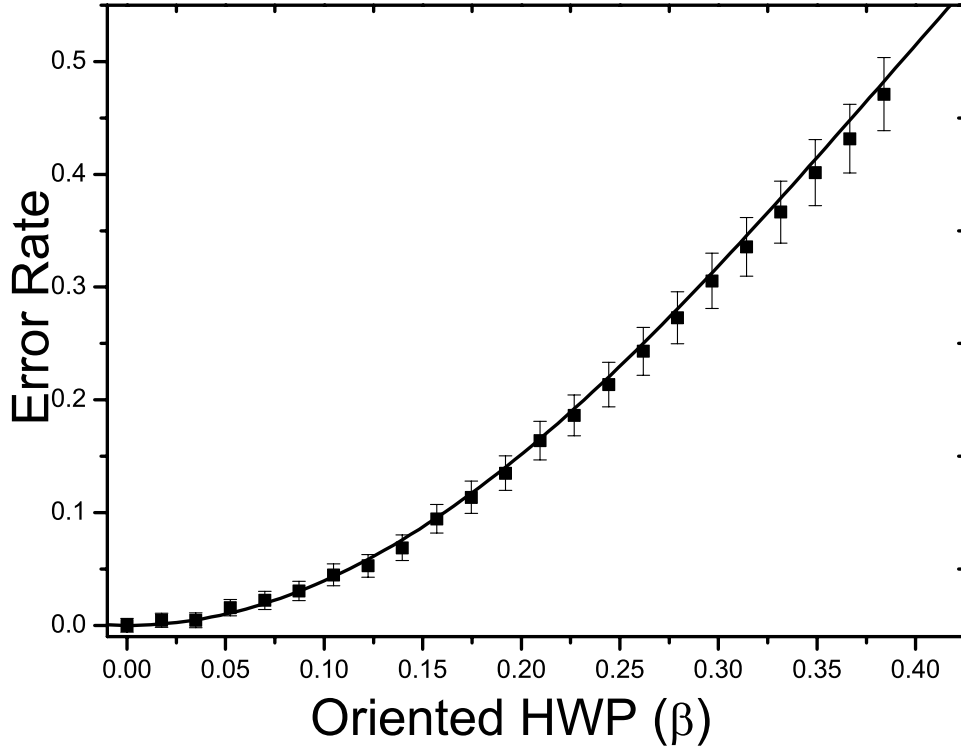


Figure 3.3: Simulated bit-flip noisy quantum channel. The curve represents the desired error rate.

dots show the measured bit flip error rate. It is clear that the engineered noisy quantum channel works nicely.

In order to show that our experiment has successfully achieved the error rejection code, the quantum states to be transmitted in mode 1 are prepared along one of the three complementary bases of $|H\rangle/|V\rangle$, $|+\rangle/|-\rangle$, and $|R\rangle/|L\rangle$. The error rates in the engineered quantum channel can be varied by simultaneously changing the axis of each half-wave plate. Specifically, we vary the angle θ to achieve various error rates from 0 to 0.40 with an increment 0.05 in the quantum channel.

The experimental results of three different input states, after passing through the noisy quantum channel, are shown in Fig. 3.4. The triangle dots in Fig. 3.4, corresponding to the bit-flip error rates of single photons, were measured by directly sending the quantum state of photon 1 (after passing through a polarizer and some wave-plates for state preparing, not shown in Figure) through the engineered quantum channel while with both PBS_1 and PBS_2 removed. These dots also shows the quality of the simulated error of the quantum noisy channel. The quadrangle dots show the final bit-flip error rates after performing encoding and decoding operation for error rejection with the help of PBS_1 and PBS_2 . Fig. 3.4a, 3.4b and 3.4c shows the experimental results for the input states $|V\rangle$, $|-\rangle$, and $|L\rangle$, respectively. The other three input states have the similar results as the one with the same basis respectively. And Fig. 3.4d shows the average QBER calculated over all

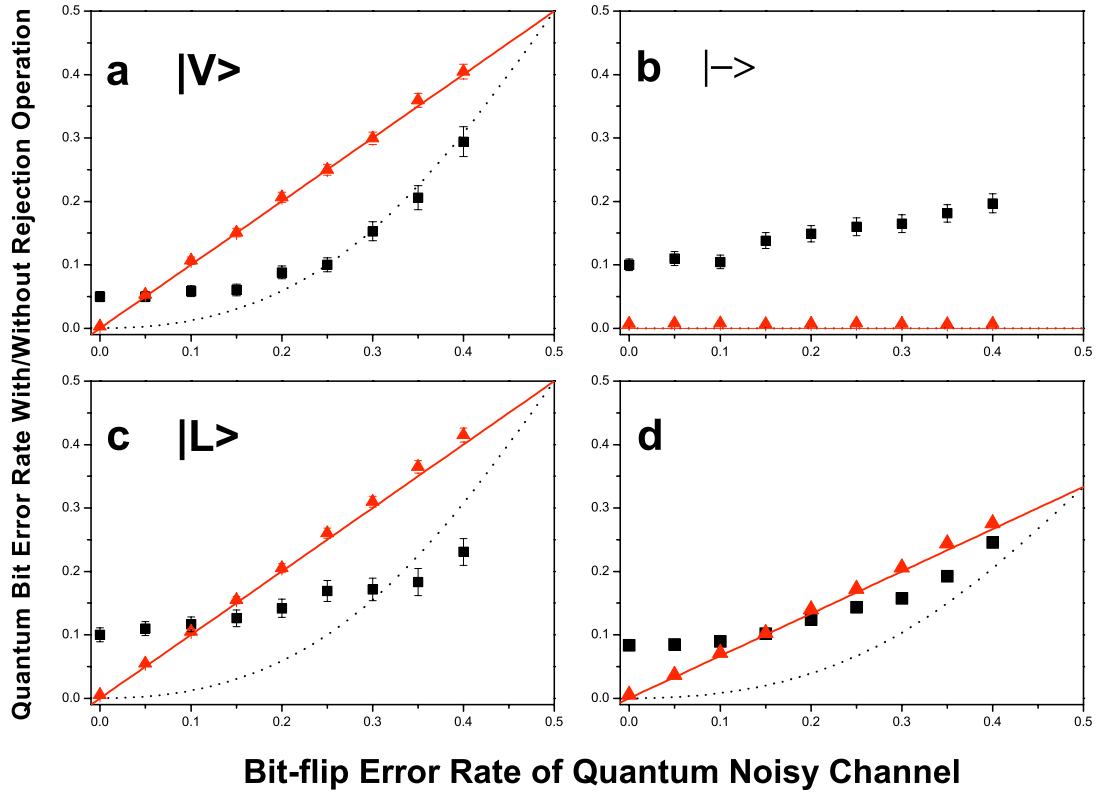


Figure 3.4: Experimental results for three different initial states $|V\rangle$ (a), $|-\rangle$ (b) and $|L\rangle$ (c), and (d) shows the average QBER (calculated over all the six states). The quadrangle and the triangle dots are corresponding to the cases that error-rejection and no error-rejection was made, and the solid curves and the dot curves show the theoretically prediction of QBER for the cases without and with error rejection respectively.

six input states.

In Fig. 3.4, one can clearly see that our error-rejection operation itself also introduces significant error rates, even with $E_0 = 0$. Therefore, if the original E_0 is comparable with the error rate caused by the experimental imperfection, no improvement will be gained after error-rejection. In the $|H\rangle/|V\rangle$ experiment, the experimental error rate is about 5%. In both $|+\rangle/|-\rangle$ and $|R\rangle/|L\rangle$ experiments an experimental error rate of 10% is observed.

We notice that, whereas both the $|+\rangle/|-\rangle$ and $|R\rangle/|L\rangle$ experiments have roughly the same visibility, a better visibility is obtained in the $|H\rangle/|V\rangle$ experiment. This is mainly due to our two-photon entanglement source, which has a better visibility in the $|H\rangle/|V\rangle$ basis (97%) than in the $|+\rangle/|-\rangle$ or $|R\rangle/|L\rangle$ basis (94%). Moreover, it is partly due to the imperfect birefringent compensation at the PBS_1 and PBS_2 [57], which leads a reduction of interference visibility, hence imperfect encoding and decoding process. Moreover, the imperfect encoded state passing through the noisy channel also leads that in the $|+\rangle/|-\rangle$ basis the result become deteriorate as increasing of artificial noise.

3.5 Discussion

From Fig. 3.4a and 3.4c, it is obvious that our error-rejection method can significantly reduce the bit-flip error as long as E_0 is larger than the experimental error rates. However, although ideally in the $|+\rangle/|-\rangle$ experiment no error should occur after the error-rejection operation, an error rate no less than 10% is observed, which is in accordance with the limited visibility of 80%.

Although our experimental results are imperfect, they are sufficient to show a proof of principle of a bit-flip error rejection protocol for error-reduced transfer of quantum information through a noisy quantum channel. Moreover, Fig. 3.4d shows that for a substantial region our experimental method does provide an improved QBER over the standard scheme in a six-state QKD. This implies, with further improvement, the error-rejection protocol may be used to improve the threshold of tolerable error rate over the quantum noisy channel in QKD [110].

Our experimental realization of bit-flip error rejection deserves some further comments. First, the same method can be applied to reject the phase-shift error because phase errors can be transformed into bit-flip errors by a 45° polarization rotation. In this way we can reject all the 1 bit phase-shift error instead of bit-flip error. Second, by encoding unknown states into higher multi-photon (N -photon) entanglement and performing multi-particle parity check measurement [104] either the higher order (up to $N - 1$) bit-flip error or phase-shift error can be rejected for more delicate quantum communication.

In summary, our experiment shows a proof of principle of a bit-flip error rejection protocol for error-free transfer of quantum information through a noisy quantum channel. Moreover, by further improvement of the quality of the resource for multi-photon entanglement, the method may also be used to enhance the bit error rate tolerance [111, 112] over the noisy quantum channel and offer a novel way to achieve long-distance transmission of the fragile quantum states in the future QKD.

Chapter 4

Violation of Bell's Inequality beyond Tsirelson's bound

4.1 Introduction

Bell's theorem [86, 91], derived from Einstein, Podolsky and Rosen's notion of local realism [4] is recognized as "the most profound discovery of science" [113]. It states that the value of certain measured statistical correlations between multiple systems predicted by quantum mechanics can be higher than the highest value allowed by local realism. The most commonly form may be so-called Clauser-Horne-Shimony-Holt (CHSH) [114] inequality, which states that in local realism the absolute value of a combination of four correlations is bounded by 2. While quantum mechanics allows $2\sqrt{2}$ in principle. It is widely believed that "quantum theory does not allow any stronger violation of the CHSH inequality than the one already achieved in Aspect's experiment [47] $2\sqrt{2}$ " [115].

However, as stressed by Peres [115], Bell inequalities [86, 91] have nothing to do with quantum mechanics. They are constraints imposed by local realistic theories on the values of linear combinations of the averages (or probabilities) of the results of experiments on two or more separated systems. Therefore, when examining data obtained in experiments to test Bell inequalities, it is legitimate to do it from the perspective (i.e., under the assumptions) of local realistic theories, without any reference to quantum mechanics. This approach leads to some apparently paradoxical results. A remarkable one is that, while it is a standard result in quantum mechanics that no quantum state can violate the CHSH Bell inequality [114] beyond Tsirelson's bound (also written as Cirel'son's bound), namely $2\sqrt{2}$ [116], the correlations between two qubits belonging to a three-qubit system can violate the CHSH-Bell inequality beyond $2\sqrt{2}$ [117]. In particular, if we use a three-qubit GHZ state [90], we can even obtain the maximum allowed violation of the CHSH-Bell inequality, namely 4 [117].

In this chapter, we report the first observation of a violation of the CHSH-Bell inequality beyond Tsirelson's bound by using a three-photon polarization-entangled GHZ state produced by Type-II spontaneous parametric down-conversion. In addition, since the experiment also provides all the data required for testing Mermin's three-party Bell inequality [92], we use our results to demonstrate the violation of this inequality.

4.2 CHSH-Bell inequality

The main idea behind the CHSH-Bell inequality [114] is that, in local realistic theories, the absolute value of a particular combination of correlations between two distant particles i and j is bounded

by 2:

$$|C(A, B) - mC(A, b) - nC(a, B) - mnC(a, b)| \leq 2 \quad (4.1)$$

where m and n can be either -1 or 1 , and A and a (B and b) are physical observables taking values -1 or 1 , referring to local experiments on particle i (j). The correlation $C(A, B)$ of A and B is defined as

$$C(A, B) = P_{AB}(1, 1) - P_{AB}(1, -1) - P_{AB}(-1, 1) + P_{AB}(-1, -1), \quad (4.2)$$

where $P_{AB}(1, -1)$ denotes the joint probability of obtaining $A = 1$ and $B = -1$ when A and B are measured.

The bound 2 in inequality (4.1) can be easily derived as follows. In local realistic theories, for any individual system, the observables A , a , B and b have predefined value v_A , v_a , v_B and v_b , either -1 or 1 . Therefore, for an individual system the combination of correlations appearing in (4.1) can be calculated as

$$v_B(v_A - nv_a) - mv_b(v_A + nv_b), \quad (4.3)$$

which is either -2 or 2 , because one of the expressions between parentheses in (4.3) is necessarily zero and the other is either -2 or 2 . Therefore, the absolute value of the corresponding averages is bound by 2.

4.2.1 Tsirelson's bound

However, Tsirelson proved that, for a two particle system prepared in any quantum state $|\psi\rangle$, the absolute value of the combination of quantum correlations appearing in the inequality (4.1) is bounded by $2\sqrt{2}$ [116],

$$|C_Q(A, B) - mC_Q(A, b) - nC_Q(a, B) - mnC_Q(a, b)| \leq 2\sqrt{2} \quad (4.4)$$

where the quantum correlation of A and B , $C_Q(A, B)$ is defined as $\langle \psi | \hat{A}\hat{B} | \psi \rangle$. Here \hat{A} and \hat{B} are the self-adjoint operators which represent observable A and B . Tsirelson's bound can easily be derived as follows [118]. Consider the operator with the same structure as the combination which appears in inequality (4.4),

$$\hat{C} = \hat{A}\hat{B} - m\hat{A}\hat{b} - n\hat{a}\hat{B} - mn\hat{a}\hat{b}. \quad (4.5)$$

Since $\hat{A}^2 = \hat{a}^2 = \hat{B}^2 = \hat{b}^2 = \mathbf{I}$, where \mathbf{I} is the identity operator,

$$\hat{C}^2 = 4\mathbf{I} - mn[\hat{A}, \hat{a}][\hat{B}, \hat{b}]. \quad (4.6)$$

Given the fact for all \hat{F} and \hat{G} bounded operators we have

$$\|[\hat{F}, \hat{G}]\| \leq \|\hat{F}\hat{G}\| + \|\hat{G}\hat{F}\| \leq 2\|\hat{F}\|\|\hat{G}\|. \quad (4.7)$$

Thus, $\|\hat{C}^2\| \leq 8$, or $\|\hat{C}\| \leq 2\sqrt{2}$. That is Tsirelson's bound [116].

However, from the inequality (4.1) itself, a simple question would be if it is possible to violate the CHSH inequality to 4 instead of $2\sqrt{2}$, since 4 would be the maximum bound allowed if the four correlations in the CHSH inequality (4.1) were independent. Assuming local realistic theories' point of view, the correlations predicted by quantum mechanics between two distant qubits belonging to a three-qubit system can violate the CHSH-Bell inequality beyond Tsirelson's bound [117].

4.2.2 Violation beyond Tsirelson's bound

To show the principle of violation beyond Tsirelson's bound, let's consider three distant qubits, which are polarization-entangled photons prepared in the GHZ state:

$$|\Psi\rangle = \frac{1}{\sqrt{2}} (|H\rangle|H\rangle|H\rangle + |V\rangle|V\rangle|V\rangle), \quad (4.8)$$

where H (V) denotes horizontal (vertical) linear polarization. During the experiment, we will analyze the polarization of each photon in one of two different basis: either in the X basis, or in the Y basis. These polarization bases can be expressed in terms of the H/V basis as (2.3). The measurement results $+$ (R) and $-$ (L) are denoted by 1 and -1 , respectively.

For each three-photon system prepared in the state (4.8), we will define as photons i and j those two giving the result -1 when making X measurement on all three photons; the third photon will be denoted as k . If all three photons give the result 1, photons i and j could be any pair of them. Since no other combination of results is allowed for the state (4.8), i and j are well defined for every three-photon system.

We are interested in the correlations between two observables, A and a , of photon i and two observables, B and b , of photon j . In particular, let us choose $A = X_i$, $a = Y_i$, $B = X_j$, and $b = Y_j$, where X_q and Y_q are the polarizations of photon q along the basis X and Y , respectively. The particular CHSH-Bell inequality (4.1) we are interested in is the one in which $m = n = y_k$, where y_k is one of the possible results, -1 or 1 (although we do not know which one), of measuring Y_k . With this choice we obtain the CHSH-Bell inequality

$$|C(X_i, X_j) - y_k C(X_i, Y_j) - y_k C(Y_i, X_j) - C(Y_i, Y_j)| \leq 2, \quad (4.9)$$

which holds for local realistic theories, regardless of the particular value, either -1 or 1 , of y_k .

We could force photons i and j to be those in locations 1 and 2, by measuring X on the photon in location 3, and then selecting only those events in which the result of this measurement is 1. This procedure guarantees that our definition of photons i and j is physically meaningful. By the definition of qubits i and j , and taking into account that the three-photon state (4.8) is an eigenstate of the self-adjoint operator $\hat{X}_i \hat{X}_j \hat{X}_k$ with eigenvalue 1, the only possible results will be $X_i = X_j = 1$ and $X_i = X_j = -1$. Thus we obtain

$$C(X_i, X_j) = 1. \quad (4.10)$$

On the other hand, the state (4.8) is an eigen state of $\hat{X}_i \hat{Y}_j \hat{Y}_k$ with eigenvalue -1 , therefore, we can obtain

$$C(X_i, Y_j) = -y_k, \quad (4.11)$$

because the only possible results will be $X_i = 1, Y_j = -y_k$ and $X_i = -1, Y_j = y_k$. Given the fact that the state (4.8) is an eigenstate of $\hat{Y}_i \hat{Y}_j \hat{X}_k$ with eigenvalue -1 , the only possible results are $Y_i = y_k, X_j = -1$ and $Y_i = -y_k, X_j = 1$. Thus, we obtain

$$C(Y_i, X_j) = -y_k. \quad (4.12)$$

In the end, by the definition of qubit k as the one in which $X_k = 1$, and taking into account that state (4.8) is an eigenstate of $\hat{Y}_i \hat{Y}_j \hat{X}_k$ with eigenvalue -1 , we can obtain

$$C(Y_i, Y_j) = -1, \quad (4.13)$$

since the only possible result are $Y_i = -Y_j = 1$ and $Y_i = -Y_j = -1$. From Eq. (4.10–4.13), the left-hand side of inequality (4.9) is 4, which is the maximum value allowed by the definition of correlation. Other choices of three-qubit entangled quantum states and observables lead to violations of the CHSH inequality in the range of $2\sqrt{2}$ to 4.

4.3 Experiment proposal

Because it does not allow us to measure Y on photon k , the experimental test can not be simply a test on. The key point for testing inequality (4.9) is noticing that we do not need to know in which locations are photons i , j , and k for every three-photon system. We can obtain the required data

by performing suitable combinations of measurements of X or Y on the three photons. In order to see this, let us first translate inequality (4.9) into the language of joint probabilities. Assuming that the expected value of any local observable cannot be affected by anything done to a distant particle, the CHSH-Bell inequality (4.9) can be transformed into a more convenient experimental inequality [119, 120]:

$$\begin{aligned} -1 \leq & P_{X_i X_j}(-1, -1) - P_{X_i Y_j}(-1, -y_k) \\ & - P_{Y_i X_j}(-y_k, -1) - P_{Y_i Y_j}(y_k, y_k) \leq 0. \end{aligned} \quad (4.14)$$

This can be proved as follows. Since $P_{AB}(a, b) = \frac{1}{4} \langle (\mathbf{I} + a\hat{A}) \otimes (\mathbf{I} + b\hat{B}) \rangle$, here a and b can be either -1 or 1 . Thus, the middle term in inequality (4.14) can be expanded as,

$$\begin{aligned} & P_{X_i X_j}(-1, -1) - P_{X_i Y_j}(-1, -y_k) - P_{Y_i X_j}(-y_k, -1) - P_{Y_i Y_j}(y_k, y_k) \\ &= \frac{1}{4} \langle (\mathbf{I} - \hat{X}_i) \otimes (\mathbf{I} - \hat{X}_j) \rangle - \langle (\mathbf{I} - \hat{X}_i) \otimes (\mathbf{I} - y_k \hat{Y}_j) \rangle \\ &\quad - \langle (\mathbf{I} - y_k \hat{Y}_i) \otimes (\mathbf{I} - \hat{X}_j) \rangle - \langle (\mathbf{I} + y_k \hat{Y}_i) \otimes (\mathbf{I} + y_k \hat{Y}_j) \rangle \\ &= \frac{1}{4} \left(\langle \hat{X}_i \hat{X}_j \rangle - y_k \langle \hat{X}_i \hat{Y}_j \rangle - y_k \langle \hat{Y}_i \hat{X}_j \rangle - \langle \hat{Y}_i \hat{Y}_j \rangle - 2 \right) \\ &= \frac{1}{4} (C(X_i, X_j) - y_k C(X_i, Y_j) - y_k C(Y_i, X_j) - C(Y_i, Y_j) - 2). \end{aligned} \quad (4.15)$$

Consequently, the inequality (4.14) is equivalent with inequality (4.9). And the bounds l of inequalities (4.1) and (4.9) are transformed into the bounds $(l-2)/4$ of inequality (4.14). Therefore, the local realistic bound in (4.14) is 0, Tsirelson's bound is $(\sqrt{2}-1)/2$, and the maximum value is $1/2$.

To measure the inequality (4.14), we must relate the four joint probabilities appearing in (4.14) to the probabilities of coincidences in an experiment with three spatial locations, 1, 2, and 3. For instance, it can be easily seen that

$$\begin{aligned} P_{X_i X_j}(-1, -1) = & P_{X_1 X_2 X_3}(1, -1, -1) + P_{X_1 X_2 X_3}(-1, 1, -1) \\ & + P_{X_1 X_2 X_3}(-1, -1, 1) + P_{X_1 X_2 X_3}(-1, -1, -1). \end{aligned} \quad (4.16)$$

In addition, $P_{X_i Y_j}(-1, -y_k)$ and $P_{Y_i X_j}(-y_k, -1)$ are both less than or equal to

$$\begin{aligned} & P_{X_1 Y_2 Y_3}(-1, 1, -1) + P_{X_1 Y_2 Y_3}(-1, -1, 1) \\ & + P_{Y_1 X_2 Y_3}(1, -1, -1) + P_{Y_1 X_2 Y_3}(-1, -1, 1) \\ & + P_{Y_1 Y_2 X_3}(1, -1, -1) + P_{Y_1 Y_2 X_3}(-1, 1, -1). \end{aligned} \quad (4.17)$$

Finally,

$$P_{Y_i Y_j}(y_k, y_k) = P_{Y_1 Y_2 Y_3}(1, 1, 1) + P_{Y_1 Y_2 Y_3}(-1, -1, -1). \quad (4.18)$$

Therefore, by performing measurements in 5 specific configurations (XXX , XYX , YXX , YXY , and YYY), we can obtain the value of the middle side of inequality (4.14).

In the state (4.8), the first three probabilities in the right-hand of (4.16) are expected to be $1/4$, and the fourth is expected to be zero; the six probabilities in (4.17) are expected to be zero, and the two probabilities in the right hand side of (4.18) are expected to be $1/8$. Therefore, the middle side of inequality (4.14) is expected to be $1/2$, which means that the left-hand side of inequality (4.9) is 4, which is not only beyond Tsirelson's bound, $2\sqrt{2}$, but is also the maximum possible violation of inequality (4.9).

4.4 Experimental setup

To generate the three-photon GHZ state (4.8) we use the technique developed in previous experiments [39, 42] as described in § 2.2. The experimental setup for generating three-photon

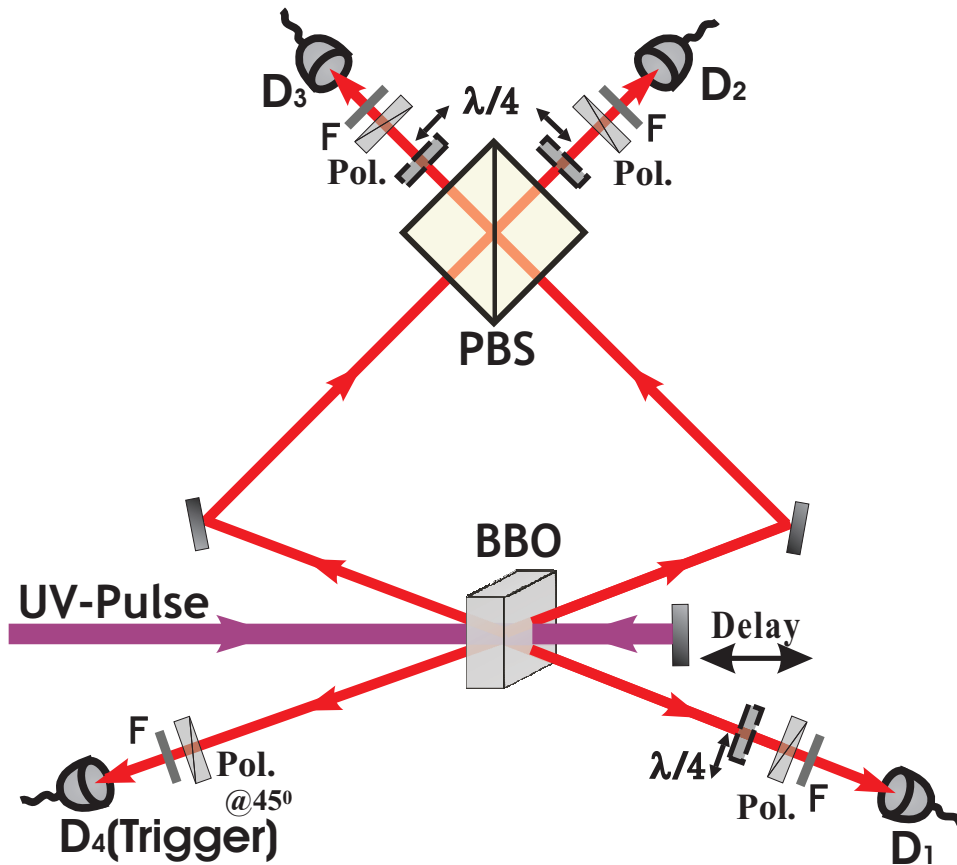


Figure 4.1: Experimental setup for generating three-photon GHZ states. An ultraviolet pulse passes twice through the + crystal to generate two pairs of polarization-entangled photons by Type-II spontaneous parametric down-conversion used to perform the preparation of three-photon GHZ state. The ultraviolet laser with a central wavelength of 394 nm has pulse duration of 200fs, a repetition rate of 76 MHz, and an average pump power of 400 mW. We observe about 2×10^4 entangled pairs per second behind 3.6 nm filters (F) of central wavelength 788 nm. Polarizers (Pol.) and quarter wave plates ($\lambda/4$) in front of the detectors are used for performing X or Y measurement.

entanglement is shown in Fig. 4.1. A pulse of ultraviolet light passes through a BBO crystal twice to produce two polarization-entangled photon pairs, where both pairs are in the state

$$|\Psi_2\rangle = 1/\sqrt{2}(|H\rangle|H\rangle + |V\rangle|V\rangle). \quad (4.19)$$

One photon out of each pair is then steered to a polarization beam splitter (PBS) where the path lengths of each photon have been adjusted (by scanning the delay position) so that they arrive simultaneously. After the two photons pass through the PBS, and exit it by a different output port each, there is no way whatsoever to distinguish from which emission each of the photons originated, then correlations due to four-photon GHZ entanglement

$$|\Psi_4\rangle = 1/\sqrt{2}(|H\rangle|H\rangle|H\rangle|H\rangle + |V\rangle|V\rangle|V\rangle|V\rangle) \quad (4.20)$$

can be observed [42]. After that, by performing a $|+\rangle$ polarization projective measurement onto one of the four outputs, the remaining three photons will be prepared in the desired GHZ state (4.8).

In the experiment, the observed fourfold coincident rate of the desired component $HHHH$ or $VVVV$ is about 1.4 per second. By performing a + projective measurement at photon 4 as the

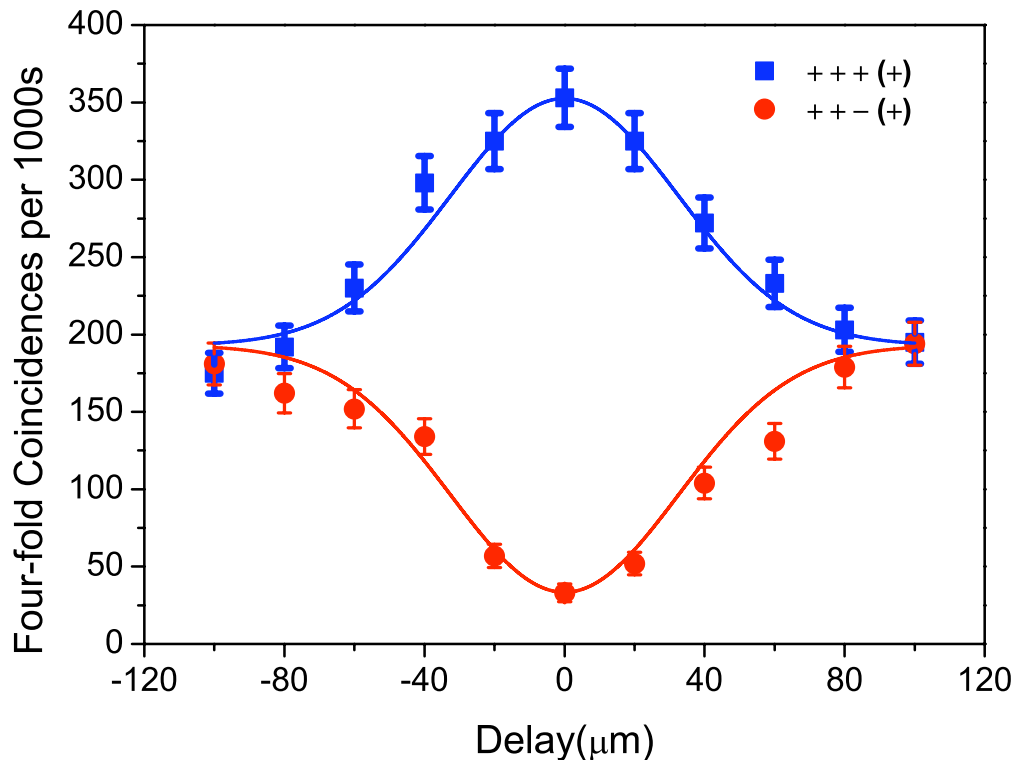


Figure 4.2: Typical experimental results for polarization measurements on all three photons in a X basis triggered by the photon 4 at the $+$ polarization. The coincidence rates of $+++$ and $++-$ components are shown as a function of the pump delay mirror position. The high visibility obtained at zero delay implies that three photons are indeed in a coherent superposition.

trigger of the fourfold coincident, the ratio between any of the desired events HHH and VVV to any of the 6 other undesired ones, e.g., HHV , is about 65 : 1. To confirm that these two events are indeed in a coherent superposition, we have performed polarization measurements in X basis. In Fig. 4.2, we compare the count rates of $+++$ and $++-$ components as we move the delay mirror (Delay) by the trigger photon 4 at the $+$ polarization. The latter component is suppressed with a visibility of 83% at zero delay, which confirms the coherent superposition of HHH and VVV .

The experiments consists of performing measurements in 5 specific configurations. As shown in Fig. 4.1, we use polarizers oriented at $\pm 45^\circ$ and $\lambda/4$ plates to perform X or Y measurements.

4.5 Experimental results

For the 5 required configurations, i.e. XXX , XYX , YXY , YYX , and YYY , the experimental results for all possible outcomes are shown in Fig. 4.3.

Substituting the experimental results (shown in Fig. 4.3) into the right-hand side of (4.16), we obtain

$$P_{X_i X_j}(-1, -1) = 0.738 \pm 0.012. \quad (4.21)$$

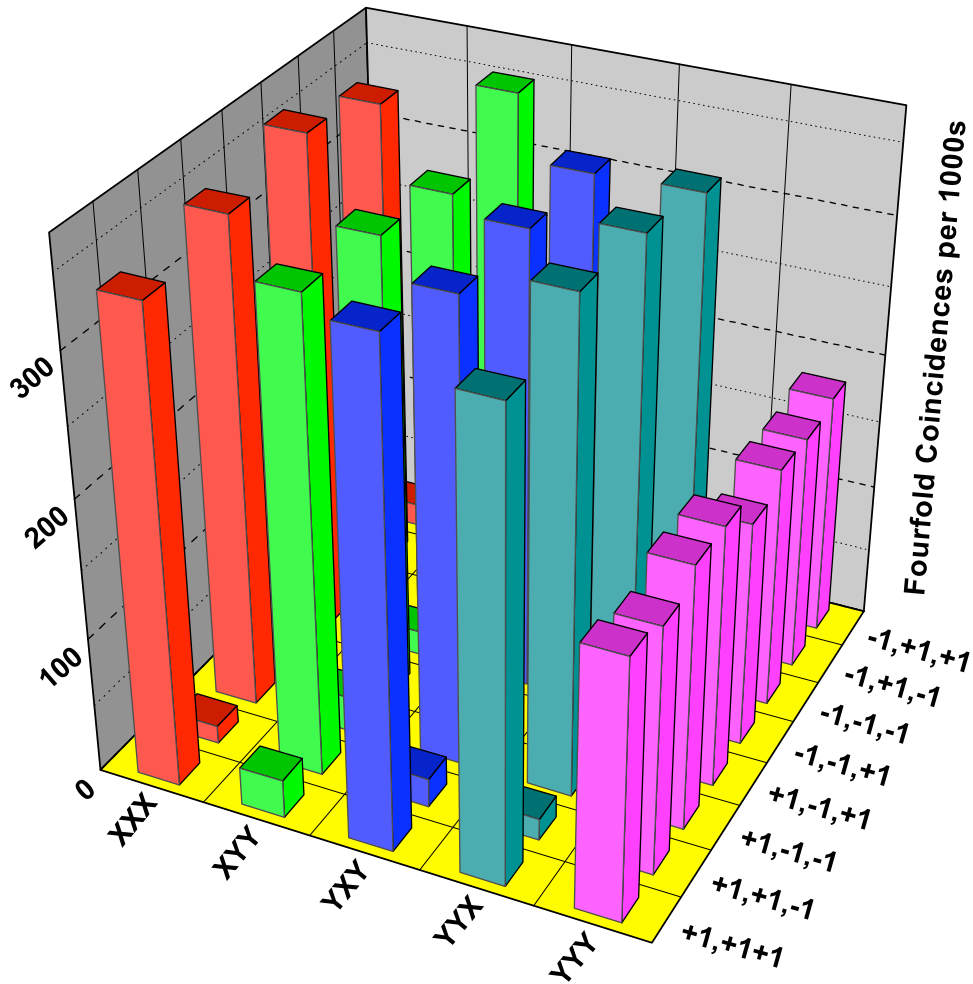


Figure 4.3: Experimental results observed for the 5 required configurations: XXX , XYY , YXY , YYX , and YYY .

Similarly, substituting the experimental results in (4.17), we obtain

$$\begin{aligned} P_{X_i Y_j}(-1, -y_k) &\leq 0.072 \pm 0.007, \\ P_{Y_i X_j}(-y_k, -1) &\leq 0.072 \pm 0.007. \end{aligned} \quad (4.22)$$

Finally, substituting the experimental results in (4.18), we obtain

$$P_{Y_i Y_j}(y_k, y_k) = 0.254 \pm 0.011. \quad (4.23)$$

Therefore, the prediction for the middle side of (4.14) is greater than or equal to 0.340 ± 0.019 , and the prediction for the right-hand side of (4.9) is greater than or equal to 3.36 ± 0.08 , which clearly violates Tsirelson's bound by 7 standard deviations.

4.5.1 Violation of Mermin's inequality

In addition, using part of the results contained in Fig. 4.3, we can test the three-particle Bell inequality derived by Mermin [92],

$$|C(X_1, Y_2, Y_3) + C(Y_1, X_2, Y_3) + C(Y_1, Y_2, X_3) - C(X_1, X_2, X_3)| \leq 2. \quad (4.24)$$

From the results in Fig. 4.3 we obtain 3.57 ± 0.04 for the left-hand side of (4.24), which is a violation of inequality (4.24) by 39 standard deviations. Note that the experiment for observing the violation beyond Tsirelson's bound also requires performing measurements in an additional configuration (YYY).

4.6 Discussion

In conclusion, we have demonstrated a violation of the CHSH-Bell inequality beyond Tsirelson's bound. It should be emphasized that such a violation is predicted by quantum mechanics and appears when examining the data from the perspective of local realistic theories [117]. In addition, it should be stressed that the reported experiment is different as previous experiments to test local realism involving three or four-qubit GHZ states [49, 50], since it is based on a definition of pairs which is conditioned to the result of a measurement on a third qubit, and requires performing measurements in additional configurations.

Chapter 5

Teleportation of two-qubit composite system

5.1 Introduction

Ever since the wheel was invented more than 5000 years ago, people have been inventing new ways to travel faster from one point to another, such as the chariot, bicycle, automobile, airplane and so on. All of these forms of transportation share the same flaw: they require us to cross a physical distance. However, in both eastern fairy tales and western myths, there exists an amazing way of transportation the so-called teleportation. Teleportation is such a condition, one object for example a person, he disappears in one place and appears in another place without moving it. In classical physics, we know we can scan all the information of the object and with the information we can reconstruct one in the other places. However, in quantum world this method is impossible since it is forbidden to extract all the information from an unknown quantum state.

Surprisingly, in 1993 six scientists proposed a scheme for transferring the state of a quantum system from one location to another which is the so-called quantum teleportation [7]. By using entanglement, one can transfer the quantum state without getting any information about the state in the course of this transformation. Later it is found that quantum teleportation is central to quantum communication [17] and plays an important role in a number of quantum computation protocols [18, 19, 20]. Experimental demonstrations have been implemented with photons [31, 32, 34] or ions [121, 122]. Very recently long-distance teleportation [123, 124] and open-destination teleportation [43] have also been realized. So far, previous experiments [31, 32, 34, 121, 122, 123, 124, 43] have only been able to teleport single qubits. However, since teleportation of single qubits is insufficient for a large-scale realization of quantum communication and computation [17, 18, 19, 20], teleportation of a composite system containing two or more qubits has been seen as a long-standing goal in quantum information science.

In this chapter we will report the first experimental demonstration of a two-photon quantum teleportation, which utilizes the six-photon interferometer techniques. In the experiment, we develop and exploit a six-photon interferometer to teleport an arbitrary polarization state of two photons. Not only does our six-photon interferometer provide an important step towards teleportation of a complex system, it will also enable future experimental investigations on a number of fundamental quantum communication and computation protocols [18, 125, 126, 23]. Realization of such a teleportation also represents the current state-of-the-art for manipulation of any qubit system.

5.2 Two-qubit teleportation scheme

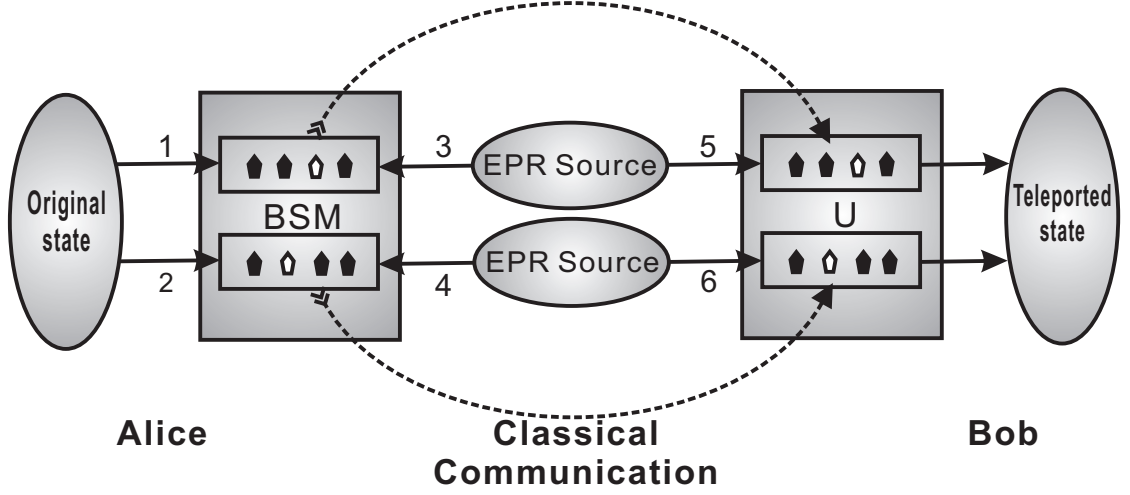


Figure 5.1: Schematic diagram showing the principle of two-qubit teleportation. Alice wants to teleport an unknown state of a system composed of photon 1 and 2 to Bob. To do so, Alice and Bob first share two entangled photon pairs (EPR source), photon pairs 3-5 and 4-6. Alice then carries out a joint Bell-state measurement (BSM) both on photons 1 and 3 and on photons 2 and 4, respectively. On receiving Alice's BSM results via classical communication, Bob can then carry out a corresponding unitary transformation (U) on both photons 5 and 6 to convert them into the original state of photons 1 and 2.

Although there exist other ways to achieve teleportation of a composite system [127, 128], our experimental scheme [19, 129] closely follows the original proposal for teleportation of single qubits [7]. In the two-qubit teleportation, the sender, Alice, wants to send an unknown state of a system composed of qubits 1 and 2,

$$|\chi\rangle_{12} = \alpha |H\rangle_1 |H\rangle_2 + \beta |H\rangle_1 |V\rangle_2 + \gamma |V\rangle_1 |H\rangle_2 + \delta |V\rangle_1 |V\rangle_2, \quad (5.1)$$

where α , β , γ and δ are four arbitrary complex numbers satisfying $|\alpha|^2 + |\beta|^2 + |\gamma|^2 + |\delta|^2 = 1$, to a distant receiver, Bob (Fig. 5.1). In order to achieve teleportation, Alice and Bob first have to share two ancillary entangled photon pairs (photon pairs 3-5 and 4-6) which are prepared in the one of Bell-states $|\Phi^+\rangle = (|HH\rangle + |VV\rangle)/\sqrt{2}$. The two-qubit teleportation scheme then works as follows.

Alice first teleports the state of photon 1 to photon 5 following the standard teleportation protocol. In terms of the four Bell-states of photons 1 and 3,

$$\begin{aligned} |\Phi^\pm\rangle_{13} &= (|H\rangle_1 |H\rangle_3 \pm |V\rangle_1 |V\rangle_3)/\sqrt{2} \\ |\Psi^\pm\rangle_{13} &= (|H\rangle_1 |V\rangle_3 \pm |V\rangle_1 |H\rangle_3)/\sqrt{2}, \end{aligned} \quad (5.2)$$

the combined state of photons 1, 2, 3 and 5 can be rewritten as

$$\begin{aligned} |\chi\rangle_{12} |\Phi^+\rangle_{35} &= \frac{1}{2} (|\Phi^+\rangle_{13} |\chi\rangle_{52} + |\Phi^-\rangle_{13} \hat{\sigma}_{5z} |\chi\rangle_{52} \\ &\quad + |\Psi^+\rangle_{13} \hat{\sigma}_{5x} |\chi\rangle_{52} + |\Psi^-\rangle_{13} (-i\hat{\sigma}_{5y}) |\chi\rangle_{52}), \end{aligned} \quad (5.3)$$

where $\hat{\sigma}_x$, $\hat{\sigma}_y$ and $\hat{\sigma}_z$ are the well-known Pauli operators. Eq. (5.3) implies, that by performing a joint Bell-state measurement (BSM) on qubits 1 and 3, Alice projects the state of qubits 5 and 2 onto one of the four corresponding states. After she has told Bob her BSM result via a classical communication channel, Bob can convert the state of qubits 5 and 2 into the original state $|\chi\rangle_{52}$ by

applying to photon 5 a corresponding local unitary transformation $(\hat{I}, \hat{\sigma}_X, \hat{\sigma}_Y, \hat{\sigma}_Z)$, independent of the original state.

Similarly, the combined state of photons 2, 4, 5 and 6 can be rewritten in terms of the four Bell-states of photons 2 and 4 as

$$\begin{aligned} |\chi\rangle_{52} |\Phi^+\rangle_{46} = & \frac{1}{2} (|\Phi^+\rangle_{24} |\chi\rangle_{56} + |\Phi^-\rangle_{24} \hat{\sigma}_{6Z} |\chi\rangle_{56} \\ & + |\Psi^+\rangle_{24} \hat{\sigma}_{6X} |\chi\rangle_{56} + |\Psi^-\rangle_{24} (-i\hat{\sigma}_{6Y}) |\chi\rangle_{56}). \end{aligned} \quad (5.4)$$

Following the above procedure, Alice can also teleport the state of photon 2 to photon 6. First, Alice performs a joint BSM on photons 2 and 4 and sends the BSM result to Bob. Upon the BSM result received, by applying to photon 6 a corresponding local unitary transformation $(\hat{I}, \hat{\sigma}_x, \hat{\sigma}_y, \hat{\sigma}_z)$, Bob can convert the state of qubits 5 and 6 into the original state

$$|\chi\rangle_{56} = \alpha |H\rangle_5 |H\rangle_6 + \beta |H\rangle_5 |V\rangle_6 + \gamma |V\rangle_5 |H\rangle_6 + \delta |V\rangle_5 |V\rangle_6 \quad (5.5)$$

to accomplish the task of the most general two-qubit teleportation.

The above scheme has a remarkable feature: it teleports the two photonic qubits, 1 and individually. This way, neither the two original qubits nor the teleported qubits have to be in the same place. Such a flexibility is desired in distributed quantum information processing, such as quantum telecomputation [20] and quantum secret sharing [94, 130]. Moreover, the above method of teleporting each qubit of a composite system individually can be easily generalized to teleport a N -qubit complex system.

5.3 A stable high-intensity entangled photon source

Although significant experimental advances have been achieved in teleportation of single qubits (photons and ions), the realization of teleportation of a composite system containing two or more qubits has remained a real experimental challenge. This is because, on one hand the recent photonic experiments [123, 124, 43] would have a too low six-photon coincidence rate. On the other hand, the experiments with trapped ions [122, 121] are limited by the finite life time of ion qubits due to decoherence and the nonideal fidelity of quantum logic operation between ion qubits. Since photons are robust against decoherence and high precision unitary transformations for photons can be performed with linear optical devices, in the present experiment we still chose to use polarization-entangled photon pairs via parametric down-conversion [53] as the main resource while various efforts have been made to greatly improve the brightness and stability of the entangled photon sources.

A natural way to obtain a brighter entangled photon source is to increase the power of the ultraviolet light necessary for parametric down-conversion. To significantly increase the ultraviolet power, we would need a more powerful ultra-fast infrared laser system for the up-conversion process. To achieve this, we have used an all-solid-state CW laser Verdi-V18 instead of Verdi-V10 to pump a modified mode-locked Ti:sapphire laser system Mira900-F (Mira) as is shown in Fig. 5.2. Unfortunately, the conversion efficiency of the Ti:sapphire crystal will drop greatly when the pump power is beyond a certain threshold, typically 10 in the commercial Mira. This is because the pump laser Verdi-V18 will bring more heat to the Ti:sapphire crystal. To solve this problem, a better cooling cycle system around the Ti:sapphire crystal is used. Moreover, a brighter pump laser in the Mira cavity will make the output infrared pulse unstable. A new output coupler with higher transmission efficiency is used in the cavity to stabilize the output laser. After these innovations, we achieved an ultra fast infrared pulse with an output power of about 2.9W with the Verdi-V18 operated at 14W, which is almost twice as high as before.

The high power infrared pulse was properly focused on the LiB_3O_5 (LBO) crystal to achieve the best up-conversion efficiency. To avoid damage to the LBO, caused by the focused laser beam,

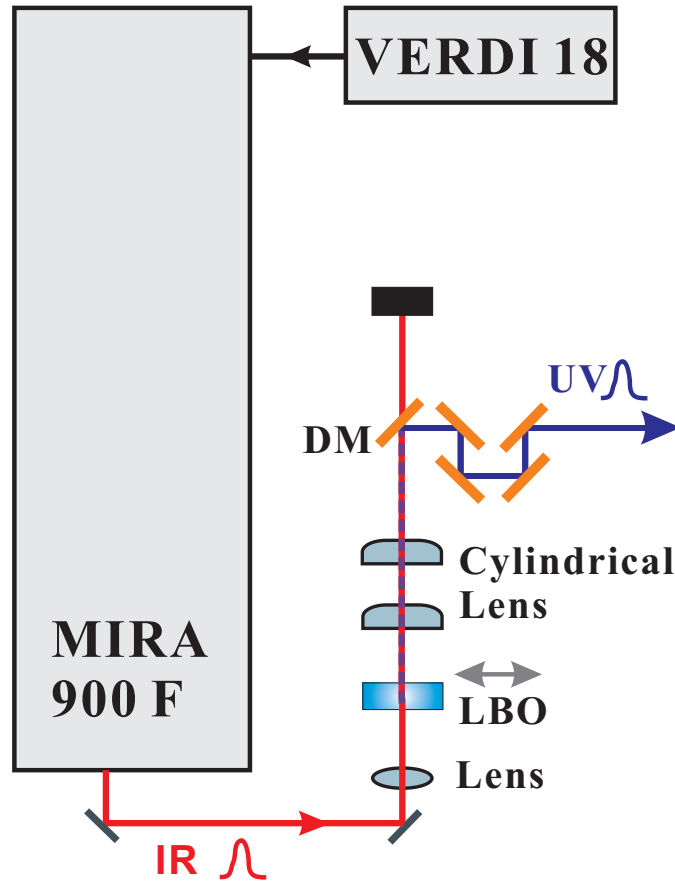


Figure 5.2: The method to increase the power of the ultraviolet light. A modified mode-locked Ti:sapphire laser (MIRA), pumped with an all-solid-state CW laser Verdi-V18 (operating at 14W), is used to produce high-intensity ultra-fast infrared light pulses. The infrared light pulse passes through the LBO crystal to generate via up-conversion the ultraviolet pulse necessary for parametric down-conversion. Behind the LBO, two cylindrical lenses with orthogonal axes, (one horizontal and one vertical) are used to shape and focus the ultraviolet beam and five dichroic mirrors (DM) are used to separate the ultraviolet from the infrared light.

the LBO is mounted on a motorized translation stage and will be moved by a distance of to another point once the reference - single count rate of detector D5H (see Fig. 5.3)- is below a certain threshold. Since back-reflection of the LBO into the Mira system can destroy the mode-lock condition, perfect control of the LBO motion is crucial. Due to the brighter infrared pulse, much more noise (i.e., infrared light) is introduced to the ultraviolet light during the up-conversion process. To compensate for this, two additional dichroic mirrors are added in comparison to former experiments to further separate the ultraviolet light with the infrared noise.

To have a better collection efficiency of entangled photon pairs, we significantly shortened the distance between the BBOs and the fiber couplers to make our setup more compact. Besides the improvement in collection efficiency, a compact setup also helps to significantly improve the stability of the whole six-photon interferometer. To optimize the collection efficiency for all three entangled photon pairs, we chose a 10 cm focus lens between the two BBOs and a 20 cm radius concave mirror behind the second BBO to refocus the ultraviolet pulse such that it has the same beam size in all three BBO pumping processes. With these modifications, we achieved a stable high-intensity entangled photon source.

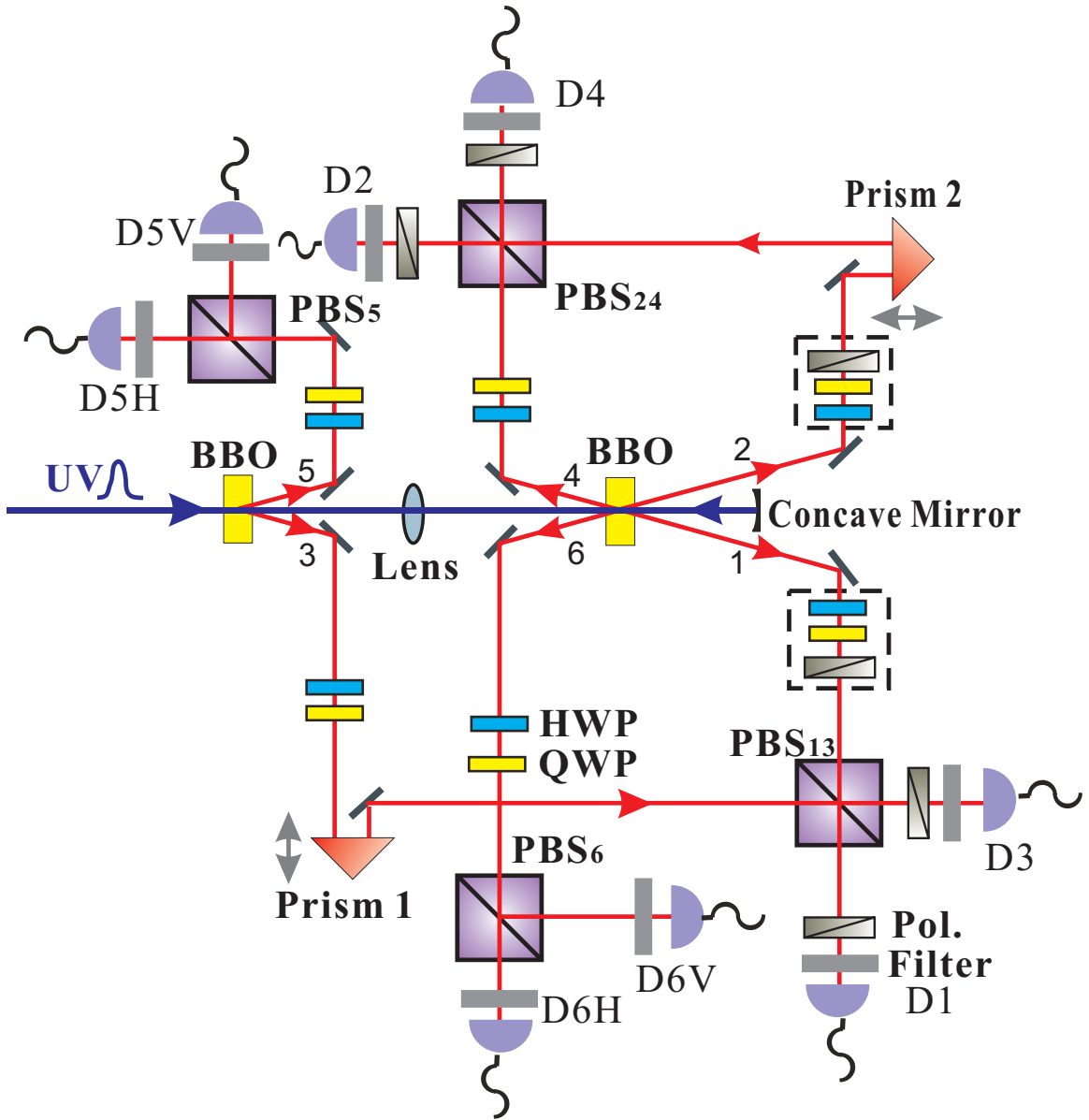


Figure 5.3: A schematic diagram of the experimental setup. The ultraviolet pulse passes through a BBO crystal to generate a polarization-entangled photon pair in mode 3 and 5 (that is, the first ancillary entangled photon pair). After the first BBO, a 10-cm-focus lens is introduced to refocus the ultraviolet pulse pumps once more into the second BBO and generates the third entangled photon pair in modes 4 and 6 (that is, the second ancillary photon pair). Prisms 1 and 2, both mounted on step motors, are used to compensate the time delay for the interference on polarizing beam splitters PBS13 and PBS24, respectively. PBS5 and PBS6 are used to verify the teleported state with the help of wave plates in front of them. The photons are all detected by silicon avalanche single-photon detectors. Coincidences are recorded with a coincidence unit clocked by the infrared laser pulses. Pol. are linear polarizers and Filter labels the narrow band filter with $\Delta\lambda_{FWHM} = 2.8\text{nm}$.

5.4 Experimental setup

A schematic diagram of our experimental setup is shown in Fig. 5.3. The developed high-intensity ultraviolet laser successively passes through two BBO crystals to generate three polarization-entangled photon pairs [53]. The ultraviolet laser with a central wavelength of 390 nm has a pulse duration of 180 fs, a repetition rate of 76 MHz and an average power of 1.0 W. All three photon pairs are originally prepared in the Bell state $|\Phi^+\rangle = (|HH\rangle + |VV\rangle)/\sqrt{2}$. As we described in last section, besides the high-intensity ultraviolet laser, significant efforts have been made to achieve better collection efficiency and stability of the entangled photon sources. Following these efforts, we managed to observe on average 10^5 photon pairs per second from each source. This is almost five times brighter than the source achieved in recent teleportation experiment [43]. With this high-intensity entangled photon source we could obtain in total 10 six-photon events per minute. This is two orders magnitude higher than any former photonic teleportation experiments could have achieved.

With the help of wave plates and polarizers, we prepared photon pair 1-2 in the desired two-qubit state $|\chi\rangle_{12}$ that is to be teleported. Photon pairs 3-5 and 4-6, which are in the state $|\Phi^+\rangle$, are used as the two ancillary pairs.

To implement two-qubit teleportation, it is necessary to perform a joint BSM on photons 1 and 3 and photons 2 and 4, respectively. To demonstrate the working principle of two-qubit teleportation it is sufficient to identify one of the four Bell-states in both BSMs, although this will result in a reduced efficiency—the fraction of success—of 1/16. In the experiment, we decide to analyze the Bell-state $|\Phi^+\rangle$. This is achieved by interfering photons 1 and 3 and photons 2 and 4 on the polarizing beam-splitters, PBS₁₃ and PBS₂₄, respectively. To interfere photons 1 and 3 (photons 2 and 4) on the PBS₁₃ (PBS₂₄), it has to be guaranteed that the two photons have good spatial and temporal overlap at the PBS such that they are indistinguishable. To achieve this, the two outputs of the PBSs are spectrally filtered ($\Delta\lambda_{FWHM} = 2.8nm$) and monitored by fiber-coupled single-photon detectors [109]. Moreover, perfect temporal overlap is accomplished by adjusting the path length of photon 3 (photon 2) by a delay prism 1 (prism 2) to observe “Hong-Ou-Mandel”-type interference fringes behind the PBS₁₃ (PBS₂₄) in the $+/-$ basis [42]. The required projection of photons 1 and 3 (2 and 4) onto $|\Phi^+\rangle$ can then be achieved by detecting behind PBS₁₃ (PBS₂₄) a $|+\rangle|+\rangle$ or $|-\rangle|-\rangle$ coincidence between detectors D1 and D3 (D2 and D 4) [42]. Note that, in the experiment, only the $|+\rangle|+\rangle$ coincidence is registered, which further reduces the teleportation efficiency to 1/64. However, by inserting one PBS and two detectors behind each output of PBS₁₃ and PBS₂₄, respectively, both $|\Phi^+\rangle$ (by detecting a $|+\rangle|+\rangle$ or $|-\rangle|-\rangle$ coincidence) and $|\phi^-\rangle$ (by detecting a $|+\rangle|-\rangle$ or $|-\rangle|+\rangle$ coincidence) can be identified and thus the efficiency can be increased up to 1/4 [104].

As shown in equations (5.3) and (5.4), the projection measurements onto $|\Phi^+\rangle_{13}$ and $|\Phi^+\rangle_{24}$ leave photons 5 and 6 in the state $|\chi\rangle_{56}$, that is, the original state of photons 1 and 2. To demonstrate that our two-qubit teleportation protocol works for a general unknown polarization state of photons 1 and 2, we decide to teleport three different initial states: $|\chi\rangle_A = |H\rangle_1|V\rangle_2$, $|\chi\rangle_B = (|H\rangle_1 + |V\rangle_1)(|H\rangle_2 - i|V\rangle_2)/2$ and $|\chi\rangle_C = (|H\rangle_1|V\rangle_2 - |V\rangle_1|H\rangle_2)/\sqrt{2}$. $|\chi\rangle_A$ is simply one of the four computational basis vectors in the two-qubit Bloch sphere; $|\chi\rangle_B$ is composed by a linear polarization state and a circular polarization state, which is also a superposition of all the four computational basis vectors; and $|\chi\rangle_C$ is a maximally entangled state.

5.5 Experimental results

We quantify the quality of our teleportation experiment by looking at the fidelity as defined by

$$F = Tr(\hat{\rho}|\chi\rangle\langle\chi|) \quad (5.6)$$

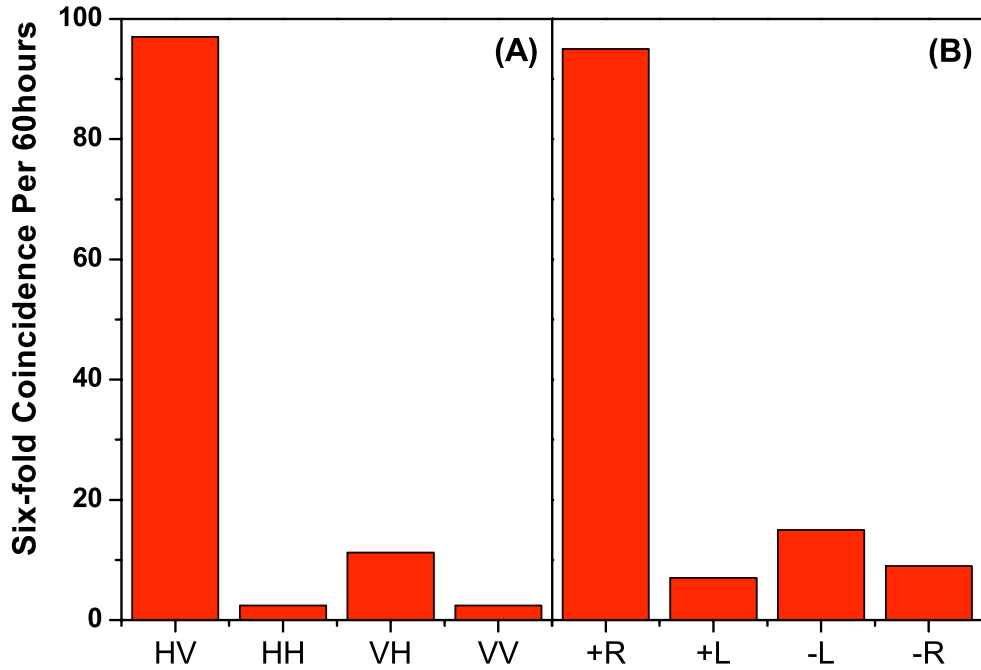


Figure 5.4: Experimental results for the teleportation of the $|\chi\rangle_A$ state and the $|\chi\rangle_B$ state. Each measurement takes 60 h. **A**, The $|\chi\rangle_A$ state. We measured photon 5 and 6 in $|H\rangle/|V\rangle$ basis. **B**, The $|\chi\rangle_B$ state. We measured photon 5 in $|+\rangle/|-\rangle$ basis and photon 6 in $|R\rangle/|L\rangle$ basis. The fraction of $|H\rangle|V\rangle$ ($|+\rangle|R\rangle$) to the sum of all counts shows the fidelity for the teleportation of the $|\chi\rangle_A$ ($|\chi\rangle_B$) state in **A** (**B**).

where $|\chi\rangle$ is the original state and $\hat{\rho}$ is the density matrix of the teleported state. To measure the fidelity of two-qubit teleportation, two PBSs (PBS₅ and PBS₆) and corresponding wave plates (HWP and QWP), as shown in Fig. 5.3, are combined properly to analyze the teleported state of photons 5 and 6.

The fidelity measurements for the $|\chi\rangle_A$ and $|\chi\rangle_B$ teleportation are straight forward. Conditioned on detecting a $|+\rangle|+\rangle$ coincidence between D1 and D3, D2 and D4, respectively, we analyze the teleported state of photons 5 and 6 in the H/V basis for the $|\chi\rangle_A$ teleportation; whereas we analyze photon 5 in the \pm basis and photon 6 in the R/L basis for the $|\chi\rangle_B$ teleportation. As the above state analysis only involves orthogonal measurements on individual qubits, the fidelity of the teleported state is directly given by the fraction of observing a $|\chi\rangle_A$ or $|\chi\rangle_B$ state at detectors D5 and D6. The measurement results are shown in Fig. 5.4. The experimental integration time for each fidelity measurement was about 60 hours and we recorded about 100 desired two-qubit teleportation events. The intergration time is slightly longer than would be expected from the original source rate, due to the additional losses at the interference PBSs. On the basis of our original data, we conclude that the fidelity for $|\chi\rangle_A$ or $|\chi\rangle_B$ is 0.86 ± 0.03 or 0.75 ± 0.02 , respectively.

The measurement on the fidelity of the $|\chi\rangle_C$ teleportation is a bit more complex, since a complete Bell-state analysis on photons 5 and 6 usually requires nonlinear interaction between them. Fortunately, the fidelity can still be determined by local measurements on individual qubits.

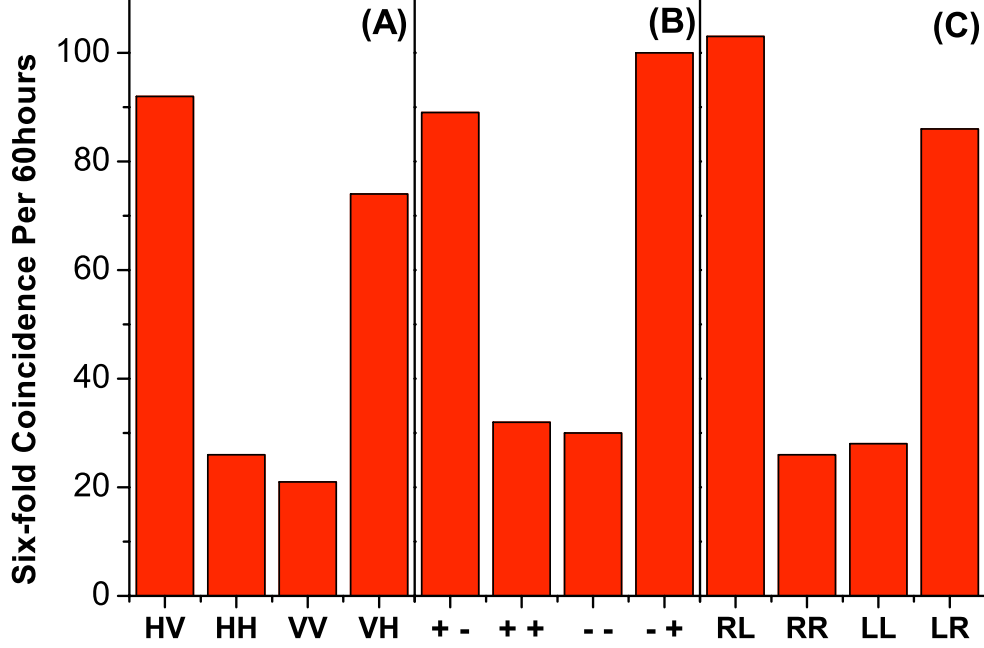


Figure 5.5: Experimental results for $|\chi\rangle_C$ teleportation. Three complementary bases were used: (A) $|H\rangle/|V\rangle$, (B) $|+\rangle/|-\rangle$ and (C) $|R\rangle/|L\rangle$ corresponding to the three different local measurements $\hat{\sigma}_x\hat{\sigma}_x$, $\hat{\sigma}_y\hat{\sigma}_y$ and $\hat{\sigma}_z\hat{\sigma}_z$. Each measurements takes 60 h. In (A) whenever there is a $|H\rangle|H\rangle$ or $|V\rangle|V\rangle$ coincidence, the result of the $\hat{\sigma}_x\hat{\sigma}_x$ is +1, whereas $|H\rangle|V\rangle$ or $|V\rangle|H\rangle$ represents -1. In (B), $|+\rangle|+\rangle$ or $|-\rangle|-\rangle$ represents +1, whereas $|+\rangle|-\rangle$ or $|-\rangle|+\rangle$ represents -1. In (C), $|R\rangle|R\rangle$ or $|L\rangle|L\rangle$ displaces +1, whereas $|R\rangle|L\rangle$ or $|L\rangle|R\rangle$ displaces -1.

To see this, we write the density matrix of $|\chi\rangle_C$ in terms of the Pauli matrices:

$$|\chi\rangle_C \langle\chi| = |\Psi^-\rangle \langle\Psi^-| = \frac{1}{4}(\hat{I} - \hat{\sigma}_x\hat{\sigma}_x - \hat{\sigma}_y\hat{\sigma}_y - \hat{\sigma}_z\hat{\sigma}_z). \quad (5.7)$$

By Eq. (5.6), we have:

$$F = Tr(\hat{\rho} |\Psi^-\rangle \langle\Psi^-|) = \frac{1}{4}Tr[\hat{\rho}(\hat{I} - \hat{\sigma}_x\hat{\sigma}_x - \hat{\sigma}_y\hat{\sigma}_y - \hat{\sigma}_z\hat{\sigma}_z)]. \quad (5.8)$$

This implies that, we can obtain the fidelity of $|\chi\rangle_C$ teleportation by consecutively carrying out three local measurements $\hat{\sigma}_x\hat{\sigma}_x$, $\hat{\sigma}_y\hat{\sigma}_y$ and $\hat{\sigma}_z\hat{\sigma}_z$ on the two teleported qubits. The measurement results for the three operators are shown in Fig. 5.5, each of which took about 60 hours. Using equation (5.8) we determine an experimental fidelity of 0.65 ± 0.03 .

5.6 Discussion

As can be seen from the above experimental results, all the teleportation fidelities are well beyond the state estimation limit of 0.40 for a two-qubit composite system [131], hence successfully demonstrating quantum teleportation of a two-qubit composite system. The imperfection of the fidelities

| Original States | Fidelities | Fidelities after subtraction of noise |
|--|-----------------|---------------------------------------|
| $ H\rangle V\rangle$ | 0.86 ± 0.03 | 0.97 ± 0.03 |
| $(H + V\rangle H - iV\rangle)/2$ | 0.75 ± 0.02 | 0.83 ± 0.02 |
| $(H\rangle V\rangle - V\rangle H\rangle)/\sqrt{2}$ | 0.65 ± 0.03 | 0.77 ± 0.03 |
| Average | 0.75 ± 0.03 | 0.86 ± 0.03 |

Table 5.1: Fidelities of quantum teleportation of a two-qubit composite system.

is mainly due to the noise caused by emission of two pairs of down-converted photons by a single source [31]. In our experiment, this noise contributes around 10 spurious six-fold coincidences in 60 h and was not subtracted in the fidelity estimation. As comparison, by taking into account the experimental parameters, as done in a former experiment [31], subtracting this kind of noise clearly improves the fidelities, as shown in the last column of Table 5.1. Besides the double pair emission, the limited interference visibility and imperfect entangled state also reduce our teleportation fidelities. We notice that the fidelities of $|\chi\rangle_B$ and $|\chi\rangle_C$ teleportation are worse than those of $|\chi\rangle_A$. This is because the fidelities of $|\chi\rangle_B$ and $|\chi\rangle_C$ teleportation depend on the interference visibility on PBS13 and PBS24, while the $|\chi\rangle_A$ teleportation fidelity does not. Moreover, as the quality of the initial entangled state $|\chi\rangle_C$ is not as good as for the disentangled states $|\chi\rangle_A$ and $|\chi\rangle_B$, the fidelity of $|\chi\rangle_C$ teleportation is worse than that of the other two.

In summary we have developed and exploited a six-photon interferometer to report the first experimental demonstration of a two-qubit composite system. Not only does our experiment present an important step towards teleportation of a complex system, the techniques developed also enable immediate experimental investigations on novel quantum communication and computation protocols. First, by reinterpreting the teleportation of state as a process of entangling two distant photons 5 and 6 that never interacted our experiment can be seen as a two-stage realization of entanglement swapping, which allows new studies on the advantages of quantum relay [125]. Second, exactly the same experimental setup used in the teleportation can be used to observe a six-photon Schrödinger Cat state and test its quantum nonlocality [92]. Moreover, using a slightly modified experimental setup one can first prepare photons 3, 4, 5 and 6 in a four-photon cluster state [132] and further exploit the four-photon cluster state to demonstrate teleportation-based CNOT operation between photons 1 and 2, which is the kernel of fault-tolerant quantum computation [18]. Finally, whereas a modified six-photon interferometer can be used to prepare a six star-ring cluster state [133] and further implement universal quantum error-correction code [134] by performing a projection measurement on the input qubit, our six-photon interferometer can also be modified to produce various four, five and six-photon clusters [84] which are essential resources for one-way quantum computation [23, 51].

Chapter 6

One-way quantum computing

6.1 Introduction

Highly entangled multipartite states, so-called cluster states, have recently raised enormous interests in quantum information processing. This sort of states are crucial to be a fundamental resource and a building block aiming at one-way universal quantum computing [23, 24, 135]. They are also the essential elements for various quantum error correction codes and quantum communication protocols [136, 130]. Moreover the entanglement are shown to be robust against decoherence [137], be persistent against loss of qubits [24], and thus are exceptionally well suitable for quantum computing and many tasks [23, 24, 135, 136, 130]. Considerable efforts have been stepped toward generating and characterizing cluster states in linear optics [84, 138, 139, 51, 140, 141, 45]. Recently the principal feasibility of one-way quantum computing model has been experimentally demonstrated through 4-photon cluster state successfully [51, 141, 142].

So far, preparing photonic cluster state still suffers from several serious limitations. Due to the probabilistic nature and Poissonian distribution of the parametric down-conversion process, the generation rate of 4-photon cluster states is quite low [139, 138, 51, 141], and largely restricts speed of computing. Besides, the quality and fidelity of prepared cluster states are relatively low [138, 51, 141], which are difficult to be improved substantially. These disadvantages consequently impose great challenges of advancement even for few-qubit quantum computing.

Fortunately, motivated by the progress that an important type of states termed hyper-entangled states have been experimentally generated [55, 56, 143, 144], we have the possibility to produce a new type of cluster state (2-photon 4-qubit cluster state) with nearly perfect fidelity and high generation rate. The hyper-entangled states have been used to test “All-Versus-Nothing” (AVN) quantum nonlocality [145, 146, 55, 56], and are shown to lead to an enhancing violation of local realism [147, 148]. The states also enable to perform complete deterministic Bell state analysis [149] as demonstrated in [144, 150].

In this chapter, we present an experimental realization of one-way quantum computing with such a 2-photon 4-qubit cluster state. The key idea is to develop and employ a bright source which produces a 2-photon state entangled both in polarization and spacial modes. We are thus able to implement the Grover’s algorithm and quantum gates with excellent performances. The genuine four-partite entanglement and high fidelity of better than 88% are characterized by an optimal entanglement witness. Inheriting the intrinsic two-photon character, our scheme promises a brighter source by 4 orders of magnitude than the usual multi-photon source, which offers a significantly high efficiency for optical quantum computing. It thus provides a simple and fascinating alternative to complement the latter. With ease of manipulation and control, the nearly perfect quality of this source allows to perform highly faithful and precise quantum computing.

6.2 State preparation

The desired four-particle cluster state can be written in the form

$$|C_4\rangle = (|0000\rangle_{1234} + |0011\rangle_{1234} + |1100\rangle_{1234} - |1111\rangle_{1234})/2. \quad (6.1)$$

To generate the cluster state, unlike the experiments presented in former chapters, we use the technique developed in previous experiments [55] with type-I SPDC source [151] instead of type-II SPDC source. The experimental setup is shown in Fig. 6.1a. A pump pulse of ultraviolet light has a central wavelength of 355 nm with a repetition rate of 80 MHz and an average power of 200 mW. After it pass through two contiguous BBO with optic axes aligned in perpendicular planes, with a small probability, via the parametric down-conversion, it produce a polarization entangled photon pair in the forward direction with a state

$$\frac{1}{\sqrt{2}}(|H\rangle_A |H\rangle_B + |V\rangle_A |V\rangle_B) \quad (6.2)$$

on spacial (path) modes $L_{A,B}$. Now if the pump pulse is reflected and passes through the BBO crystal a second time, then by properly adjust the QWP for another possibility, it generate polarization entangled photon pairs in the backward direction with a state

$$\frac{1}{\sqrt{2}}(|H\rangle_A |H\rangle_B - |V\rangle_A |V\rangle_B) \quad (6.3)$$

on modes $R_{A,B}$.

Through perfect temporal overlaps of modes R_A and L_A and of modes R_B and L_B , one can obtain a state with coherent superposition

$$\left((|H\rangle_A |H\rangle_B + |V\rangle_A |V\rangle_B) |L\rangle_A |L\rangle_B + e^{i\theta} (|H\rangle_A |H\rangle_B - |V\rangle_A |V\rangle_B) |R\rangle_A |R\rangle_B \right) / 2. \quad (6.4)$$

By properly adjusting the distance between the concave mirror and the crystal so that $\theta = 0$, the state (6.4) will be

$$\left((|H\rangle_A |H\rangle_B + |V\rangle_A |V\rangle_B) |L\rangle_A |L\rangle_B + (|H\rangle_A |H\rangle_B - |V\rangle_A |V\rangle_B) |R\rangle_A |R\rangle_B \right) / 2. \quad (6.5)$$

To do so, the concave mirror and the prism are scanned by a motor translation stage and piezo translation stage respectively. The interference fringe is observed, as shown in Fig. 6.2, by measuring the twofold coincidence between the output modes toward detectors D_1 and D_2 behind 22.5° HWPs and corresponded PBSs. By setting the piezo system to a position where we observe maximum twofold coincidence of $D_1 - D_2$, we achieve $\theta = 0$.

In this way, the generated state will be exactly the desired cluster state (6.1) if we identify photon A to be qubits 2,3 and photon B to be qubits 1,4 and encode logical qubits as

$$\begin{aligned} |H(V)\rangle_B &\leftrightarrow |0(1)\rangle_1 \\ |H(V)\rangle_A &\leftrightarrow |0(1)\rangle_2 \\ |L(R)\rangle_A &\leftrightarrow |0(1)\rangle_3 \\ |L(R)\rangle_B &\leftrightarrow |0(1)\rangle_4. \end{aligned} \quad (6.6)$$

We observe a cluster state generation rate about 1.2×10^4 per second for 200mw ultraviolet pump, which is 4 order of magnitude brighter than the usual 4-photon cluster state production [51, 141, 138] where only a rate of about 1 per second is achieved .

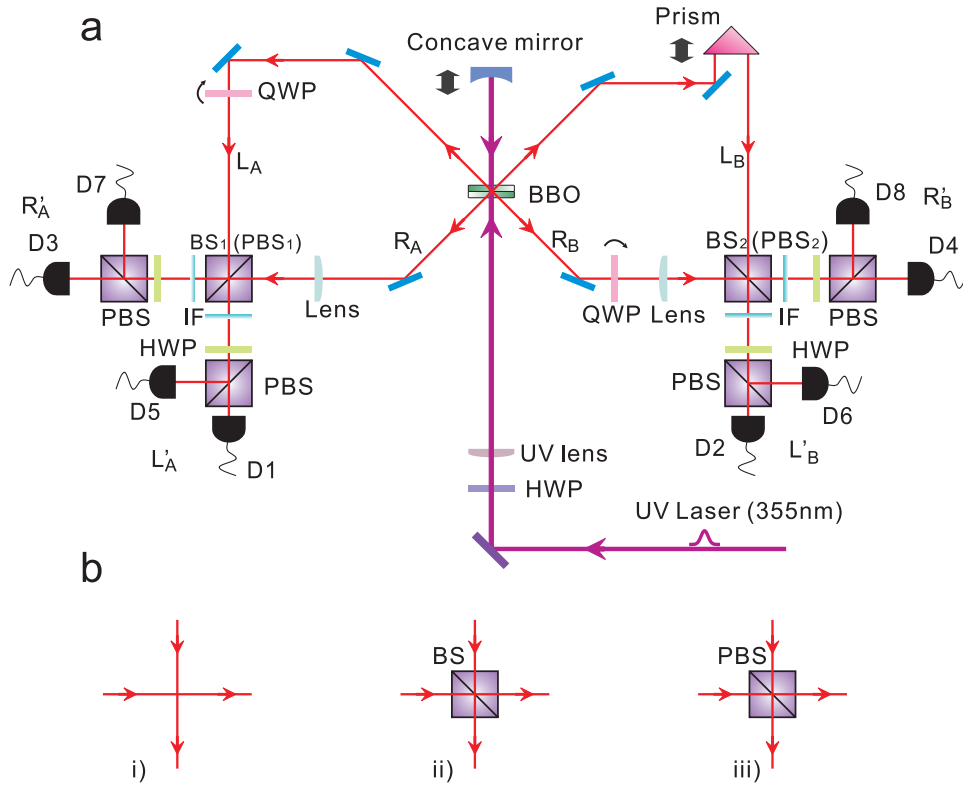


Figure 6.1: Schematic of experimental setup. (a). By pumping a two-crystal structured in a double pass configuration, one polarization entangled photon pair is generated either in the forward direction or in the backward direction. Two QWPs are tilted along their optic axis to vary relative phases between polarization components to attain two desired possibilities for entangled pair creation. Concave mirror and prism are mounted on translation stages to optimize interference on two beam splitters (BS_{1,2}) or polarizing beam splitters (PBS_{1,2}) for achieving the target cluster state. HWPs together with PBS and 8 single-photon detectors (D1-D8) are used for polarization analysis of the output state. IF are 3 nm filters with central wavelength 710 nm. (b). In the place where BS_{1,2} or PBS_{1,2} are located, three apparatuses are for measuring all necessary observables. Setup (i) is for Z measurement while setup (ii) is used for X measurement for spacial modes. If an α phase shifter is inserted at one of the input modes in (ii), an arbitrary measurement along basis $B(\alpha)$ can be achieved. Setup (iii) can be for Z measurement of spacial mode and, simultaneously, for Z measurement of polarization.

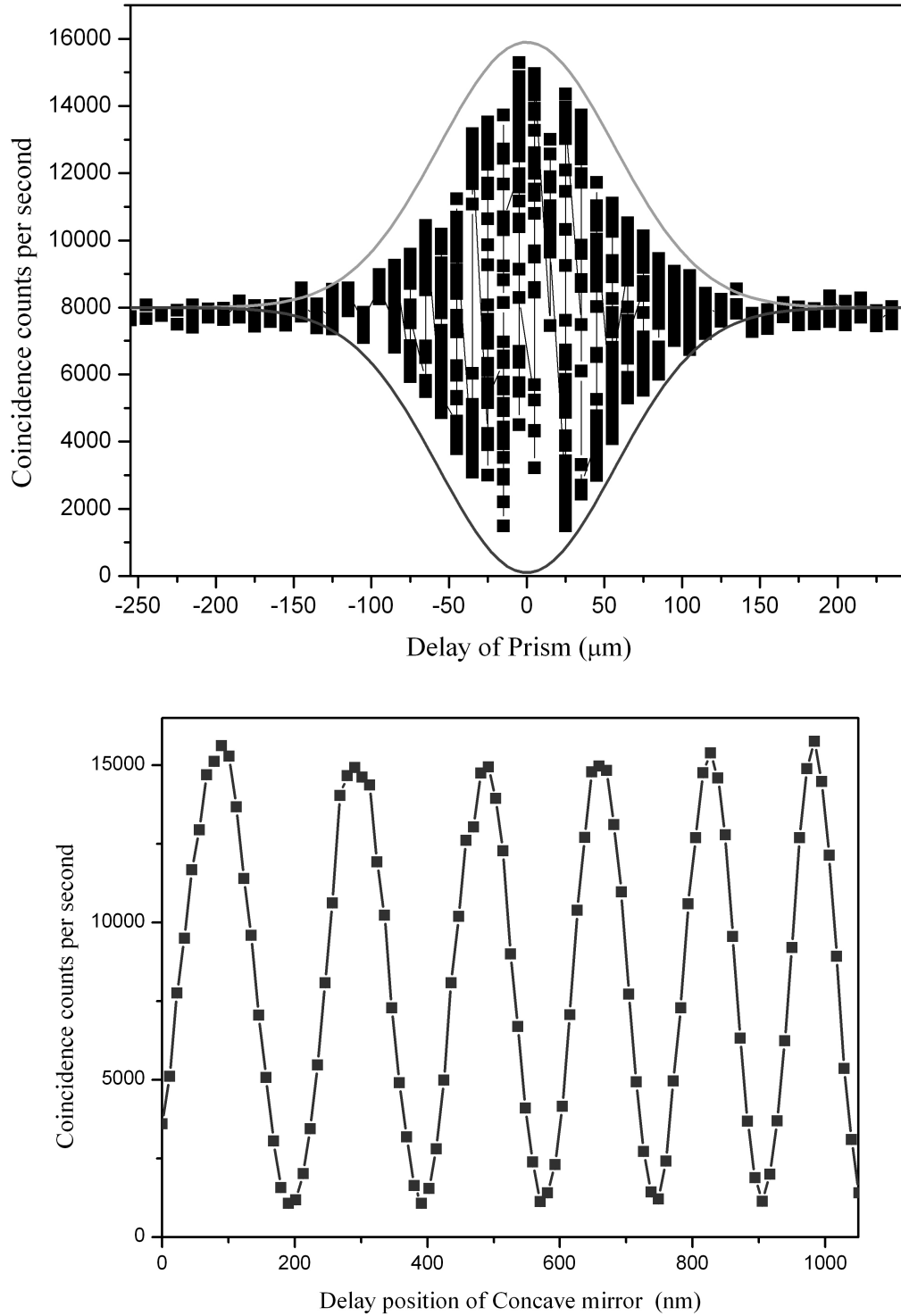


Figure 6.2: Interference fringe observed when the concave mirror and the prism being moved to achieve perfect temporal overlap and to adjust the phase $\theta = 0$. **a** We measure the two fold coincidence between the output modes toward detectors D_1 and D_2 behind 22.5° HWP and PBS, by scanning the position of the prism. The envelope of the observed twofold coincidence varies indicating the visibility of the two photon coherence. Inside the coherent region, the best visibility is obtained at the position where perfect temporal overlap is achieved. **b** We use a piezo translation stage to move the concave mirror to perform a fine scan around the centre of the envelope. By setting the piezo system to a position where we observe maximum twofold coincidence of D_1 - D_2 , we then achieve $\theta = 0$.

| Observable | Value | Observable | Value |
|------------|---------------------|------------|---------------------|
| $XXIZ$ | 0.9070 ± 0.0036 | $IZXX$ | 0.9071 ± 0.0037 |
| $XXZI$ | 0.9076 ± 0.0035 | $ZIXX$ | 0.8911 ± 0.0040 |
| $IIZZ$ | 0.9812 ± 0.0016 | $ZZII$ | 0.9372 ± 0.0030 |

Table 6.1: Experimental values of all the observable on the state $|C_4\rangle$ for the entanglement witness \mathcal{W} measurement. Each experimental value corresponds to measure in an average time of 1 sec and considers the Poissonian counting statistics of the raw detection events for the experimental errors.

6.2.1 State analysis

To evaluate the quality of the state, we apply an optimal entanglement witness [152]. The witness is of form

$$\mathcal{W} = \left(4 \cdot I^{\otimes 4} - (XXIZ + XXZI + IIZZ + IZXX + ZIXX + ZZII) \right) / 2, \quad (6.7)$$

where I is a 2-dimensional identity matrix while

$$\begin{aligned} Z &= (|0\rangle\langle 0| - |1\rangle\langle 1|), \\ X &= (|0\rangle\langle 1| + |1\rangle\langle 0|) \end{aligned} \quad (6.8)$$

are Pauli matrices. A negative value for the witness implies 4-partite entanglement for a state close to $|C_4\rangle$ and will be optimally as -1 for a perfect cluster state. Two experimental settings of $XXZZ$ and $ZZXX$ are needed. $XXZZ$ can be attained by measuring in the $+/-$ basis for the polarization in each output arm after apparatus (i) in Fig. 6.1b. while $ZZXX$ can be realized by measuring in the H/V basis after apparatus (ii). This is because BS acts exactly as a Hadamard transformation for the path modes to change Z basis to X basis for measurement, namely,

$$\begin{aligned} |L\rangle_{A,B} &\rightarrow \frac{1}{\sqrt{2}}(|R'\rangle_{A,B} + |L'\rangle_{A,B}) \\ |R\rangle_{A,B} &\rightarrow \frac{1}{\sqrt{2}}(|R'\rangle_{A,B} - |L'\rangle_{A,B}). \end{aligned} \quad (6.9)$$

All of the observables for evaluating the witness are listed in Table 6.1. Substituting their experimental values into Eq. (6.7) yields $\langle \mathcal{W} \rangle_{exp} = -0.766 \pm 0.004$, which clearly proves the genuine four-partite entanglement by about 200 standard deviations. As shown in [152], one can obtain a lower bound for fidelity of experimental prepared state to $|C_4\rangle$

$$F \geq \frac{1}{2} - \frac{1}{2} \langle \mathcal{W} \rangle_{exp} = 0.883 \pm 0.002. \quad (6.10)$$

This proves to be a better cluster source than the ones in [51, 141, 138] where fidelities are about 0.63 [51, 141] and 0.74 [138] respectively. We attribute impurity of our state to imperfect overlapping on BS, deviations of BS from 50%, as well as imperfections in the polarization and path modes analysis devices. To get a qualitative depiction for these imperfections, we scan the concave mirror with piezo translation stage displacements and observe interference after $BS_{1,2}$. By measuring along H/V basis in each output arm, we have obtained visibility of $0.842 \pm 0.008, 0.943 \pm 0.006, 0.968 \pm 0.004, 0.949 \pm 0.006$ for coincidences among detectors D1-D2, D1-D4, D3-D2 and D3-D4 respectively.

6.3 Cluster state based one-way computing

A cluster state can be represented by an array of nodes, where each node is initially in the state of $|+\rangle = (|0\rangle + |1\rangle)/\sqrt{2}$. Every connected line between nodes experiences a controlled-phase

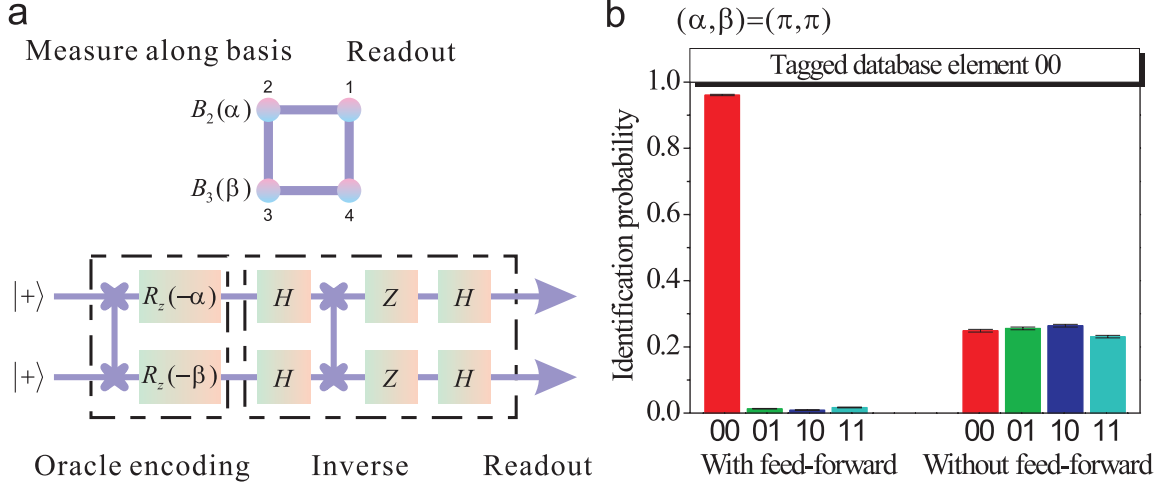


Figure 6.3: Demonstration of Grover’s algorithm. **a.** Equivalent quantum circuit of Grover’s algorithm using box cluster state. The ‘oracle’ encodes the element ‘00’ by measuring along basis $B_{2,3}(\pi)$, while the inverse and readout sections will find this entry with certainty by a single query. **b.** A successful identification probability of $(96.1 \pm 0.2)\%$ is achieved deterministically with feed-forward, while it is $(24.9 \pm 0.4)\%$ without feed-forward. This is in an excellent agreement with theoretical expectations. The trick is that the black box provides only outcomes but not basis information for feed-forward. Thus the oracle encoding is hidden before feed-forward on readout.

(“CPhase”) gates acting as [24, 23, 135]

$$|j\rangle|k\rangle \rightarrow (-1)^{jk} |j\rangle|k\rangle, \quad j, k \in \{0, 1\}. \quad (6.11)$$

For a given cluster state, consecutive single-qubit measurements in basis $B_k(\alpha) = \{|\alpha_+\rangle_k, |\alpha_-\rangle_k\}$ will define a quantum computing in addition to feed-forward of measurement outputs, where

$$|\alpha_{\pm}\rangle_k = (|0\rangle \pm e^{i\alpha} |1\rangle)_k / \sqrt{2}, \quad (\alpha \in \mathbb{R}). \quad (6.12)$$

A measurement output of $|\alpha_+\rangle_k$ means ‘0’ while $|\alpha_-\rangle_k$ signifies ‘1’. This measurement basis determines a rotation $R_z(\alpha) = \exp(-i\alpha Z/2)$, followed by a Hadamard operation $H = (X + Z)/\sqrt{2}$ of encoded qubits. The state $|C_4\rangle$ can be represented by a box type graph shown in Fig. 6.3a, up to a local unitary transformation.

6.3.1 Grover’s algorithm

For an unsorted database with N entries, Grover’s search algorithm gives a quadratic speed-up for with $\sim \sqrt{N}$ consultations on average [22]. Striking linear optics implementations have been achieved in [153, 154], although it is questionable whether the algorithm is truly ‘quantum’ due to a demonstration [154] based on interference of classical waves. One-way realizations have been carried out [51, 141] recently. In the case of four entries $|00\rangle, |01\rangle, |10\rangle, |11\rangle$, a single quantum search will find the marked element. An execution goes as follows: an oracle encodes a desired entry by changing its sign through a black box with initial state $|++\rangle$. After an inversion-about-the-mean operation, the labeled element will be found with certainty by readout. It is shown in [51] that this can be exactly finished with the box cluster state in Fig. 6.3a. For demonstration, we experimentally tag the element $|00\rangle$ on qubits 2, 3 and make the readout on qubits 1, 4 all along basis $B(\pi)$. Noting the fact that the state Eq. (6.1) differs the box cluster from a H transformation

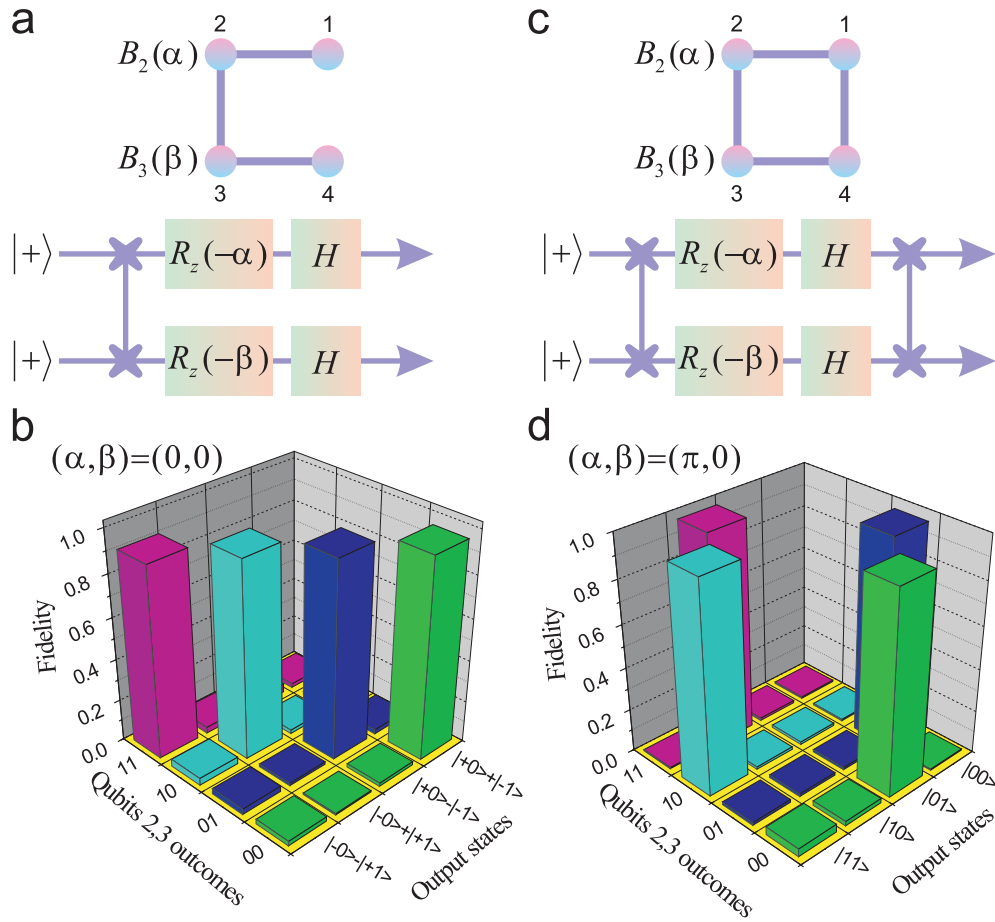


Figure 6.4: Two-qubit quantum gates realizations. **a.** CPhase gate realization with the horseshoe cluster. **b.** Experimental measured fidelities of output states to the ideal Bell states (unnormalized) in the lab basis. They are 0.954 ± 0.003 , 0.940 ± 0.004 , 0.936 ± 0.005 , 0.910 ± 0.005 for outcomes 00,01,10,11 on qubits 2,3 respectively. **c.** Quantum gate implementation that does not generate entanglement with the box cluster. **d.** Measured fidelities of output states to the ideal product states in the lab basis. They are 0.935 ± 0.005 , 0.962 ± 0.004 , 0.969 ± 0.003 , 0.975 ± 0.003 for outcomes 00,01,10,11 on qubits 2,3 respectively.

on every qubit and a swap between qubits 2 and 3, this amounts to measure along the V/H basis after apparatus (iii) in Fig. 6.1b. Two PBS here are for interfering, to ensure the desired cluster state. In the meantime they are acting as polarization measurement devices, which is equivalent to use apparatus (i) in this case. The outputs of the algorithm are two bits $\{s_3 \oplus s_4, s_1 \oplus s_2\}$ in lab basis by feed-forwarding outcomes of qubits 2,3, where s_i are measurement outcomes on qubits i . The experimental results are sketched in Fig. 6.3b.

6.3.2 Quantum gates

Non-trivial two-qubit quantum gates such as the CPhase gate are at the heart of universal quantum computation, that can be realized by cluster states conveniently. Depending on the initial cluster state and measurement basis, states with different degrees of entanglement can be generated. The horseshoe or box cluster shown in Fig. 6.4a and 6.4c can realize such important gates. For the case of horseshoe cluster in Fig. 6.4a, depending on the outcomes when measuring along basis $B_2(\alpha)$

and $B_3(\beta)$, the output state on qubits 1,4 would be

$$|\Omega_{out}\rangle = (X^{s_2} \otimes X^{s_3})(H \otimes H)(R_z(-\alpha) \otimes R_z(-\beta))\text{CPhase}|\Omega_{in}\rangle \quad (6.13)$$

where $|\Omega_{in}\rangle = |++\rangle$. The state $|\Omega_{out}\rangle$ is always a maximal entangled state. Taking $\alpha = \beta = 0$ and consider outcomes ‘00’ in qubits 2,3. This implies a final Bell state of $|\Omega_{out}\rangle = (|+\rangle|0\rangle + |-\rangle|1\rangle)/\sqrt{2}$. Note that the horseshoe cluster state is equivalent to the state Eq. (6.1) up to a HHH transformation, in lab basis this amounts to the fact that the output state is exactly $|\Omega_{out}\rangle$, that is symmetric under HH transformation. To characterize quality of quantum gates outputs, we put a birefringent crystal in path R_B to make a transformation $|+\rangle \leftrightarrow |-\rangle$ for polarization. After BS_2 , all the Bell states on qubits 1,4 will change as

$$\begin{aligned} (|+\rangle_1|0\rangle_4 \pm |-\rangle_1|1\rangle_4)/\sqrt{2} &\longrightarrow |+\rangle_1|\pm\rangle_4, \\ (|-\rangle_1|0\rangle_4 \pm |+\rangle_1|1\rangle_4)/\sqrt{2} &\longrightarrow |-\rangle_1|\pm\rangle_4, \end{aligned} \quad (6.14)$$

which can be completely and deterministically discriminated by measuring along $|\pm\rangle$ basis. The fidelities of the output states in the lab basis to the ideal Bell state are shown in Fig. 6.4b. Similarly, for the box cluster state shown in Fig. 6.4c, measurements on qubits 2,3 along basis $\{B_2(\alpha), B_3(\beta)\}$ will give an output state on qubits 1,4 with

$$|\Omega_{out}\rangle = (Z \otimes X)^{s_3}(X \otimes Z)^{s_2}\text{CPhase}(H \otimes H)(R_z(-\alpha) \otimes R_z(-\beta))\text{CPhase}|\Omega_{in}\rangle \quad (6.15)$$

which is a product state when $\alpha = \pi$ and $\beta = 0$. Since we can completely distinguish 4 different products states, output fidelities can be obtained directly, as shown in Fig. 6.4d. By employing the techniques developed in [141] with active feed-forward, one can expect to achieve deterministically quantum computing with excellent quality outputs.

6.4 Discussion

We remark that other 2-qubit states can be generated, by suitable measurements on qubits 2,3. However, an arbitrary single-qubit rotation needs generally 3 single-qubit measurements on a cluster for one-way implementation [51, 141], which is a big consuming of resource. Fortunately, this rotation can be easily attained by linear optical components both for polarization and spacial modes. Therefore a hybrid framework would be more practical with one-way realization of two-qubit gates and the usual single-qubit gates. Due to low efficiency for producing multi-photon and concurrent occupations for polarization-spacial degrees of freedom of the photons, our source is not yet scalable, the same as the multi-photon source [141]. However, the scheme developed here leads to quantum computing with a quality and efficiency at present largely unmatched by previous methods.

In summary, we have developed a scheme for preparation of a 2-photon 4-qubit cluster state, designed and demonstrated the first proof-of-principle realization of one-way quantum computing employing such a source. The excellent quality of the state with fidelity better than 88% is achieved. The high count rates enable quantum computing by 4 orders of magnitude more efficient than previous methods. We have implemented the Grover’s algorithm with a successful probability of about 96% and quantum gates with high fidelities of about 95% on average. Our scheme helps to make a significant advancement of quantum information processing, and the source constitutes a promising candidate for efficient and high quality one-way optical quantum computing. By using more photons and more degrees of freedom, one can expand our ability to generate many-qubit cluster states for performing quantum computing and other complex tasks. Our results can also find rapid applications in quantum error correction codes, multi-partite quantum communication protocols [136, 130], as well as novel types of AVN tests for nonlocality [145, 146].

Part II

Manipulation of Atoms: Quantum Memory

Chapter 7

Atomic ensemble based quantum repeater

7.1 Introduction

While photons are the ideal information carriers for long-distance quantum communication, the photon losses and the decoherence which both scales exponentially with the length of the communication channel. Entangled swapping [33, 3] and entanglement purification [35, 37] are proposed to solve these two serious problems. Significant experimental advances in both proposals have been achieved [34, 155, 38, 98] in laboratory via SPDC source, however, the probabilistic property of SPDC source makes the the requirement of resources increases exponentially with the communication length. Fortunately, the quantum repeater protocol [17, 68] enables to establish high-quality long-distance entanglement in the communication time increasing only polynomially with transmission distance.

Early physical implementations of a quantum repeater were based on atoms trapped in high-finesse cavities [69], where strong coupling between atoms and photons is required. However, these techniques require a extremely complicated experimental setup. In a seminal paper [70], Duan *et al.* (DLCZ) proposed an implementation of the quantum repeater by using atomic ensembles and linear optics. In this protocol atomic ensembles are used as memory qubits to avoid the challenging requirement for strong coupling between atoms and photons. In the efforts of realizing the atomic ensemble based quantum repeater protocol, significant experimental advances have been achieved recently. Non-classical correlated photon pairs were generated from a MOT and a hot vapor cell [71, 72]. Controllable single photons were generated from atomic ensembles with the help of “event-ready” detection and feedforward circuit [73, 74, 75]. Interference of photons emitted from different atomic ensembles are studied [76, 77, 78]. Entanglement between two atomic ensembles either in the same MOT or in two MOTs were generated by detecting single photons [79, 80] and used for memory-built-in quantum teleportation between photonic and atomic qubits [81]. Recently, a segment of the DLCZ protocol was demonstrated [82].

However, the DLCZ protocol has an inherent drawback which is severe enough to make long-distance quantum communication extremely difficult [156]. In this Chapter, first we will introduce the basic conception of original DLCZ protocol and show that the phase stability problem in the DLCZ protocol is so severe that it makes a long-distance quantum communication impossible. Then we will propose a robust quantum repeater architecture building on the DLCZ protocol, which is insensitive to phase stability. The robustness is improved about 7 orders of magnitude higher in comparison with the original DLCZ protocol.

7.2 The DLCZ protocol

7.2.1 Light-atoms coupling

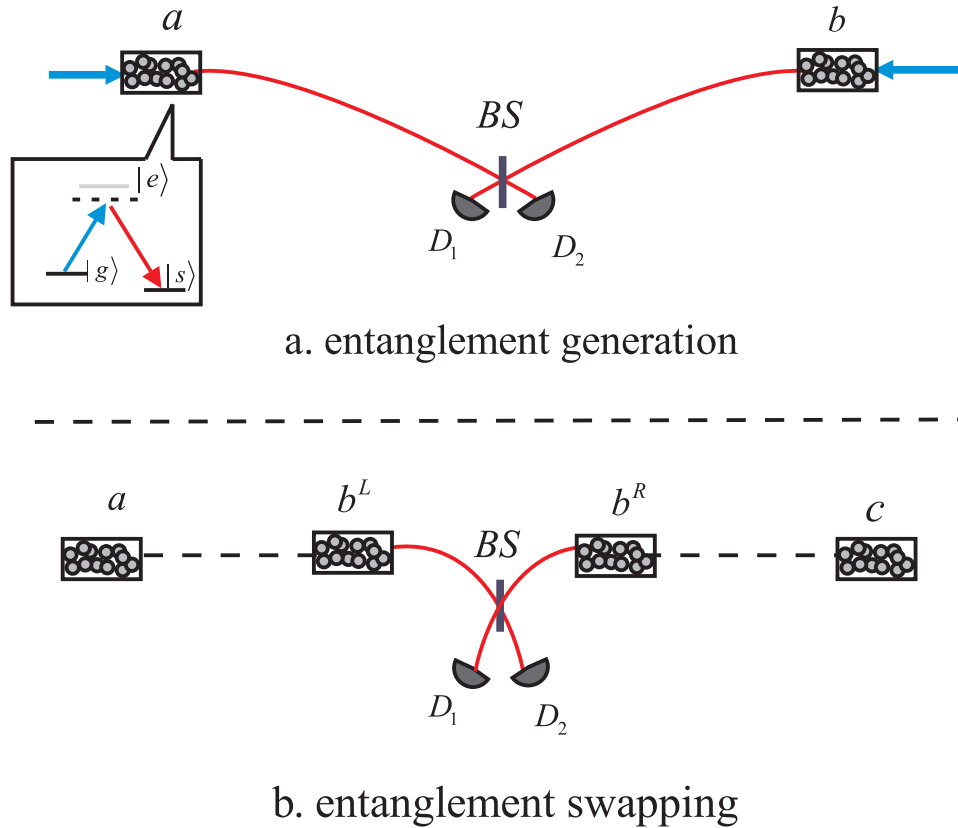


Figure 7.1: Setups for entanglement generation and entanglement swapping in the DLCZ protocol. a). Forward-scattered anti-Stokes photons, generated by an off resonant Write laser pulse via spontaneous Raman transition, are directed to beam splitter (BS) at the center. Entanglement is generated between atomic ensembles at sites a and b , once there is a click on either of the detectors. The inset shows the atomic level structure, with a pair of metastable state $|g\rangle$ and $|s\rangle$, and excited state $|e\rangle$. b). Entanglement has been generated between atomic ensembles (a, b^L) and (b^R, c) . The atomic ensembles at site b are illuminated by near resonant Read laser pulses, and the retrieved Stokes photons are subject to BS at the center. A click on either of the detectors will prepare the atomic ensembles at a and c into an entangled state.

Let us first consider a pencil shaped atomic sample of N atoms with Λ level structure (see inset in Fig. 7.1), a pair of metastable lower states $|g\rangle$ and $|s\rangle$ and the excited state $|e\rangle$. Initially, all the atoms are prepared in the ground state $|g\rangle$. The so-called “Write” pulse, an off-resonant weak light pulse with the transition $|g\rangle \rightarrow |e\rangle$, induces a spontaneous Raman transition into the metastable atomic state $|s\rangle$, which prepares the forward-scattered anti-Stokes mode¹ and collective

¹The radiation emitted during Raman scattering is separated by its detuning from the original laser frequency: red detuned radiation has the name Stokes light, while the blue detuned is called anti-Stokes light. Since in all the experiments described in Part II, the initial ground state has a higher energy level as the other metastable state, thus we call the light field scattered by ‘Write’ process as anti-Stokes light and the one by ‘Read’ process as Stokes light.

atomic state into a two mode squeezed state [70]. The light-atom system can be described as

$$|\psi\rangle = |0_a 0_s\rangle + e^{i\phi} \sqrt{\chi} S^\dagger a^\dagger |0_a 0_s\rangle + O(\chi) \quad (7.1)$$

where ϕ is an phase which is determined by that of the write pulse, $|0_a\rangle = \bigotimes_i |g\rangle_i$ is the ground state of the atomic ensemble and $|0_s\rangle = |vac\rangle$ denotes the vacuum state of the Stokes photons. Here, a^\dagger is the creation operator of the Stokes mode, and the collective atomic excitation operator is defined by $S^\dagger = \frac{1}{\sqrt{N}} \sum_i |s\rangle_i \langle g|$, since one is not able to tell which atom is transferred. The small excitation probability $\chi \ll 1$ can be achieved by manipulating the write laser pulse [157].

The pair of metastable lower states $|g\rangle$ and $|s\rangle$ can be hyperfine or Zeeman sublevels of the electronic ground state of alkali-metal atoms so that collective atomic state has a long coherence lifetime. By sending in a so-called ‘‘Read’’ pulse resonant with the transition $|s\rangle \rightarrow |e\rangle$, the collective spin excitation can be retrieved back to Stokes light field at the transition $|e\rangle \rightarrow |g\rangle$. The reading process is closely related to an electromagnetically induced transparency process [158]. The resultant state of the anti-Stokes – Stokes modes can be written as

$$|\psi\rangle_{AS,S} = |0\rangle_{AS} |0\rangle_S + e^{i\phi'} \sqrt{\chi} |1\rangle_{AS} |1\rangle_S + O(\chi), \quad (7.2)$$

ϕ' is determined by both write and read pulses. Thus, the photon numbers in the two modes are correlated. The nonclassical correlation between anti-Stokes and Stokes are experimentally verified and will be described in Chapter 8. Moreover, an anti-Stokes detection click will herald the atoms in the collective state $S^\dagger |vac\rangle$, and thus can be used to generate single photons on demand (see also Chapter 8).

7.2.2 Entanglement generation

The schematic entanglement generation setup is shown in Fig. 7.1a. Let us consider two atomic ensembles at site a and b at a distance of $L_0 \leq L_{att}$, with L_{att} the channel attenuation length². Two write pulses excite both ensembles simultaneously, and the anti-Stokes photons generated from both sites are directed to the beam splitter (BS) at the center. Once there is a click on the detectors, entanglement between communication sites a and b is established

$$|\psi\rangle_{a,b} = (S_a^\dagger + e^{i\Delta\phi} S_b^\dagger) / \sqrt{2} |vac\rangle + O(\sqrt{\chi}), \quad (7.3)$$

where $\Delta\phi$ denotes the difference of the phase shifts between the left and the right side of channel.

7.2.3 Entanglement connection

The maximum distance between the entangled ensemble a and b is limited by the attenuation length L_{att} of the communication channels. To extend the distance, one can apply then entanglement connection via entanglement swapping. The entanglement swapping setup is depicted in Fig. 7.1b. Assume we have created entangled states (7.3) between atomic ensembles (a, b^L) and (b^R, c) as

$$|\psi\rangle_{a,b^L} = (S_a^\dagger + e^{i\phi^L} S_{b^L}^\dagger) / \sqrt{2} |vac\rangle, \quad (7.4)$$

$$|\psi\rangle_{b^R,c} = (S_{b^R}^\dagger + e^{i\phi^R} S_c^\dagger) / \sqrt{2} |vac\rangle, \quad (7.5)$$

neglecting the higher order excitations. The two atomic ensembles b^L and b^R are illuminated simultaneously by read laser pulses. The retrieved Stokes photons are subject to the BS, and a click on either of the single photon detectors will prepare the atomic ensembles at sites a and c into an entangled state. In this way, the entangled pair can be connected to arbitrary distance via entanglement swapping.

Note that, once the entanglement at one site is generated, it can be hold due to the quantum memory until another pair is ready. This is an important advantage of the quantum repeater idea, which is responsible for the polynomial growth with the communication distance.

²The length that the channel attenuation reaches $1/e$.

7.2.4 Phase instability analysis

However, as we present above, both entanglement generation and entanglement swapping in DLCZ protocol depend on Mach-Zehnder-type interference. Thus, relative phase between two remote entangled pairs is sensitive to path length instabilities, which has to be kept constant within a fraction of photon's wavelength. Moreover, entanglement generation and entanglement swapping are probabilistic. If connecting neighboring entangled pairs does not succeed after performing entanglement swapping, one has to repeat all previous procedures to reconstruct the entangled pairs. This means the path length fluctuation must be stabilized until the desired remote entangled pairs are successfully generated. A particular analysis shows that, to maintain path length phase instabilities at the level of $\lambda/10$ (λ : wavelength; typically $\lambda \sim 1 \mu\text{m}$ for photons generated from atomic ensembles) requires the fine control of timing jitter at a sub-femto second level over a timescale of a few tens of seconds, no matter whether entanglement generation is performed locally or remotely [156]. It is extremely difficult for current technology to meet this demanding requirement, since the lowest reported jitter is about a few tens of femto-seconds for transferring a timing signal over kilometer-scale distances for averaging times of ≥ 1 s [159]. Thus the requirement to stabilize the relative phase in the DLCZ scheme is still extremely demanding for current techniques [156].

7.3 Robust quantum repeater

7.3.1 Motivation

As is well known, the two-photon Hong-Ou-Mandel-type interference is insensitive to phase instability [160]. The path length fluctuations should be kept on the length scale within a fraction of photon's coherence length (say, 1/10 of the coherence length, which is about 3 m for photons generated from atomic ensembles [73]). Therefore the robustness is improved about 7 orders of magnitude higher in comparison with the single-photon Mach-Zehnder-type interference in DLCZ protocol. The interference of two photons from independent atomic ensembles has been reported recently [76, 77, 78]. This type of two-photon interference has been widely used in quantum communication and quantum computation [161, 162, 163, 164, 84].

To exploit the advantage of two-photon interference, it is natural to extend the DLCZ protocol by polarization encoding a memory qubit with two atomic ensembles [80, 81], and entangling two memory qubits at neighboring sites via a two-photon Bell-state measurement. Unfortunately, as shown below, the Bell-state measurement will not create the desired entangled state, but a complex superposition state with spurious contributions from second-order excitations, which preclude further entanglement manipulation.

7.3.2 Basic protocol

Let us consider two communication sites A and B at a distance of L_0 . A schematic setup of entanglement generation is shown in Fig. 7.2. Each site has two atomic ensembles encoded as one memory qubit and the two atomic ensembles at each node are excited simultaneously by write laser pulses. We assume the Stokes photons generated from the two atomic ensembles at the same site have orthogonal polarization state, e.g., $|H\rangle$ and $|V\rangle$, which denote horizontal and vertical linear polarization, respectively. In this way the memory qubit is effectively entangled in the polarization states of the emitted Stokes photons.

The anti-Stokes photons generated from both sites are directed to the PBS and subject to BSM-I in the center to entangle the two neighboring memory qubits. However, the two-photon state generated in the second-order spontaneous Raman process will also induce coincidence counts on the detectors. Thus the BSM-I can only prepare the neighboring memory qubits into a complex superposition state with spurious contributions from second-order excitations. For instance, a

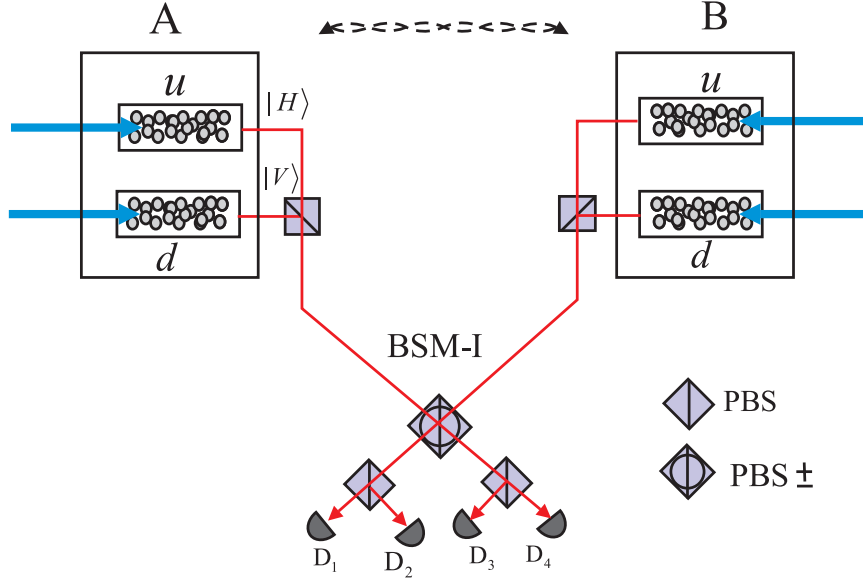


Figure 7.2: Setup for entanglement generation between sites A and B . Forward-scattered anti-Stokes photons, generated by an off-resonant write laser pulse via spontaneous Raman transition, are subject to Bell-state measurement (BSM-I) at the center. The Stokes photons generated at the same site are assumed to have different polarization i.e., $|H\rangle$ and $|V\rangle$. PBS (PBS $_{\pm}$) reflects photons with polarization $|V\rangle$ ($|-\rangle$) and transmits photons with polarization $|H\rangle$ ($|+\rangle$), where $|\pm\rangle = \frac{1}{\sqrt{2}}(|H\rangle \pm |V\rangle)$. After passing through the PBS $_{\pm}$ and PBS successively, the Stokes photons are detected by single photon detectors. A coincidence count between single photon detectors D_1 and D_4 (D_1 and D_3) or D_2 and D_3 (D_2 and D_4) will project the four atomic ensembles into the complex entangled state $|\psi\rangle_{AB}$ up to a local unitary transformation.

coincidence count between D_1 and D_4 projects the two memory qubits into

$$|\psi\rangle_{AB} = \left(\frac{e^{i(\phi_A + \phi_B)} S_{uA}^\dagger S_{uB}^\dagger + S_{dA}^\dagger S_{dB}^\dagger}{2} + \frac{e^{i2\phi_A} S_{uA}^{\dagger 2} + e^{i2\phi_B} S_{uB}^{\dagger 2} - e^{i2\phi_A} S_{dA}^{\dagger 2} - e^{i2\phi_B} S_{dB}^{\dagger 2}}{4} \right) |vac\rangle, \quad (7.6)$$

where ϕ_A and ϕ_B are the phases that the photons acquire, respectively, from site A and B during the BSM-I. The atomic ensembles are distinguished by subscript (u, d) and (A, B). The first part is the maximally entangled state needed for further operations, while the second part is the spurious two-excitation state coming from second-order excitations. The success probability is on the order of $O(\chi^2 \eta_1^2 e^{-L_0/L_{att}})$, where η_1 is the detection efficiency. The time needed in this process is

$$T_0 \approx \frac{T_{cc}}{\chi^2 \eta_1^2 e^{-L_0/L_{att}}},$$

with $T_{cc} = L_0/c$ the classical communication time.

It is obvious that the phases ϕ_A and ϕ_B only lead to a multiplicative factor $e^{i(\phi_A + \phi_B)}$ before the desired entangled state and thus have no effect on the desired entanglement. The prize to pay is that some spurious coincidence counts from the two-excitation terms are also registered, which obviously prevents further entanglement manipulation and must be eliminated by some means. However, we find that it is not necessary to worry about these terms, because they can be automatically washed out if the Bell-state measurement in the entanglement swapping step is

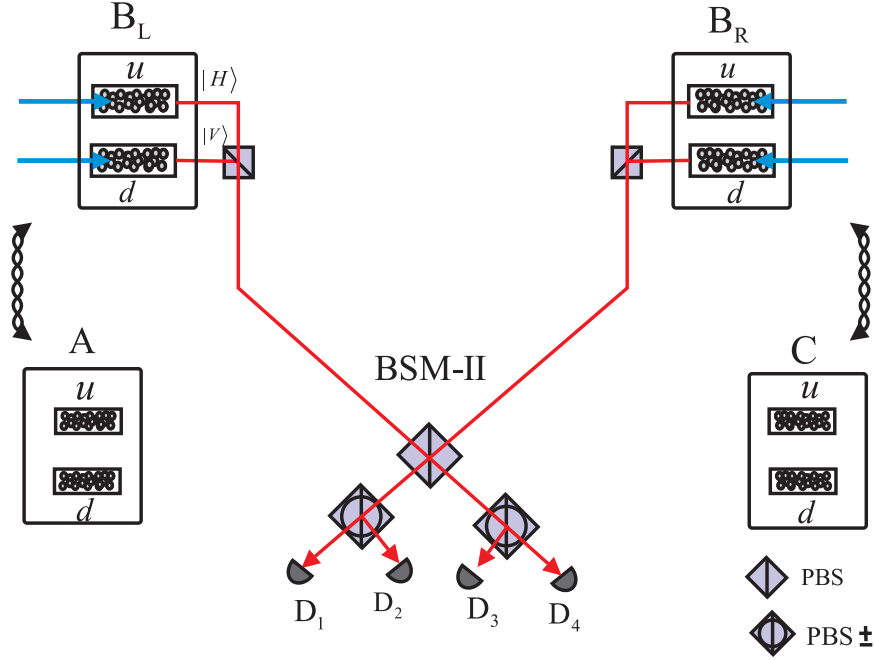


Figure 7.3: Setup for entanglement connection between sites A and C via entanglement swapping. Complex entangled states have been prepared in the memory qubits between sites (A, B_L) and (B_R, C) . The memory qubits at site B are illuminated by near resonant read laser pulses, and the retrieved anti-Stokes photons are subject to BSM-II at the center. The Stokes photons at the same site have different polarizations $|H\rangle$ and $|V\rangle$. After passing through PBS and PBS_\pm successively, the Stokes photons are detected by single photon detectors. Coincidence counts between D_1 and D_4 (D_1 and D_3) or D_2 and D_3 (D_2 and D_4) are registered. The memory qubits will be projected into an effectively maximally entangled state ρ_{AC} up to a local unitary transformation. Note that the sequence of PBSs in BSM-II is different from BSM-I. This helps to eliminate the spurious contributions from second-order excitations.

carefully designed. In the ideal case a maximally entangled state can be created by implementing entanglement swapping.

The entanglement swapping setup is depicted in Fig. 7.3. Let us consider three communication sites A, B and C , and assume that we have created the complex entangled states (Eq. 7.6) $|\psi\rangle_{AB_L}$ and $|\psi\rangle_{B_R C}$ between (A, B_L) and (B_R, C) , respectively³. The memory qubits B_L and B_R at site B are illuminated simultaneously by read laser pulses. The retrieved Stokes photons are subject to BSM-II. Note that the sequence of the PBSs in BSM-II is different from BSM-I. The BSM-II is designed like this in order that the two-photon states converted from the spurious two-excitation terms are directed into the same output and thus will not induce a coincidence count on the detectors. In the ideal case, if the retrieve efficiency is unity and perfect photon detectors are used to distinguish photon numbers, only the two-photon coincidence count will be registered and project the memory qubits into a maximally entangled state. For instance, when a coincidence count between D_1 and D_4 is registered one will obtain

$$|\phi^+\rangle_{AC} = (S_{u_A}^\dagger S_{u_C}^\dagger + S_{d_A}^\dagger S_{d_C}^\dagger) / \sqrt{2} |vac\rangle. \quad (7.7)$$

³Note that in Ref. [165], both entanglement swapping and entanglement generation is performed remotely, so we need at least two atomic ensembles at each node. Here entanglement swapping is performed locally following the standard quantum repeater protocol [24], and thus we have to manipulate at least four atomic ensembles at each communication site.

In this way a maximally entangled state across sites A and C is generated by performing entanglement swapping. The maximally entangled state can be extended by further entanglement swapping as usual. Both the entanglement creation and entanglement connection in our scheme rely on two-photon interference, so the improvement in insensitivity to path length fluctuations, as compared to the DLCZ scheme, is about 7 orders of magnitude.

In practice, the retrieve efficiency η_r is determined by optical depth of the atomic ensembles [166]. Furthermore, current single photon detectors are incapable of distinguishing photon numbers. Taking into account these imperfections, the multi-photon coincidence counts in the BSM-II have to be considered. Through some simple calculations, one can find that the coincidence counts will prepare the memory qubits into a mixed entangled state of the form

$$\rho_{AC} = p_2\rho_2 + p_1\rho_1 + p_0\rho_0, \quad (7.8)$$

where the unnormalized coefficients are calculated to be

$$\begin{aligned} p_2^{(u)} &= \frac{\eta_r^2\eta_1^2}{32}, \\ p_1^{(u)} &= \frac{\eta_r^2(1-\eta_r)\eta_1^2}{16} + \frac{\eta_r^3}{32}\left(\frac{\eta_1\eta_2}{2} + \eta_1^2\right), \\ p_0^{(u)} &= \frac{\eta_r^3}{32}(1-\eta_r)\left(\frac{1}{2}\eta_1\eta_2 + \eta_1^2\right) + \\ &\quad \frac{\eta_r^2(1-\eta_r)^2\eta_1^2}{32} + \frac{\eta_r^4}{64}\left(\frac{1}{4}\eta_2^2 + \eta_1^2\right), \end{aligned} \quad (7.9)$$

where η_1 and η_2 are the detector efficiency for single photon state and two photon state. The success probability of entanglement swapping is $p = p_2^{(u)} + p_1^{(u)} + p_0^{(u)}$. $\rho_2 = |\phi^+\rangle_{AC}\langle\phi^+|$ is a maximally entangled state, ρ_1 is a maximally mixed state, where only one of the four atomic ensembles has one excitation, and ρ_0 is the vacuum state where all atomic ensembles are in the ground states.

It is easy to see that ρ_{AC} is in fact an effectively maximally entangled states, which can be projected automatically to a maximally entangled state in the entanglement-based quantum cryptography schemes. When implementing quantum cryptography via the Ekert protocol [11], we randomly choose the detection basis at the remote sites and detect the photons retrieved from the atomic ensembles. Then we compare the detection basis by classical communication. In this process, only the coincidence counts are registered and used for quantum cryptography. In our case only the first term ρ_2 will contribute to a coincidence count between the detectors at the two sites and will be registered after classical communication. The maximally mixed state term ρ_1 and the vacuum term ρ_0 have no contribution to the experimental results, and thus ρ_{AC} is equivalent to the Bell state $|\phi^+\rangle_{AC} = (S_{u_A}^\dagger S_{u_C}^\dagger + S_{d_A}^\dagger S_{d_C}^\dagger)/\sqrt{2}|vac\rangle$.

7.3.3 Entanglement connection and scalability

Effectively entangled states can be connected to a longer communication distance via further entanglement swapping. To implement a quantum repeater protocol, a nesting scheme is used in entanglement connection process [17, 68]. Taking into account higher-order excitations, the generated effectively entangled pair Eq. (7.8) can be re-written as

$$\rho' = \rho + p'_2\rho'_2 + p'_3\rho'_3,$$

where the normalized density matrix ρ'_2 and ρ'_3 denote the two-excitation mixed state and three-excitation mixed state generated due to higher-order excitations in the spontaneous Raman process, and the small coefficients p'_2 and p'_3 are on the order of $O(\chi) \ll 1$. After the j -th swapping step, the effectively entangled pair can be described as [156]

$$\rho'_{s_j} = p_{2s_j}\rho_{2s_j} + p_{1s_j}\rho_{1s_j} + p_{0s_j}\rho_{0s_j} + p'_{2s_j}\rho'_{2s_j} + p'_{3s_j}\rho'_{3s_j}. \quad (7.10)$$

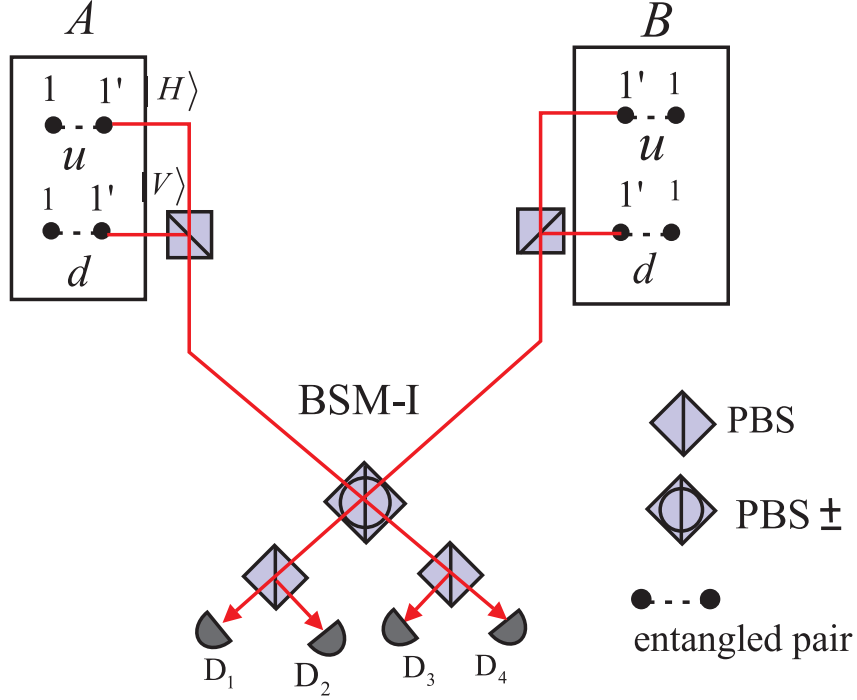


Figure 7.4: Elementary entangled pairs are first locally generated via the standard DLCZ protocol. The anti-Stokes photons are subject to BSM-I to connect neighboring communication nodes. We also assume the anti-Stokes photons retrieved from atomic ensembles at the same site have different polarization. Note that BSM-I also helps to eliminate the spurious contributions from higher order excitations.

Here ρ_{2s_j} is the maximally entangled state between two memory qubits at a distance of $L = 2^j L_0$, and ρ_{1s_j} and ρ_{0s_j} are also the maximally mixed state and vacuum state, respectively. Note that $\rho'_{s_1} = \rho'$ is just the mixed entangled state created after the first entanglement swapping step. The coefficients can be estimated to be

$$p'_{2s_j} \sim O(j\chi), \quad p'_{3s_j} \sim O(\chi), \quad (7.11)$$

$$p_{\alpha s_j} \approx p_{\alpha s_{j-1}} + O(j\chi), \quad (\alpha = 0, 1, 2). \quad (7.12)$$

From Eq. (7.11), it is easy to see that the contributions from higher-order excitations ρ'_{2s_j} and ρ'_{3s_j} can be safely neglected, as long as the small excitation probability fulfills $j\chi \ll 1$, which can be easily achieved by tuning the write laser pulse. One can also see that the coefficients p_{2s_j} , p_{1s_j} and p_{0s_j} are stable to the first order of $j\chi$, therefore the probability to find an entangled pair in the remaining memory qubits is almost a constant and will not decrease significantly with distance during the entanglement connection process. The time needed for the j -th connection step satisfies the iteration formula

$$T_{s_j} = \frac{1}{p_{s_j}} [T_{s_{j-1}} + 2^{j-1} T_{cc}]$$

with p_{s_j} the success probability of the j -th swapping step. The total time needed for the entanglement connection process is

$$T_{tot} \approx T_0 \prod_j p_{s_j}^{-1} \approx \frac{T_{cc}}{\chi^2 \eta_1^2} e^{L_0/Latt} (L/L_0)^{\log_2 1/\eta}, \quad (7.13)$$

where $\eta = \eta_r^2 \eta_1^2$ is a constant. The excitation probability can be estimated to be $\chi \sim L_0/L$, and then the time needed in the entanglement connection process

$$T_{tot} \propto (L/L_0)^{2+\log_2 1/\eta}$$

scales polynomially or even quadratically with the communication distance.

One can modify our protocol by performing entanglement generation locally and entanglement swapping remotely. It will help to increase the scalability, since entanglement generation is usually the rate-limiting stage due to the low excitation probability. Local entanglement can also be generated via the standard DLCZ protocol and then connected by two-photon Hong-Ou-Mandel interference, because local path length fluctuations can be well controlled. The experimental setup is shown in Fig. 7.4. Here we need BSM-I to eliminate spurious contributions from high-order excitations. Note that the setup in Fig. 7.4 is a simple variation of the scheme proposed Jiang *et al.* [167], where entanglement swapping is performed locally and entanglement generation is performed remotely – thus, it still requires a fine control of timing jitter at a sub-femto second level over a timescale of a few tens of seconds. Therefore, we remark that such a simple modification is crucial to long-distance quantum communication, as entanglement generation relies on single-photon interference and must be performed locally.

7.3.4 Alternative approach

The locally entangled memory qubits can be generated by other means. Atomic ensembles can also serve as a quantum memory to store a photonic state [168, 169]. By applying a time dependent classical control laser pulse of a Rabi frequency Ω_c , the whole system has a particular zero-energy eigenstate, i.e., the dark-state-polariton. The single-polariton state is

$$|D, 1\rangle = \frac{\Omega_c(t)}{\sqrt{\Omega_c^2(t) + g^2 N}} |1\rangle_p |0\rangle_a - \frac{g\sqrt{N}}{\sqrt{\Omega_c^2(t) + g^2 N}} |0\rangle_p S^\dagger |0\rangle_a, \quad (7.14)$$

with g being the coupling constant for the $|g\rangle - |e\rangle$ transition. Here $|0\rangle_p$ ($|1\rangle_p$) is the vacuum (single-photon) state of the quantized field to be stored. The quantum memory works by adiabatically changing $\Omega_c(t)$ such that one can coherently map $|D, 1\rangle$ onto either purely atom-like state $|0\rangle_p S^\dagger |0\rangle_a$ where the single photon is stored, or purely photon-like state $|1\rangle_p |0\rangle_a$, which corresponds to the release of the single photon.

To exploit the advantage of two-photon Hong-Ou-Mandel-type interference, we need a quantum memory for the photonic polarization qubits. Figure 7.5 shows quantum memory for storing any single-photon polarization states by the dark-state-polariton method. Two atomic ensembles being a quantum memory for polarization qubits at each node are thus the required localized memory qubit in our scheme. Thus transformation between an arbitrary photon polarization state $\alpha |H\rangle + \beta |V\rangle$ and the corresponding state stored in atomic ensembles $(\alpha S_h^\dagger + \beta S_v^\dagger) |0\rangle$ can be achieved by adiabatically manipulating the control laser pulse. Importantly, our quantum memory works even when the two probability amplitudes in the stored state $\alpha |H\rangle + \beta |V\rangle$ are not c -numbers but quantum states of other photonic qubits. As a result, two memory qubits U and D at one site (see Fig. 7.6a) can be deterministically entangled in their “polarizations” by storing two polarization-entangled photons, e.g.,

$$\frac{1}{\sqrt{2}} (S_{h_U}^\dagger S_{h_D}^\dagger + S_{v_U}^\dagger S_{v_D}^\dagger) |vac\rangle \leftrightarrow \frac{1}{\sqrt{2}} (|H\rangle |H\rangle + |V\rangle |V\rangle). \quad (7.15)$$

The latter state in Eq. (7.15) are generated by a deterministic polarization-entangler using four single photons, linear optics and an event-ready detection [170]. With an overall success probability of $\frac{1}{8}$ for perfect photon counting, such an “event-ready” entangler can deterministically generate two maximally polarization-entangled qubits.

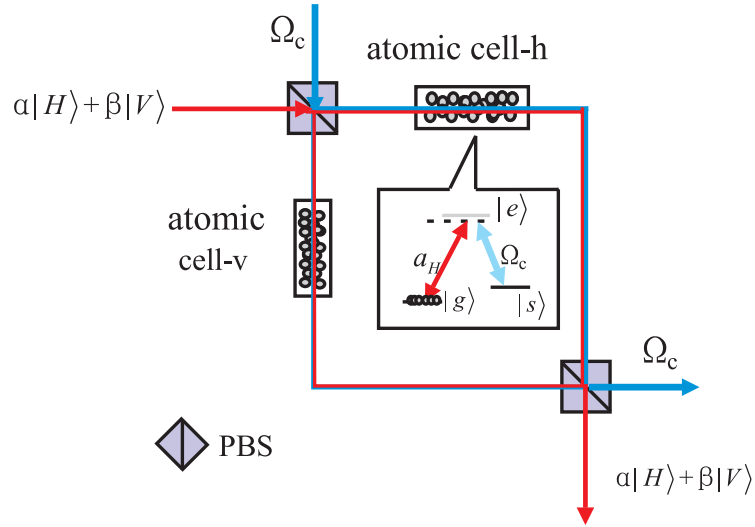


Figure 7.5: Quantum memory for photonic polarization qubits. Two ensembles are a classical control field. Classical and quantized light fields are fed into the first PBS and will leave at two different outputs of the second PBS. As each atomic cell works as quantum memory for single photons with polarization $|H\rangle$ or $|V\rangle$ via the adiabatic transfer method, the whole setup is then quantum memory of any single-photon polarization states. The inset shows the relevant level structure of the atoms. The $|e\rangle - |s\rangle$ transition is coherently driven by the classical control field of Rabi frequency Ω_c , and the $|g\rangle - |e\rangle$ transition is coupled to a quantized light field.

Polarization encoding allows a two-photon interference entanglement swapping to construct entanglement between adjacent sites. As shown in Fig. 7.6, one can first create each memory pair in a maximal event-ready entanglement at two adjacent communication nodes and then the two photons stored in the two U memories are simultaneously retrieved and subject to a two-photon Bell-state measurement at the center. Conditioned on the result of this Bell-state measurement, the remaining two D memory qubits are maximally entangled, also in an event-ready way. Usual entanglement swapping can be applied to the polarization encoding memory qubits and thus allows the implementation of a robust quantum repeater.

7.3.5 Entanglement purification

With imperfect entanglement and erroneous local operations, entanglement connection, together with decoherence, will reduce the fidelity of entanglement. Then at certain stage of entanglement connection, the less entangled states have to be purified via the entanglement purification protocol [37, 38] to enable further entanglement connection. Fig. 7.7 shows how to achieve linear optical entanglement purification between any specified two nodes, e.g., node- I and node- J , across which one has less entangled pairs of quantum memories.

Assume two effectively mixed entangled pairs of fidelity F are created in parallel via entanglement connection as we discussed above. The effectively entangled states stored in the four memory qubits are converted into entangled photons by the read laser pulses, and then subject to two PBSs, respectively. The photons in mode b_1 and b_2 are detected in $|\pm\rangle = \frac{1}{\sqrt{2}}(|H\rangle \pm |V\rangle)$ basis by single photon detectors, and will project the photons in mode a_1 and a_2 into an effectively maximally entangled state of higher fidelity F' [37, 38]. The higher-fidelity entangled pair in mode a_1 and a_2 can be restored into two distant memory qubits at nodes I and J by means of the dark-state-polariton method for further manipulation.

To generate a remote entangled pair, the nested quantum purification has to be implemented

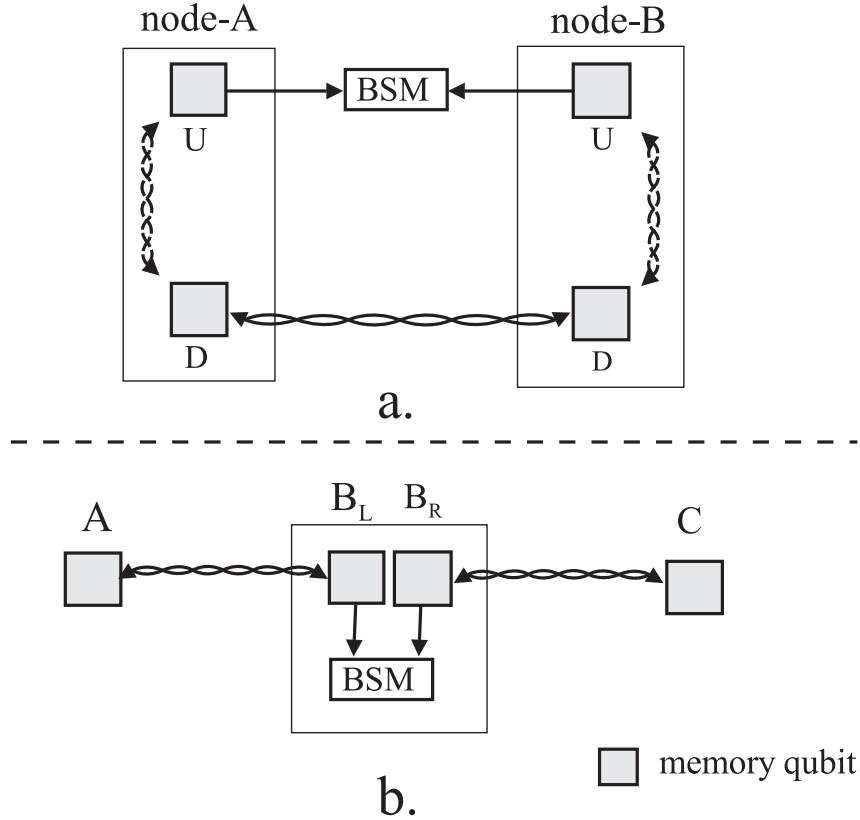


Figure 7.6: a). Entanglement swapping between adjacent communications nodes A and B . Two pairs of entangled memory qubits are first generated by storing the event-ready entanglement of two photons at each node. Then the two photons stored in the U memory at the two nodes are simultaneously retrieved and subject to a two-photon Bell-state measurement at the center. This entanglement swapping process will in an “event-ready” way entangle the two distant D memory qubits. b). Entanglement connection to extend the communication length. Two well entangled pairs of memory qubits, one across nodes (A, B_L) and (B_R, C) are prepared in parallel. The Bell-state measurement on the two photons released simultaneously from the two memories at node B results in, with a probability of $1/2$, well entangled quantum memories across nodes A and C in a definite Bell state.

[17, 68]. The total time overhead to create entanglement across two communication nodes at a distance of 1280 km can be numerically estimated. In our calculation, we assume the distance $L_0 = 10$ km and the photon loss rate is 0.1 dB/km in free space. To improve the scalability, we assume entanglement generation is performed locally as described in § 7.3.4 and the entanglement generation time is considered to be $100 \mu s$. The fidelity of the adjacent entangled memory qubits is $F = 0.88$, as can be estimated by connecting two adjacent memories from two pairs of photon-memory entanglement after 5 km free space transmission of both photons [67]. One of the major factors affecting the efficiency of our scheme is single-photon detection. Fortunately, high-efficiency photon counting is feasible by using quantum state transfer and state-selective fluorescence detection with nearly unit efficiency [171, 172]. To increase the efficiency, we assume photon counting detectors with detection efficiency 99% are used, and the retrieve efficiency is considered to be 98%. Entanglement purification is performed three times during the entanglement connection process to improve the fidelity. Our numerical results give a total time of about 23 seconds to create an effectively entangled pair, with a probability of 0.75 to get the entangled pair of fidelity 94%.

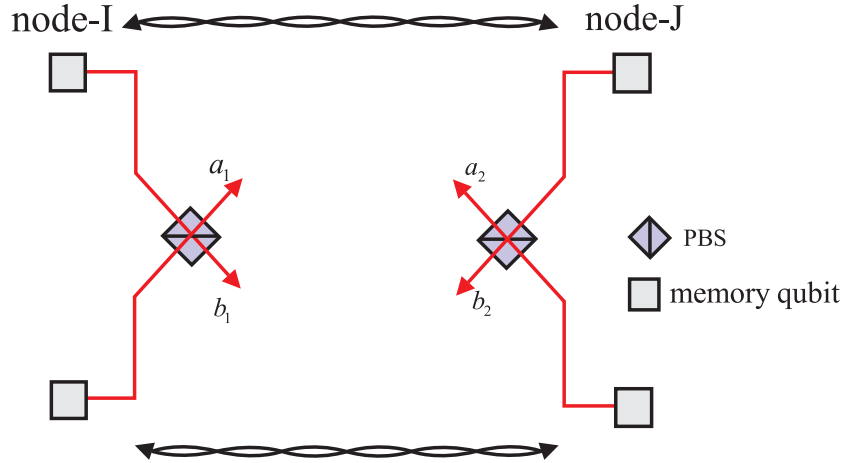


Figure 7.7: Setup for quantum entanglement purification. Entangled states have been prepared in the memory qubits between two distant nodes I and J . The memory qubits at the two sites are illuminated by near resonant read laser pulse, and the retrieved entangled photon pairs are directed to two PBS respectively. The photons in mode b_1 and b_2 are detected in $|\pm\rangle = \frac{1}{\sqrt{2}}(|H\rangle \pm |V\rangle)$ basis and the remaining photons in mode a_1 and a_2 are restored in the memory qubits at the two sites respectively.

7.4 Conclusion

In summary, we have given a particular analysis on phase stability problem of the DLCZ protocol. This problem can be overcome by taking advantage of two-photon Hong-Ou-Mandel-type interference, which alleviates the phase stability requirements by about 7 orders of magnitude. Most of the ingredients in our protocol have been experimentally realized in recent years [78, 81] (see Chapter 9 and 10). A long storage time is crucial for implementing atomic ensemble based quantum repeater protocol. Storage time of up to $30 \mu s$ was reported recently [80]. An optical dipole trap may have the potential to extend the storage time to 1 second. According to a recent proposal, quantum memory with nuclear atomic spins might have very long storage time of about hours [173]. Our scheme also relies on the ability to reliably transfer of photon's polarization states over a free-space or optical fiber channel. Two recent experiments demonstrated this ability up to 100 km in free space [174] and in fiber [175]. Our scheme faithfully implements a robust quantum repeater and thus enables a realistic avenue for relevant long-distance quantum communication.

Chapter 8

Deterministic single photon source

8.1 Introduction

Although weak coherent beams can be used as a pseudo single-photon source, the advent of quantum information processing has placed stringent requirements on single photons either on demand or heralded [176]. In particular, linear optical quantum computation [19] depends on the availability of such single-photon sources. The single-photon nature guarantees unconditional security and high efficiency in quantum cryptography [3]. Different approaches have been attempted in the last decade to develop an on-demand single-photon source, such as quantum dots [177, 178], single atoms and ions [179, 180], and color centers [181]. However, all of them are confronted with different challenges. For example, the single-atom implementation provides spectrally narrow single photons with a well defined spatial mode, but the manipulation of single atoms requires sophisticated techniques and expensive setups [179]. Quantum dots are a potential source with high single-photon rate, but the requirement of spectral filtering entails inevitable losses. It is very difficult to prepare truly identical sources due to inhomogeneities in both the environment of the emitters and the emitters itself [182]. Color centers are excellent sources, even at room temperature, however, the high peak intensities of a pulsed excitation can lead to complex and uncontrollable dark states [176]. So it has been taken as a formidable task to develop a promising deterministic single-photon source.

Moreover, an important challenge in distributed quantum information processing is the controllable transfer of quantum state between flying qubit and macroscopic matter. Starting from a recent proposal for long-distance quantum communication with atomic ensembles [70], it is possible to implement both a single-photon source on demand and controllable transfer of quantum state between a photonic qubit and macroscopic matter, provided that proper feedback is applied. A single spin excitation can be generated in an atomic ensemble by applying a series of subsequent clean (optical pumping) and write pulses stimulating spontaneous Raman scattering. The successful generation of a spin excitation is indicated by the detection of a corresponding Raman photon. This information is used as feedback to stop the sequence, and further on to start the next process, for example to convert the spin excitation back into a single photon. Such a sequence can be taken as having a feed-forward ability for the deterministically converted single photon.

Recently, significant experimental progresses have been achieved in demonstration of quantum storage and single-photon sources [71, 183, 184, 73], and even entanglement between two atomic ensembles [80, 79] has been generated. However, coincidence-based post-selection was used in these experiments. No feedback was applied and consequently the requirement of resources would increase exponentially with each new step of operation. This significantly limits the scalability of the schemes [19, 70].

In this chapter, we present an experimental realization of a deterministic and storable single-

photon source. Single spin excitations in an atomic ensemble are generated by detecting anti-Stokes photons from spontaneous Raman scattering. This detection allows to implement feed-forward and convert the spin excitations into single photons at a predetermined time. It is shown that the single-photon quality is conserved while the production rate of single photons can be enhanced significantly by the feedback circuit. In principle, the spatial mode, bandwidth, and frequency of single-photon pulses are determined by the spatial mode, intensity and frequency of the retrieve laser [73]. It is feasible to integrate such a single-photon source with the storage medium, atomic ensembles. Our controllable single-photon source potentially paves the way for the construction of scalable quantum communication networks [70, 17] and linear optical quantum computation [19].

8.2 Basic conception

8.2.1 Non-classical photon pair generation

The basic primitive integral to the DLCZ scheme is the generation of non-classical pair. Specifically, an initial write pulse is employed to create a state of collective atomic excitation as heralded by photoelectric detection of an anti-Stokes photon. After a programmable delay δt , a subsequent read pulse interrogates the atomic sample, leading to the emission of a Stokes photon. The manifestly quantum (or nonclassical) character of the correlations between the anti-Stokes and Stokes photon can be verified by way of the observation of cross-correlation. Any classical correlation would have a cross-correlation of 1 and coherent pulse has a cross-correlation of 2. Any correlation bigger than 2 represents the quantum property.

The basic concept of our experiments is shown in Fig. 8.1. Cold atoms with Λ -type level configuration (two ground state $|a\rangle$, $|b\rangle$ and an excited state $|e\rangle$) collected by a magneto-optical trap (MOT) are used as the media for quantum memory. The atoms are initially optically pumped to state $|a\rangle$ by a pump laser. Then a weak classical *write* pulse, with the Rabi frequency Ω_w , close to the resonance of transition $|a\rangle$ to $|e\rangle$ is introduced in the atomic cloud. Due to the spontaneous Raman process, a photon of anti-Stokes field \hat{a}_{AS} is emitted into the forward scattering mode. Simultaneously, a collective spin excitation corresponding to the mode of the anti-Stokes field \hat{a}_{AS} is generated in the atomic ensemble [70, 185]. The state of the field \hat{a}_{AS} and the collective spin state of the atoms can be expressed by the superposed state

$$|\Psi\rangle \sim |0_{AS}0_b\rangle + \sqrt{\chi}|1_{AS}1_b\rangle + \chi|2_{AS}2_b\rangle + O(\chi^{3/2}), \quad (8.1)$$

where χ is the excitation probability of one spin flip, $|i_{AS}i_b\rangle$ denotes the i -fold excitation of the anti-Stokes field and the collective spin. Ideally, conditioned on detecting one and only one anti-Stokes photon in detector D1, a single spin excitation is generated in the atomic ensemble with certainty. After a controllable time delay δt (in the order of the lifetime τ_c of the spin excitation), another classical *read* pulse with the Rabi frequency Ω_R , which is on-resonance with the transition from $|b\rangle$ to $|e\rangle$, is applied to retrieve the spin excitation and generate a photon of Stokes field \hat{a}_S .

In our present experiment, more than 10^8 ^{87}Rb atoms are collected by the MOT with an optical depth of about 5 and the temperature of about 100 μK . The earth magnetic field is compensated by three pairs of Helmholtz coils. The two ground states $|a\rangle$ and $|b\rangle$ and the excited state $|e\rangle$ in the Λ -type system are $|5S_{1/2}, F=2\rangle$, $|5S_{1/2}, F=1\rangle$, and $|5P_{1/2}, F=2\rangle$, respectively. The write laser is tuned to the transition from $|5S_{1/2}, F=2\rangle$ to $|5P_{1/2}, F=2\rangle$ with detuning of 10 MHz and the read laser is locked on resonance to the transition from $|5S_{1/2}, F=1\rangle$ to $|5P_{1/2}, F=2\rangle$. By using orthogonal polarizations, write and read beams are spatially overlapped on a polarized beam splitter (PBS1), and then focused into the cold atoms with the beam waist of 35 μm . After passing the atomic cloud, the two beams are split by PBS2 which serves as the first stage of filtering the write (read) beam out from the anti-Stokes (Stokes) field. The leakage of write (read) field from PBS2 propagating with the anti-Stokes (Stokes) field will be further filtered by a thermal cell filled

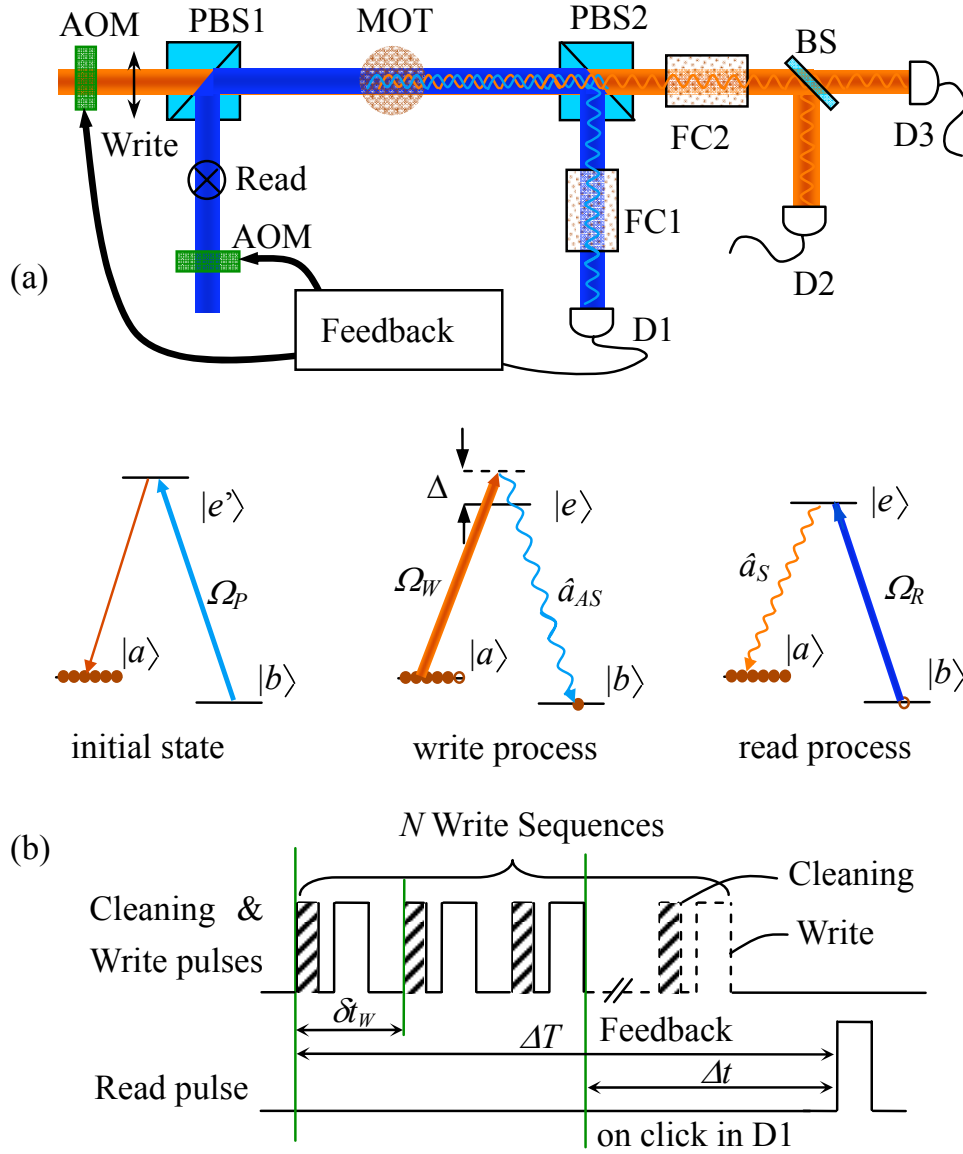


Figure 8.1: Illustration of the experimental setup (a) and the time sequence with the feedback circuit for the *write* and *read* process (b). The atomic ensemble is firstly prepared in the initial state $|a\rangle$ by applying a pump beam resonant with the transition $|b\rangle$ to $|e'\rangle$. A write pulse with the Rabi frequency Ω_W is applied to generate the spin excitation and an accompanying photon of the mode \hat{a}_{AS} . Waiting for a duration Δt , a read pulse is applied with orthogonal polarization and spatially overlap with the write beam in PBS1. The photons, whose polarization is orthogonal to that of the write beam, in the mode \hat{a}_{AS} are spatially extracted from the write beam by PBS2 and detected by detector D1. Similarly, the field \hat{a}_S is spatially extracted from the Read beam and detected by detector D2 (or D3). Here, FC1 and FC2 are two filter cells, BS is a 50/50 beamsplitter, and AOM1 and AOM2 are two acousto-optic modulators.

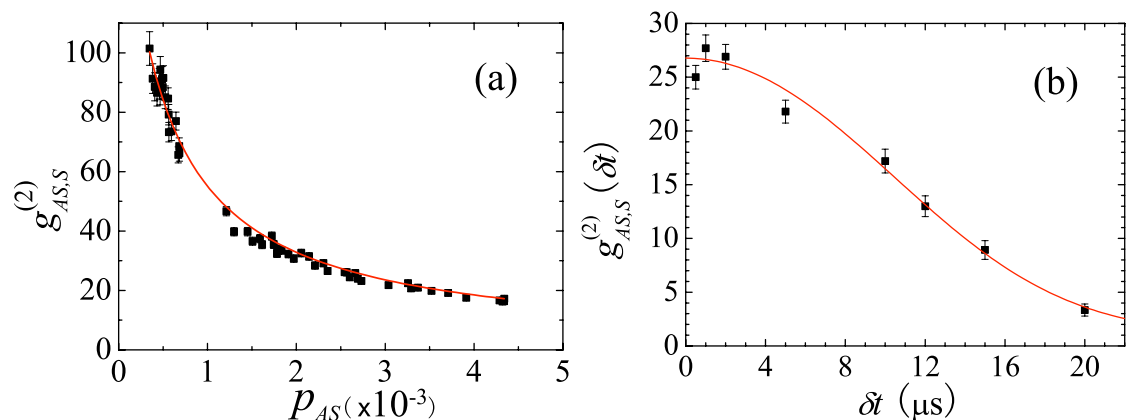


Figure 8.2: Intensity correlation function $g_{AS,S}^{(2)}$ along the excitation probability p_{AS} with $\delta t = 500$ ns (a) and along the time delay δt between read and write pulses with $p_{AS} = 3 \times 10^{-3}$ (b). The black dots are obtained from current experiment and the curves correspond to a least-square fit procedure according to Eq. (8.2) and (8.3). The observed lifetime is $\tau_c = 12.5 \pm 2.6 \mu\text{s}$.

with ^{87}Rb atoms, in which the rubidium atoms are prepared in state $|5S_{1/2}, F = 2\rangle$ ($|5S_{1/2}, F = 1\rangle$) initially. Coincident measurements among D1, D2 and D3 are performed with a time resolution of 2 ns.

After switching off the MOT, the atoms are optically pumped to the initial state $|a\rangle$. The write pulse containing about 10^4 photons with a duration of 100 ns is applied onto the atomic ensemble, to induce the spontaneous Raman scattering via $|a\rangle \rightarrow |e\rangle \rightarrow |b\rangle$. The state of the induced anti-Stokes field and the collective spin in Eq. (8.1) is generated with a probability $\chi \ll 1$. After a controllable delay of δt , the read pulse with the duration of 75 ns is applied for converting the collective excitation into the Stokes field. In comparison, the intensity of the read pulse is about 100 times stronger than that of the write one.

Assume the probability to have an anti-Stokes (Stokes) photon is p_{AS} (p_S), and the coincident probability between the Stokes and anti-Stokes channels is $p_{AS,S}$, then the intensity correlation function $g_{AS,S}^{(2)} = p_{AS,S}/(p_{AS}p_S)$. We measured the variation of $g_{AS,S}^{(2)}$ as a function of p_{AS} shown in Fig. 8.2(a) with a time delay of $\delta t = 500$ ns. Considering the background in each channel, we obtain

$$p_{AS} = \chi\eta_{AS} + B\eta_{AS}, \quad (8.2a)$$

$$p_S = \chi\gamma\eta_S + C\eta_S, \quad (8.2b)$$

$$p_{AS,S} = \chi\gamma\eta_{AS}\eta_S + p_{AS}p_S. \quad (8.2c)$$

Here, η_{AS} and η_S are the overall detection efficiencies in the anti-Stokes and Stokes channels respectively, which include the transmission efficiency η_t of filters and optical components, the coupling efficiency η_c of the fiber couplers, and the quantum efficiency η_q of single photon detectors (η_{AS} includes an additional spatial mode-match efficiency η_m [184]), γ is the retrieve efficiency which is a time-dependent factor, and B (C) is determined by the background in the anti-Stokes (Stokes) channel. The red curve in Fig. 8.2(a) is the least-square fit result according to Eq. (8.2), assuming $B = 0$ for simplicity. The efficiency in the anti-Stokes channel is observed as $\eta_{AS} \sim 0.07$ and the retrieve efficiency $\gamma \sim 0.3$. The largest correlation $g_{AS,S}^{(2)}$ (101 ± 6) appears at the lowest excitation probability p_{AS} of 3.5×10^{-4} .

The finite lifetime of the spin excitation results from the dephasing of the collective state due to the Larmor precession of the spins in the residual magnetic field. It can be characterized by the decay of the retrieve efficiency $\gamma(\delta t) = \gamma_0 \exp(-\delta t^2/\tau_c^2)$ [184], where τ_c is the lifetime of the

collective state. It can be determined from the decay of the measured intensity correlation function $g_{AS,S}^{(2)}(\delta t)$ as shown in Fig. 8.2(b), taken at $p_{AS} = 0.003$. Using Eq. (8.2), the intensity correlation function reads

$$g_{AS,S}^{(2)}(\delta t) = 1 + \frac{\gamma(\delta t)}{(B + \chi)\gamma(\delta t) + D}, \quad (8.3)$$

where C is absorbed by the new constant D . Our data give a lifetime of $\tau_c = 12.5 \pm 2.6 \mu s$. The cross correlation of the first point is slightly lower which might be caused by noise arising from the elastic scattering of the write beam.

8.2.2 Single photon source

The excellent correlation between anti-Stokes and Stokes photon pair allow us generating a heralded single photon source [186, 187]. The key idea of is that a single photon (here, Stokes photon) can be generated at a predetermined time if we know that the medium contains an atomic excitation. The presence of the latter is heralded by the measurement of a scattered photon in the write process. After this point one simply waits and reads out the excitation at the predetermined time. The performance of heralding measurements represents a conditional process.

Moreover, by applying more write pulses in each experimental trial, and a feedback protocol, we can greatly increase the generation probability of the single photon while the single photon quality will conserve. To do so, as shown in Fig. 8.1(b), in the time interval ΔT , N independent write sequences with a period of δt_w are applied to the atomic ensemble. Each write sequence contains a cleaning pulse (the optical pumping to the initial state) and a write pulse. Once an anti-Stokes photon is detected by D1 the feedback circuit stops the further write sequence and enables the read pulse to retrieve the single Stokes photon after a time delay Δt . The maximum number of trials (N) is given by the life time of the excitation. The feedback protocol enhances the production rate of Stokes photons according to the new excitation probability

$$P_{AS} = \sum_{i=0}^{N-1} p_{AS}(1 - p_{AS})^i$$

while the single-photon quality is conserved.

Our protocol can be executed in different modes. In a first mode, one can fix the retrieve time ΔT . Therefore, the delay Δt varies because the spin excitation is created randomly by one of the write sequences. Single photons are produced at a given time with a high probability, ideally approaching unity if $N \gg 1$. Furthermore, the retrieve efficiency could be improved significantly by an increased optical depth of the atomic ensemble and an optimal retrieve protocol [166]. This mode serves as a deterministic single-photon source. In a second mode, we retrieve the single photon with a fixed delay Δt after a successful write. More general the imprinted single excitation can be converted into a single photon at any given time with the life time τ_c . This is well suited for a quantum repeater [17, 70] where one needs to synchronize the nodes.

In the first experiment, we fixed $\Delta T = 12.5 \mu s$ and $\delta t_w = 1 \mu s$, and $N = 12$ subsequent write sequences were applied. The quality of the single-photon source can be characterized by the anti-correlation parameter α [186], which is equivalent to the second-order auto-correlation function $g_{S,S}^{(2)}$ of the Stokes photon on the condition of an anti-Stokes photon is detected. When we use N write pulses and the feedback protocol, the detection probabilities in D2, D3 and the coincidence detection probability D23 conditioned on a registration of an anti-Stokes photon in D1 are

$$P_{m|AS} = \frac{\sum_{i=0}^{N-1} p_{AS}(1 - p_{AS})^i p_{m|AS}(\Delta T - n \cdot \delta t_w)}{\sum_{i=0}^{N-1} p_{AS}(1 - p_{AS})^i}, \quad (8.4)$$

where $m = 2, 3, 23$ and $p_{m|AS}(\Delta T - n \cdot \delta t_w)$ is a time-dependent probability conditioned on a click in the anti-Stokes channel. The anti-correlation parameter α is given by $P_{23|AS}/(P_{2|AS}P_{3|AS})$.

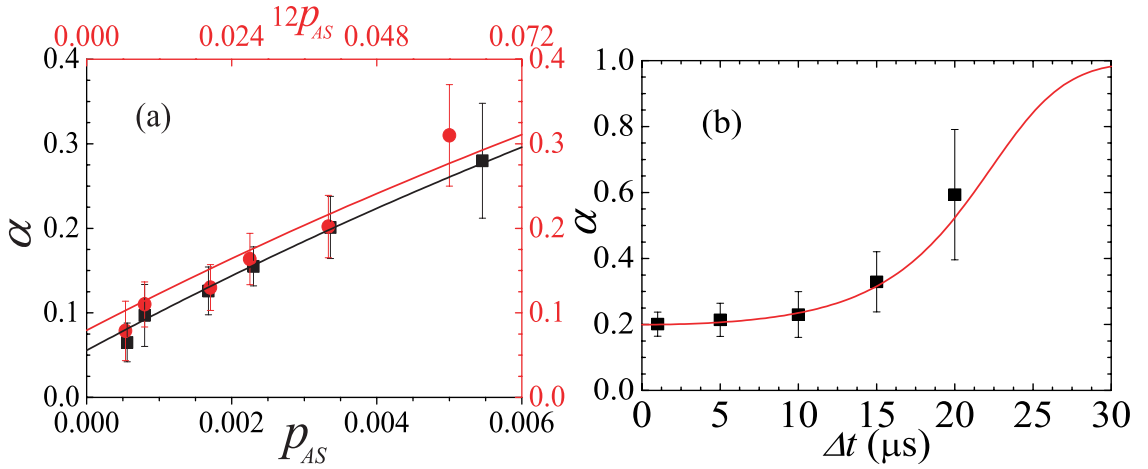


Figure 8.3: The anti-correlation parameter as a function of p_{AS} (a) and Δt (b). In Fig (a), the data in black correspond to the experiment without feedback circuit, in which each write sequence is followed by one read pulse. The data in red correspond to the experiment with feedback circuit, in which 12 successive write sequences are followed by one read pulse. The red curve is the theoretical evaluation taking into account the fitted background of the black dots. In Fig (b), 12 write sequences were applied in each trial while measuring.

Fig. 8.3(a) shows the measured α as a function of the excitation probability p_{AS} . For $N = 1$ (black) the variation of α is nearly linear in the region of $p_{AS} = 0 \sim 0.006$. The black curve is the fit according to Eq. (8.4). When using 12 successive write sequences, we plot α versus $12p_{AS}$ as red dots. The red line is a no free parameter calculation from Eq. (8.4), taking the fitted parameters from $N = 1$ setting $N = 12$. We note that, for $p_{AS} \rightarrow 0$ the value of α is 0.057 ± 0.028 , which in principle should be 0. This offset comes from noise including residual leakage of the write and read beams, stray light, and dark counts of the detectors. However, the advantage of the feedback protocol is not degraded by such noise. It is verified that α is conserved even with enhanced excitation probability. If the lifetime of the spin excitation is sufficiently long to allow many write sequences, the excitation probability can reach unity while the single-photon nature is still conserved. Then the generation efficiency then only depends on the retrieve efficiency itself.

In the second experiment, we use $\delta t_w = 1 \mu\text{s}$ and $N = 12$. Fig. 8.3(b) shows the measured α as a function of Δt . For every Δt , ΔT varies due to the random creation of the spin excitation by the N write sequences. The behavior of $\alpha(\Delta t)$ is related to a reversed profile of $g_{AS,S}^{(2)}(\delta)$ in Fig. 8.2(b). For the delay $\Delta t < \tau_c$, the value of α stays at a low level and varies slowly. For $\Delta t > \tau_c$, $\alpha(\Delta t)$ increases towards 1. But even for a delay of 20 μs ($\sim 2\tau_c$) we find $\alpha \sim 0.6$. A satisfying agreement is observed between the theoretical curve and the experimental data.

8.3 Discussion

Typically, the single spin excitation can be produced at a rate of 600 per second, while the detection success probability per trial is 2.5%, the overall detection rate of single-photon production is $\sim 15 \text{ s}^{-1}$. As demonstrated in the present work, the lifetime of collective states is important for the quality and production rate of single photons. In the atomic ensemble, the coherence time of the collective state suffers from the residual magnetic field around the MOT and the thermal motion of the atoms. The latter effect is negligible because of the very low temperature of the atomic cloud. Using a better compensation of residual magnetic field or using field insensitive clock states we can significantly increase the lifetime of the collective state. Moreover, by further improving the

control circuit, i.e. reducing the period of write pulses due to electronic delays, we can apply more write pulses within the lifetime. In particular, in the case with $p_{AS} = 0.003$ and a write period of 300 ns, we can obtain a single-photon source with a probability as high as 95% within a lifetime of 300 μ s.

In conclusion, we have demonstrated an experimental realization of an controllable single-photon source with atomic storage. The lifetime of the collective spin excitation reaches 12.5 μ s. A feedback circuit was constructed to control the generation of the spin excitation and the storage time δt . Being a key device in the scalable quantum communication network, this circuit also shows a promising performance in the enhancement of the excitation probability while the single-photon quality is conserved. This single-photon source is able to work at either a deterministic mode or a time controllable mode heralded by the feedback circuit. The single-photon source based on atomic ensemble has the advantages of narrow band, high quality and controllable character, which is helpful for the construction of scalable quantum information processing system in the future.

Chapter 9

Interference of photons from independent atomic ensembles

9.1 Introduction

Synchronized generation of either deterministic and storable single photons or entangled photon pairs is essential for scalable linear optical quantum information processing (LOQIP). With the help of quantum memory and feed-forward, one can thus achieve long-distance quantum communication [17, 37, 70] and efficient quantum computation [19, 23, 25, 84]. Very recently, interfering synchronized independent single photons [188] and entangled photon pairs [155] have been experimentally achieved with two pulsed spontaneous parametric down-conversion sources pumped by two synchronized but mutually incoherent femto-second lasers. However, due to the absence of quantum memory for broad-band (a few nm) single photons no feedback was applied in the above experiments, single photons or entangled photon pairs were merely generated probabilistically in each experimental run, i.e. with a small probability p . Thus, in an experiment concerning manipulation of N synchronized single (or entangled) photon sources, the experimental efficiency will decrease exponentially with the number of sources (proportional to p^N). Moreover, the short coherence time of down-converted photons (\sim a few hundred fs, defined by the bandwidth of interference filters) also makes hard the overlap of photon wavepackets coming from two distant sites. These two drawbacks together make the above experiments inappropriate for scalable LOQIP.

Following a recent proposal for long-distance quantum communication with atomic ensembles [70] (see also the improved schemes [156]), it is possible to generate narrow-band single photons or entangled photon pairs in a deterministic and storable fashion. In the past years, significant experimental progresses have been achieved in demonstration of quantum storage and single-photon sources [184, 73], and even entanglement in number basis for two atomic ensembles has been demonstrated experimentally [79]. Moreover, deterministic narrow-band single-photon sources have been demonstrated most recently with the help of quantum memory and electronic feedback circuits [74, 189, 75].

In this Chapter, we develop further the techniques used in Chapter 8 to implement synchronized generation of two independent single-photon sources from two remote atomic ensembles provided by MOT. The two synchronized single photons are further used to demonstrate efficient generation of entangled photon pairs. Since our single-photon sources are generated in principle in a deterministic and storable fashion, with the help of feed-forward the experimental methods can be used for scalable generation of photonic entanglement. Moreover, compared to the short coherence time of down-converted photons in Refs. [188, 155] the coherence time of our synchronized narrow-band single photons is about 25 ns, four orders longer, which makes it much easier to overlap independent photon wavepackets from distant sites for further applications of LOQIP. Finally, it is worth noting

that the read and write lasers used for different single-photon sources are fully independent to each other. The synchronization was achieved by separate electronic signals generated by the control electronics.

9.2 Experiment

The basic concept of our experiment is illustrated in Fig. 9.1. Atomic ensembles collected by two MOT's 0.6 m apart function as the media for quantum memories and deterministic single-photon sources. Each ensemble consists of about 10^8 ^{87}Rb atoms. The two hyperfine ground states $|5S_{1/2}, F=2\rangle=|a\rangle$ and $|5S_{1/2}, F=1\rangle=|b\rangle$ and the excited state $|5P_{1/2}, F=2\rangle=|e\rangle$ form a Λ -type system $|a\rangle-|e\rangle-|b\rangle$. The atoms are initially optically pumped to state $|a\rangle$. A write pulse Ω_w with the detuning of $\Delta = 10$ MHz and a beam diameter about $400 \mu\text{m}$ is applied to generate the spin excitation and an accompanying photon of the anti-Stokes field \hat{a}_{AS} with a beam diameter about $100 \mu\text{m}$. The mode \hat{a}_{AS} , tilted 3° from the direction of the write beam, is coupled in a single-mode fiber (SMF) and guided to a single-photon detector. The superposed state of the anti-Stokes field \hat{a}_{AS} and a collective spin state of the atoms can be described as,

$$|\Psi\rangle \sim |0_{AS}0_b\rangle + \sqrt{\chi}|1_{AS}1_b\rangle + \chi|2_{AS}2_b\rangle + O(\chi^{3/2}), \quad (9.1)$$

where $\chi \ll 1$ is the excitation probability of one spin flip, and $|i_{AS}i_b\rangle$ denotes the i -fold excitation of the anti-Stokes field and the collective spin. Ideally, conditioned on detecting one and only one anti-Stokes photon, a single spin excitation is generated in the atomic ensemble with certainty. In practice, considering photon loss in the detection, this condition can be fulfilled by keeping $\chi \ll 1$ so as to make the multi excitations negligibly small. After a controllable time delay δt_R (in the order of the lifetime τ_c of the spin excitation), another classical *read* pulse with the Rabi frequency Ω_R is applied with orthogonal polarization and spatially mode-matched with the write beam from the opposite direction. The spin excitation in the atomic ensemble will be retrieved into a single photon of the Stokes field \hat{a}_S , which propagates to the opposite direction of the field \hat{a}_{AS} and is also coupled in SMF. If the retrieve efficiency reaches unity, the Stokes photon is no longer probabilistic because of the quantum memory and feedback control [75, 189, 74], which now can serve as a deterministic single-photon source. As shown in Fig. 9.1, Alice and Bob both have such a source. They prepare collective spin excitations independently and the one who finishes the preparation first will wait for the other while keeping the collective spin excitation in her/his quantum memory. After they agree that both have finished the preparation, they retrieve the excitations simultaneously at anytime they want within the lifetime of the collective state. Therefore the retrieved photons arrive at the beam splitter with the required timing.

Compared to a probabilistic photon source, the present implementation with atomic ensembles contributes a considerable enhancement to the coincidence rate of single photons coming from Alice and Bob. For instance, we consider a similar setup but without feedback circuit, where Alice and Bob apply write and read in every experimental trial and thereafter measure the four-fold coincidence of anti-Stokes and Stokes photons in the four channels D1, D2, C1 and C2. Assume the probability to have an anti-Stokes photon in channel D1 (D2) is p_{AS1} (p_{AS2}) and the corresponding retrieve efficiency for conversion of the spin excitation to a Stokes photon coupled into channel C1 (C2) is $\gamma_1(\delta t_R)$ [$\gamma_2(\delta t_R)$], then the probability of four-fold coincidence is

$$p_{4c} = p_{AS1}\gamma_1(\delta t_R)p_{AS2}\gamma_2(\delta t_R).$$

This has to be compared with using the feedback circuits shown in Fig. 9.1, where we can apply at most N (limited by the lifetime of the quantum memory and the speed of the feedback circuit)

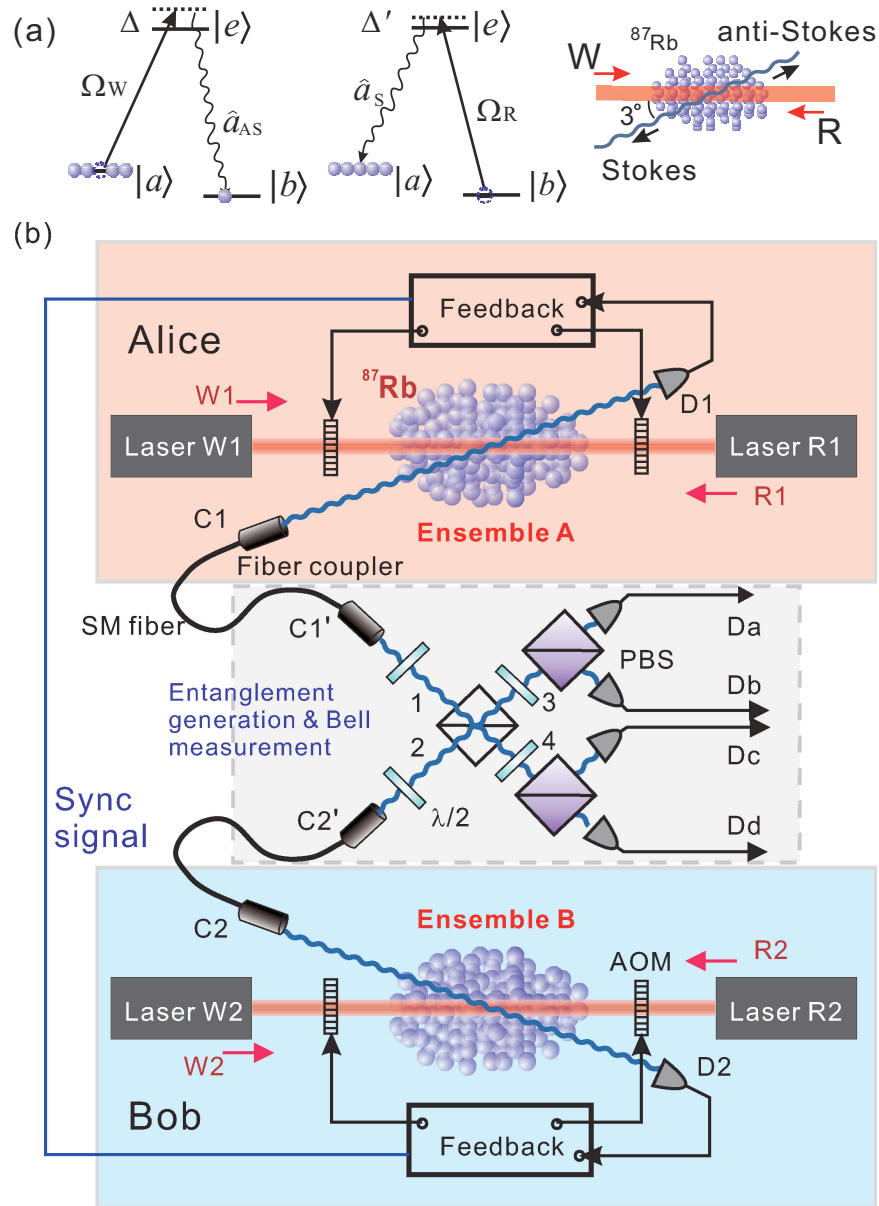


Figure 9.1: Illustration of the relevant energy levels of the atoms and arrangement of laser beams (a) and the experimental setup (b). Alice and Bob each keeps a single-photon source at two remote locations. As elucidated in Chapter 8, Alice applies write pulses continuously until an anti-Stokes photon is registered by detector D1. Then she stops the write pulse, holds the spin excitations and meanwhile sends a synchronization signal to Bob and waits for his response (This is realized by the feedback circuit and the acousto-optic modulators, AOM). In parallel Bob prepares a single excitation in the same way as Alice. After they both agree that each has a spin excitation, each of them will apply a read pulse simultaneously to retrieve the spin excitation into a light field \hat{a}_S . The two Stokes photons propagate to the place for entanglement generation and Bell measurement. They overlap at a 50:50 beam splitter (BS) and then will be analyzed by latter half-wave plates ($\lambda/2$), polarized beam splitters (PBS) and single photon detectors Da, Db, Dc, and Dd.

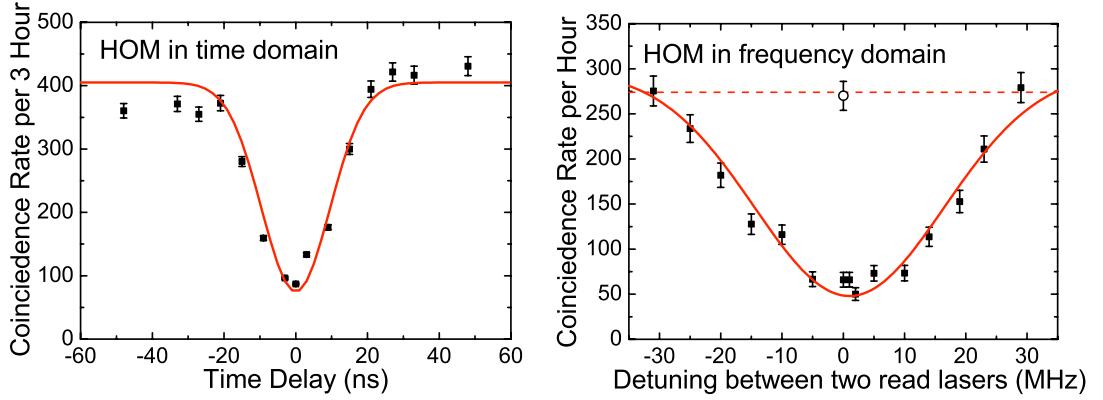


Figure 9.2: Hong-Ou-Mandel dips in time domain (left panel) and frequency domain (right panel). The circle in the right panel was obtained by setting the polarization of the two photons perpendicular to each other and zero detuning between two read lasers. The Gaussian curves that roughly connect the data points are only shown to guide the eye. The dashed line shows the plateau of the dip. Error bars represent statistical errors, which are \pm one standard deviation.

write pulses in each trial. Then the probability of four-fold coincidence becomes

$$P_{4c} = \left\{ \sum_{i=0}^{N-1} p_{AS1}(1-p_{AS1})^i \sum_{j=i}^{N-1} p_{AS2}(1-p_{AS2})^j \times \gamma_2(\delta t_R) \gamma_1[(j-i) \cdot \delta t_W + \delta t_R] \right\} + \left\{ \dots \right\}_{1 \leftrightarrow 2}, \quad (9.2)$$

where δt_W is the time interval between the sequential write pulses [75] and $\{\dots\}_{1 \leftrightarrow 2}$ is the same as the first term with index 1 and 2 being exchanged. Assume $p_{AS1} \ll 1$ and $p_{AS2} \ll 1$ and a long lifetime τ_c , we obtain

$$P_{4c} \sim N^2 p_{AS1} \gamma_1(\delta t_R) p_{AS2} \gamma_2(\delta t_R)$$

for a definite number N . So the probability of four-fold coincidence is enhanced by N^2 for each trial. For our case $p_{AS1} \approx p_{AS2} = 2.0 \times 10^{-3}$ (the relevant cross correlation $g_{AS,S}^{(2)} = 30$), $N = 12$, $\tau_c \sim 12 \mu\text{s}$, $\delta t_W = 800 \text{ ns}$, $\delta t_R = 400 \text{ ns}$, and $\gamma_1(0) \approx \gamma_2(0) = 8\%$, the enhancement is 136.

The four lasers in Fig. 9.1 are independently frequency stabilized. The linewidths of W1 and R1 are about 1 MHz while those of W2 and R2 are about 5 MHz of the full width at half maximum (FWHM). However, they will be broadened to more than 20 MHz because the laser pulse modulated by the AOM is a Gaussian-like profile with width about 40 ns FWHM. The linewidth of the retrieved single photons is determined mainly by the linewidth and intensity of the read lasers. So we try to make the profile of the two independent read pulses identical to each other.

In order to verify that the two Stokes photons coming from Alice and Bob are indistinguishable, we let them overlap at a BS with the same polarization (horizontal in our case) and measure the quantum interference indicated by the the Hong-Ou-Mandel (HOM) dip [160]. Having observed the high visibility of HOM dip in both time domain and frequency domain, we are confirmed that the two independent photons are indistinguishable. Then we put one of the two photons to vertical polarized before they enter the BS. By coincidence measurement at the two outputs of the BS, we generate the Bell state

$$|\Psi^-\rangle_{12} = \frac{1}{\sqrt{2}}(|H\rangle_1|V\rangle_2 - |V\rangle_1|H\rangle_2),$$

which is verified by the measurement of violation of Bell's Inequality.

9.3 Experimental results

Two-photon interference effect at a 50:50 standard BS can be described as follows. Quantum mechanically, the action of the beam splitter on the input modes can be written as

$$\begin{aligned} |\hat{a}_1\rangle &\longrightarrow \frac{i}{\sqrt{2}}|\hat{a}_3\rangle + \frac{1}{\sqrt{2}}|\hat{a}_4\rangle \\ |\hat{a}_2\rangle &\longrightarrow \frac{1}{\sqrt{2}}|\hat{a}_3\rangle + \frac{i}{\sqrt{2}}|\hat{a}_4\rangle \end{aligned} \quad (9.3)$$

where, e.g. $|\hat{a}_i\rangle$ describes the spatial quantum state of the particle in input beam i . Note that a standard BS is polarization independent, and thus has no effect on the polarization state of the photon. Considering two independent photons with polarization state $\alpha|H\rangle_1 + \beta|V\rangle_1$, and $\gamma|H\rangle_2 + \delta|V\rangle_2$ overlap at the BS, the input state can be described as,

$$|\psi_i\rangle = (\alpha|H\rangle_1 + \beta|V\rangle_1)|\hat{a}_1\rangle \cdot (\gamma|H\rangle_2 + \delta|V\rangle_2)|\hat{a}_2\rangle. \quad (9.4)$$

As shown in Eq. 9.3, for photons 1 and 2 passing through the beam splitter their spatial modes will undergo a corresponding unitary transformation. The state in Eq. 9.4 thus evolves into

$$|\psi_f\rangle_{12} = \frac{1}{\sqrt{2}}(\alpha|H\rangle_1 + \beta|V\rangle_1)(i|\hat{a}_3\rangle + |\hat{a}_4\rangle) \cdot \frac{1}{\sqrt{2}}(\gamma|H\rangle_2 + \delta|V\rangle_2)(|\hat{a}_3\rangle + i|\hat{a}_4\rangle). \quad (9.5)$$

If we assume that the two photons have the same frequency and arrive at the beam splitter simultaneously thus they are indistinguishable anymore after passing through the beam splitter. The total two-photon state including both the spatial and the spin part, therefore, has to obey bosonic quantum statistics. This implies that the outgoing physical state must be symmetric under exchange of labels 1 and 2. To do so, one should symmetrize the state $|\psi_f\rangle_{12}$, that is, also include its exchange wave-function

$$|\psi_f\rangle_{21} = \frac{1}{\sqrt{2}}(\alpha|H\rangle_2 + \beta|V\rangle_2)(i|\hat{a}_3\rangle + |\hat{a}_4\rangle) \cdot \frac{1}{\sqrt{2}}(\gamma|H\rangle_1 + \delta|V\rangle_1)(|\hat{a}_3\rangle + i|\hat{a}_4\rangle). \quad (9.6)$$

The final outgoing state therefore reads

$$|\psi_f\rangle = \frac{1}{\sqrt{2}}(|\psi_f\rangle_{12} + |\psi_f\rangle_{21}), \quad (9.7)$$

and consequently we have

$$\begin{aligned} |\psi_f\rangle = &\frac{1}{2}[(\alpha\gamma + \beta\delta)\Phi_{12}^+ \cdot i(|\hat{a}_3\rangle|\hat{a}_3\rangle + |\hat{a}_4\rangle|\hat{a}_4\rangle) \\ &+(\alpha\gamma - \beta\delta)\Phi_{12}^- \cdot i(|\hat{a}_3\rangle|\hat{a}_3\rangle + |\hat{a}_4\rangle|\hat{a}_4\rangle) \\ &+(\alpha\delta + \beta\gamma)\Psi_{12}^+ \cdot i(|\hat{a}_3\rangle|\hat{a}_3\rangle + |\hat{a}_4\rangle|\hat{a}_4\rangle) \\ &+(\alpha\delta - \beta\gamma)\Psi_{12}^- \cdot (|\hat{a}_4\rangle|\hat{a}_3\rangle - |\hat{a}_3\rangle|\hat{a}_4\rangle)]. \end{aligned} \quad (9.8)$$

From Eq. 9.8, it is clear that consider two parallel polarization state photon, i.e. $\alpha = \gamma$ and $\beta = \delta$ both of the photons will come out through same outputs. While in the case with two photons that are not parallel, two photons proceed after the beam splitter in different emerging beams if, and only if, their polarization state is in the state $|\Psi^-\rangle_{12}$ (refer to the fourth term of Eq. 9.8). Thus by post-selecting the two-fold coincidence in mode 3 and 4 we generate the maximally entangled state Ψ^- .

9.3.1 The measurement of HOM dip

We did two measurements to obtain the HOM dip in time domain and frequency domain respectively. To make the photons indistinguishable, the polarizations of the anti-Stokes photons were

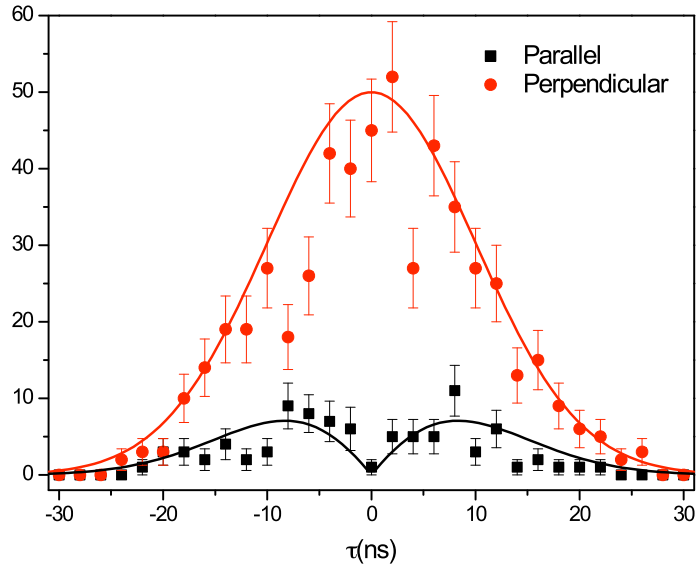


Figure 9.3: Hong-Ou-Mandel dips in time domain with coincidence window (2 ns) much shorter than the wave-package length. The red spots are measured under perpendicular polarization and the black ones are measured under parallel cases.

set to horizontal with two half-wave plates before they enter the BS as shown in Fig. 9.1. The other two half-wave plates after the BS were set to 0° .

In the first measurement, we measured the four-fold coincidence among detectors D1, D2, Da and Dd while changing the time delay between the two read pulses (Fig. 9.2, left panel). The excitation probabilities $p_{AS1} \approx p_{AS2} = 2.0 \times 10^{-3}$. The coincidence rate varies with the delay. Ideally, there should be complete destructive interference if the wavepackets of the two photons overlap perfectly. However, it is hard to make the two wavepackets absolutely identical or exactly overlapped in practice. We obtained the visibility of the dip $V = (C_{\text{plat}} - C_{\text{dip}})/C_{\text{plat}} = (80 \pm 1)\%$, where C_{plat} is the non-correlated coincidence rate at the plateau and C_{dip} is the interfering coincidence rate at the dip. The asymmetry of the profile at negative delay and positive delay shows that the two wavepackets are (a) not perfectly identical, (b) not symmetric themselves. Assume the HOM dip is a Gaussian-type profile, we estimate the coherence time is 25 ± 1 ns FWHM.

In the second measurement, we measured the four-fold coincidence among detectors D1, D2, Da and Dd while changing the frequency detuning between the two read pulses (Fig. 9.2, right panel). It is the first time to measure HOM dip in the frequency domain at single-photon level. The excitation probabilities are $p_{AS1} \approx p_{AS2} = 3.0 \times 10^{-3}$, higher than those in the time domain. Because of the limit of the current setup, the detuning can be varied from -30 MHz to 30 MHz. In order to verify the coincidence rate at largest detuning reached the plateau of HOM dip, we measured the coincidence by setting the polarization of the two photons perpendicular to each other and zero detuning between the two read lasers (shown as a circle in Fig. 9.2). The consistence of this data with those two at largest detunings shows that we have achieved the plateau of HOM dip. The visibility is $(82 \pm 3)\%$ which agrees well with that obtained in time domain. The width of the HOM dip is 35 ± 3 MHz FWHM, in accordance with the coherence time 25 ns. Therefore, the narrow-band characteristic of the present source is verified directly by the HOM dip in the frequency domain.

Table 9.1: Correlation functions E and the resulting S .

| E | $\theta_1 = 0^\circ$ | $\theta'_1 = 45^\circ$ | S |
|---------------------------|----------------------|------------------------|-----------------|
| $\theta_2 = 22.5^\circ$ | -0.613 ± 0.037 | 0.575 ± 0.039 | 2.37 ± 0.07 |
| $\theta'_2 = -22.5^\circ$ | 0.606 ± 0.038 | 0.579 ± 0.039 | |

9.3.2 Time resolved two-photon interference

Note that, in Fig. 9.2 right panel, HOM dip is measured by setting the coincidence window (here ~ 50 ns) larger than the wave-package length of the single photons (~ 25 ns). In Fig. 9.3, we measure the time-resolved two-photon quantum interference by setting the wave-package at perfect temporal overlap and setting the coincidence window (2 ns in the experiment) much shorter than the wave-package length. The red spots are measured under perpendicular polarization and the black ones are measured under parallel cases. It is clear there is also a dip at 0 delay, which is consistent with both the theoretical and experimental results [190, 191] rather than the plateau at 0 delay in ref. [76].

9.3.3 Efficient entanglement generation

As shown in Fig. 9.1, we set orthogonal polarizations (horizontal and vertical) of the Stokes photons with the two half-wave plates before the BS. Then the state of the two photons will be projected to $|\Psi^-\rangle_{12}$ if there is coincidence between the two output port 3 and 4 as shown in Eq. (9.8). With another two half-wave plates and two PBS after the BS, the entanglement of the two photons can be verified by a Clauser-Horne-Shimony-Holt (CHSH) type inequality [114], where $S \leq 2$ for any local realistic theory with

$$S = |E(\theta_1, \theta_2) - E(\theta_1, \theta'_2) - E(\theta'_1, \theta_2) - E(\theta'_1, \theta'_2)|. \quad (9.9)$$

Here $E(\theta_1, \theta_2)$ is the correlation function where θ_1 and θ'_1 (θ_2 and θ'_2) are the measured polarization angles of the Stokes photon at port 3 (4). The observed values of the correlation functions are listed in Table 9.1 resulting in $S = 2.37 \pm 0.07$, which violates Bell's Inequality by 5 standard deviations. This clearly confirms the quantum nature of the entanglement state.

9.4 Discussion

Besides the imperfect overlap of the single-photon wavepackets, the two-photon components in each of the single-photon sources affect the visibility as well. The quality of single-photon source is characterized by the anti-correlation parameter $\alpha = 2P_{\text{II}}/P_{\text{I}}^2$ [75], where P_{I} (P_{II}) is the probability of generating one (two) photon(s) for each source (the higher orders are negligible small). If the two wavepackets do not overlap at all, there is no interference between them. Then we obtain the non-correlated coincidence rate $C_{\text{plat}} = P_{\text{I}}^2/2 + P_{\text{II}}$ between Da and Dd. If they overlap perfectly, there is destructive interference leading to a coincidence rate $C_{\text{dip}} = P_{\text{II}}$. So the visibility of the HOM dip is $V = 1/(1 + \alpha)$. In our experiment, $\alpha = 0.12$ for the source prepared later (the spin excitation is retrieved immediately) and $\alpha = 0.17$ for the source prepared earlier (it has to wait for the other one). This leads to an average visibility of 87%. In the frequency domain, the average visibility is around 83% because of higher excitation probabilities.

Moreover, with our imperfect sources we do not create a perfect $|\Psi^-\rangle_{12}$. If we consider the two photon component in the photon sources the created state will be:

$$|\Psi_{\text{eff}}\rangle_{12} = \begin{cases} P_{\text{I}}^2/2, & 1/\sqrt{2}(|H\rangle_1|V\rangle_2 - |V\rangle_1|H\rangle_2); \\ P_{\text{II}}/2, & |H\rangle_1|H\rangle_2; \\ P_{\text{II}}/2, & |V\rangle_1|V\rangle_2. \end{cases} \quad (9.10)$$

From the quality of the single photons generated from the two ensembles, $\alpha = 0.12, 0.17$ and Eq. (9.10), we estimate the expected violation of Bell's Inequality is around 2.3, which is in good agreement with our measured value. It is interesting to note that a violation of Bell's Inequality needs a single photon source with $\alpha < 0.24$ according to Eq.(9.10). In order to minimize α , further improvements, e.g., a higher optical couple efficiency, a lower photon loss, a lower excitation probability and a higher retrieve efficiency, will be made in our future investigations.

In conclusion, we realized synchronized generation of narrow-band single photons with two remote atomic ensembles. The Hong-Ou-Mandel dip was observed in both time domain and frequency domain with a high visibility for independent photons coming from two distant sites, which shows the indistinguishability of these photons. By virtue of quantum memories and feedback circuits, the efficiency of generating entangled photon pairs was enhanced by a factor of 136, which claims our single-photon source as a promising candidate for the future implementation of scalable quantum computation based on linear optics [19, 23, 25, 84]. The present spatially-distributed independent single-photon sources (with fully independent write and read lasers) are pre-requirements for the long-distance quantum communication [17, 156]. The narrow-band property (which makes the overlap of the photon wavepackets at the order of nanoseconds) of single photons and high efficiency of entanglement generation also profit the present source to serve as an ideal candidate for large scale communications, e.g., satellite-based quantum communication.

Chapter 10

Teleportation between photonic and atomic qubits

10.1 Introduction

As we introduced in Chapter 5, quantum teleportation [7], the way to transfer the state of a quantum system from one place to another, is one of the most intriguing examples of how quantum entanglement can assist in realizing practical tasks and is involved in numerous quantum communication [17] and quantum computation schemes [18, 19]. Teleportation was first demonstrated between two independent photonic qubits [31]; later developments include demonstration of entanglement swapping [34], open-destination teleportation [43] and teleportation of a quantum state between two ionic qubits [122, 121]. Teleportation has also been demonstrated for continuous variable system, i.e. transferring a quantum state from one light beam to another [192] and, most recently, even from light to matter [193].

However, the above demonstrations of teleportation have severe drawbacks, especially in long-distance quantum communication. On the one hand, the absence of quantum storage makes the teleportation of light alone non-scalable. On the other hand, in teleportation of ionic qubits the shared entangled pairs were created locally which limits the distance of teleportation up to a few μm and is difficult to extend to large distances. In continuous variable teleportation between light and matter the experimental fidelity is extremely sensitive to the transmission loss - even in the ideal case only a maximal attenuation of 10^{-1} is tolerable [194]. Moreover, the complicated protocol required in retrieving the teleported state in the matter [195] is out of the reach of current technology.

Remarkably, the combination of quantum teleportation and quantum memory of photonic qubits [70, 165, 167, 156] could provide a novel way to overcome these drawbacks. Even though both of them have been demonstrated separately in many proof-of-principle experiments [31, 34, 43, 80, 73, 184], the demonstration of such memory-built-in teleportation of photonic qubits, remains an experimental challenge.

Here we achieve this appealing combination by experimentally implementing teleportation between discrete photonic (flying) and atomic (stationary) qubits. In our experiment, we use the polarized photonic qubits as the information carriers and the collective atomic qubits [70, 165, 167, 156, 80] (an effective qubit consists of two atomic ensembles, each with 10^6 ^{87}Rb atoms) as the quantum memory. In memory-built-in teleportation, an unknown polarization state of single photons is teleported onto and stored in a remote atomic qubit via a Bell-state measurement between the photon to be teleported and the photon that is originally entangled with the atomic qubit. The protocol has several distinct features: First, different from ionic system its information carrier (flying photonic qubit) is robust against decoherence and can be easily transmitted

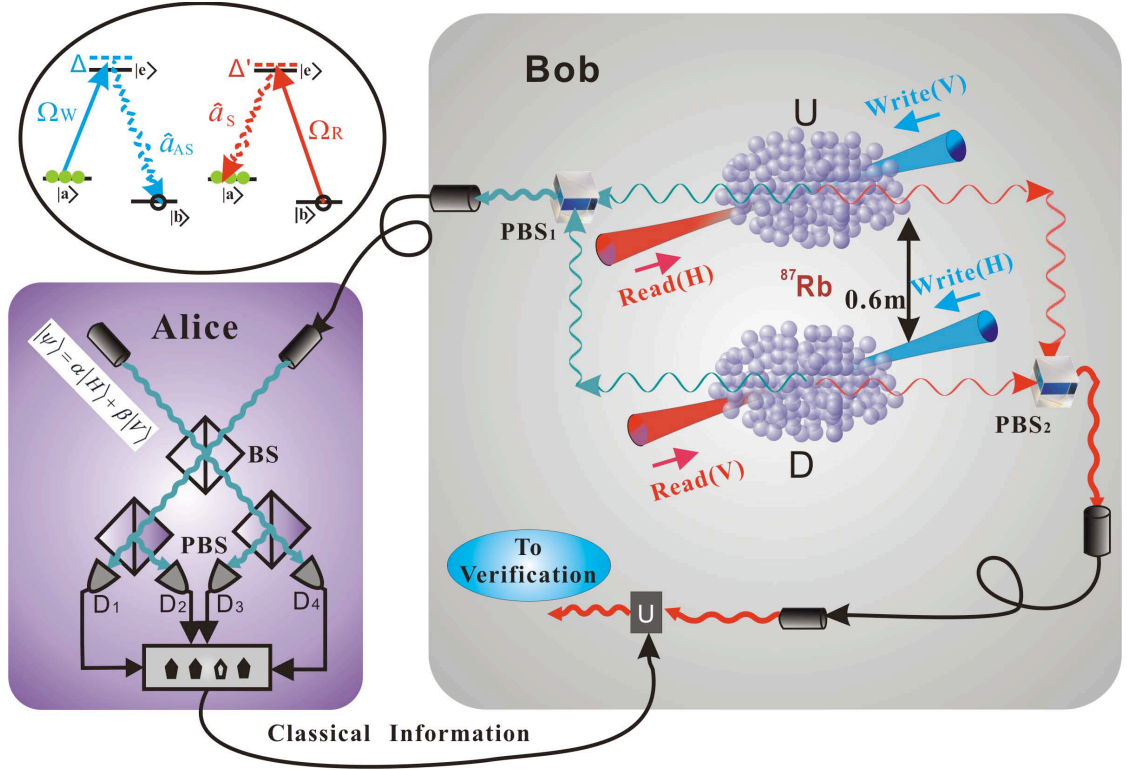


Figure 10.1: Experimental setup for teleportation between photonic and atomic qubits. The inset shows the structure and the initial populations of atomic levels for the two ensembles. At Bob’s site the anti-Stokes fields emitted from U and D are collected and combined at PBS_1 , selecting perpendicular polarizations. Then the photon travels 7 m through fibers to Alice’s to overlap with the initial unknown photon on a beam-splitter (BS) to perform the Bell-state measurement. The results of the Bell-state measurement are sent to Bob via a classical channel. The results of the Bell-state measurement are sent back to Bob via a classical channel. Bob then perform the verification of the teleported state in the U and D ensembles by converting the atomic excitation to a photonic state. A unitary operation on the converted photon is performed according to the classical information from the results of Bell-state measurement is performed.

over large distances. Second, different from continuous variable system its teleportation fidelity is insensitive to photon losses. In practice, an overall transmission attenuation of 10^{-4} is tolerable with current technology, as demonstrated in recent experiments [174, 175]. Moreover, since the collective state of atomic ensembles is used to encode an atomic qubit, the teleported state can be easily read out in a controllable time for further quantum information applications. Besides being of fundamental interest, most importantly, our memory-built-in teleportation protocol with the direct inclusion of a readable quantum memory enables efficient and scalable connection of quantum networks [165, 167, 156].

10.2 Experiment scheme

A schematic setup of our experiment is shown in Fig. 1. At Bob’s site, a pair of effective maximally entangled qubits is created by sending two classical light pulses through two atomic ensembles U (up) and D (down) which are located in two magneto-optical traps (MOTs) of ^{87}Rb 0.6 m apart. The two ground states $|a\rangle$ ($5S_{1/2}, F = 2$) and $|b\rangle$ ($5S_{1/2}, F = 1$) form together with the excited level $|e\rangle$ ($5P_{1/2}, F' = 2$) a Λ type system. Initially each ensemble is prepared in the ground state

$|a\rangle$. Shining a weak classical write pulse coupling the transition $|a\rangle \rightarrow |e\rangle$ with a red detuning Δ (10 MHz) and the Rabi frequency Ω_W into ensembles m ($m = U$ or D), creates a superposition between the anti-Stokes field \hat{a}_{AS} and a collective spin state of the atoms [70],

$$|\Psi\rangle_m = |0_{AS}0_B\rangle_m + \sqrt{\chi_m}|1_{AS}1_B\rangle_m + O(\chi_m) \quad (10.1)$$

where $\chi_m \ll 1$ is the excitation probability of one spin flip in ensemble m , and $\sqrt{\chi_m}|i_{AS}i_B\rangle_m$ denotes the i -fold excitation of the anti-Stokes field and the collective spin. We adjust $\chi_U = \chi_D$, select orthogonal polarization of the two anti-stokes fields and combine them on a polarized beam splitter (PBS₁), as illustrated in Fig. 10.1. Neglecting the vacuum state and higher order excitations, the entangled state between photonic and atomic qubits can be described as an effectively entangled state,

$$|\Psi\rangle = \frac{1}{\sqrt{2}} \left(|H\rangle|\tilde{V}\rangle + |V\rangle|\tilde{H}\rangle \right) \quad (10.2)$$

where $|\tilde{H}\rangle = |0_B\rangle_U|1_B\rangle_D$ ($|\tilde{V}\rangle = |1_B\rangle_U|0_B\rangle_D$) denotes one spin excitation in ensemble $D(U)$. Physically, the atom-photon entangled state (10.2) is exactly equivalent to the maximally polarization entangled state generated by spontaneous parametric down-conversion [53]. Note that, the coherence time of the photonic qubit in the atom-photon entangled state 10.2 is about 25 ns [78], which makes the overlap between the anti-Stokes photon and the photon to be teleported very easy.

After the effectively entangled state (10.2), the Anti-Stokes photon is sent to Alice over a 7 m long fiber. Suppose that at Alice's site, the photon to be teleported is in an unknown polarization state $|\phi\rangle = \alpha|H\rangle + \beta|V\rangle$. In terms of four Bell states $|\Psi^\pm\rangle = (|HV\rangle \pm |VH\rangle)/\sqrt{2}$, and $|\Phi^\pm\rangle = (|HH\rangle \pm |VV\rangle)/\sqrt{2}$, the combined state of the three qubits can be rewritten as

$$|\phi\rangle|\Psi\rangle = \frac{1}{2}(|\Phi^+\rangle\hat{\sigma}_x|\tilde{\phi}\rangle + |\Phi^-\rangle(-i\hat{\sigma}_y|\tilde{\phi}\rangle) + |\Psi^+\rangle|\tilde{\phi}\rangle + |\Psi^-\rangle\hat{\sigma}_z|\tilde{\phi}\rangle) \quad (10.3)$$

where $\hat{\sigma}_x$, $\hat{\sigma}_y$ and $\hat{\sigma}_z$ are the well-known Pauli operators, and $|\tilde{\phi}\rangle = \alpha|\tilde{H}\rangle + \beta|\tilde{V}\rangle$. It can thus be seen that a joint Bell-state measurement on the two photons at Alice's side projects the state of atomic qubit at Bob's side into one of the four corresponding states as shown in equation (10.3). After the Bell-state measurement, the initial state of photonic qubit is thus transferred to and stored in the atomic qubit. In standard teleportation, depending on the Bell-state measurement results Bob can then perform a unitary transformation, independent of $|\tilde{\phi}\rangle$, on the atomic qubit to convert its state into the initial state of the photonic qubit.

To achieve the required Bell-state measurement, the photon from the entangled state 10.2 and the photon to be teleported are superposed on a 50:50 beam-splitter (BS in Fig. 10.1). The BS together with the subsequent coincidence measurements is capable of identifying two of the four Bell-states [30], $|\Psi^+\rangle$ and $|\Psi^-\rangle$ in our experiment. This results in a reduced efficiency - the fraction of success - of 50%. Note that, to demonstrate the working principle of teleportation it is sufficient to identify only one of the four Bell-states, e.g. via identification of $|\Psi^+\rangle$ and verification of $|\tilde{\phi}\rangle$ [31, 34, 43].

To verify the success of teleportation, we convert the atomic excitation back to a optical excitation in a controllable time by shining in two simultaneous read pulses, coupling the transition $|b\rangle \rightarrow |e\rangle$ with a blue detuning Δ' (6 MHz) and the Rabi frequency Ω_R . The polarizations of the two read pulses are selected to be perpendicular with respect to the corresponding write pulses. The retrieved Stokes fields are then combined at PBS₂. Hence, the atomic qubit is converted back to a single-photon polarization state. Instead of performing a direct measurement on the atomic qubit, via a polarization measurement on the converted single-photon state we can thus obtain the experimental teleportation fidelity.

If teleportation occurs, conditional on detecting a $|\Psi^+\rangle$ state at Alice's side the state of the atomic qubit at Bob's side will be left in the state $|\tilde{\phi}\rangle$ (equation (10.3)). Following the above read out protocol the collective atomic state $|\tilde{\phi}\rangle$ will be converted into exactly the initial polarization

state $|\phi\rangle$. On the other hand, if a $|\Psi^-\rangle$ state is detected the state of the atomic qubit will then be left in the state $\hat{\sigma}_z|\tilde{\phi}\rangle$, which after conversion is equivalent to the initial state except for a unitary transformation $\hat{\sigma}_z$. Consequently, applying $\hat{\sigma}_z$ on the converted single-photon polarization state we will again obtain the same initial state $|\phi\rangle$. It is worth noting that, the ease of both transferring atomic excitation to optical excitation and exploiting linear optical elements to perform precise unitary transformation on single-photon states is a distinct advantage of our method.

10.3 Experimental realization

In the experiment, the MOT is loaded for 20 ms at a repetition rate of 40 Hz. The magnetic field and the cooling beams are then quickly switched off while the repumping beams stay on for 0.5 ms before being switched off in order to prepare the atoms in the initial $F = 2$ ground state $|a\rangle$. Then, within another 4.5 ms experimental trials (each consisting of successive write, read and repumping pulses) are repeated with a controllable period depending on the desired retrieve time of the teleported state. In each experimental trial, two write pulses Ω_W with the red detuning of $\Delta = 10$ MHz, beam diameter about 400 μm and orthogonal polarization are simultaneously applied to the two atomic ensembles to generate the spin excitation and two accompanying anti-Stokes fields \hat{a}_{AS} with beam diameter about 100 μm . The anti-Stokes modes, are tilted 3° from the direction of the corresponding write beam, and guided to PBS₁ and then sent to Alice's site by a single-mode fiber.

Before performing the teleportation, it is necessary to verify the entanglement. To do so, we map the atomic excitations back into a single photon by sending two classical read pulses through the two ensembles. The retrieved Stokes fields with perpendicular polarizations are combined on PBS₂ (Fig. 10.1). And, the superposition state of anti-Stokes and Stokes fields is effectively equivalent to the following maximally polarization entangled state

$$|\Psi\rangle_{AS,S} \sim |H\rangle_{AS}|V\rangle_S + e^{i(\phi_1+\phi_2)}|V\rangle_{AS}|H\rangle_S. \quad (10.4)$$

Here $\phi_{1(2)} = \Delta\theta_{W(R)} + \Delta\theta_{AS(S)}$ represents the phase difference between the two anti-Stokes (Stokes) fields at the PBS₁ (PBS₂). As shown in Fig. 10.2, $\Delta\theta_{W(R)}$ arises from the path difference of the two write (read) beams from BS₂ (BS₁) to the U and D ensembles; $\Delta\theta_{AS(S)}$ arises from the path difference between the two anti-Stokes (Stokes) fields from the U and D ensembles to the PBS₁ (PBS₂). In the experiment $\Delta\theta_W + \Delta\theta_{AS}$ and $\Delta\theta_R + \Delta\theta_S$ are actively stabilized by two Mach-Zehnder interferometers, respectively. Note that, even though the phase $\phi_{1(2)}$ might vary from trial to trial, however, the total phase $\phi_1 + \phi_2$ is actively stabilized and fixed to zero as describing later.

After the effective entanglement between the photonic and atomic qubits is generated, the photon travels 7 m through an optical fiber to Alice's site, where it is overlapped with the initial unknown photon on a BS performing the Bell-state measurement. Knowing the Bell-state measurement result from Alice by a classical channel, Bob then perform the verification of the teleported state in the U and D ensembles by converting the atomic excitation to a photonic state. If a $|\Psi^+\rangle$ is registered, Bob directly performs a polarization analysis on the converted photon to measure the teleportation fidelity. On the other hand, if a $|\Psi^-\rangle$ is registered, the converted photon is sent through a HWP via the first order diffraction of an AOM (not shown in Figure). The HWP is set at 0 degree serving as the unitary transformation of $\hat{\sigma}_z$. Then the photon is further sent through the polarization analyzer to obtain the teleportation fidelity.

10.3.1 Phase locking

In order to stabilize the phase $\phi_1 + \phi_2$ in expression (10.4) actively, two Mach-Zehnder interferometers are used as shown in Fig. 10.2. Because the spatial mode of anti-Stokes (Stokes) field and Wire (Read) beam have 3° angle, we can not lock the phase $\phi_1 (= \Delta\theta_W + \Delta\theta_{AS})$ and $\phi_2 (= \Delta\theta_R + \Delta\theta_S)$ directly. However, we can lock the phase of $\Delta\theta_W + \Delta\theta_R$ and $\Delta\theta_{AS} + \Delta\theta_S$ separately.

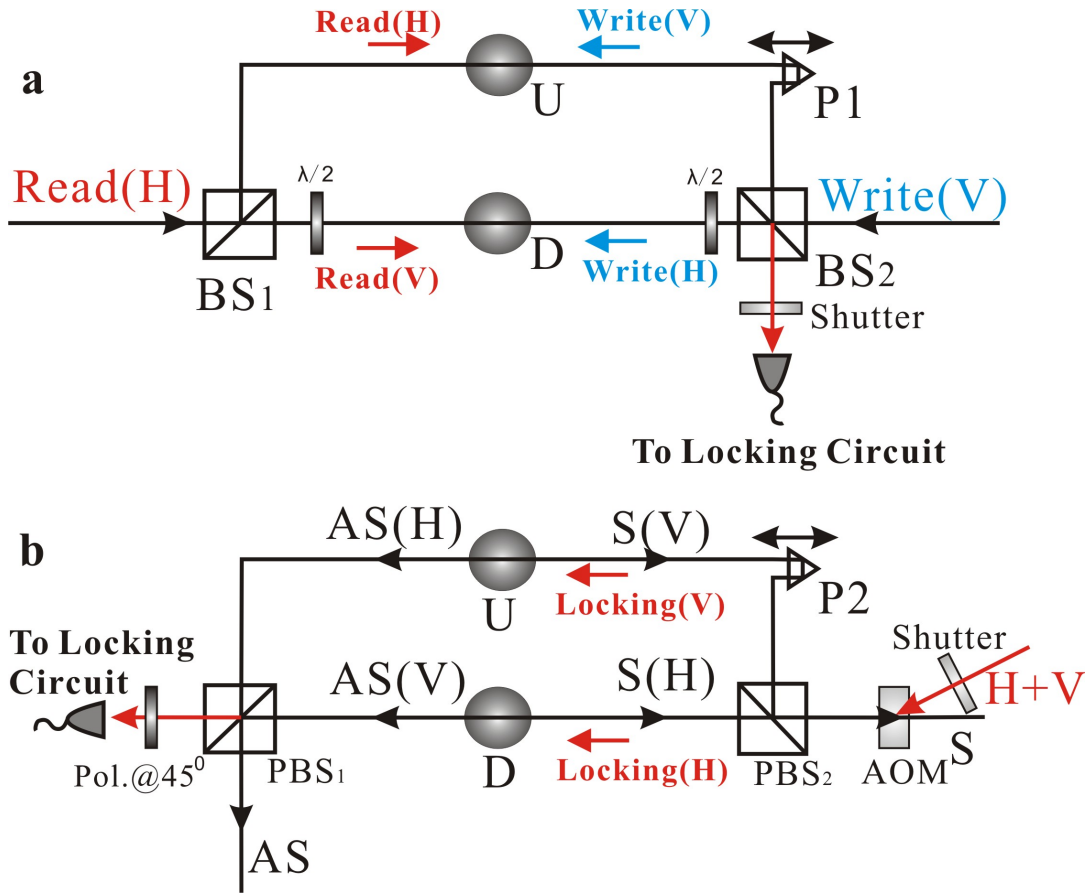


Figure 10.2: Schematic drawing of the phase locking setup. Two Mach-Zehnder interferometers are used to actively stabilize the phases between the arms of write and read paths (a) and between the arms of anti-Stokes and Stokes paths (b), respectively. H/V denotes the horizontal/vertical polarization, and AOM is for an acousto-optic modulator. A polarizer (Pol.) is set at 45° to erase the polarization information. The HWPs ($\lambda/2$) are set at 45° as well to rotate the horizontal polarization to vertical. AS (S) denotes the anti-Stokes (Stokes) photon.

To stabilize the phase of $\Delta\theta_W + \Delta\theta_R$, the read beam is switched on during the 20 ms MOT loading stage, used as the locking beam (Fig. 10.2a). During the 5 ms experimental stage, the shutter is switched off. The interference signal can be used as the error signal of a standard proportional-integrator (PI) locking circuit. The error signal is normalized by the duty cycle and then sent to the homebuilt PI circuit. By controlling the voltage of the piezo (P1) we can lock the phase $\Delta\theta_W + \Delta\theta_R$ to a set value.

To stabilize the phase of $\Delta\theta_{AS} + \Delta\theta_S$, an additional locking beam polarized at 45 degree with the frequency of read beam is sent in at the angle of the first order diffraction of the AOM (Fig. 10.2b) during the MOT loading stage. Passing through the AOM, the locking beam is overlapped with the Stokes and anti-Stokes beams. Since the anti-Stokes and Stokes light are perpendicularly polarized, the output of the locking beam is from another port of PBS₁. After the locking beam goes through a polarizer at 45 degree, the interference signal can be detected by a photodiode and used to lock the phase $\Delta\theta_{AS} + \Delta\theta_S$. During the experimental stage, the shutter and the RF power of AOM are all switched off to prevent the leakage of the locking beam from entering into the anti-Stokes – Stokes channels. In this way, the overall phase of $\phi_1 + \phi_2$ is actively locked.

Table 10.1: Fidelities of teleporting a photonic qubit at a storage time of $0.5 \mu s$. Data for teleporting each state are collected two hours. The error bars represent the statistical error, i.e. ± 1 standard deviation.

| Original state | fidelities |
|----------------|-------------------|
| $ H\rangle$ | 0.865 ± 0.017 |
| $ +\rangle$ | 0.737 ± 0.009 |
| $ R\rangle$ | 0.750 ± 0.009 |

10.3.2 Photonic qubit to be teleported

We need as well a single photon to prepare the initial state. This can be realized as the described in Chapter 8. However, to simplify the experiment, we using a weak coherent pulse which has the same frequency as anti-Stokes photon to prepare the initial state in stead of single photon. Without loss of generality, we select horizontal ($|H\rangle$), 45-degree ($|+\rangle = \frac{1}{\sqrt{2}}|H + V\rangle$) and right-hand circular ($|R\rangle = \frac{1}{\sqrt{2}}|H + iV\rangle$) polarizations as our initial states. As shown in Fig. 10.1, after knowing the BSM results at Alice's site, the atomic excitation at Bob's site is then converted back to a photonic state in a controllable time to analyze the teleportation fidelity.

With emphasis we note that, since the two-photon events from the weak coherent pulses would contribute a significant amount of spurious two-fold Bell-state measurement coincidences – which herald nothing but the arrival of two source photons and can not be distinguished from the true Bell-state measurement results, a two-fold Bell-state measurement click could only with average probability of about 40% herald the success of teleportation in our experiment, given an arbitrary initial state (see § 10.5.1). Therefore, as in previous teleportation experiments [31, 34, 43], in reality our teleportation only occurs posteriorly, i.e. conditional on detecting a three-fold coincidence.

10.4 Experimental result

With a generation probability of anti-Stokes photon 0.003, the signal-to-noise ratio between the desired ($|H\rangle_{AS}|V\rangle_S$ and $|V\rangle_{AS}|H\rangle_S$) and unwanted ($|H\rangle_{AS}|H\rangle_S$ and $|V\rangle_{AS}|V\rangle_S$) components is observed to be 15:1, corresponding to a visibility of 87.5% with a statistical error 0.4%. This confirms that the $|H\rangle_{AS}|V\rangle_S$ and $|V\rangle_{AS}|H\rangle_S$ terms are the dominant components. Furthermore, in order to prove the two terms are indeed in a coherent superposition, we also measure the signal-to-noise ratio in the 45-degree polarization basis. The experimental results of the polarization correlation exhibit an interference fringe with a visibility of $(82.2 \pm 0.4)\%$, confirming the high quality of our atom-photon entanglement.

Moreover, the probability of containing a single photon for each weak coherent pulse is 0.03. And, due to the imperfect retrieve, collection and detection efficiency of the teleported state, 30%, 75% and 50% respectively, in our experiment the overall teleportation success probability is about 10^{-6} . Table 10.1 shows the experimental result of the teleportation fidelities at a retrieve time of $0.5 \mu s$. The result shows the fidelities for different initial states are all well beyond the classical limit of two-thirds [196], confirming the success of teleportation between photonic and atomic qubits.

To show the ability to store the teleported state in our quantum memory, we further measure the fidelity of teleportation of right-hand circular polarization for different retrieval time. The result is shown in Fig. 10.3. Up to $8 \mu s$ the fidelity is still above the classical limit [196]. The fidelity drops down mainly because of the decoherence in the collective atomic state [75].

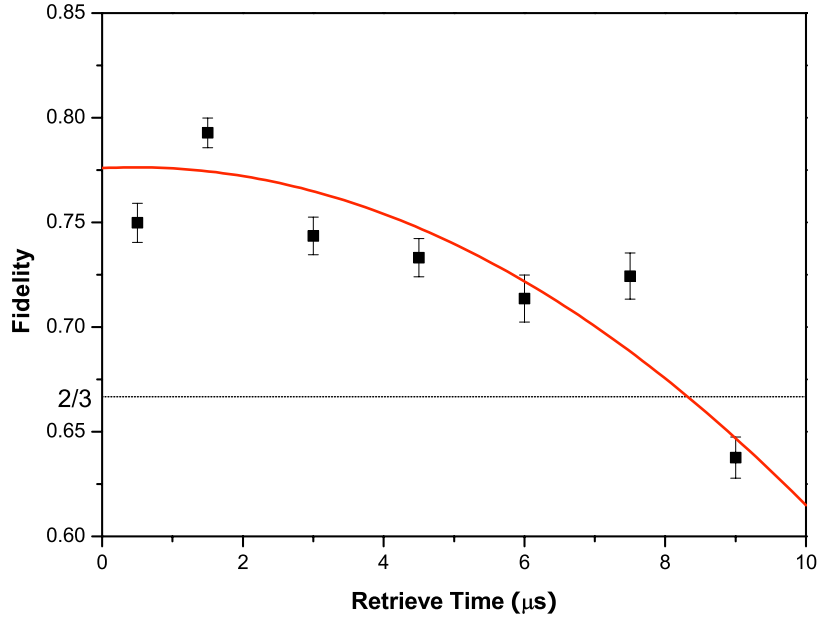


Figure 10.3: Fidelity of the teleported state in atomic ensembles along storage time. The initial state to be teleported is $H + iV$. Until $8 \mu s$ the fidelity is still well beyond the classical limit of $2/3$. Each experimental point is measured for about four hours (averagely). The curve is a Gaussian fit, due to the Gaussian decay of the retrieve efficiency. The error bars represent the statistical error, i.e. ± 1 standard deviation.

10.5 Discussion – noise estimation

In our experiment, the intensity of the write pulses is adjusted such that in each experimental run, the probability of creating an anti-Stokes photon behind the PBS_1 is $p_{AS} \sim 0.003$. The intensity of the read pulses is about 70 times higher than the write pulses. Under this condition we achieve a retrieve efficiency of $\gamma \sim 30\%$. After each write and read process, the probability of emitting a single photon in Stokes mode (denoted by p_S) is measured to be ~ 0.004 . In each weak coherent pulses, the probability of containing a single photon is $p_0 \sim 0.03$.

10.5.1 Bell-state measurement

Thus, a Bell-state measurement result, i.e. two-fold coincidence would mainly have three components:

(1) Coincidence between a single photon from the weak coherent beam and an anti-Stokes photon, which is the desired Bell-state measurement result and has a probability of

$$\sim \frac{1}{2} p_{AS} p_0 \eta^2.$$

Here η is the average overall detection efficiency of our single-photon detectors, i.e. the product of the collection efficiency ($\sim 75\%$) and the detection efficiency of the detectors ($\sim 50\%$).

(2) Spurious coincidence contributed by the double emission from the weak coherent beam. In teleportation of $|+\rangle$ and $|R\rangle$ states, the probability of registering such two-fold coincidence is given

by

$$\sim \frac{1}{4} p_0^2 \eta^2.$$

However, since only Ψ^\pm is analyzed in our Bell-state measurement, in teleportation of $|H\rangle$ state, the double emission from the weak coherent beam leads no two-fold coincidence.

(3) Spurious coincidence contributed by the double emission from the atomic ensembles, which has a probability of

$$\sim \frac{1}{4} p_{AS}^2 \eta^2.$$

Substituting the experiment parameters, we thus get that, for $|H\rangle$ teleportation, a Bell-state measurement click will with a probability of 95% herald the success of teleportation, however for $|+\rangle$ and $|R\rangle$ teleportation, a Bell-state measurement click will only with a probability of 17% herald the success of teleportation. Thus given an arbitrary input state the average probability to herald the success of teleportation will be around 40%.

10.5.2 Teleportation fidelity

Our three-fold coincidence would mainly have three components as well:

(1) Coincidence among a single photon of the initial state from the weak coherent beam, an anti-Stokes photon, and a successfully retrieved Stokes photon, which is the desired event and has a probability of

$$\sim \frac{1}{2} p_{AS} p_0 \gamma \eta^3.$$

Thus, the overall success probability of the teleportation in each experimental run is around 10^{-6} .

(2) Spurious coincidence contributed by a two-photon event (the double emission) from the weak coherent pulse and a single-photon event in Stokes mode. The same as the noise estimation in Bell state measurement (§ 10.5.1) in $|+\rangle$ and $|R\rangle$ teleportation the probability of registering such three-fold coincidence is given by

$$\sim \frac{1}{4} p_0^2 p_S \eta^3$$

and no such spurious three-fold coincidence in $|H\rangle$ teleportation.

(3) Spurious coincidence contributed by double emission from the atomic ensembles and one retrieved Stokes photon, which has a probability of

$$\sim \frac{1}{4} p_{AS}^2 (2\gamma\eta - (\gamma\eta)^2) \eta^2.$$

Moreover, the probability of dark counts in each detector is about 10^{-5} per trial, implying a signal-to-noise ratio better than 100 : 1. And the errors in polarization are less than 1%. These two errors are thus negligible. Denote the probability of the desired three-fold coincidence as

$$S = \frac{1}{2} p_{AS} p_0 \gamma \eta^3$$

and the probability of the spurious one as

$$N = \frac{1}{4} p_0^2 p_S \eta^3 \kappa_\phi + \frac{1}{4} p_{AS}^2 (2\gamma\eta - (\gamma\eta)^2) \eta^2$$

here ϕ is the initial state, $\kappa_H = 0$ and $\kappa_+ = \kappa_R = 1$. Taking into account the imperfection of entanglement source, one can thus estimate the final fidelity for $|H\rangle$ teleportation by

$$f = \frac{S(1+V)/2 + N/2}{S+N},$$

where $V \sim 0.88$ is the entanglement visibility in the H/V basis. A simple calculation shows that the final fidelity should be around 0.90, which is in good agreement with our experimental fidelity

0.865 ± 0.017 . The slight difference is probably due to the neglected dark count and polarization errors.

In teleportation of $|+\rangle$ and $|R\rangle$ states, the experimental fidelities are much lower. This is because, on the one hand we have one more spurious three-fold coincidence contribution, i.e.

$$\frac{1}{4}p_0^2 p_S \eta^3.$$

More importantly, the imperfect overlap of the wavepackets on the BS, typically around 90% in our experiment [78], will further reduce the fidelities significantly. However, note that such imperfection has no effect on the $|H\rangle$ teleportation. Taking these into account, a similar calculation shows that the final fidelity for $|+\rangle$ and $|R\rangle$ teleportation should be around 0.79. Given the neglected dark count and polarization errors, our experimental results again well agree with the calculated fidelities.

10.6 Conclusion

In summary, we have demonstrated quantum teleportation between photonic and atomic qubits. The ability - teleporting the unknown quantum state of a photonic qubit onto an atomic qubit and then converting it back to a photonic state in a controllable time - is essential for the recent quantum repeater protocols [165, 167, 156] that address the extremely difficult phase stabilization, as required in the original scheme for long-distance quantum communication [70]. However, we would like to note that, due to the low success probability of teleportation and short life-time of quantum memory, significant improvements are still needed in order for our method to be really useful for practical applications. For example, we could use active feed-forward to achieve both a deterministic entanglement source [165, 167, 156] and a high-quality single-photon source [74, 75], by which the overall success teleportation rate can be greatly increased while the spurious coincidence is suppressed. This, given our present excitation rate of anti-Stokes photons, would require a lifetime of quantum memory up to 1 ms. Moreover, in order to achieve long-distance quantum communication, e.g. free-space quantum teleportation over 100 km the same order of storage time is required. To do so, one can confine the atoms in an optical trap and exploiting a clock state to store the collective spin excitation [197], this could potentially extend the lifetime up to 1 s. Finally, comparing former photonic teleportation [31, 34, 43], where the coherence time of down-converted photons is only about a few hundred fs, the narrowband feature of our anti-Stokes photon source (coherence time ~ 25 ns) makes the overlap of independent photon wavepackets from distant sites much easier. This advantage together with the feasible long lifetime quantum memory may provide an ideal solution for large-scale quantum communications, e.g., satellite-based quantum communication [198, 67].

Chapter 11

A novel entanglement source

11.1 Introduction

Quantum communication provides an absolutely secure approach to transfer information by means of quantum cryptography or faithful teleportation of unknown quantum states. Unfortunately, the photon transmission loss and the decoherence scale exponentially with the length of the communication channel. This makes it extremely hard to deliver quantum information over long distance effectively. A quantum repeater protocol [17, 68] combining the entanglement swapping, purification and quantum memory provides a remarkable way to establish high-quality long-distance quantum networks, and makes the communicating resources increase only polynomially with transmission distance.

Following the DLCZ scheme [70], in recent years, significant experimental advances have been achieved towards the implementation of the quantum repeater protocol by using the atomic ensemble and linear optics [71, 184, 73, 80, 79, 75, 82]. However, the DLCZ protocol has an inherent drawback which is severe enough to make a long distance quantum communication extremely difficult [165, 156]. The phase fluctuation caused by path length instability over long distance is very hard to overcome. Recently, a more robust quantum repeater architecture was proposed to bypass the phase fluctuation over long distance [165]. This architecture is based on the two-photon Hong-Ou-Mandel-type interference, which is insensitive to the relative phase between two photons. Several experiments have proven that the path length fluctuations only need to be kept on the scale of the photon's coherent length, from hundreds of micrometer [155] to tens of meters [76, 77, 78]. In our original protocol [165, 156] (see also Chapter. 7), two laser beams with fixed relative phase are needed to excite two atomic ensembles in order to generate the atom-photon entanglement for the local communication node. Only the path length between two ensembles in the local node need to be stabilized to sub-wavelength scale. Some recent works close to the requirements of our protocol have provided the techniques to generate atom-photon entanglement with spin excitation of magnetic sublevels [199, 189] or dual-species atomic ensemble to prevent for the propagating phase difference [200]. But for each of these there remain problems like balancing the excitation between the ensembles or the complexity and efficiency of frequency mixing, which make it hard to implement the full protocol over long distance. Another kind of atom-photon entanglement is realized using the orbital angular momentum states [201], which could also extend to high-dimensional entanglement. However, the divergence property of different orbital angular momentum modes makes it impractical for long-distance quantum communication [202].

In the last Chapter, we use two write excite two atomic ensembles simultaneously, by an active phase-stabilization scheme, we can generate atom-photon entanglement, which is exactly as proposed in ref. [165]. However, the property of two atomic ensembles working as one logic qubit makes a realistic quantum repeater very complicate (eight atomic ensembles are needed to deterministi-

cally generate one pair of entanglement between two distant locations as described in Chapter. 7). In this Chapter, we present a new approach to effectively generate the entanglement between the atomic qubit and photonic qubit based on atomic ensemble in a local MOT. It fulfil the requirements of the improved protocol [165]. Contrast to the previous experiments [80, 79, 199, 189, 200], the atomic ensemble is excited by only one write beam with single frequency, while two spontaneous Raman scattered fields (anti-Stokes fields) in different spatial modes are combined on a polarizing beam splitter and serve as the photonic qubit. The corresponding collective spin excitations in the atomic ensemble represent the atomic qubit. This new scheme makes the local phase stabilization simple. Moreover, the relative phase difference between the two selected modes is actively stabilized by the local build-in Mach-Zehnder interferometer (see § 10.3.1). Besides, by extending the approach to select more spatial modes of collective excitation, high-dimensional entanglement and hyper-entangled state could be easily realized.

11.2 Experimental conception

The basic setup of our experiment is shown in Fig. 11.1. A cold ^{87}Rb atomic cloud with temperature about $100\ \mu\text{K}$ in the MOT is used as the medium to generate and store the information of the quantum excitation. The two hyperfine ground states $|5S_{1/2}, F=2\rangle=|a\rangle$ and $|5S_{1/2}, F=1\rangle=|b\rangle$ and the excited state $|5P_{1/2}, F=2\rangle=|e\rangle$ form a Λ -type system. After loading the MOT, the atoms are first pumped to initial state $|a\rangle$. A single weak 75 ns write beam illuminates the atom cloud with beam waist of $240\ \mu\text{m}$ and 10 MHz red-detuned to $|a\rangle \rightarrow |e\rangle$ transition. Two anti-Stokes fields ($|e\rangle \rightarrow |b\rangle$ Laguerre-Gauss LG_{00} mode, $70\ \mu\text{m}$ waist) AS_L and AS_R induced by the write beam via spontaneous Raman scattering are collected at $\pm 3^\circ$ relative to the propagating direction of the write beam. This also defines the spatial mode of the atomic ensemble L and R . With small excitation probability, the atom-light field can be expressed as [70]

$$|\Psi\rangle_m \sim |0_{AS}0_b\rangle_m + \sqrt{\chi_m}|1_{AS}1_b\rangle_m + O(\chi_m), \quad (11.1)$$

where $\chi_m \ll 1$ is the excitation probability of one collective spin in ensemble m ($m = L, R$), and $\sqrt{\chi_m}|i_{AS}i_b\rangle_m$ denote the i -fold excitation of the anti-Stokes light field and the collective spin in atomic ensemble.

When the write beam excites the atomic ensemble and an anti-Stokes photon is generated, it also transfers the momentum to the collective spin excitation in the atomic ensemble. To fulfill the momentum conservation, the overall k -vector of the collective excitation after the spontaneous Raman scattering is $\vec{k}_{atom} = \vec{k}_W - \vec{k}_{AS}$, where \vec{k}_{AS} and \vec{k}_W are the wave vector of the anti-Stokes field and write beam, respectively. If no other external field disturbs the atomic state, during the storage time τ , the momentum of the collective excitation is kept. When the read pulse is applied on the atomic ensemble to retrieve the collective excitation back into a correlated Stokes field, the momentum of the collective excitation is transferred back to the Stokes field. The wave vector of the Stokes field becomes $\vec{k}_S = \vec{k}_R + \vec{k}_{atom}$, where \vec{k}_R represents the wave vector of the read beam. Then after the retrieve process, the wave vector of the correlated Stokes field fulfill the mode-matching condition [203]

$$\vec{k}_S = \vec{k}_R + \vec{k}_W - \vec{k}_{AS}. \quad (11.2)$$

Under the counter-propagating condition of read and write beams (shown in Fig. 11.1), we will have

$$\vec{k}_S \simeq -\vec{k}_{AS}.$$

To characterize the light field, we measure the cross correlation $g_{AS,S}^{(2)}$ [71, 75], which marks the degree of quantum correlation, between the anti-Stokes and the Stokes fields. As two anti-Stokes fields AS_L and AS_R are detected at two different spatial modes, two corresponding Stokes fields

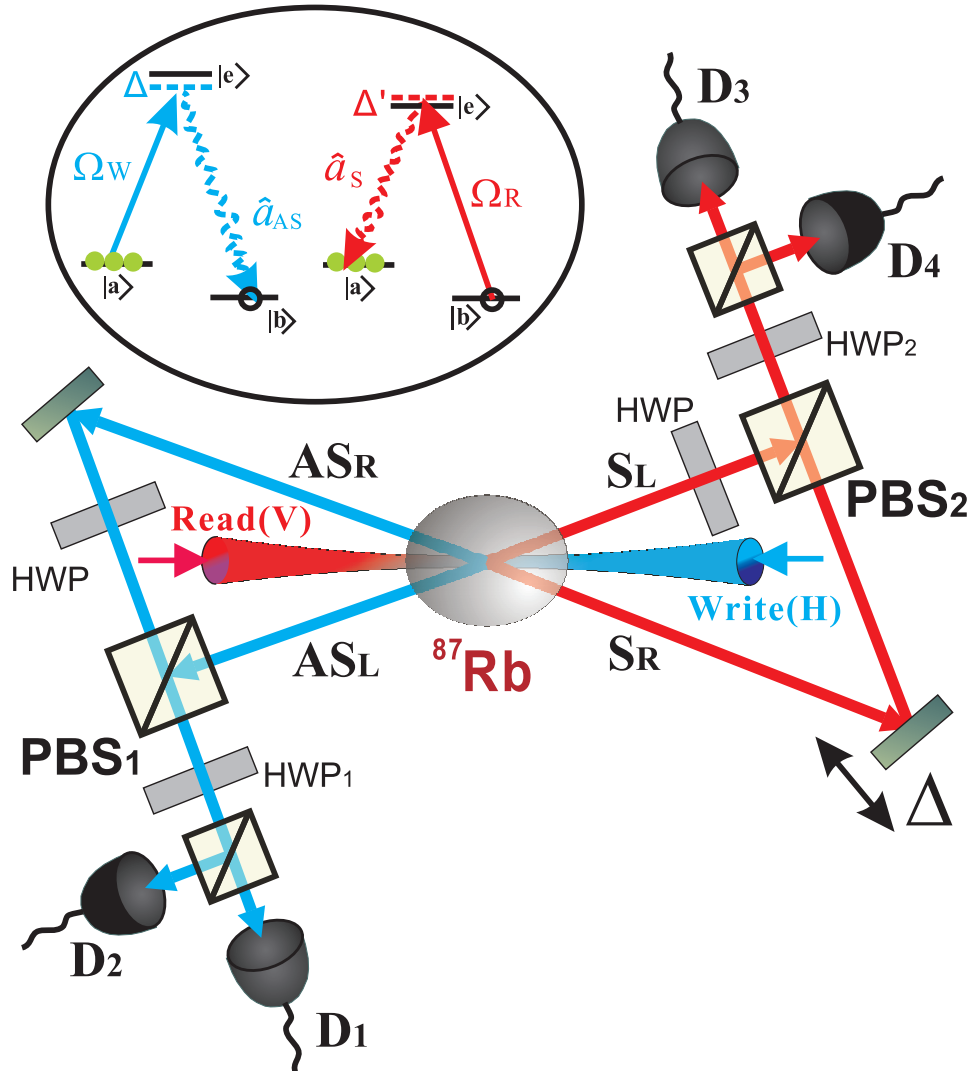


Figure 11.1: Illustration of the scheme of the experiment setup and the relevant energy levels of the ^{87}Rb atoms. Cold ^{87}Rb atoms captured by MOT are initially prepared in state $|a\rangle$. A weak write pulse Ω_w with a beam waist of $240\ \mu\text{m}$ illuminates the atom cloud to generate the spin excitation. The spontaneous Raman scattered anti-Stokes field AS_L and AS_R are detected at $\pm 3^\circ$ to the propagating direction of the write beam, with the beam waist of $70\ \mu\text{m}$, defining the spatial mode of the atomic ensembles L and R , respectively. The two anti-Stokes field are combined on a polarizing beam splitter PBS_1 and sent to the polarization analyzer. This creates the entanglement between the polarization of the anti-Stokes field and the spatial modes of spin excitation of atoms in atomic ensemble. After a controlled storage time τ , the entanglement is verified by retrieving the spin excitation back to the Stokes fields S_L and S_R by a strong read pulse, which is overlapped and counter-propagates to the write beam. After overlap the Stokes fields on PBS_2 , the entanglement can be proved.

S_L and S_R can be detected during the retrieve process. For the mode-matched fields S_L and AS_L (S_R and AS_R), the cross correlation $g_{AS,S}^{(2)} \gg 1$ when $\chi \ll 1$, which means good quantum correlation between those fields. But for the unmatched fields S_L and AS_R (S_R and AS_L), no quantum correlation is observed ($g_{AS,S}^{(2)} \sim 1$), which means there's no cross talk between these two different modes. The viability of our new approach is guaranteed by this condition.

We adjust the two modes L and R to be equal excited ($\chi_L = \chi_R = \chi$). The two anti-Stokes field are combined on PBS₁ and sent into a polarization analyzer, as illustrated in Fig. 11.1. Neglecting the vacuum state and high order excitations, the entangled states between the photonic and the atomic qubit can be described as,

$$|\Psi\rangle = \frac{1}{\sqrt{2}}(|H\rangle|R\rangle + e^{i\phi_1}|V\rangle|L\rangle) \quad (11.3)$$

where $|H\rangle/|V\rangle$ denotes horizontal/vertical polarizations of the single anti-Stokes photon and $|L\rangle/|R\rangle$ denotes single collective spin excitation in ensemble L/R , ϕ_1 is the propagating phase difference between the two anti-Stokes fields before they overlap at PBS₁. Physically, the atom-photon entangled state (11.3) is equivalent to the maximally polarization entangled state generated by spontaneous parametric down-conversion [53].

11.3 Characterization of atom-photon entanglement

To verify the entanglement between the anti-Stokes field and the atomic spin excitation, a relative strong read pulse with 75 ns close to resonance of $|e\rangle \rightarrow |b\rangle$ transition counter-propagating with the write beam is applied after a controllable time τ to convert the atomic collective excitation back into Stokes fields.

After combine the two Stokes fields on PBS₂ (see Fig. 11.1), the superposition state of anti-Stokes and Stokes fields is the following maximally polarization entangled state

$$|\Psi\rangle_{AS,S} = \frac{1}{\sqrt{2}}|H\rangle_{AS}|H\rangle_S + e^{i(\phi_1+\phi_2)}|V\rangle_{AS}|V\rangle_S, \quad (11.4)$$

where ϕ_2 represent the propagating phase difference between two Stokes fields before they overlap at the PBS₂. In our experiment, the total phase $\phi_1 + \phi_2$ is actively stabilized via the build in Mach-Zehnder interferometer and fixed to zero [81]. After the phase stabilization, the short term phase fluctuation is measured to be smaller than $\pi/30$ and long term drift is cancelled, which guarantees the stability of our experiment.

11.3.1 Entanglement visibility

To characterize the quality of generated atom-photon entanglement, the scaling of entanglement with the excitation probability χ is investigated. To do so, we measure the visibility V of the interference fringes of the coincidence rate between anti-Stokes and Stokes photons for various value of χ with fixed memory time $\tau = 500$ ns. The half waveplate HWP₁ (see Fig. 11.1) is set to $+22.5^\circ$ to measure the anti-Stokes fields under X base and rotate HWP₂ to measure the Stokes fields under different bases. As χ increases, the high order term in Eq. (11.1) can not be neglected. The visibility V can be expressed as the function of cross correlation between the anti-Stokes and Stokes fields [189]

$$V = \frac{g_{AS,S}^{(2)} - 1}{g_{AS,S}^{(2)} + 1}. \quad (11.5)$$

Ideally, the relationship of the excitation rate χ and cross correlation $g_{AS,S}^{(2)}$ is $g_{AS,S}^{(2)} = 1 + 1/\chi$ at low excitation limit ($\chi \ll 1$). Considering the overall detection efficiency of the anti-Stokes

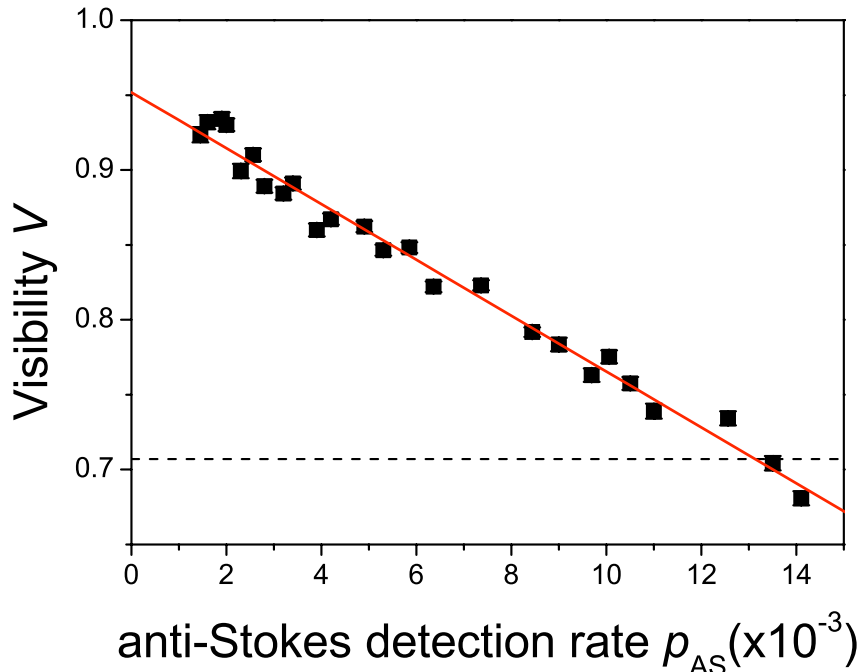


Figure 11.2: Visibility of the interference fringes V between anti-Stokes fields and Stokes fields various with the changing of the detected rate of anti-Stokes field p_{AS} . The solid line is the fit corresponding to Eq.(11.6). The dashed line shows the bound of $1/\sqrt{2}$ which mark the limit to violate the CHSH-type Bell's inequality.

field η_{AS} , we have the detection rate of the anti-Stokes photon $p_{AS} = \eta_{AS}\chi$. Thus, at the small excitation rate limit ($\chi \ll 1$), the visibility can be expressed as

$$V = 1 - 2p_{AS}/\eta_{AS}. \quad (11.6)$$

In our experiment, $\eta_{AS} \sim 8\%$. Figure 11.2 shows the measured visibility V varying with p_{AS} . As the excitation rate χ decrease, which corresponds to decrease of p_{AS} , the visibility V increases as does the degree of entanglement. The solid line is the linear fit for the experiment data. At $p_{AS} \rightarrow 0$, V is near 0.95. This imperfection is mainly caused by the overlap of the two anti-Stokes fields AS_L and AS_R , the noise of the single photon detectors and the phase fluctuation in the interferometer. As the detection rate p_{AS} increases, the probability of high order excitations increases faster than that of the single excitation. Then the correlation $g_{AS}^{(2)}$ decreases, as well as the visibility. At $p_{AS} < 1.3 \times 10^{-2}$, V is larger than $1/\sqrt{2}$ which marks the bound of violation of the Clauser-Horne-Shimony-Holt (CHSH) type Bell's inequality [189, 114]. Moreover, the cross correlation between different spatial modes, e.g. between AS_L and S_R , is measured to be 1.1 ± 0.5 , which means the negligible of the crosstalk caused by the Stokes photons emit to the wrong mode.

11.3.2 Storage of entanglement

To further study the storage ability of the atomic ensemble quantum memory, we characterize the temporal decay of entanglement with storage time τ . Here we measure the decay of the S parameter, sum of the correlation function in CHSH type Bell's inequality, where $S \leq 2$ for any

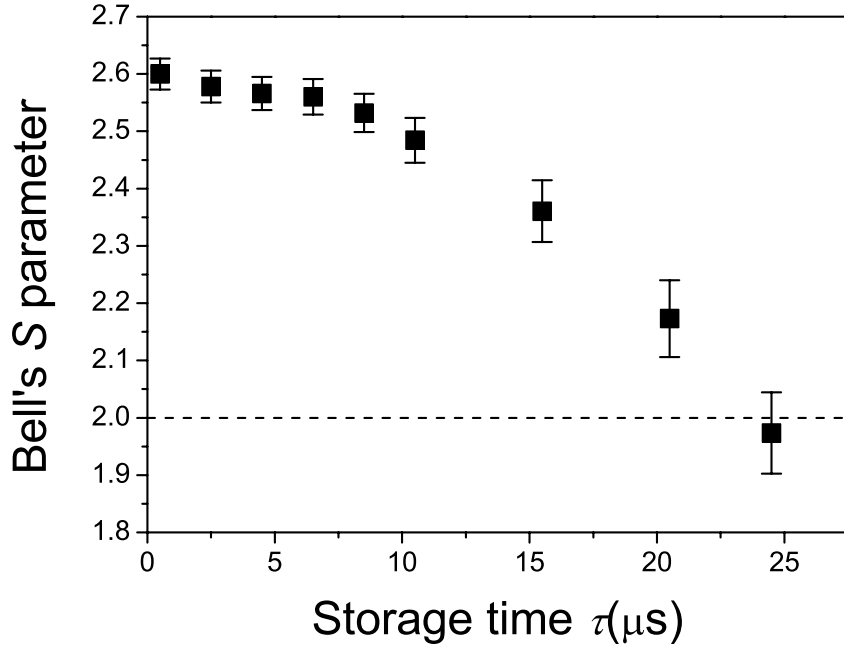


Figure 11.3: Decay of the S parameter in the Bell's inequality measurement with the storage time τ . The dashed line shows the classical bound of $S = 2$.

local realistic theory with

$$S = |E(\theta_1, \theta_2) - E(\theta_1, \theta'_2) - E(\theta'_1, \theta_2) + E(\theta'_1, \theta'_2)|, \quad (11.7)$$

here $E(\theta_1, \theta_2)$ is the correlation function, where θ_1 and θ'_2 (θ'_1 and θ_2) are the measured polarization bases of the anti-Stokes field and Stokes field. During the measurement, the HWP₁ and HWP₂ are set to different angles to make the bases settings at $(0^\circ, 22.5^\circ)$, $(0^\circ, -22.5^\circ)$, $(45^\circ, 22.5^\circ)$ and $(45^\circ, -22.5^\circ)$, respectively. The excitation rate χ was fixed to having $p_{AS} = 2 \times 10^{-3}$, and the result of measurement is shown in Fig. 11.3. At the storage time of 500 ns, $S = 2.60 \pm 0.03$, which violates Bell's inequality by 20 standard deviations. As the storage time increases, the S parameter decreases, indicating the decoherence of the entanglement. At storage time $\tau = 20.5 \mu\text{s}$, we still get $S = 2.17 \pm 0.07$, which means the character of quantum entanglement is still well preserved. The decay of S parameter with increasing storage time τ is caused by the residual magnetic field which inhomogeneously broadens the ground state magnetic sublevels. This process can be observed from the decay of the retrieve efficiency and the cross correlation between anti-Stokes and Stokes fields.

Shown in Fig. 11.4, the retrieve efficiency and the cross correlation between anti-Stokes and Stokes field all decreases with increasing the storage time τ . At $\tau = 500$ ns, the overall retrieve efficiency (including the transmission loss and the detector efficiency) is $12.2 \pm 0.4\%$ and the cross correlation $g_{AS,S}^{(2)} = 38 \pm 1$. At $\tau = 20.5 \mu\text{s}$, the retrieve efficiency and cross correlation decrease to $2.2 \pm 0.1\%$ and $g_{AS,S}^{(2)} = 9.8 \pm 0.7$, respectively. These values are still sufficient to violate the CHSH-type Bell's inequality. When τ is longer than $24 \mu\text{s}$, $g_{AS,S}^{(2)} < 6$ makes it insufficient to violate the Bell's inequality.

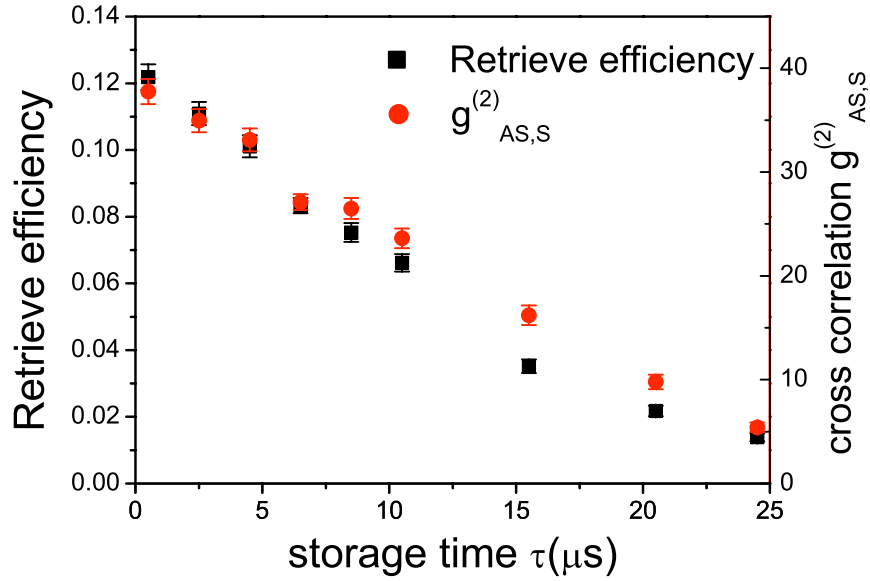


Figure 11.4: The decay of retrieve efficiency and cross correlation $g_{12}^{(2)}$ with the storage time τ . The anti-Stokes detection rate is fixed at $p_{AS} = 2 \times 10^{-3}$. The square dots show the decay process of the retrieve efficiency of the Stokes fields, round dots show the decay of the cross correlation $g_{AS,S}^{(2)}$ between anti-Stokes field and Stokes field.

11.4 Discussion

In conclusion, we have generated a robust atom-photon entanglement with a novel approach. A single write beam and a single atomic ensemble are used to generate the collective spin excitations. Two spatial modes of collective excitations are defined by the collection modes of anti-Stokes fields. The conservation of momentum during the atom-photon interaction prevent for the cross talk between different excited spatial modes. The visibility of the entanglement and violation of the CHSH type Bell's inequality are measured to prove the atom-photon entanglement between anti-Stokes photon and collective excitation in atomic ensemble. Also with the help of the build-in quantum memory, the violation of the Bell's inequality still exists after $20.5 \mu\text{s}$, corresponding to the time of light propagating 4 km in an optical fiber. That means we have successfully achieved a memory build-in atom-photon entanglement source which can work as a node of the long-distance quantum communication networks. Moreover, if more anti-Stokes modes are selected at different angles corresponding to the write beam, this approach can be easily extended to generate higher order entanglement, which could be very useful in the complex quantum cryptography and quantum computation.

Chapter 12

Entanglement swapping

12.1 Introduction

Quantum memories or registers are fundamental requirements in future networks of quantum information processing like what we are familiar with in traditional computers used in our everyday life. However, the manipulations on quantum bits, such as storage, retrieve and transportation, are conceptually different from those on classical electronic bits because of the non-cloning character of quantum states. Even it is a challenging task to implement high-quality storage and retrieve of a quantum bit, there have been a few investigations on quantum state transfer between matter and light. An atom (ion) [204, 205], an atom in an optical cavity [206, 207], and a cloud of atoms [82, 200, 73, 75, 208] have been used as the medium to store a quantum bit. A distributed quantum network requires entanglement among two and more remote memories, which has not been accomplished yet. In the frame of a quantum repeater protocol [17], a significant progress is the DLCZ scheme that Duan *et al* [70] proposed to implement long-distance quantum communication with atomic ensembles and linear optics, where single-photon interference is used to generate entanglement between atomic ensembles. However, two serious problems make the DLCZ scheme unlikely to become reality. First, the phase requirement of single-photon interference, where the fluctuation of fiber length should much less than a wavelength, is too strict to be satisfied in large scale (say kilometers long) communication. Second, imperfections of photon loss and inefficiency of detection make the undesired vacuum components in the state increase very fast with communication distance and therefore account for a sharp decrease of the communication fidelity. Two simultaneously proposed schemes [165, 167] provide solutions to overcome the above problems, where two-photon interference is used to generate long-distance entanglement. As we described in Chapter 7 the fluctuation of fiber length is limited to the order of a coherence length of the photons, which is 7 order loose than that in the DLCZ scheme. The vacuum component will be suppressed and no longer a dominant term after a few connections.

Most recently, with two-photon interference the entanglement of two remote $^{171}\text{Yb}^+$ atoms has been reported [209]. A future advantage in this experiment is that single-atom quantum memories allow the implementation of conditional quantum gates through photonic channels. However, there are two shortcomings: first of all, the success probability is very low due to low collection efficiency of the spontaneous radiation while the contribution from dark count events is considerably high which makes the fidelity pretty low; secondly, the read-out of an atomic bit to a photonic one is extremely hard since there is no preferential optical mode of the read-out light until the atom could be coupled to an optical cavity. So, such entanglement is not ready for use in scalable quantum applications.

In this Chapter, by further developing the atom-photon entanglement introduced in Chapter 11, we report a scalable unit for long-distance quantum communication [165]. This unit is imple-

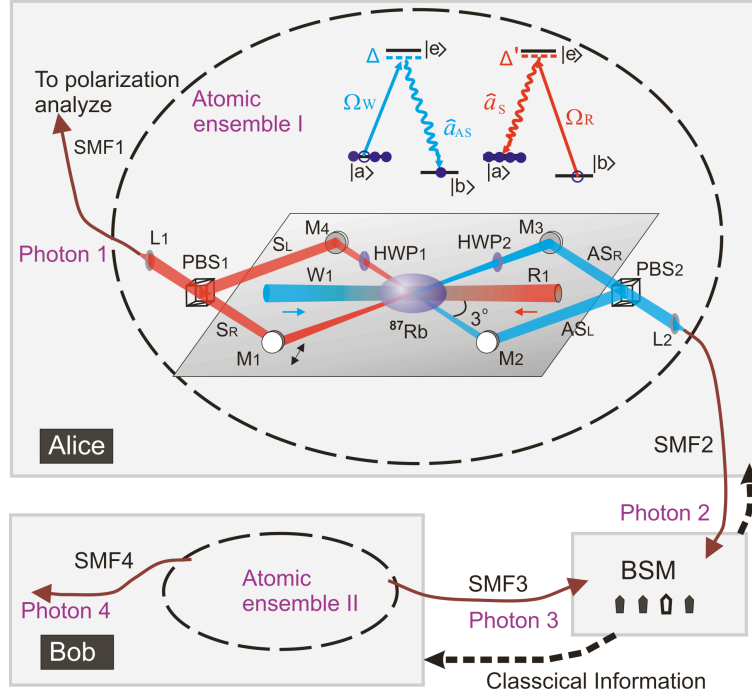


Figure 12.1: Illustration of the relevant energy levels of the atoms and the experimental setup. At Alice’s site, ^{87}Rb atoms are prepared in the initial state $|a\rangle = |5S_{1/2}, F = 2\rangle$. A write pulse Ω_w with the detuning of $\Delta = -10$ MHz and a beam waist of $240\ \mu\text{m}$ is applied to generate the spin excitation (with one atom excited to $|b\rangle = |5S_{1/2}, F = 1\rangle$) through Raman scattering $|a\rangle \rightarrow |e\rangle \rightarrow |b\rangle$, where $|e\rangle = |5P_{1/2}, F = 2\rangle$) and an accompanying photon of the anti-Stokes field \hat{a}_{AS} with a beam waist of $70\ \mu\text{m}$. The light modes in channels AS_L and AS_R , tilted $\pm 3^\circ$ relative to the direction of the write beam, are overlapped at PBS2 selecting perpendicular polarizations and coupled in a single-mode fiber (SMF2) for a future Bell-state measurement. Bob has the same apparatus and simultaneously does the same as Alice. Photon 2 and 3 overlap at BSM through which the entanglement between the two atomic ensembles I and II is generated. After a time interval δt_s , the spin excitations in the two atomic ensembles are retrieved back to single photons and the entanglement can be verified through polarization analysis of photons 1 and 4.

mented with two clouds of atomic ensembles. By means of entanglement swapping, entanglement is generated between two remote atomic ensembles connected with either 6 m or 300 m fiber-based optical channel, where the flying qubits—two emitted photons from the atomic ensembles are sent to an intermediate station for a joint BSM. Afterwards, the measurement induced entanglement between the atomic ensembles are verified by the violation of an Bell’s inequality and by an entanglement witness. The striking features, phase-error insensitiveness and scalable flexibility, promise the present setup as a fundamental unit for future quantum information processing. This unit is feasible to be assembled in scalable networks of quantum information processing due to its properties of scalability, narrow band, and high quality of entanglement.

12.2 Experimental setup

12.2.1 Atom-photon entanglement

To generate and verify the entanglement between two remote atomic ensembles, we use three steps which are implementing two atom-photon entanglement sources [210], sending the flying qubits—photons to a station for BSM, and verifying the entanglement between the stationary qubits—

atomic ensembles. The basic principle is shown in Fig. 12.1. Alice and Bob both have a cold atomic ensemble consisting of about 10^8 ^{87}Rb atoms with the temperature ~ 100 μK . After loading the atoms in two magneto-optical traps (MOT) within 20 ms, they switch off the MOTs and start the experiment which is 5 ms long. At each site, after the atoms are prepared at the initial state $|a\rangle$, a single weak (50 ns long, ~ 1 μW) write beam illuminates the atomic cloud with a beam waist of 240 μm and 10 MHz red-detuned with respect to $|a\rangle \rightarrow |e\rangle$ transition. Two anti-Stokes fields (70 μm waist, $|e\rangle \rightarrow |b\rangle$) AS_L and AS_R induced by the write beam via spontaneous Raman scattering are collected at $\pm 3^\circ$ angle relative to the propagating direction of the write beam. This also defines the spatial modes of the atomic ensemble L and R . With a low excitation probability, the state of the atom-photon field can be expressed as [70]

$$|\Psi\rangle_m \sim |0_{AS}0_b\rangle_m + \sqrt{\chi_m}|1_{AS}1_b\rangle_m + O(\chi_m), \quad (12.1)$$

where $\chi_m \ll 1$ is the excitation probability of one collective spin in ensemble m ($m = L, R$), and $|i_{AS}i_b\rangle_m$ denote the i -fold excitation of the anti-Stokes field and the collective spin in the atomic ensemble. When the experimental inefficiencies (e.g. the coupling efficiency of light modes, the transmission loss and detection efficiency of single photon detectors) are taken into account, the excitation probability $\chi\eta_{AS} = 2 \times 10^{-3}$, where η_{AS} is the overall efficiency for each anti-Stokes channel (either AS_L or AS_R).

The two modes L and R are adjusted to be identical ($\chi_L = \chi_R = \chi$), and overlapped at a polarizing beam splitter PBS2 with orthogonal polarizations. Neglecting the vacuum state and higher order excitations, the entangled states between the atomic qubit and the photonic qubit can be described as,

$$|\Psi\rangle_{\text{at-ph}} = \frac{1}{\sqrt{2}} (|H\rangle|R\rangle + e^{i\phi_1}|V\rangle|L\rangle) \quad (12.2)$$

where $|H\rangle/|V\rangle$ denotes horizontal/vertical polarization of the single anti-Stokes photon and $|L\rangle/|R\rangle$ denotes single collective spin excitation in ensemble L/R , ϕ_1 is the propagating phase difference between the two anti-Stokes fields before they overlap at PBS2. Physically, the atom-photon entangled state (12.2) is equivalent to the maximally polarization-entangled state generated by spontaneous parametric down-conversion [53].

At this stage we have finished the first step of implementing two atom-photon entanglement sources at sites Alice and Bob respectively. Before the next step, entanglement swapping, this entanglement can be verified by converting the atomic spin into a single photon (a Stokes field) and measuring the correlation functions between this photon and the previous anti-Stokes field. To do this, a relative strong read pulse (with 50 ns long, ~ 60 μW) close to resonance of $|e\rangle \rightarrow |b\rangle$ transition and counter-propagating with the write beam is applied after a controllable time δt_s to convert the atomic collective excitation back into a Stokes field. Ideally, the retrieve efficiency reaches unit relying on the mode-match condition and collective enhancement of the atoms [70]. However, there are imperfections, e.g., photon loss, low optical depth of the atomic ensembles, coupling efficiency of light fields, detection efficiency of single photon detectors, which limit the overall retrieve efficiency to about 15% in practice. After combine the two Stokes fields on PBS1 (see Fig. 12.1), the superposition state of the anti-Stokes and Stokes fields is the following maximally polarization-entangled state

$$|\Psi\rangle_{AS,S} = \frac{1}{\sqrt{2}} (|H\rangle_{AS}|H\rangle_S + e^{i(\phi_1+\phi_2)}|V\rangle_{AS}|V\rangle_S), \quad (12.3)$$

where ϕ_2 represent the propagating phase difference between two Stokes fields before they overlap at the PBS2. In our experiment, the total phase $\phi_1 + \phi_2$ is actively stabilized via the built-in Mach-Zehnder interferometer and fixed to zero [81]. As shown in Chapter 11 the entanglement in Eq. (12.3) still exists with a storage time up to $\delta t_s = 20$ μs measured by the violation of a CHSH-type Bell's inequality [210].

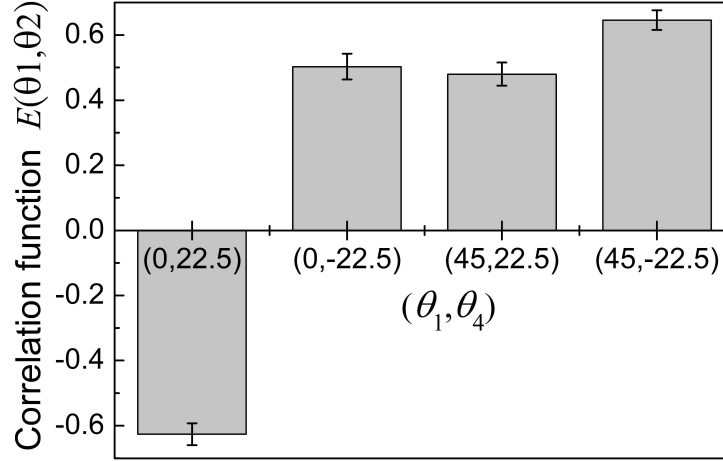


Figure 12.2: Correlation functions of a CHSH-type Bell's inequality with the storage time $\delta t_s = 500$ ns. Error bars represent statistical errors, which are ± 1 standard deviation.

12.2.2 Entanglement swapping

Having known the entanglement quality at each site, we generate the entanglement between atomic ensembles I and II via entanglement swapping [34, 165]. As shown in Fig. 12.1, photon 2 from Alice and photon 3 from Bob are sent to a station (with each traveling 3 m or 150m in an optical fiber) for BSM. On condition of the output of the BSM, in our case we choose

$$|\Phi^+\rangle_{2,3} = \frac{1}{\sqrt{2}} (|H\rangle_2|H\rangle_3 + |V\rangle_2|V\rangle_3),$$

the state of the two remote atomic ensembles is projected to

$$|\phi^+\rangle_{I,II} = \frac{1}{\sqrt{2}} (|R\rangle_I|R\rangle_{II} + |L\rangle_I|L\rangle_{II}).$$

It is worthy to note here, the double excitations in either atomic ensemble I or II will cause false events in the BSM [165], which reduces the success probability of entanglement swapping by a factor of 1/2. However the false events can be eliminated at the stage of entanglement verification by the four-fold coincidence measurement of photons 1, 2, 3 and 4 (Note here, the arriving time of photons 1 and 4 is later than that of photons 2 and 3 by a interval δt_s , which is the storage time in the memories).

12.3 Experimental result

12.3.1 Violation of CHSH-Bell inequality

Triggered by the output of the BSM, the established entanglement between atomic ensembles I and II is ready to be verified by converting the atomic spins into single photons 1 and 4 whose state should be $|\Psi^-\rangle_{1,4}$. Here we measure the S parameter, sum of the correlation functions in a CHSH-type Bell's inequality, where $S \leq 2$ for any local realistic theory with

$$S = |E(\theta_1, \theta_4) - E(\theta_1, \theta'_4) - E(\theta'_1, \theta_4) - E(\theta'_1, \theta'_4)|, \quad (12.4)$$

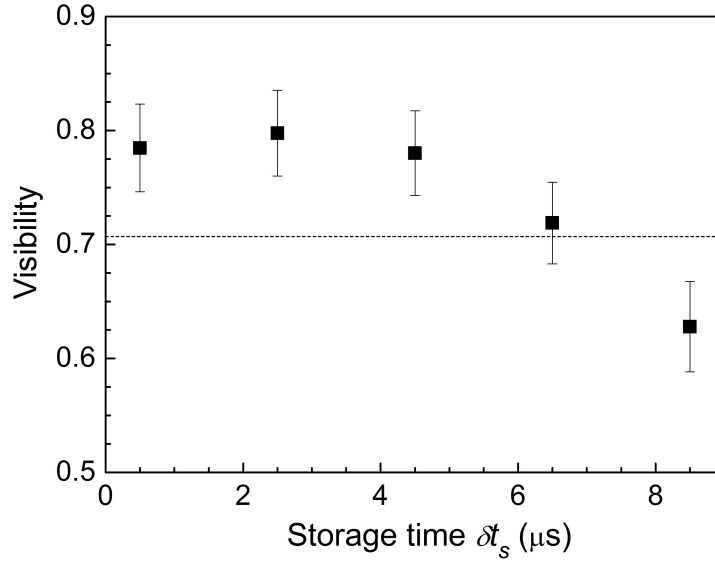


Figure 12.3: Visibility as a function of the storage time. Black dots are for the visibility and the dashed line shows the threshold for the violation of the CHSH-type Bell’s inequality. Error bars represent statistical errors, which are ± 1 standard deviation.

and $E(\theta_1, \theta_4)$ is the correlation function, in which θ_1 and θ'_1 (θ_4 and θ'_4) are the measured polarization bases of photon 1 (4). During the measurement, the polarization settings are $(0^\circ, 22.5^\circ)$, $(0^\circ, -22.5^\circ)$, $(45^\circ, 22.5^\circ)$ and $(45^\circ, -22.5^\circ)$, respectively. With the above excitation rate $\chi\eta_{\text{AS}} = 2 \times 10^{-3}$, the probability of coincidence between photons 2 and 3 is $p_{2,3} = 2(\chi\eta_{\text{AS}})^2 = 8 \times 10^{-6}$.

When the storage time $\delta t_s = 500$ ns, the measured correlation functions are shown in Fig. 12.2, resulting in $S = 2.26 \pm 0.07$, which violates Bell’s inequality by 3 standard deviations. The four-fold coincidence rate is observed as $\sim 30 \text{ hour}^{-1}$. In order to show the storage ability of the quantum memories, we measure the interference visibility of photons 1 and 4 as a function of the storage time (shown in Fig. 12.3). When the storage time is shorter than $6 \mu\text{s}$, the visibility is higher than the threshold $1/\sqrt{2}$, which means the entanglement still exists between photons 1 and 4. With these quantum memories, communication can be established between such stationary qubits when the flying qubits travel 1.8 km in free space, which has never been demonstrated till now. The entanglement between the atomic ensembles can be improved by reducing the transmission loss of single photons, extending the lifetime of the quantum memory and increasing the retrieve efficiency of collective excitations.

12.3.2 Entanglement witness

For an illustration of remote quantum connection between two atomic ensembles, we change the length of the two fibers SMF2 and SMF3 from 3 m to 150 m. The anti-Stokes photon is delayed 730 ns and the connection length is 300 m between atomic ensembles I and II. Relaxation of the fiber tension was observed by a measurement of the polarization rotation of an input light. This relaxation was compensated by two quarter-wave plates and one half-wave plate.

To prove the entanglement of the photons 1 and 4 (therefore atomic ensembles I and II), we use the method of entanglement witnesses [211]. An entanglement witness is an observable that has a positive expectation value on all biseparable states. Thus, a negative expectation value proves the

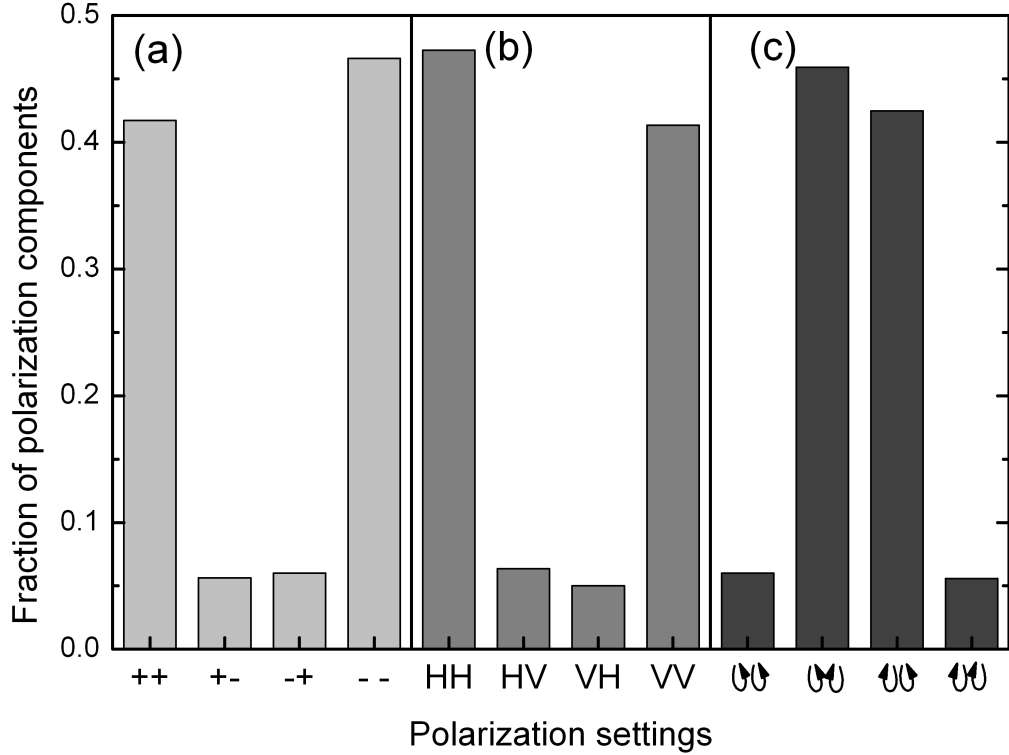


Figure 12.4: Experimental outcomes of the fractions at different polarization settings. The polarization bases are chosen as (a) $|+\rangle$ and $|-\rangle$, (b) $|H\rangle$ and $|V\rangle$, and (c) $|\odot\rangle$ and $|\oslash\rangle$ respectively.

presence of multipartite entanglement. In our case, we use the witness

$$\begin{aligned}
 W = \frac{1}{2} (&|HV\rangle\langle HV| + |VH\rangle\langle VH| + |+-\rangle\langle +-| \\
 &+ |-+\rangle\langle -+| - |\odot\odot\rangle\langle \odot\odot| - |\oslash\oslash\rangle\langle \oslash\oslash|).
 \end{aligned} \tag{12.5}$$

Here $|+\rangle = (1/\sqrt{2})(|H\rangle + |V\rangle)$ and $|-\rangle = (1/\sqrt{2})(|H\rangle - |V\rangle)$ denote diagonally polarized single photon states, while $|\odot\rangle = (1/\sqrt{2})(|H\rangle + i|V\rangle)$ and $|\oslash\rangle = (1/\sqrt{2})(|H\rangle - i|V\rangle)$ correspond to the left and right circular polarization states. The above operator can be locally measured by choosing correlated measurement settings that allow detection of the linear, diagonal, and circular polarization for both photons.

After a storage time of 1230 ns (with a 730 ns delay being taken account), the photons 1 and 4 (shown in Fig. 12.1) are sent to their own polarization analyzer at the same time. Three series of polarization settings are used and the measured local observables are shown in Fig. 12.4. The resulting $\langle W \rangle = \text{Tr}(W\rho_{\text{exp}}) = -0.33 \pm 0.02$, which is negative by 16 standard deviations and therefore proves the presence of entanglement between the two atomic ensembles.

12.3.3 Fidelity

The entanglement swapping can be quantified by the fidelity of the measured state of the atomic ensembles. To determine the fidelity, we write the density matrix of $|\phi^+\rangle$ in terms of the Pauli matrices:

$$|\phi^+\rangle\langle\phi^+| = \frac{1}{4} (\hat{I} + \hat{\sigma}_x\hat{\sigma}_x - \hat{\sigma}_y\hat{\sigma}_y + \hat{\sigma}_z\hat{\sigma}_z). \tag{12.6}$$

By Eq. (12.6), we have:

$$F = \text{Tr}(\rho_{\text{exp}}|\phi^+\rangle\langle\phi^+|_{\text{I,II}}) = \text{Tr}\left(\rho_{\text{exp}}\left(\hat{I} + \hat{\sigma}_x\hat{\sigma}_x - \hat{\sigma}_y\hat{\sigma}_y + \hat{\sigma}_z\hat{\sigma}_z\right)\right). \quad (12.7)$$

Substituting the experimental results in Eq. (12.7) we obtain the fidelity of final state on $|\phi^+\rangle$ is $F = 0.83 \pm 0.02$. Note that, to violate the CHSH-Bell inequality, $F = 0.78$ is needed for Werner state. Hence, we successfully demonstrating the entanglement swapping to the atomic ensembles.

12.4 Discussion

In summary, we have demonstrate a scalable unit for long-distance quantum communication. It is of great importance that two macroscopic quantum memories have been entangled at a long distance of either 6 m or 300 m by entanglement swapping, which paves the way for construction of future networks of quantum information processing. By the optimization of the quality of local atom-photon entangled pairs and suppression of the noise, it is expected a much higher count rate and a better entanglement of the two remote atomic ensembles. Furthermore, the lifetime of the entanglement source is 24 μs [210], which is expected to be extended to the order ~ 10 ms if the atoms can be confined in a dipole trap with “clock states” [197] as the memory states. Then the combination of stationary qubits (quantum memories) and flying qubits (photons) will certainly contribute to the future global quantum communication network.

Part III

Conclusion

Chapter 13

Conclusion and outlook

Quantum information science and atomic optics are the most active fields in modern physics. In this thesis, we further developed the technique of manipulation of atoms and photons to investigate the possibility of combining these two active field. In order to conclude this thesis we want to give a summary of its main points as well as an outlook to future work.

We have first investigated the applications of SPDC source in linear optical QIP by manipulation of multi-photon entanglement: by a full realization of encode and decode process for error-rejection we showed a proof-in-principle demonstration of error-free transfer for quantum information through a noisy quantum channel; by exploiting a three-photon polarization-entangled state, properly defining the pairs which is conditioned to the result of a measurement on a third qubit and performing measurements in additional configuration we violated the CHSH-Bell inequality *beyond* Tsirelson's bound; by developing a scheme for creation and characterization of a two-photon-four-qubit cluster state, we demonstrated successfully one-way computing, both Grover's algorithm and quantum gates with excellent fidelity and high generation rates, which enables high efficient computing; further by developing a tweaked high-intensity laser to exploit a unique six-photon interferometer, the combined state of two photons have been teleported – while preserving their entanglement – and this could bring large-scale quantum communication and computation a step closer.

However, large scale linear optical QIP requires quantum memory. By manipulation of atomic ensembles, we have successfully demonstrated capabilities proposed in the seminal DLCZ and the improved protocols, including the generation of two non-classical photon pair and further exploited to a deterministic single photon source. The indistinguishability of two independent photon emitted from two distant atomic ensemble is experimentally investigated and by an active feed-forward circuit we efficiently generate polarization-entangled photon pairs. Two atomic ensembles as one atomic qubit have been exploited to generate atom-photon entanglement. when demonstrating quantum teleportation, an unknown photonic qubit state has been teleported into the atomic qubit, stored in the atomic memory and subsequently transferred from the atomic qubit back to photonic qubit. A new approach to effectively generate the entanglement between the atomic qubit and photonic qubit has been proposed and implemented. The atomic ensemble is excited by only one write beam with a single frequency, while two spontaneously scattered Raman fields in different spatial modes are combined on a polarizing beam splitter and serve as the photonic qubit. The corresponding collective spin excitations in the atomic ensemble represent the atomic qubit. Based on such an atom-photon entanglement, entanglement between two distant atomic qubits has been generated via entanglement swapping. These experiments demonstrate a simple and promising approach toward building a scalable quantum memory.

Although various protocols have been demonstrated in laboratory, we are still on the way to large scale linear optical QIP. An obvious drawback of the current quantum memory realization is the storage time is limited to about 15 μs . By exploiting a well-controlled magnetic field one has

potential to improve the memory time up to hundreds of microseconds, limitation is due to the diffusion of atom into and out of the desired regions of the atomic ensembles. However, in order to archive both a deterministic entanglement source and a high-quality single-photon source by active feed-forward ability, a lifetime of quantum memory up to milliseconds is needed. Moreover, in order to achieve long-distance quantum communication, e.g. free-space quantum teleportation over hundreds of kilometers the same order of storage time is required. To do so, one can confine the atoms in an optical trap and exploiting the collective spin excitation into a decoherence-free subspace – a magnetic field insensitive clock state [197], this could potentially extend the lifetime of quantum memory up to the order of seconds.

Even with long memory time, the original DLCZ protocol is still impractical for long distance quantum communication [156]: it has serious phase stabilization problem [165]; the scalability is low [167]; the errors increase significantly and there is no purification. So far, all the improved protocols can only solve part of these problems [165, 167, 212]. Fortunately, recently we find that all these problems might be solved by a quasi-pair-source protocol ¹.

It is expected that an implementation of scalable and long lifetime quantum memory and the techniques combining manipulation of photons and atoms would open up realistic prospective for large scale QIP and dramatically change not only our world view, but also our everyday life. An enhancement of quality of life is to be expected by taking further efforts into the direction of yet unachieved, very ambitious goals.

¹More research on this protocol is ongoing.

APPENDIX:

Associated publications

Within the frame work of the presented thesis the following publications have been achieved:

- **Yu-Ao Chen**, An-Ning Zhang, Zhi Zhao, Xiao-Qi Zhou, Jian-Wei Pan, Experimental Quantum Error Rejection for Quantum Communication. *Phys. Rev. Lett.* **96**, 220504 (2006). (Chapter 3)
- **Yu-Ao Chen**, Tao Yang, An-Ning Zhang, Zhi Zhao, Adan Cabello and Jian-Wei Pan. Experimental Violation of Bell's Inequality beyond Tsirelson's Bound. *Phys. Rev. Lett.* **97**, 170408 (2006). (Chapter 4)
- Qiang Zhang, Alexander Goebel, Claudia Wagenknecht, **Yu-Ao Chen**, Bo Zhao, Tao Yang, Alois Mair, Jörg Schmiedmayer and Jian-Wei Pan, Experimental quantum teleportation of a two-qubit composite system. *Nature Physics* **2**, 678 (2006). (Chapter 5)
- Kai Chen, Che-Ming Li, Qiang Zhang, **Yu-Ao Chen**, Alexander Goebel, Shuai Chen, Alois Mair, Jian-Wei Pan, Experimental realization of one-way quantum computing with two-photon four-qubit cluster states. *Phys. Rev. Lett.* **99**, 120503 (2007). (Chapter 6)
- Bo Zhao, Zeng-Bing Chen, **Yu-Ao Chen**, Jörg Schmiedmayer and Jian-Wei Pan. Robust creation of entanglement between remote memory qubits. *Phys. Rev. Lett.* **98**, 240502 (2007). (Chapter 7)
- Zeng-Bing Chen, Bo Zhao, **Yu-Ao Chen**, Jörg Schmiedmayer and Jian-Wei Pan. Fault-tolerant quantum repeater with atomic ensembles and linear optics. *Phys. Rev. A* **76**, 022329 (2007). (Chapter 7)
- Shuai Chen, **Yu-Ao Chen**, Thorsten Strassel, Zhen-Sheng Yuan, Bo Zhao, Jörg Schmiedmayer and Jian-Wei Pan. Deterministic and storable single-photon source based on a quantum memory. *Phys. Rev. Lett.* **97**, 173004 (2006). (Chapter 8)
- Zhen-Sheng Yuan, **Yu-Ao Chen**, Shuai Chen, Bo Zhao, Markus Koch, Thorsten Strassel, Yong Zhao, Gan-Jun Zhu, Jörg Schmiedmayer and Jian-Wei Pan. Synchronized Independent Narrow-band Single Photons and Efficient Generation of Photonic Entanglement *Phys. Rev. Lett.* **98**, 180503 (2007). (Chapter 9)
- **Yu-Ao Chen**, Shuai Chen, Zhen-Sheng Yuan, Bo Zhao, Chih-Sung Chuu, Jörg Schmiedmayer, Jian-Wei Pan, Memory-built-in quantum teleportation with photonic and atomic qubits. *Nature Physics*, in press (2007); preprint available at <http://xxx.lanl.gov/abs/0705.1256>. (Chapter 10)

- Shuai Chen, **Yu-Ao Chen**, Bo Zhao, Zhen-Sheng Yuan, Jörg Schmiedmayer, Jian-Wei Pan, Demonstration of a stable atom-photon entanglement source for quantum repeaters. Phys. Rev. Lett. **99**, 180505 (2007). (Chapter [11](#))

Acknowledgment

Strength exists when we hold our hands, and ways are there because we cooperate. This thesis is the result of three and half years of work whereby I have been accompanied and supported by many people. It is a pleasant aspect that I have now the opportunity to express my gratitude for all of them.

First and most important, I would like to thank Prof. Jian-Wei Pan who opened for me the possibility to work in this absolutely fascinating and beautiful area of quantum optics and quantum information. No word can express my sincere gratitude. I could not have imagined having a better advisor and mentor for my Ph.D. His overly enthusiasm and integral view on research and his mission for providing “only high-quality work and not less”, has made a deep impression on me. He could not even realize how much I have learned from him. Besides of being an excellent supervisor, Jian-Wei was as close as a relative and a good friend to me. I am really glad that I have come to get know Jian-Wei Pan in my life.

I am very grateful to my second advisor, Prof. Jörg Schmiedmayer, who warmly recommended and supported my application for the Fellowship of “Eliteförderung der Deutsche Telekom Stiftung”, which enabled my continuation of physics study in Germany. I want sincerely acknowledge him for his many years of guidance and support, for his natural feeling of the experiment, and for his accepting to review my thesis. Thank-you to my other examiners, Prof. Peter Schmelcher and Prof. Zhong Zhang.

Starting with an empty atomic lab, starting with no working experience with neutral atoms, without the guidance of Dr. Shuai Chen it would be no possible building up the entire compact and complicate setup. I would like to thank Dr. Shuai Chen for introducing me the laser spectroscopy, laser cooling, experimental control and so on, and for his patience and encouragement during the hard times.

Thank you to Mr. Thorsten Strassel for his endless patience and organization skills and for helping me in the German translation of the abstract and the interim reports of my scholarship as well. I enjoyed our discussions about physics, the meaning of life, and all the rest.

The quantum memory results of my thesis could become possible owing to a coordinated team work and a friendly climate reigned in our lab. I thank Dr. Shuai Chen, Dr. Zhen-Sheng Yuan and Mr. Thorsten Strassel for the inspiring atmosphere they created while working on the experiment with me, for sharing happiness for every progress, and for immeasurable amount of knowledge, both experimental and theoretical, I have learned from them.

I am indebted to Dr. Qiang Zhang, who was my roommate for two years, for the many comments and discussions at any time of the day. Sometime we had a quite hard discussion, even people thought that we were fighting, but actually we were sharing ideas. I really enjoyed it, my best friend, Qiang. Moreover, his knowledge, reasoning, vivid interest on vast areas and emanating peacefulness were also a great help to me.

I am grateful to Mr. Bo Zhao, who married his wife at the same day as me, for the encouragement when we met the problem of applying the marriage. Also, I am very grateful that he gave me full theoretical support and has been always available to discuss the many problems and questions I brought him. I would also like to thank Prof. Zeng-Bing Chen for theoretical guidance and helpful discussion.

In a foreign country, there is always difficulties during daily life and I am very grateful to Alexander Goebel, Thorsten Strassel and Claudia Wagenknecht for helping me dealing with all kinds of documents in German, communicating with others who speaks no English and so on. All these kindly efforts made my years in Heidelberg very easy.

I would like to thank Dr. You-Jin Deng and Mr. Thorsten Strassel for their helpful discussions and kindness to read and correct this thesis.

All my colleagues of the QUO group gave me the feeling of being at home at work. Kai Chen, Shuai Chen, Chih-Sung Chuu, Zeng-Bing Chen, You-Jin Deng, Alexander Goebel, Koch Markus, Thorsten Strassel, Claudia Wagenknecht, Zhen-Sheng Yuan, Bo Zhao and Yong Zhao, many thanks for being your colleague and for your kindly helping during the past years in both scientific research and daily life.

My thanks also refer to Ms. Claudia Wallenwein, the secretary of the institute, for her quite efficiency in the office, and for her continuous help on various matters throughout the years.

Without our electronic and mechanic workshops the development of our experiment setup would have been much slower. I would like to thank the staff of our workshops for their amazing work, for their collaborative and active developments. I would like to particularly thank Mr. Peter von Walter for introducing me the field of hardware programing, which makes our experimental control possible.

This research has been supported and funded by various organizations including the Deutsche Forschungsgemeinschaft (DFG), the Alexander von Humboldt Foundation, the Marie Curie Excellence Grant of the EU, the Chinese Academy of Sciences (CAS), the National Fundamental Research Program (Grant No. 2006CB921900) and the Deutsche Telekom Stiftung. I thank them all for their confidence in our project.

Among the many very good teachers I met throughout my academic career, I especially thank Professor Yong-de Zhang, my undergraduate advisor, for his outstanding guidance and continuous concern about my career.

I sincerely thank all my friends, from all over the world, who have ever concerned me or helped me.

My huge thanks belong to my parents for their love, for giving me the best education, and for their support, wherever in the world I am and whatever incomprehensible things I happen to be doing there.

Last but not least, I would like to thank my darling wife Yan-Nan for her love, support and patience during the Ph.D period.

Bibliography

- [1] C. H. Bennett. "Quantum and classical information: Transmission and computation". *Physics Today*, 48(10):24–30, 1995.
- [2] D. Bouwmeester, A. Ekert, and A. Zeilinger. *The Physics of quantum information*. Springer-Verlag Berlin: Heidelberg, 2000.
- [3] N. Gisin, G. Ribordy, W. Tittel, and H. Zbinden. Quantum cryptography. *Rev. Mod. Phys.*, 74:145, 2002.
- [4] A. Einstein, B. Podolsky, and N. Rosen. Can quantum mechanical description of physical reality be considered complete? *Phys. Rev.*, 47:777, 1935.
- [5] E. Schrödinger. Die gegenwärtige Situation in der Quantenmechanik. 23:807–812; 823–828; 844–849, 1935.
- [6] N. Bohr. Can quantum-mechanical description of physical reality be considered complete? *Phys. Rev.*, 48:696, 1935.
- [7] C. H. Bennett, G. Brassard, C. Crepeau, R. Jozsa, A. Peres, and W. K. Wothers. Teleporting an unknown quantum state via dual classic and Einstein-Podolsky-Rosen channels. *Phys. Rev. Lett.*, 70:1895–1899, 1993.
- [8] A. Ekert and R. Jozsa. Quantum computation and shor's factoring algorithm. *Rev. Mod. Phys.*, 68:733–753, 1996.
- [9] B. Schumacher. Quantum coding. *Phys. Rev. A*, 51:2738–2747, 1995.
- [10] W. K. Wothers and W. H. Zurek. A single quantum cannot be cloned. *Nature*, 299:802–803, 1982.
- [11] A. K. Ekert. Quantum cryptography based on Bell's theorem. *Phys. Rev. Lett.*, 67:661–663, 1991.
- [12] C. H. Bennett and G. Brassard. in *Proc. IEEE Int. Conf. on Computers, systems, and signal processing*, Bangalore, India:(IEEE, New York, 1984), 175.
- [13] C. H. Bennett and S. J. Wiesner. Communication via one- and two-particle operators on Einstein-Podolsky-Rosen states. *Phys. Rev. Lett.*, 69:2881–2884, 1992.
- [14] R. L. Rivest, A. Shamir, and L. M. Adleman. A method of obtaining digital signatures and public-key cryptosystems. *Commun. ACM*, 21:120–126, 1978.
- [15] P. W. Shor. Polynomial-time algorithms for prime factorization and discrete logarithms on a quantum computer. In *Proceedings of the 35th Annual Symposium on Foundations of Computer Science*, 1994.

- [16] G. Vernam. Cipher printing telegraph systems for secret wire and radio telegraphic communications. *J. Am. Inst. Electr. Eng.*, 45:109–115, 1926.
- [17] H. J. Briegel, W. Dur, J. I. Cirac, and P. Zoller. Quantum repeaters: the role of imperfect local operations in quantum communication. *Phys. Rev. Lett.*, 81:5932–5935, 1998.
- [18] D. Gottesman and I. L. Chuang. Demonstrating the viability of universal quantum computation using teleportation and single-qubit operations. *Nature*, 402:390–393, 1999.
- [19] E. Knill, R. Laflamme, and G. J. Milburn. A scheme for efficient quantum computation with linear optics. *Nature*, 409:46–52, 2001.
- [20] L. K. Grover. Quantum teleportation. arXiv:quant-ph/9704012.
- [21] P. W. Shor. Polynomial-time algorithms for prime factorization and discrete logarithms on a quantum computer. *SIAM J. Comp.*, 26:1484–1509, 1997.
- [22] L. K. Grover. Quantum mechanics helps in searching for a needle in a haystack. *Phys. Rev. Lett.*, 79:325, 1997.
- [23] R. Raussendorf and H. J. Briegel. A one-way quantum computer. *Phys. Rev. Lett.*, 86:5188–5191, 2001.
- [24] H. J. Briegel and R. Raussendorf. Persistent entanglement in arrays of interacting particles. *Phys. Rev. Lett.*, 86:910–913, 2001.
- [25] M. A. Nielsen. Optical quantum computation using cluster states. *Phys. Rev. Lett.*, 93:040503, 2004.
- [26] P. W. Shor. Scheme for reducing decoherence in quantum computer memory. *Phys. Rev. A*, 52:R2493–R2496, 1995.
- [27] A. M. Steane. Error correcting codes in quantum theory. *Phys. Rev. Lett.*, 77:793–797, 1996.
- [28] C. H. Bennett, D. P. DiVincenzo, J. A. Smolin, and W. K. Wootters. Mixed-state entanglement and quantum error correction. *Phys. Rev. A*, 54:3824–3851, 1996.
- [29] R. Laflamme, C. Miquel, J. P. Paz, and W. H. Zurek. Perfect quantum error correcting code. *Phys. Rev. Lett.*, 77:198–201, 1996.
- [30] K. Mattle, H. Weinfurter, P. G. Kwiat, and A. Zeilinger. Dense coding in experimental quantum communication. *Phys. Rev. Lett.*, 76:4656–4659, 1996.
- [31] D. Bouwmeester, J.-W. Pan, K. Mattle, M. Eibl, H. Weinfurter, and A. Zeilinger. Experimental quantum teleportation. *Nature*, 390:575–579, 1997.
- [32] D. Boschi, S. Branca, F. De Martini, L. Hardy, and S. Popescu. Experimental realization of teleporting an unknown pure quantum state via dual classical and Einstein-Podolsky-Rosen channels. *Phys. Rev. Lett.*, 80:1121–1125, 1998.
- [33] M. Żukowski, A. Zeilinger, M. A. Horne, and A. K. Ekert. “event-ready-detectors” Bell experiment via entanglement swapping. *Phys. Rev. Lett.*, 71:4287–4290, 1993.
- [34] J.-W. Pan, D. Bouwmeester, H. Weinfurter, and A. Zeilinger. Experimental entanglement swapping: entangling photons that never interacted. *Phys. Rev. Lett.*, 80:3891–3894, 1998.
- [35] C. H. Bennett, G. Brassard, S. Popescu, B. Schumacher, J. A. Smolin, and W. K. Wootters. Purification of noisy entanglement and faithful teleportation via noisy channels. *Phys. Rev. Lett.*, 76:722–725, 1996.

-
- [36] D. Deutsch, A. Ekert, R. Jozsa, C. Macchiavello, S. Popescu, and A. Sanpera. Quantum privacy amplification and the security of quantum cryptography over noisy channels. *Phys. Rev. Lett.*, 77:2818–2821, 1996.
- [37] J.-W. Pan, C. Simon, C. Brukner, and A. Zeilinger. Entanglement purification for quantum communication. *Nature*, 410:1067–1070, 2001.
- [38] J.-W. Pan, S. Gasparoni, U. Rupert, G. Weihs, and A. Zeilinger. Experimental entanglement purification of arbitrary unknown states. *Nature*, 423:417–422, 2003.
- [39] D. Bouwmeester, J.-W. Pan, M. Daniell, H. Weinfurter, and A. Zeilinger. Observation of three-photon greenberger-horne-zeilinger entanglement. *Phys. Rev. Lett.*, 82:1345, 1999.
- [40] A. Rauschenbeutel, G. Nogues, S. Osnaghi, P. Bertet, M. Brune, J.-M. Raimond, and S. Haroche. Step-by-step engineered multiparticle entanglement. *Science*, 288:2024–2028, 2000.
- [41] C. A. Sackett, D. Kielpinski, B. E. King, C. Langer, V. Meyer, C. J. Myatt, M. Rowe, Q. A. Turchette, W. M. Itano, D. J. Wineland, and C. Monroe. Experimental entanglement of four particles. *Nature*, 404:256–259, 2000.
- [42] J.-W. Pan, M. Daniell, S. Gasparoni, G. Weihs, and A. Zeilinger. Experimental demonstration of four-photon entanglement and high-fidelity teleportation. *Phys. Rev. Lett.*, 86:4435, 2001.
- [43] Z. Zhao, Y.-A. Chen, A.-N. Zhang, T. Yang, H. Briegel, and J.-W. Pan. Experimental demonstration of five-photon entanglement and open-destination teleportation. *Nature*, 430:54–57, 2004.
- [44] D. Leibfried, E. Knill, S. Seidelin, J. Britton, R. B. Blakestad, J. Chiaverini, D. B. Hume, W. M. Itano, J. D. Jost, C. Langer, R. Ozeri, R. Reichle, and D. J. Wineland. Creation of a six-atom ‘Schrödinger cat’ state. *Nature*, 438:639–642, 2005.
- [45] C.-Y. Lu, X.-Q. Zhou, O. Gühne, W.-B. Gao, J. Zhang, Z.-S. Yuan, A. Goebel, Tao Yang, and Jian-Wei Pan. Experimental entanglement of six photons in graph states. *Nature Physics*, 3:91–95, 2007.
- [46] H. Häffner, W. Hänsel, C. F. Roos, J. Benhelm, D. Chek al kar1, M. Chwalla, T. Körber, U. D. Rapol, M. Riebe, P. O. Schmidt, C. Becher, O. Gühne, W. Dür, and R. Blatt. Scalable multiparticle entanglement of trapped ions. *Nature*, 438:643–646, 2005.
- [47] A. Aspect, J. Dalibard, and G. Roger. Experimental test of Bell’s inequalities using time-varying analyzers. *Phys. Rev. Lett.*, 49:1804–1807, 1982.
- [48] A. Aspect, P. Grangier, and G. Roger. Experimental realization of Einstein-Podolsky-Rosen-Bohm gedankenexperiment: A new violation of Bell’s inequalities. *Phys. Rev. Lett.*, 49:91–94, 1982.
- [49] J.-W. Pan, D. Bouwmeester, M. Daniell, H. Weinfurter, and A. Zeilinger. Experimental test of quantum nonlocality in three-photon Greenberger-Horne-Zeilinger entanglement. *Nature*, 403:515–519, 2000.
- [50] Z. Zhao, T. Yang, Y.-A. Chen, A.-N. Zhang, M. Żukowski, and J.-W. Pan. Experimental violation of local realism by four-photon Greenberger-Horne-Zeilinger entanglement. *Phys. Rev. Lett.*, 91:180401, 2003.
- [51] P. Walther, K. J. Resch, T. Rudolph, E. Schenck, H. Weinfurter, V. Vedral, M. Aspelmeyer, and A. Zeilinger. Experimental one-way quantum computing. *Nature*, 434:169–176, 2005.

- [52] D. C. Burnham and D. L. Weinberg. Observation of simultaneity in parametric production of optical photon pairs. *Phys. Rev. Lett.*, 25:84–87, 1970.
- [53] P. G. Kwiat, K. Mattle, H. Weinfurter, A. Zeilinger, A. V. Sergienko, and Y. Shih. New high-intensity source of polarization-entangled photon pairs. *Phys. Rev. Lett.*, 75:4337–4341, 1995.
- [54] J.-W. Pan, Z.-B. Chen, M. Żukowski, H. Weinfurter, and Anton Zeilinger. Multi-photon entanglement and interferometry. *Rev. Mod. Phys.*, in press (2007).
- [55] T. Yang, Q. Zhang, J. Zhang, J. Yin, Z. Zhao, M. Żukowski, Z.-B. Chen, and J.-W. Pan. All-versus-nothing violation of local realism by two-photon, four-dimensional entanglement. *Phys. Rev. Lett.*, 95:240406, 2005.
- [56] C. Cinelli, M. Barbieri, R. Perris, P. Mataloni, and F. De Martini. All-versus-nothing non-locality test of quantum mechanics by two-photon hyperentanglement. *Phys. Rev. Lett.*, 95:240405, 2005.
- [57] J.-W. Pan, S. Gasparoni M. Aspelmeyer, T. Jennewein, and A. Zeilinger. Experimental realization of freely propagating teleported qubits. *Nature*, 421:721–725, 2003.
- [58] T. Jennewein, C. Simon, G. Weihs, H. Weinfurter, and A. Zeilinger. Quantum cryptography with entangled photons. *Phys. Rev. Lett.*, 84:4729–4732, 2000.
- [59] D. S. Naik, C. G. Peterson, A. G. White, A. J. Berglund, and P. G. Kwiat. Entangled state quantum cryptography: Eavesdropping on the ekert protocol. *Phys. Rev. Lett.*, 84:4733–4736, 2000.
- [60] W. Tittel, J. Brendel, H. Zbinden, and N. Gisin. Quantum cryptography using entangled photons in energy-time bell states. *Phys. Rev. Lett.*, 84:4737–4740, 2000.
- [61] Y.-A. Chen, A.-N. Zhang, Z. Zhao, X.-Q. Zhou, C.-Y. Lu, C.-Z. Peng, T. Yang, and J.-W. Pan. Experimental quantum secret sharing and third-man quantum cryptography. *Phys. Rev. Lett.*, 95:200502, 2005.
- [62] S. Gasparoni, J.-W. Pan, P. Walther, T. Rudolph, and A. Zeilinger. Realization of a photonic controlled-not gate sufficient for quantum computation. *Phys. Rev. Lett.*, 93:020504, 2004.
- [63] Z. Zhao, A.-N. Zhang, Y.-A. Chen, H. Zhang, J.-F. Du, T. Yang, and J.-W. Pan. Experimental demonstration of a nondestructive controlled-NOT quantum gate for two independent photon qubits. *Phys. Rev. Lett.*, 94:030501, 2005.
- [64] X.-H. Bao, T.-Y. Chen, Q. Zhang, J. Yang, H. Zhang, T. Yang, and J.-W. Pan. Optical nondestructive controlled-NOT gate without using entangled photons. *Phys. Rev. Lett.*, 98:170502, 2007.
- [65] I. Marcikic, H. de Riedmatten, W. Tittel, H. Zbinden, M. Legré, , and N. Gisin. Distribution of time-bin entangled qubits over 50 km of optical fiber. *Phys. Rev. Lett.*, 93:180502, 2004.
- [66] C. Gobby, Z. L. Yuan, and A. J. Shields. Quantum key distribution over 122 km of standard telecom fiber. *Appl. Phys. Lett.*, 84:3762, 2004.
- [67] C.-Z. Peng, T. Yang, X.-H. Bao, J. Zhang, X.-M. Jin, F.-Y. Feng, B. Yang, J. Yang, J. Yin, Q. Zhang, N. Li, B.-L. Tian, and J.-W. Pan. Experimental free-space distribution of entangled photon pairs over 13 km: towards satellite-based global quantum communication. *Phys. Rev. Lett.*, 94:150501, 2005.

- [68] W. Dür, H.-J. Briegel, J. I. Cirac, and P. Zoller. Quantum repeaters based on entanglement purification. *Phys. Rev. A*, 59:169–181, 1999.
- [69] S.J. van Enk, J.I. Cirac, and P. Zoller. Photonic channels for quantum communication. *Science*, 279:205–208, 1998.
- [70] L.-M. Duan, M. D. Lukin, J. I. Cirac, and P. Zoller. Long-distance quantum communication with atomic ensembles and linear optics. *Nature*, 414:413–418, 2001.
- [71] A. Kuzmich, W. P. Bowen, A. D. Boozer, A. Boca, C. W. Chou, L.-M. Duan, and H. J. Kimble. Generation of nonclassical photon pairs for scalable quantum communication with atomic ensembles. *Nature (London)*, 423:731, 2003.
- [72] C. H. van der Wal, M. D. Eisaman, A. André, R. L. Walsworth, D. F. Phillips, A. S. Zibrov, , and M. D. Lukin. Atomic memory for correlated photon states. *Science*, 301:196–200, 2003.
- [73] M. D. Eisaman, A. André, F. Massou, M. Fleischhauer, A. S. Zibrov, and M. D. Lukin. Electromagnetically induced transparency with tunable single-photon pulses. *Nature*, 438:837, 2005.
- [74] D. N. Matsukevich, T. Chanelière, S. D. Jenkins, S.-Y. Lan, T. A. B. Kennedy, and A. Kuzmich. Deterministic single photons via conditional quantum evolution. *Phys. Rev. Lett.*, 97:013601, 2006.
- [75] S. Chen, Y.-A. Chen, T. Strassel, Z.-S. Yuan, B. Zhao, J. Schmiedmayer, and J.-W. Pan. Deterministic and storable single-photon source based on quantum memory. *Phys. Rev. Lett.*, 97:173004, 2006.
- [76] D. Felinto, C. W. Chou, J. Laurat, E. W. Schomburg, H. de Riedmatten, and H. J. Kimble. Conditional control of the quantum states of remote atomic memories for quantum networking. *Nature Physics*, 2:844, 2006.
- [77] T. Chanelière, D. N. Matsukevich, S. D. Jenkins, S.-Y. Lan, R. Zhao, T. A. B. Kennedy, and A. Kuzmich. Quantum interference of electromagnetic fields from remote quantum memories. *Phys. Rev. Lett.*, 98:113602, 2007.
- [78] Z.-S. Yuan, Y.-A. Chen, S. Chen, B. Zhao, M. Koch, T. Strassel, Y. Zhao, G.-J. Zhu, J. Schmiedmayer, and J.-W. Pan. Synchronized independent narrow-band single photons and efficient generation of photonic entanglement. *Phys. Rev. Lett.*, 98:180503, 2007.
- [79] C. W. Chou, H. de Riedmatten, D. Felinto, S. V. Polyakov, S. J. van Enk, and H. J. Kimble. Measurement-induced entanglement for excitation stored in remote atomic ensembles. *Nature*, 438:828–832, 2005.
- [80] D. N. Matsukevich and A. Kuzmich. Quantum state transfer between matter and light. *Science*, 306:663, 2004.
- [81] Y.-A. Chen, S. Chen, Z.-S. Yuan, B. Zhao, C.-S. Chu, J. Schmiedmayer, and J.-W. Pan. Memory-built-in quantum teleportation with photonic and atomic qubits. *arXiv:quant-ph/0705.1256*, 2007.
- [82] Chin-Wen Chou, Julien Laurat, Hui Deng, Kyung Soo Choi, Hugues de Riedmatten, Daniel Felinto, and H. Jeff Kimble. Functional quantum nodes for entanglement distribution over scalable quantum networks. *Science*, 316:1316, 2007.
- [83] N. Yoran and B. Reznik. Deterministic linear optics quantum computation with single photon qubits. *Phys. Rev. Lett.*, 91:037903, 2003.

- [84] D. E. Browne and T. Rudolph. Resource-efficient linear optical quantum computation. *Phys. Rev. Lett.*, 95:010501, 2005.
- [85] P. Kok, W. J. Munro, K. Nemoto, T. C. Ralph, J. P. Dowling, and G. J. Milburn. Linear optical quantum computing with photonic qubits. *Rev. Mod. Phys.*, 79:135–174, 2007.
- [86] J. S. Bell. On the Einstein Poldolsky Rosen paradox. *Physics (Long Island City, N.Y.)*, 1:195, 1964.
- [87] M. O. Scully, B.-G. Englert, and H. Walther. Quantum optical tests of complementarity. *Nature*, 351:111–116, 1991.
- [88] A. Aspect, P. Grangier, and G. Roger. Experimental tests of realistic local theories via Bell’s theorem. *Phys. Rev. Lett.*, 47:460–463, 1981.
- [89] M. H. Rubin, D. N. Klyshko, Y. H. Shih, and A. V. Sergienko. Theory of two-photon entanglement in type-II optical parametric down-conversion. *Phys. Rev. A* 50, 5122 - 5133 (1994), 50:5122–5133, 1994.
- [90] D.M. Greenberger, M.A. Horne, and A. Zeilinger. *Bell’s Theorem, Quantum Theory, and Conceptions of the Universe*, page 69. Kluwer, Dordrecht, 1989.
- [91] J. S. Bell. *Speakable and Unspeakable in Quantum Mechanics*. Cambridge University Press, Cambridge, England, 1987.
- [92] N.D. Mermin. Extreme quantum entanglement in a superposition of macroscopically distinct states. *Phys. Rev. Lett.*, 65:1838–1840, 1990.
- [93] M. Ardehali. Bell inequalities with a magnitude of violation that grows exponentially with the number of particles. *Phys. Rev. A*, 46:5375–5378, 1992.
- [94] M. Hillery, V. Bužek, and A. Berthiaume. Quantum secret sharing. *Phys. Rev. A*, 59:1829–1834, 1999.
- [95] M. Żukowski, A. Zelinger, M. A. Horne, and H. Weinfurter. Quest for ghz states. *Acta Phys. Pol.*, 93:187, 1998.
- [96] G. Krenn and A. Zeilinger. Entangled entanglement. *Phys. Rev. A*, 54:1793–1797, 1996.
- [97] B. Julsgaard, J. Sherson, J. I. Cirac, J. Fiurášek, and E. S. Polzik. Experimental demonstration of quantum memory for light. *Nature*, 432:482–486, 2004.
- [98] Z. Zhao, T. Yang, Y.-A. Chen, A.-N. Zhang, and Jian-Wei Pan. Experimental realization of entanglement concentration and a quantum repeater. *Phys. Rev. Lett.*, 90:207901, 2003.
- [99] H. de Riedmatten, I. Marcikic, W. Tittel, H. Zbinden, D. Collins, and N. Gisin. Long distance quantum teleportation in a quantum relay configuration. *Phys. Rev. Lett.*, 92:047904, 2004.
- [100] D. G. Cory, M. D. Price, W. Maas, E. Knill, R. Laflamme, W. H. Zurek, T. F. Havel, and S. S. Somaroo. Experimental quantum error correction. *Phys. Rev. Lett.*, 81:2152–2155, 1998.
- [101] E. Knill, R. Laflamme, R. Martinez, and C. Negrevergne. Benchmarking quantum computers: The five-qubit error correcting code. *Phys. Rev. Lett.*, 86:5811–5814, 2001.
- [102] J. Chiaverini, D. Leibfried, T. Schaetz, M. D. Barrett, R. B. Blakestad, J. Britton, W. M. Itano, J. D. Jost, E. Knill, C. Langer, R. Ozeri, and D. J. Wineland. Realization of quantum error correction. *Nature*, 432:602–605, 2004.

-
- [103] D. Bouwmeester. Bit-flip-error rejection in optical quantum communication. *Phys. Rev. A*, 63:040301(R), 2001.
- [104] J.-W. Pan and A. Zeilinger. Greenberger-Horne-Zeilinger-state analyzer. *Phys. Rev. A*, 57:2208–2211, 1998.
- [105] X.-B. Wang. Quantum error-rejection code with spontaneous parametric down-conversion. *Phys. Rev. A*, 69:022320, 2004.
- [106] T. B. Pittman, B. C. Jacobs, and J. D. Franson. Probabilistic quantum encoder for single-photon qubits. *Phys. Rev. A*, 69:042306, 2004.
- [107] M. Ricci, F. De Martini, N. J. Cerf, R. Filip, J. Fiurášek, and C. Macchiavello. Experimental purification of single qubits. *Phys. Rev. Lett.*, 93:170501, 2004.
- [108] L.-P. Lamoureux, E. Brainis, N. J. Cerf, P. Emplit, M. Haelterman, and S. Massar. Experimental error filtration for quantum communication over highly noisy channels. *Phys. Rev. Lett.*, 94:230501, 2005.
- [109] M. Żukowski, A. Zeilinger, and H. Weinfurter. Entangling photons radiated by independent pulsed source. *Ann. N.Y. Acad. Sci.*, 755:91, 1995.
- [110] X.-B. Wang. Quantum key distribution with two-qubit quantum codes. *Phys. Rev. Lett.*, 92:077902, 2001.
- [111] H. F. Chau. Practical scheme to share a secret key through a quantum channel with a 27.6% bit error rate. *Phys. Rev. A*, 66:060302(R), 2002.
- [112] D. Gottesman and H.-K. Lo. Proof of security of quantum key distribution with two-way classical communications. *IEEE Trans. Inf. Theory*, 49:457, 2003.
- [113] H. P. Stapp. Bell’s theorem and world process. *Nuovo Cimeto Soc. Ital. Fis.*, 29B:270, 1975.
- [114] J. F. Clauser, M. A. Home, A. Shimony, and R. A. Holt. Proposed experiment to test local hidden-variable theories. *Phys. Rev. Lett.*, 23:880–884, 1969.
- [115] A. Peres. *Quantum Theory: Concepts and Methods*. Kluwer, Dordrecht, 1993.
- [116] B. S. Cirelăşon. Quantum generalizations of bell’s inequality. *Lett. Math. Phys.* 4, 93, 4:93, 1980.
- [117] A. Cabello. Violating Bell’s inequality beyond Cirel’son’s bound. *Phys. Rev. Lett.*, 88:060403, 2002.
- [118] L. J. Landau. On the violation of Bell’s inequality in quantum theory. *Phys. Lett. A*, 120:54, 1987.
- [119] J. F. Clauser and M. A. Horne. Experimental consequences of objective local theories. *Phys. Rev. D*, 10:526–535, 1974.
- [120] N. D. Mermin. The best version of Bell’s theorem. *Ann. N.Y. Acad. Sci.*, 755:616, 1995.
- [121] M. D. Barrett, J. Chiaverini, T. Schaetz, J. Britton, W. M. Itano, J. D. Jost, E. Knill, C. Langer, D. Leibfried, R. Ozeri, and D. J. Wineland. Deterministic quantum teleportation of atomic qubits. *Nature*, 429:737–739, 2004.
- [122] M. Riebe, H. Häffner, C. F. Roos, W. Hänsel, J. Benhelm, G. P. T. Lancaster, T. W. Körber, C. Becher, F. Schmidt-Kaler, D. F. V. James, and R. Blatt. Deterministic quantum teleportation with atoms. *Nature*, 429:734–737, 2004.

- [123] I. Marcikic, H. de Riedmatten, W. Tittel, H. Zbinden, and N. Gisin. Long-distance teleportation of qubits at telecommunication wavelengths. *Nature*, 421:509–513, 2003.
- [124] R. Ursin, T. Jennewein, M. Aspelmeyer, R. Kaltenbaek, M. Lindenthal, P. Walther, and A. Zeilinger. Communications quantum teleportation across the danube. *Nature*, 430:849, 2004.
- [125] B. C. Jacobs, T. B. Pittman, and J. D. Franson. Quantum relays and noise suppression using linear optics. *Phys. Rev. A*, 66:052307, 2002.
- [126] A. R. Calderbank and P. W. Shor. Good quantum error-correcting codes exist. *Phys. Rev. A*, 54:1098–1105, 1996.
- [127] J. Lee and M. S. Kim. Entanglement teleportation via Werner states. *Phys. Rev. Lett.*, 84:4236–4239, 2000.
- [128] Y. Yeo and W. K. Chua. Teleportation and dense coding with genuine multipartite entanglement. *Phys. Rev. Lett.*, 96:060502, 2006.
- [129] G. Rigolin. Quantum teleportation of an arbitrary two-qubit state and its relation to multipartite entanglement. *Phys. Rev. A*, 71:032303, 2005.
- [130] R. Cleve, D. Gottesman, and H.-K. Lo. How to share a quantum secret. *Phys. Rev. Lett.*, 83:648–651, 1999.
- [131] A. Hayashi, T. Hashimoto, and M. Horibe. Reexamination of optimal quantum state estimation of pure states. *Phys. Rev. A*, 72:032325, 2005.
- [132] X.-B. Zou and W. Mathis. Generating a four-photon polarization-entangled cluster state. *Phys. Rev. A*, 71:032308, 2005.
- [133] M. Hein, J. Eisert, and H. J. Briegel. Multiparty entanglement in graph states. *Phys. Rev. A*, 69:062311, 2004.
- [134] A. R. Calderbank and P. W. Shor. Good quantum error-correcting codes exist. *Phys. Rev. A*, 54:1098, 1996.
- [135] R. Raussendorf, D. E. Browne, and H. J. Briegel. Measurement-based quantum computation on cluster states. *Phys. Rev. A*, 68:022312, 2003.
- [136] D. Schlingemann and R. F. Werner. Quantum error-correcting codes associated with graphs. *Phys. Rev. A*, 65:012308, 2002.
- [137] M. Hein, W. Dür, and H. J. Briegel. Entanglement properties of multipartite entangled states under the influence of decoherence. *Phys. Rev. A*, 71:032350, 2005.
- [138] N. Kiesel, C. Schmid, U. Weber, G. Tóth, O. Gühne, R. Ursin, and H. Weinfurter. Experimental analysis of a four-qubit photon cluster state. *Phys. Rev. Lett.*, 95:210502, 2005.
- [139] P. Walther, M. Aspelmeyer, K. J. Resch, and Anton Zeilinger. Experimental violation of a cluster state Bell inequality. *Phys. Rev. Lett.*, 95:020403, 2005.
- [140] T. P. Bodiya and L.-M. Duan. Scalable generation of graph-state entanglement through realistic linear optics. *Phys. Rev. Lett.*, 97:143601, 2006.
- [141] R. Prevedel, P. Walther, F. Tiefenbacher, P. Böhi, R. Kaltenbaek, T. Jennewein, and A. Zeilinger. High-speed linear optics quantum computing using active feed-forward. *Nature*, 445:65–69, 2007.

-
- [142] M. S. Tame, R. Prevedel, M. Paternostro, P. Böhi, M. S. Kim, and A. Zeilinger. Experimental realization of Deutsch's algorithm in a one-way quantum computer. *Phys. Rev. Lett.*, 98:140501, 2007.
- [143] J. T. Barreiro, N. K. Langford, N. A. Peters, and Paul G. Kwiat. Generation of hyperentangled photon pairs. *Phys. Rev. Lett.*, 95:260501, 2005.
- [144] C. Schuck, Gerhard Huber, C. Kurtsiefer, and Harald Weinfurter. Complete deterministic linear optics Bell state analysis. *Phys. Rev. Lett.*, 96:190501, 2006.
- [145] A. Cabello. "all versus Nothing" inseparability for two observers. *Phys. Rev. Lett.*, 87:010403, 2001.
- [146] Z.-B. Chen, J.-W. Pan, Y.-D. Zhang, C. Brukner, and A. Zeilinger. All-Versus-Nothing violation of local realism for two entangled photons. *Phys. Rev. Lett.*, 90:160408, 2003.
- [147] A. Cabello. Bipartite Bell inequalities for hyperentangled states. *Phys. Rev. Lett.*, 97:140406, 2006.
- [148] Marco Barbieri, F. De Martini, P. Mataloni, G. Vallone, and A. Cabello. Enhancing the violation of the Einstein-Podolsky-Rosen local realism by quantum hyperentanglement. *Phys. Rev. Lett.*, 97:140407, 2006.
- [149] P. G. Kwiat and H. Weinfurter. Embedded Bell-state analysis. *Phys. Rev. A*, 58:R2623–R2626, 1998.
- [150] M. Barbieri, G. Vallone, P. Mataloni, and F. De Martini. Complete and deterministic discrimination of polarization Bell states assisted by momentum entanglement. *Phys. Rev. A*, 75:042317, 2007.
- [151] P. G. Kwiat, E. Waks, A. G. White, L. Appelbaum, and P. H. Eberhard. Ultrabright source of polarization-entangled photons. *Phys. Rev. A*, 60:R773–R776, 1999.
- [152] G. Tóth and O. Gühne. Entanglement detection in the stabilizer formalism. *Phys. Rev. A*, 72:022340, 2005.
- [153] P.G. Kwiat, J.R. Mitchell, P.D.D. Schwindt, and A. G. White. Grover's search algorithm: An optical approach. *J. Mod. Opt.*, 47:257, 2000.
- [154] N. Bhattacharya, H.B. van Linden van den Heuvell, and R.J.C. Spreeuw. Implementation of quantum search algorithm using classical fourier optics. *Phys. Rev. Lett.*, 88:137901, 2002.
- [155] Tao Yang, Qiang Zhang, Teng-Yun Chen, Shan Lu, Juan Yin, Jian-Wei Pan, Zhi-Yi Wei, Jing-Rong Tian, and Jie Zhang. Experimental synchronization of independent entangled photon sources. *Phys. Rev. Lett.*, 96(11):110501, 2006.
- [156] Z.-B. Chen, B. Zhao, Y.-A. Chen, J. Schmiedmayer, and J.-Wei Pan. Fault-tolerant quantum repeater with atomic ensembles and linear optics. *Phys. Rev. A*, 76:022329, 2007.
- [157] A. André. *Nonclassical States of Light and Atomic Ensembles: Generation and New Applications*. PhD thesis, Harvard University, Graduate School of Arts and Sciences, 2005.
- [158] M. Fleischhauer, A. Imamoglu, and J. P. Marangos. Electromagnetically induced transparency: Optics in coherent media. *Rev. Mod. Phys.*, 77:633–673, 2005.
- [159] K.W. Holman, D.D. Hudson, J. Ye, and D. J. Jones. Remote transfer of a high-stability and ultralow-jitter timing signal. *Opt. Lett.*, 30:1225, 2005.

- [160] C. K. Hong, Z. Y. Ou, and L. Mandel. Measurement of subpicosecond time intervals between two photons by interference. *Phys. Rev. Lett.*, 59:2044–2046, 1987.
- [161] S. Bose, P. L. Knight, M. B. Plenio, , and V. Vedral. Proposal for teleportation of an atomic state via cavity decay. *Phys. Rev. Lett.*, 83:5158– 5161, 1999.
- [162] D.E. Browne, M.B. Plenio, and S.F. Huelga. Robust creation of entanglement between ions in spatially separate cavities. *Phys. Rev. Lett.*, 91:067901, 2003.
- [163] X.-L. Feng, Z.-M. Zhang, X.-D. Li, S.-Q. Gong, and Zhi-Zhan Xu. Entangling distant atoms by interference of polarized photons. *Phys. Rev. Lett.*, 90:217902, 2003.
- [164] C. Simon and W. T. M. Irvine. Robust long-distance entanglement and a loophole-free Bell test with ions and photons. *Phys. Rev. Lett.*, 91:110405, 2003.
- [165] B. Zhao, Z.-B. Chen, Y.-A. Chen, J. Schmiedmayer, and J.-W. Pan. Robust creation of entanglement between remote memory qubits. *Phys. Rev. Lett.*, 98:240502, 2007.
- [166] A. V. Gorshkov, A. André, M. Fleischhauer, A. S. Sørensen, and M. D. Lukin. Universal approach to optimal photon storage in atomic media. *Phys. Rev. Lett.*, 98:123601, 2007.
- [167] L. Jiang, J. M. Taylor, and M. D. Lukin. A fast and robust approach to long-distance quantum communication with atomic ensembles. *Phys. Rev. A*, 76:012301, 2007.
- [168] M. D. Lukin, S. F. Yelin, and M. Fleischhauer. Entanglement of atomic ensembles by trapping correlated photon states. *Phys. Rev. Lett.*, 84:4232–4235, 2000.
- [169] M. Fleischhauer and M. D. Lukin. Dark-state polaritons in electromagnetically induced transparency. *Phys. Rev. Lett.*, 84:5094–5097, 2000.
- [170] Q. Zhang, X.-H. Bao, C.-Y. Lu, X.-Q. Zhou, T. Yang, T. Rudolph, and J.-W. Pan. Demonstration of efficient scheme for generation of “event ready” entangled photon pairs from single photon source. *arXiv:quant-ph/0610145*, 2006.
- [171] D. F. V. James and P. G. Kwiat. Atomic-vapor-based high efficiency optical detectors with photon number resolution. *Phys. Rev. Lett.*, 89:183601, 2002.
- [172] A. Imamoglu. High efficiency photon counting using stored light. *Phys. Rev. Lett.*, 89:163602, 2002.
- [173] A. Dantan, G. Reinaudi, A. Sinatra, F. Laloë, E. Giacobino, and M. Pinard. Long-lived quantum memory with nuclear atomic spins. *Phys. Rev. Lett.*, 95:123002, 2005.
- [174] T. Schmitt-Manderbach, H. Weier, M. Fürst, R. Ursin, F. Tiefenbacher, T. Scheidl, J. Perdigues, Z. Sodnik, C. Kurtsiefer, J. G. Rarity, A. Zeilinger, and H. Weinfurter. Experimental demonstration of free-space decoy-state quantum key distribution over 144 km. *Phys. Rev. Lett.*, 98:010504, 2007.
- [175] C.-Z. Peng, J. Zhang, D. Yang, W.-B. Gao, H.-X. Ma, H. Yin, H.-P. Zeng, T. Yang, X.-B. Wang, and J.-W. Pan. Experimental long-distance decoy-state quantum key distribution based on polarization encoding. *Phys. Rev. Lett.*, 98:010505, 2007.
- [176] B. Lounis and M. Orrit. Single-photon sources. *Rep. Prog. Phys.*, 68:1129–1179, 2005.
- [177] P. Michler, A. Kiraz, C. Becher, W. V. Schoenfeld, P. M. Petroff, L. D. Zhang, E. Hu, and A. Imamoglu. A quantum dot single-photon turnstile device. *Science*, 290:2282–2285, 2000.
- [178] C. Santori, M. Pelton, G. Solomon, Y. Dale, and Y. Yamamoto. Triggered single photons from a quantum dot. *Phys. Rev. Lett.*, 86:1502–1505, 2001.

-
- [179] Axel Kuhn, Markus Hennrich, and Gerhard Rempe. Deterministic single-photon source for distributed quantum networking. *Phys. Rev. Lett.*, 89:067901, 2002.
- [180] M. Keller, B. Lange, K. Hayasaka, W. Lange, and H. Walther. Continuous generation of single photons with controlled waveform in an ion-trap cavity system. *Nature*, 431:1075–1078, 2004.
- [181] C. Kurtsiefer, S. Mayer, P. Zarda, and H. Weinfurter. Stable solid-state source of single photons. *Phys. Rev. Lett.*, 85:290–293, 2000.
- [182] C. Santori, D. Fattal, J. Vuckovic, G. S. Solomon, and Y. Yamamoto. Single-photon generation with InAs quantum dots. *New J. Phys.*, 6:89, 2004.
- [183] C. W. Chou, S. V. Polyakov, A. Kuzmich, and H. J. Kimble. Single-photon generation from stored excitation in an atomic ensemble. *Phys. Rev. Lett.*, 92:213601, 2004.
- [184] T. Chanelière, D. N. Matsukevich, S. D. Jenkins, S.-Y. Lan, T. A. B. Kennedy, and A. Kuzmich. Storage and retrieval of single photons transmitted between remote quantum memories. *Nature*, 438:833–836, 2005.
- [185] M. D. Lukin. Colloquium: Trapping and manipulating photon states in atomic ensembles. *Rev. Mod. Phys.*, 75:457–472, 2003.
- [186] P. Grangier, G. Roger, and A. Aspect. Experimental evidence for a photon anticorrelation effect on a beam splitter: a new light on single-photon interferences. *Europhys. Lett.*, 1:173–179, 1986.
- [187] C. K. Hong and L. Mandel. Experimental realization of a localized one-photon state. *Phys. Rev. Lett.*, 56:58, 1986.
- [188] Rainer Kaltenbaek, Bibiane Blauensteiner, Marek Zukowski, Markus Aspelmeyer, and Anton Zeilinger. Experimental interference of independent photons. *Phys. Rev. Lett.*, 96(24):240502, 2006.
- [189] H. de Riedmatten, J. Laurat, C.W. Chou, E.W. Schomburg, D. Felinto, and H. J. Kimble. Direct measurement of decoherence for entanglement between a photon and stored atomic excitation. *Phys. Rev. Lett.*, 97:113603, 2006.
- [190] T. Legero, T. Wilk, A. Kuhn, and G. Rempe. Time-resolved two-photon quantum interference. *Appl. Phys. B*, 77:797, 2003.
- [191] T. Legero, T. Wilk, M. Hennrich, G. Rempe, and A. Kuhn. Quantum beat of two single photons. *Phys. Rev. Lett.*, 93:070503, 2004.
- [192] A. Furusawa, J. L. Sørensen, S. L. Braunstein, C. A. Fuchs, H. J. Kimble, and E. S. Polzik. Unconditional quantum teleportation. *Science*, 282:706–709, 1998.
- [193] J. F. Sherson, H. Krauter, R. K. Olsson, B. Julsgaard, K. Hammerer, I. Cirac, and E. S. Polzik. Quantum teleportation between light and matter. *Nature*, 443:557–560, 2006.
- [194] K. Hammerer, E. S. Polzik, and J. I. Cirac. Teleportation and spin squeezing utilizing multimode entanglement of light with atoms. *Phys. Rev. A*, 72:052313, 2005.
- [195] A. E. Kozhekin, K. Mølmer, and E. S. Polzik. Quantum memory for light. *Phys. Rev. A.*, 62:033809, 2000.
- [196] S. Massar and S. Popescu. Optimal extraction of information from finite quantum ensembles. *Phys. Rev. Lett.*, 74:1259–1263, 1995.

- [197] D. M. Harber, H. J. Lewandowski, J. M. McGuirk, and E. A. Cornell. Effect of cold collisions on spin coherence and resonance shifts in a magnetically trapped ultracold gas. *Phys. Rev. A*, 66:053616, 2002.
- [198] M. Aspelmeyer, H. R. Böhm, T. Gyatso, T. Jennewein, R. Kaltenbaek, M. Lindenthal, G. Molina-Terriza, A. Poppe, K. Resch, M. Taraba, R. Ursin, P. Walther, and A. Zeilinger. Long-distance free-space distribution of quantum entanglement. *Science*, 301:621–623, 2003.
- [199] D. N. Matsukevich, T. Chanelière, M. Bhattacharya, S.-Y. Lan, S. D. Jenkins, T. A. B. Kennedy, and A. Kuzmich. Entanglement of a photon and a collective atomic excitation. *Phys. Rev. Lett.*, 95:040405, 2005.
- [200] S.-Y. Lan, S. D. Jenkins, T. Chaneliere, D. N. Matsukevich, C. J. Campbell, R. Zhao, T. A. B. Kennedy, and A. Kuzmich. Dual species matter qubit entangled with light. *Phys. Rev. Lett.*, 98:123602, 2007.
- [201] R. Inoue, N. Kanai, T. Yonehara, Y. Miyamoto, M. Koashi, and M. Kozuma. Entanglement of orbital angular momentum states between an ensemble of cold atoms and a photon. *Phys. Rev. A*, 74:053809, 2006.
- [202] A. Vaziri, J.-W. Pan, T. Jennewein, G. Weihs, and A. Zeilinger. Concentration of higher dimensional entanglement: Qutrits of photon orbital angular momentum. *Phys. Rev. Lett.*, 91:227902, 2003.
- [203] Danielle A. Braje, Vlatko Balić, Sunil Goda, G. Y. Yin, and S. E. Harris. Frequency mixing using electromagnetically induced transparency in cold atoms. *Phys. Rev. Lett.*, 93:183601, 2004.
- [204] Wenjamin Rosenfeld, Stefan Berner, Jürgen Volz, Markus Weber, and Harald Weinfurter. Remote preparation of an atomic quantum memory. *Phys. Rev. Lett.*, 98:050504, 2007.
- [205] P. Maunz, D. L. Moehring, S. Olmschenk, K. C. Younge, D. N. Matsukevich, and C. Monroe. Quantum interference of photon pairs from two remote trapped atomic ions. *Nature Physics*, 3:538–541, 2007.
- [206] T. Wilk, S. C. Webster, A. Kuhn, and G. Rempe. Single-atom single-photon quantum interface. *Science*, 317:488–490, 2007.
- [207] A. D. Boozer, A. Boca, R. Miller, T. E. Northup, and H. J. Kimble. Reversible state transfer between light and a single trapped atom. *Phys. Rev. Lett.*, 98:193601, 2007.
- [208] James K. Thompson, Jonathan Simon, Huanqian Loh, and Vladan Vuletić. A high-brightness source of narrowband, identical-photon pairs. *Science*, 313:74, 2006.
- [209] D. L. Moehring, P. Maunz, S. Olmschenk, K. C. Younge, D. N. Matsukevich, L.-M. Duan, and C. Monroe. Entanglement of single-atom quantum bits at a distance. *Nature*, 449:68–71, 2007.
- [210] S. Chen, Y.-A. Chen, B. Zhao, Z.-S. Yuan, J. Schmiedmayer, and J.-W. Pan. Demonstration of a stable atom-photon entanglement source for quantum repeaters. *Phys. Rev. Lett.*, 99:180505, 2007.
- [211] O. Gühne, P. Hyllus, D. Bruß, A. Ekert, M. Lewenstein, C. Macchiavello, and A. Sanpera. Detection of entanglement with few local measurements. *Phys. Rev. A*, 66:062305, 2002.
- [212] C. Simon, H. de Riedmatten, M. Afzelius, N. Sangouard, H. Zbinden, and N. Gisin. Quantum repeaters with photon pair sources and multimode memories. *Phys. Rev. Lett.*, 98:190503, 2007.